Thesis for the degree of Master of Philosophy

Faculty of Engineering

University of London

1968

DIGITAL POSITION CONTROL OF A LATHE TOOL

F.J.Robinson, B.Sc.

Queen Mary College, London

Acknowledgements

I would like to thank Dr. C.R.Webb, Reader in Mechanical Engineering at Queen Mary College, London, who has acted as my supervisor for this work, for his advice guidance and co-operation during my course of study and the preparation of this thesis.

In addition I would also like to thank the Governors, the Principal and the executive Head of the Faculty of Technology of Enfield College of Technology, to whom I owe a large part of the laboratory facilities used; and also Messrs. T.S.Harrison and Sons, Ltd., of Heckmondwike, Yorkshire, who very kindly loaned the lathe on which the tests were carried out.

Finally I thank Stanley Millward of Enfield College of Technology for his assistance and advice in the preparation of the computer programme which forms an essential part of the analysis.

F.J.Robinson

1968

INDEX

	Page
ABSTRACT	1
INTRODUCTION	3
SECTION 1 Description of the Harrison L6 Lathe	8
SECTION 2 Description of the Digital Servomechanism	16
SECTION 3 Performance of the Hydraulic Servo	26
SECTION 4 Analysis of the Digital Servo	50
SECTION 5 Performance of the Digital Servo	88
SECTION 6 Mounting the Servo on the Lathe	114
SECTION 7 Machining Tests	127
SECTION 8 Conclusions	140
SECTION 9 References	145
APPENDIX 1 Detailed results for Section 3	146
APPENDIX 2 Computer Programme	171
APPENDIX 3 Detailed results for Section 5	188
APPENDIX 4 Detailed results for Section 7	206

Abstract: Digital Position Control of a Lathe Tool

In this work a digital position control servomechanism, which had previously been developed by the author and a co-worker , has been fitted to the saddle of a copy turning lathe so that the positioning of the servo ram controls the setting of the lathe tool relative to the main spindle axis. In this way required workpiece diameters may be preset by means of the input to the digital servo, and it is intended to further develop the system to full numerical control of the machine.

The subject of the thesis is the analysis of the performance of the digital servo, both theoretically and practically, the mounting of the servo on the lathe and subsequent accuracy checks on workpieces machined according to preset commands at the input to the servo. Analysis of the performance of the digital servo involved the use of a general purpose digital computer to simmulate the non-linear response characteristics of the system, and the performance tests were carried out using a data sampling technique which is fully described.

Since in operation the complete system involves the use of two position servomechanisms in series, and since no overall feedback link is provided, it was also necessary to investigate

the performance of the hydraulic positioning system already fitted to the copying slide of the lathe. A series of experiments was therefore set up to measure the lag and response of the hydraulic servo under typical working conditions, in order to establish that this lag could be ignored compared to the lag in the digital system in deciding the overall accuracy of the combined equipment. This work complete with the experimental results obtained is also included.

Introduction

The work described in this thesis forms a part of a much larger research project, namely the development of a low cost numerical control system suitable for small centre lathes, which has been proceeding at Enfield College of Technology for the past three years. The first stage of the work was completed by the author and Mr. G.A.H.Thomas of Enfield College of Technology in 1965, and subsequent work on the project, including all the tests and analyses in this thesis, are due to the author.

In principle the system operates by positioning the stylus of a lathe equipped for hydraulic copy turning, by means of a small servo operated screw jack mechanism which is fitted to the machine in place of the normal copying template and holding fixture. By making use of the copy turning lathe it has been possible, with some limitations, to design a numerically controlled machine tool, capable of producing three-dimensional workpieces, with only one axis fitted with closed loop position control. This feature together with the use of cheap electronics components and parallel arithmetic in the control console has enabled the low cost principle to be met.

The lathe tool is in fact positioned by a hydraulically operated tool slide, mounted on the saddle, which is controlled by a built-in hydraulic servo valve supplied by a separate source

of pressurized hydraulic fluid. For normal copy turning operations, the servo valve is in contact with a lever system fitted with a stylus that contacts a template, and as the lathe saddle moves along the bed of the machine the stylus follows the template profile, thereby causing deflections of the servo valve which cause the tool slide to trace out in space the form of the template.

In the application described in this thesis the template is replaced by an electrically driven screw jack mechanism which is the output element of a digital position servomechanism. The hydraulic servomechanism which is fitted to the machine is described in Section 1 , and it may be seen to be of a conventional type, having a built-in mechanical feedback path for positioning errors. The digital system is an original mechanism provided with position feedback between its input and comparator elements and is fully described in Section 2 .

In developing this equipment, the overall requirement was one of positioning accuracy, rather than speed of response or reduction in lag, and emphasis has been placed on the relatively slow speeds that the system will be required to operate. This feature has enabled steps to be taken which would not be satisfactory in other fields. In addition to positioning accuracy it was also necessary to build a system which would be 'dead beat'

and as free as possible from all forms of positional oscillation.

The accuracy requirement has been met by the use of a digital system and careful design and manufacture of the output element. In this thesis the performance of the digital system is analyzed, and being non-linear in nature use was made of a digital computer to calculate stations on the response curve for the system. This work is described in Section 4, and the source listing and block diagram for the computer programme are given in Appendix 2. Having established the theoretical response of the digital servo, a series of tests was then carried out to determine the actual response of the equipment built, over its normal operating range. Since the equipment is digital it was necessary to develop a data sampling technique to record positioning errors during response to continuous ramp input functions, and this series of tests is described in Section 5.

For certain types of applications the operation of two positioning systems in series could lead to difficulties, especially if they had similar response characteristics. In this work it is shown that the hydraulic lag in the slide positioning system is very much smaller than that of the digital equipment, and in addition the speed of response required is so low, that the hydraulic servo may be taken as a solid link for the purpose

of combined system analysis. In order to establish that this is in fact the case a series of experiments was carried out to investigate the response of the hydraulic servo over the operating range in question. Continuous records of positions error or lag were obtained for the system with the aid of a proximity transducer and U.V. recording oscilloscope, the work being described in Section 3, and the oscillograms are provided in Appendix 1.

The digital system was then fitted to the saddle of the lathe, and a series of tests were run to establish the positioning accuracy achieved. A full description of the mounting and setting-up procedure is given in Section 7, and the results are provided in Appendix 4.

Fig. 1-1 General View of the Harrison L 6 Lathe used in this work, with the prototype Control Cabinet at the left hand side of the figure

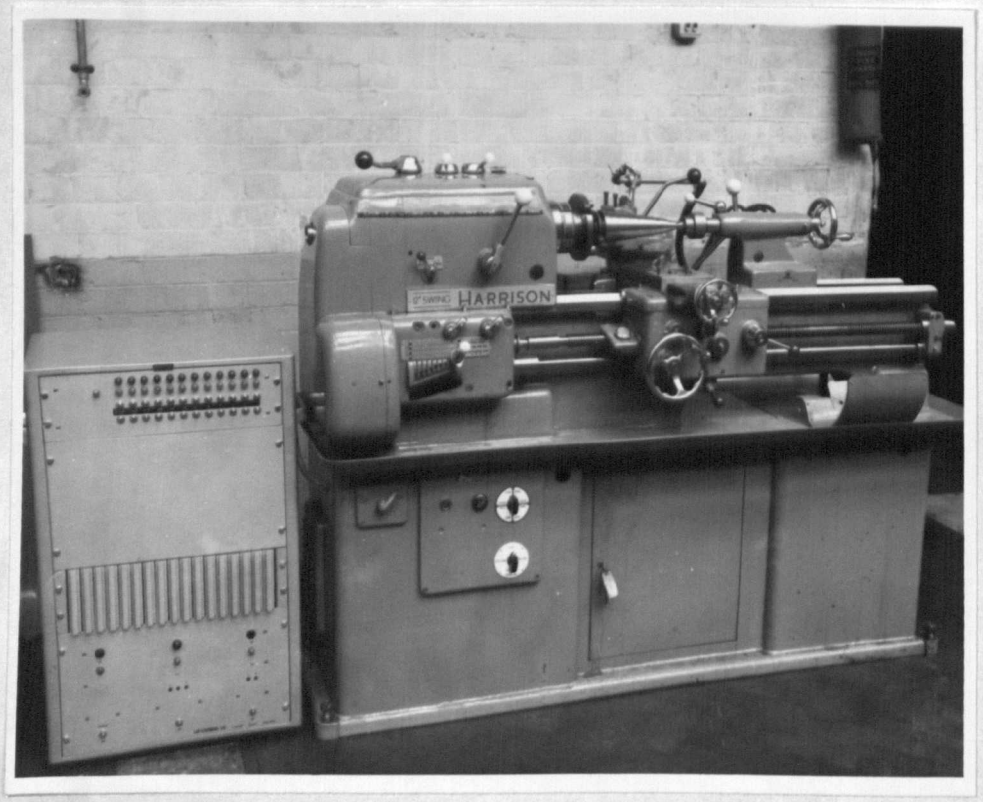

SECTION 1 : Description of the Harrison L 6 Copy Turning Lathe

The machine is a conventional 12-in. swing centre lathe, fitted with a special cross slide that incorporates a hydraulically operated copy turning slide, hydraulic servo valve, manually adjustable tool slide and tracer assembly. In addition the rear face of the lathe bed is fitted with a template holding fixture, and a separate motor driven hydraulic power unit is supplied to drive the copying servo. A view of the L 6 lathe employed in this work, together with the prototype control cabinet, is given in Fig.1-1.

Lathes in this series are either supplied with a standard cross slide and fitted with the Harrison taper turning attachment, or with the cross slide mentioned above, in which case they are termed copy turning lathes. In either case the machine can be operated as a normal centre lathe when required, since all lathes are supplied with a tool post at the front of the cross slide which may be positioned by means of the conventional manually operated screw mechanism.

Fig.1-2 is a diagram showing the general arrangement of the tool slides on an L 6 lathe fitted with the manufacturers copy turning equipment. (Ref 1 Section 9) In this diagram the chuck, tailstock, bed and saddle are shown at A,B,C and D respectively, and E is the tool post and top slide assembly for normal centre lathe working which may be seen to be mounted at the front of the cross slide member F. The copying slide G is angled 30° towards the tailstock from the cross slide axis, and incorporates a hydraulic cylinder and servo valve assembly H,

Fig. 1-2 General Arrangement of the Tool Slides on an L 6 Lathe fitted with Copy Turning Equipment

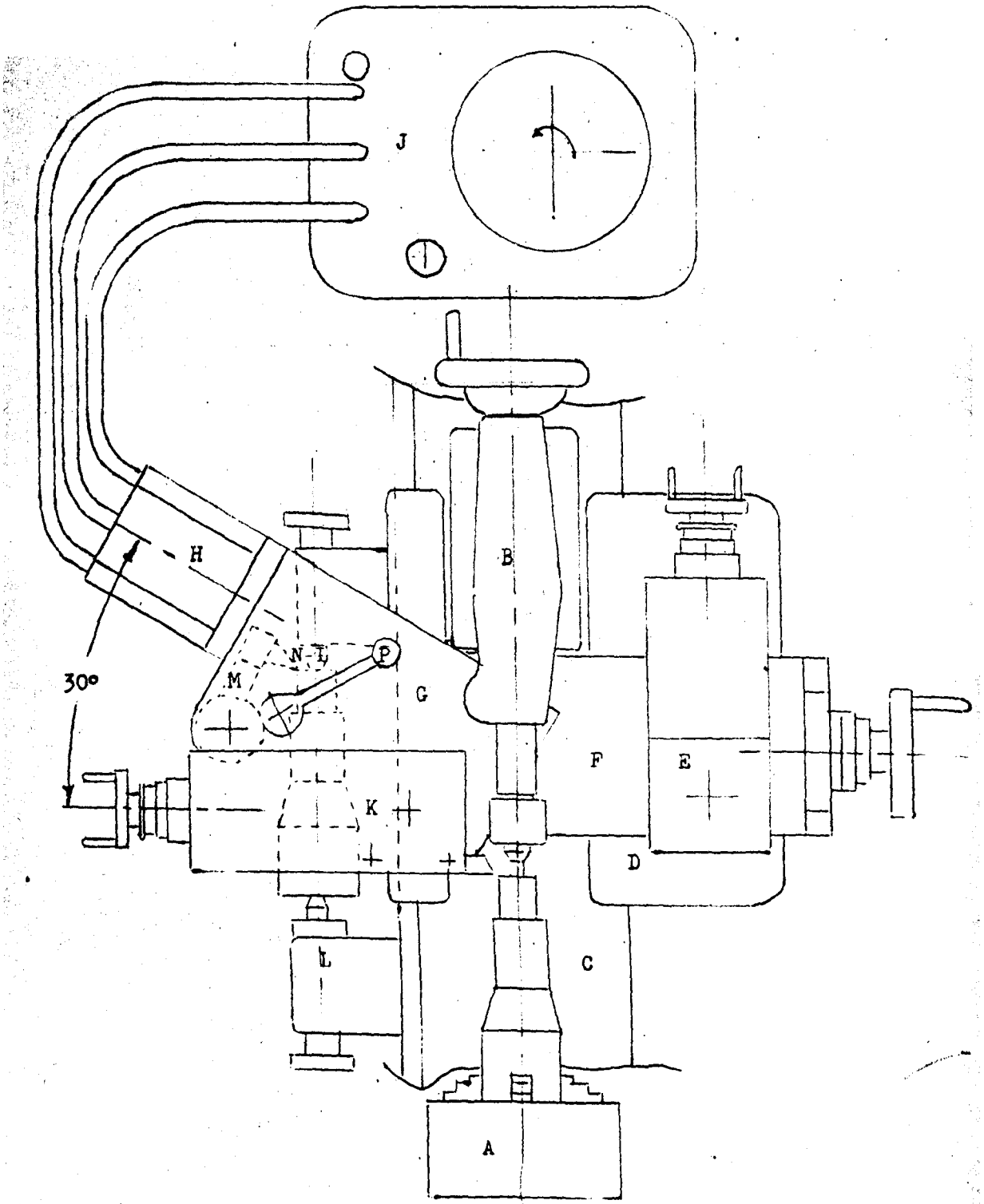

driven by power unit J. During copy turning operations the cutting tool is mounted in a tool post fitted to slide K, which is at the rear of the cross slide and mounted on an extension of the copying slide. For this type of work the lathe spindle is normally rotated in reverse compared to conventional centre lathe practice,ie. clockwise when viewed from the tailstock end of the bed.

Templates in the form of actual workpieces in the finished condition are mounted between centres L at the rear of the lathe bed, so that the surface of the template is in contact with stylus M. The stylus is mounted at one end of the tracer arm N, which pivots at a fulcrum provided with a tapered roller bearing assembly housed in the copying slide casting, and there is a lug projecting from arm N that contacts the end of the servo valve spool. In addition, an override control P is fitted, which takes the form of an eccentric on a vertical shaft fitted with a hand lever, so that rotation of the shaft causes the eccentric to move arm N, thereby depressing the valve spool which causes the copying slide to move away from the lathe axis. During copy turning the override control is set so that the eccentric is clear of arm N, thereby allowing the valve spool to be moved only by deflections of the stylus M.

Movement of the stylus causes the tracer arm to deflect which depresses the end of the valve spool. Fig.1-3 is a cross sectional view of the servo valve and hydraulic cylinder assembly, from which it may be seen that deflections of the spool result in the hydraulic system becomming unbalanced so that there is a net force on the slide piston

in a direction governed by the spool deflection. It is arranged that this force produces motion of the copying slide in the same sense as the spool deflection, thereby returning the system to a state of equilibrium, which is as the system is shown in the figure. The valve spool is lightly loaded to the left in the figure, which keeps it in contact with the stylus, and the force of this spring is the load experienced by the tracer arm.

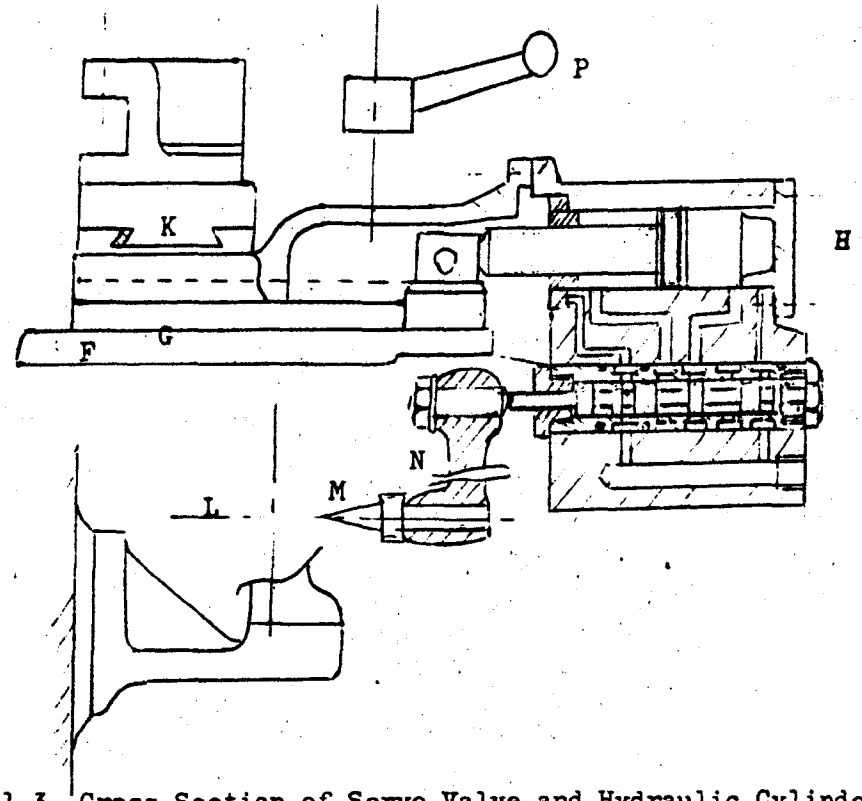

Fig. 1-3 Cross Section of Servo Valve and Hydraulic Cylinder

As has already been mentioned the copying slide is angled with respect to the cross slide axis which provides the copying tool with two components of motion, axial and radial, as the slide is retracted relative to the axis of the lathe bed. In copy turning, the saddle is moved steadily along the lathe bed throughout operations, and since the axial component of tool motion is in the opposite sense to for-

ward saddle traverse, it is possible to arrest the axial motion of the cutting tool due to saddle movement without stopping the saddle, and at the same time retain the radial component of tool motion. This effect is employed for machining faces or steps in workpieces by copy turning.

The copying equipment for the Harrison lathe is in effect a hydraulic position servomechanism, which uses a 1:1 model of the required profile as its input and a spool valve as the position sensing device. In the machine system employed in these tests, the spool valve was of the '3-way' type in order to simplify manufacture, whereas the normal valve supplied by the Harrison Company is of the '4-way' type. Drive for the copying slide comes from a hydraulic cylinder, shown at H in Fig.1-3, and the force amplification of the system is fixed by the piston diameter, and the pressure generated by the separate hydraulic power unit.

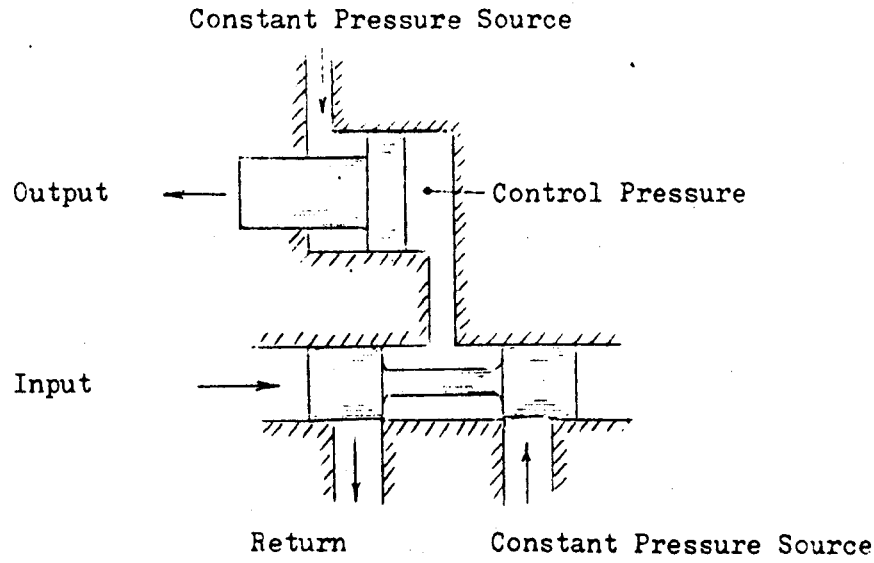

Fig.1-4 Schematic Diagram of a '3-way' type hydraulic Servo Valve

A simple explanation of the operation of tracer controlled hydraulic copying lathes is given by H.C.Town (Ref.2 Section 9), and a description of the operation of '3-way' servo valves is given in 'Design of Hydraulic Control Systems' by Lewis and Stern (Ref.3 Section9). The lands on the spool valve, and the bores in the valve body are machined to extremely fine limits, so that there is virtually no leakage of hydraulic fluid past them, and in addition the lands and ports are positioned very accurately.

In the schematic diagram in Fig.1-4, a constant pressure source of hydraulic fluid is supplied to the valve, and also to one side of the piston. It is arranged that one side of the piston has a smaller area than the other (one half in the case of the valve fitted to the Harrison machine), so that when the valve is moved to the right in the figure, the pressure is the same on both sides of the piston which results in a net force to the left acting on the piston. When the valve is moved to the left, however, the pressure is cut off from the large area side of the piston, which results in a force to the right. With the valve at an intermediate position, the two valve ports act as a pressure reducing nozzle, dropping the constant pressure source to one half its nominal value, so that there is no net force on the piston.

A more detailed analysis of spool valves is given by A.C.Morse (Ref.4 Section 9), in which it is pointed out that the flow characteristics across ports of this type can lead to instabilities, and that simple mathematical treatments of the hydraulic resistance is only reasonable for very small port openings. The effect of 'hydraul-

ic lag' on copy turning is not serious, provided that very great feed rates are not employed. Generally step input functions are not possible, all inputs being of the ramp type, and the ramp slopes are always very small by comparison with other types of position control mechanisms

Due to the very low input rates employed, the lag is always small with the result that non-linear effects in the port flow characteristics do not cause any bother. It is important, however, that position accuracy and stability are of a high order. The first requirement is met by the standard of manufacture of the valve unit, and the second places a restriction on the maximum pressure with which the system can be operated, which in turn governs the maximum value of slide response. On the Harrison machine employed in this work, the copying accuracy is claimed to be better than 0.002 in. on workpiece diameter. This would indicate that the lag in the hydraulic copying slide must at all time be less than 0.001 in., and this figure also indicates the maximum deflection of the spool valve to be encountered during copy turning operations.

Fig. 2-1 Schematic Diagram of the Digital Position Servo-mechanism

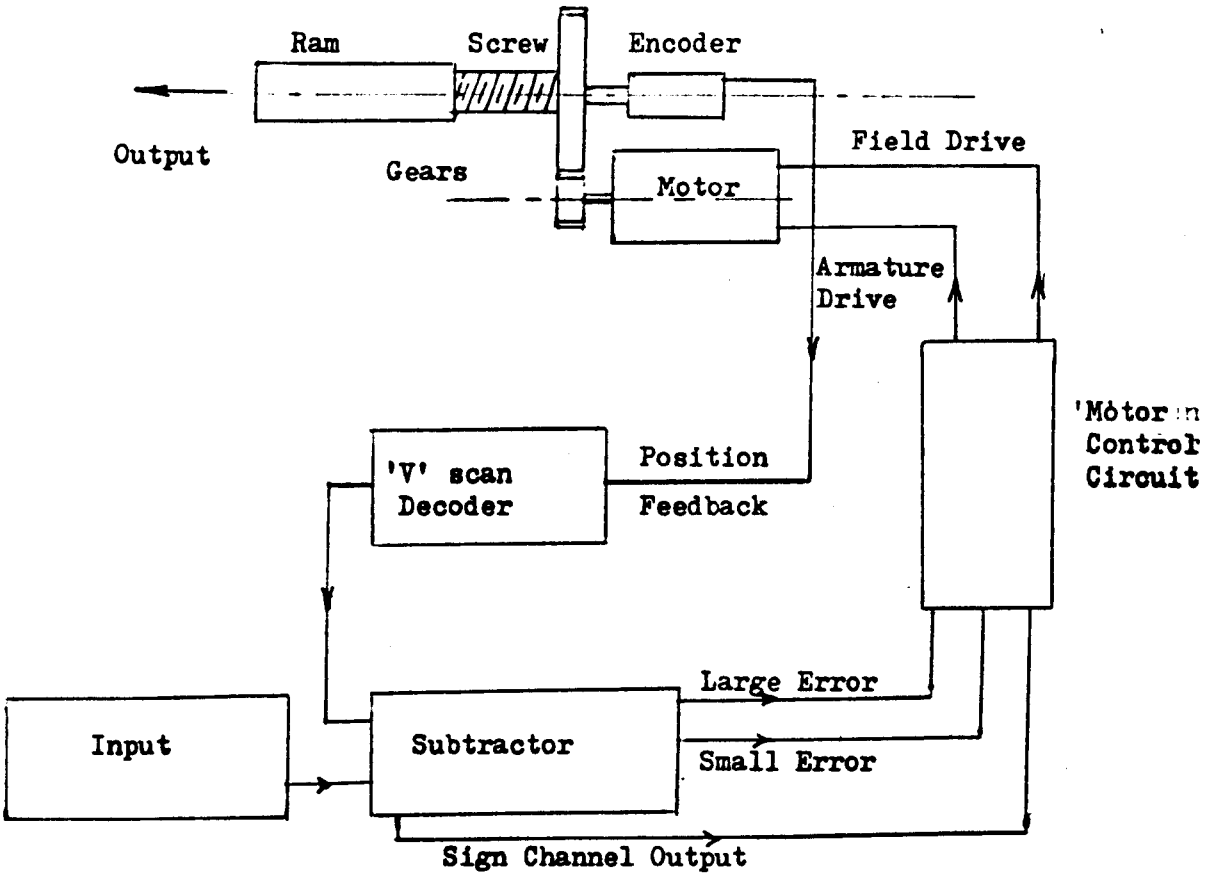

SECTION 2 : The Digital Position Servomechanism

Illustrated diagramatically in Fig.2-1, the digital positioning system employed in this work is the result of research carried out at Enfield College of Technology by the author and a co-worker, G.A.H. Thomas of Enfield College. The system was fully described in two papers which were published in 'Machinery' (Ref.5 Section 9), and the prototype equipment was displayed at the Physics Exhibition in 1965.

Basically the equipment comprises a simple positioning system which employs digital command and feedback signals, and it is electrical in operation. The measuring element is a Moore Reed 11 DV 104 contact type shaft encoder coupled to an accurately machined screw, and the comparator stage is a 12-bit parallel binary subtractor built from solid state logic elements. Input commands are supplied to the subtractor by means of a bank of tumbler switches, on which a 12-bit binary word may be set up, and it is arranged that the unit then generates an error signal in the form of another 12-bit word plus sign. The subtractor carries out the operation: Command - Feedback, giving the true numerical answer in binary code, and also the sign of the answer.

The moving element of the system is an electrically driven screw jack, which is mounted on a gearbox, and also incorporates the previously mentioned feedback encoder. Position feedback signals and also the motor control leads are connected to this unit by means of miniature multi-core cables in order to provide for the remote mounting of

the device relative to the other parts of the system, which are housed in an electronics cabinet.

The screw jack member is driven through a gear train by a small electric motor, which operates on direct current and has a wound field in order to provide for reverse rotation. In addition, for very slow 'inching' speeds, and also to overcome the effects of 'stiction' in the system, the motor armature is energized by pulsed d.c. signals having a constant amplitude of 24 V, and the motor speed is controlled by varying the mark-to-space ratio of these pulses according to the size of the error signal generated by the subtractor unit.

All electronics equipment and the command switches, are housed in a separate cabinet, that also has space available for tape reading equipment, which will be the input to the system when it has been developed into a lathe numerical control system.

SUBTRACTOR

Design of this part of the system is due to G.A.H.Thomas, and is based on the use of NOR logic elements. It was decided to employ parallel binary numbers as the digital signals in the system since this allows the use of encoders as absolute positioning mechanisms. In order to simplify the electronics as far as possible it was also decided to use normal binary numbers, instead of such modified patterns as the 'Gray' code, and this was made practicable by the availability of 'V' and 'U' scan type shaft encoders, which are dealt with later in this description.

As stated on the previous page, the signals are 12-bit binary words which means that the subtractor has 12 similar channels, thereby enabling the signals to be dealt with at once. This technique was adopted in favour of various serial subtracting systems since it was required that the comparator unit should generate its error signal as rapidly as possible, and that during each calculation no information should be lost. A logic diagram for a single channel of the subtractor unit is given below in Fig.2-2.

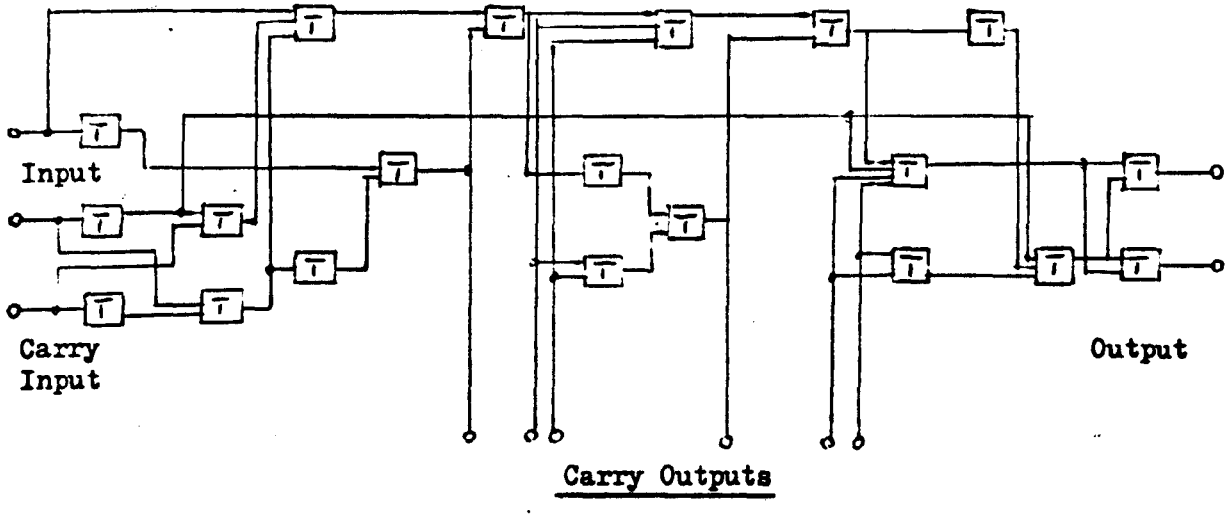

Fig.2-2 Logic Diagram for a single channel of the Subtractor

Each NOR element employed in the system is to a standard design, the circuit for which is given in Fig.2-3 on the following page. Cheap germanium transistors are employed and the total cost of each element has been held as low as possible. Speed of operation of the electronics equipment has been sacrificed in favour of simplicity and low cost, since the number of elements required for a parallel acting sys-

tem is rather large. On the other hand, the fact that the system deals with the complete binary number at once, and also since it has been designed to control the relatively low velocities of machine tool slides, justifies this decision.

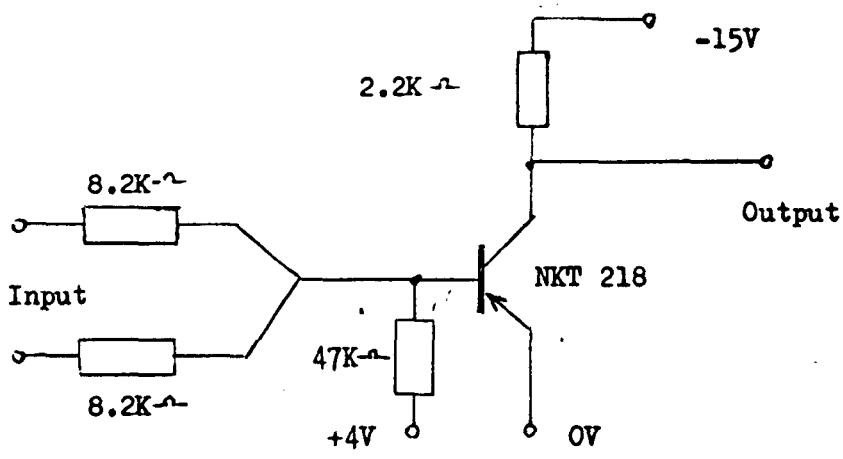

Fig.2-3 Circuit Diagram for a NOR Logic Element (2 input type)

Input to the subtractor comes from a bank of tumbler switches which in turn supply signals to a number of bistable elements forming the 'memory' of the system and coupled directly to the subtractor. These elements are necessary to hold a command, and avoid its being taken as zero, while a new command is being set up. The state of each bistable circuit is indicated by a green signal lamp for each element mounted on the front panel of the electronics cabinet. Output from each stage of the subtractor is fed to the motor control circuit, and also to a series of amber signal lamps on the front of the cabinet. These lamps, therefore, provide an indication of the error in binary code at any instant. In addition the unit generates the sign of the error signal, and this is indicated by a thirteenth amber lamp, which comes on for positive errors and vice versa. Circuit diagrams for the input switch and bistable element, and also for the signal lamps are

given below in Fig.2-4 and 2-5 respectively.

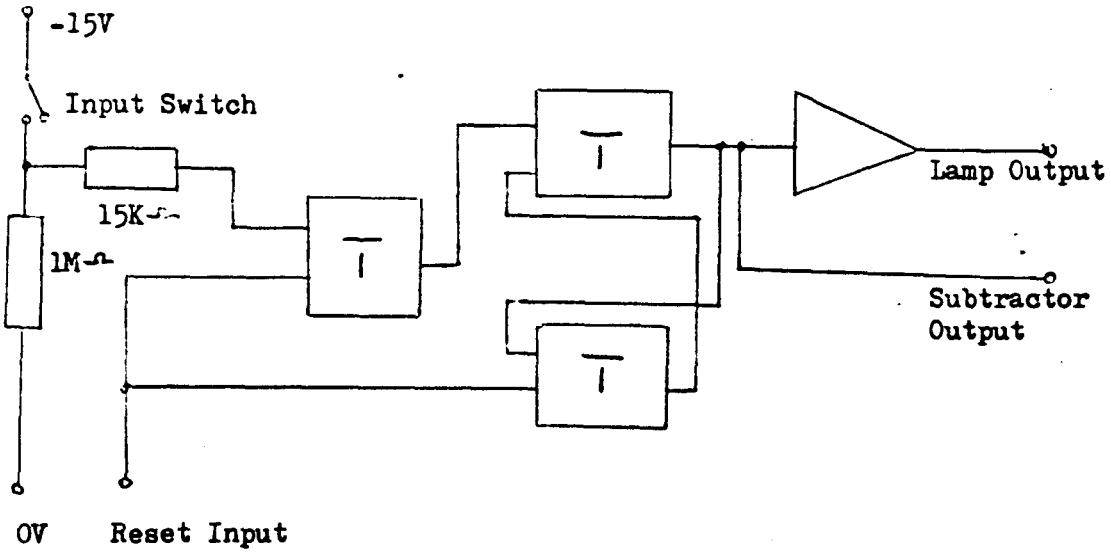

Fig.2-4 Circuit Diagram for Input Switch and Bistable Element

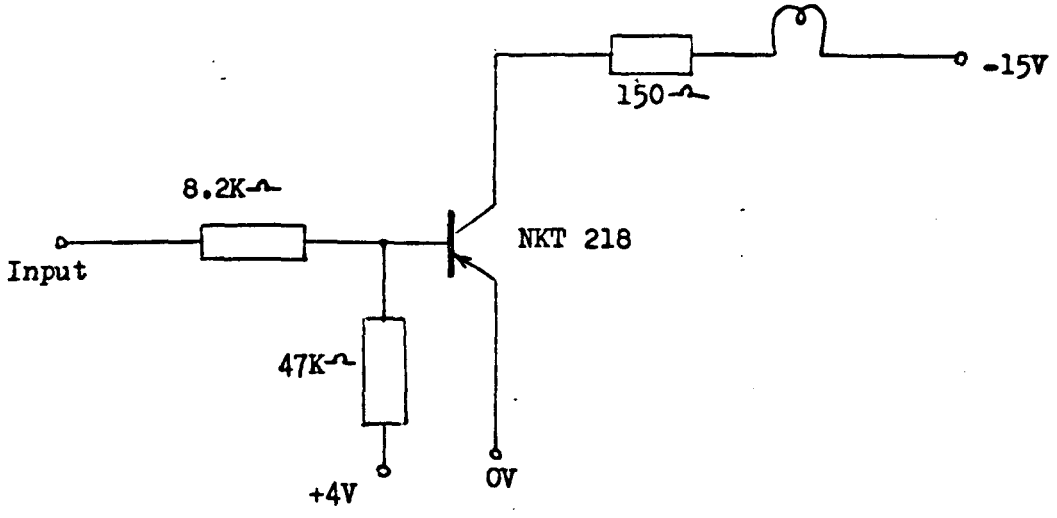

Fig.2-5 Circuit Diagram for Signal Lamp

RAM UNIT AND ENCODER

For this series of tests the unit was modified to enable it to be mounted on the Harrison lathe (see Section 6). In order to avoid backlash errors, the end of the positioning screw is fitted with a small

collet through which it is coupled directly to the encoder shaft. The screw has 16 threads per inch, and is arranged to fit the ram nut with as small an amount of backlash as possible. The ram itself is cylindrical, and provided with two longitudinal flats which are in contact with a pair of adjustable bronze cheeks bolted to the ram housing, thereby preventing rotation of the ram as the screw revolves. Drive for the screw comes from the motor through a 3:1 reduction gear train, made up of two aluminium spur gears, the backlash between which does not affect the accuracy of the system.

As already mentioned the encoder employed is of the 'V' scan type in order to avoid multi brush transition errors. This effect, together with its avoidance by the use of a 'V' scan encoder is discussed in detail in Ref.5 Section 9. Encoder output signals have to be decoded in order to produce the required binary feedback signal, since each track is fitted with a pair of brushes, lagging and leading, and the decoding circuit ensures that the correct brush is read on each track at any instant, to give the true binary output for the position reached. Fig.2-6 is the logic diagram for the decoding circuit fitted to each pair of output leads from the encoder.

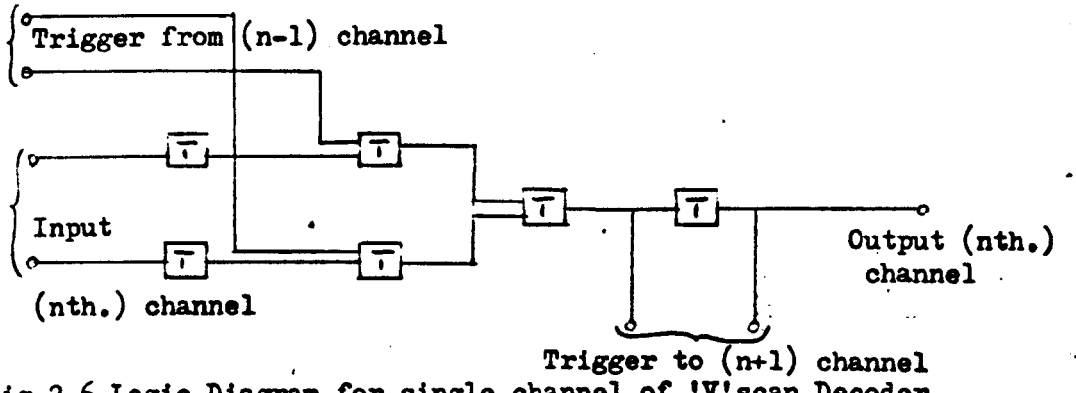

Fig.2-6 Logic Diagram for single channel of 'V'scan Decoder

The 11 DV 104 encoder provides a full count when it has been rotated through 32 revolutions, and the full count is 8192 in decimal since it is a 13-channel device. The system, however, only requires a 12-bit number as position feedback, so the least significant digit in the encoder output is ignored after decoding, which makes the full count of the device 4096 for 32 revolutions. Since 32 revolutions of the screw moves the ram through 2 inches, one binary bit is therefore very nearly equal to a ram displacement of 0.0005 in., or more accurately 0.0004869 in. The ram position is therefore indicated by the encoder to an accuracy of better than 0.0005in. over its operating range of 2 in.

MOTOR CONTROL CIRCUIT

Drive direction is controlled by altering the field polarity of the motor according to the state of the sign channel of the subtractor unit. This is effected by arranging that the output from the sign channel is coupled to a relay that is connected up as a reversing switch. The motor field, which takes only a small current, is therefore always energized which has the effect of providing a degree of braking when the armature current is cut off.

Motor speed control is effected by changing the mark-to-space ratio of the d.c. pulses supplied to the armature. The circuit for carrying out this function is based on published material by Texas Instruments, Ltd., and is acknowledged in Ref.5 Section 9. Provision was made whereby the mark-to-space ratio could be varied in 12 steps

according to the magnitude of the error signal, but preliminary tests with the servomechanism indicated that such a large number of steps was not necessary for satisfactory operation of the equipment.

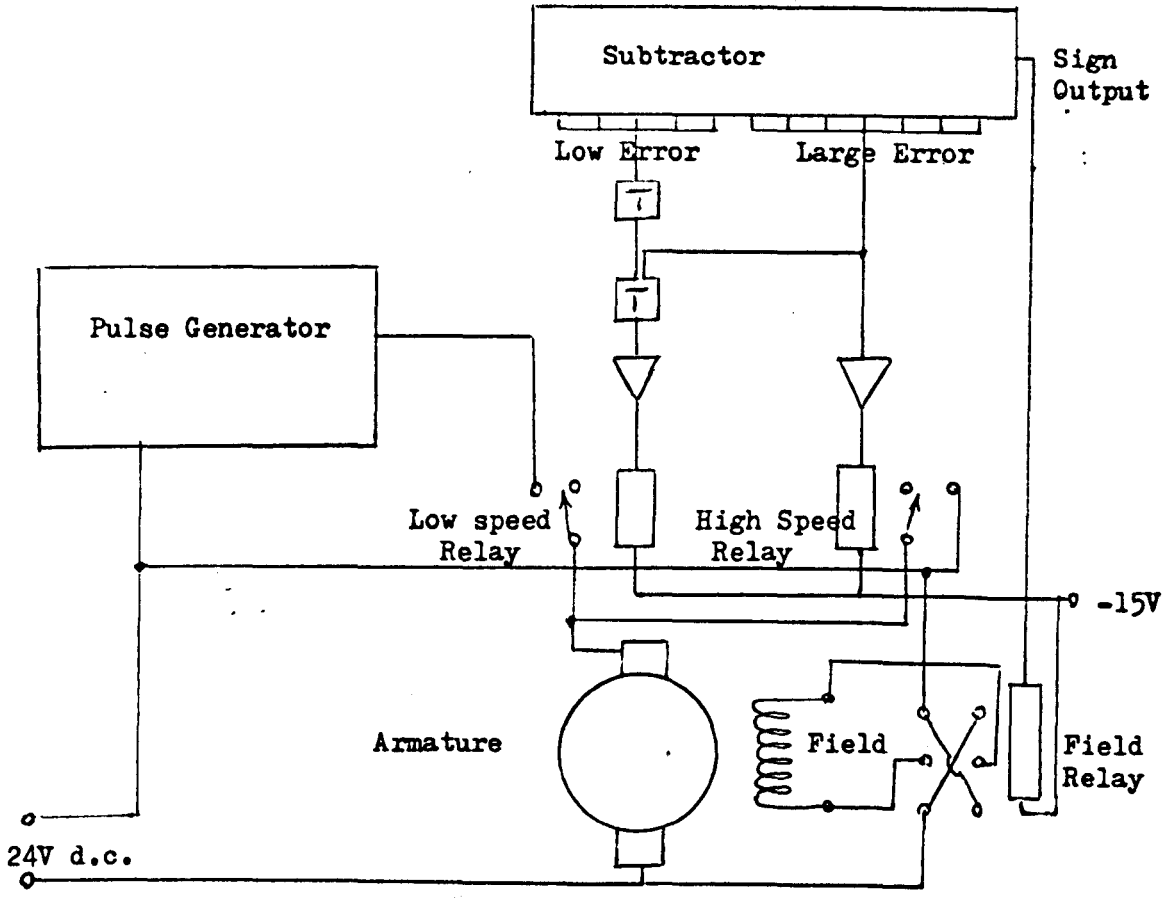

Fig.2-7 Schematic Diagram of the Motor Control Circuit

Final arrangements employed for these tests are shown above in Fig.2-7, from which it may be seen that the system is provided with two speeds, the slow rate being employed at values of error signal less than a small specified amount, which is independent of error sign. Full speed of the motor is achieved by energizing a relay which supplies 24 V d.c. to the armature, and when the error signal falls to the small specified figure the relay is switched off, and a second

relay is closed which connects the d.c. pulses from the control circuit to the armature. A preset potentiometer is fitted to the control circuit, so that the value of the mark-to-space ratio employed for the low speed mode of operation may be varied to suit the ram unit and to prevent overshooting the required position.

Positioning accuracy tests were carried out on the prototype system when it was first built, and the results of these tests are given in Ref.5 Section 9. For comparison with the present work, the results and the associated accuracy curve are included in this thesis in Table A4.1, Appendix 4, and Fig.7-1 Section 7 respectively.

Fig.3-1 Schematic Diagram of Equipment for measuring Position Errors in the Hydraulic Servomechanism

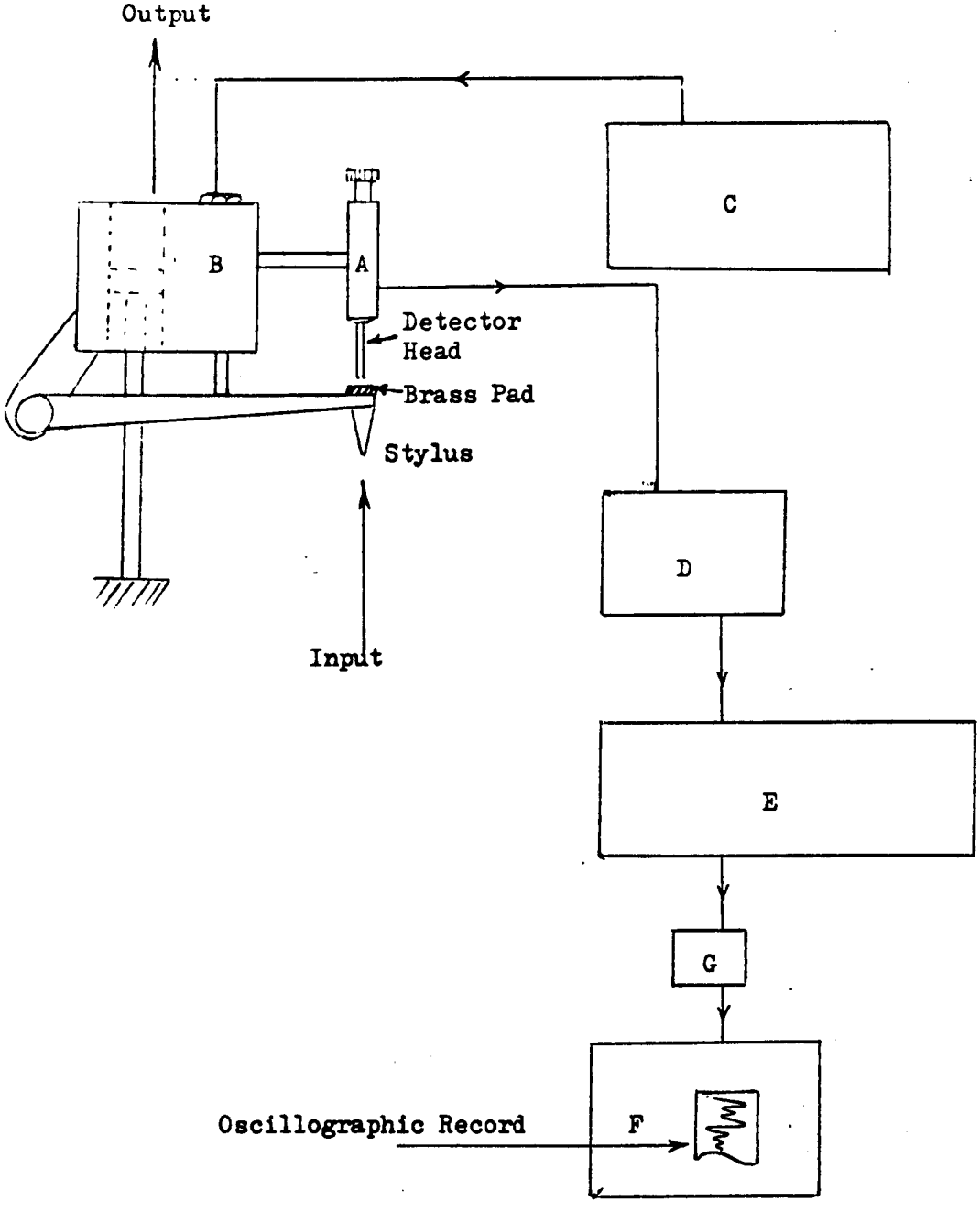

SECTION 3 : Performance of The Harrison Hydraulic Servomechanism

As has already been stated the L 6 lathe employed in this work is fitted with a hydraulic position servomechanism that operates a special tool slide for copy turning operations. It was decided to test this system for positioning accuracy and response in order to establish the magnitude of its errors for comparison with those of the digital servo which is used to drive it.

Since the system comprises a hydraulic cylinder which is controlled by a 3-way type spool valve, supplied from an external hydraulic power unit, position errors of the system are proportional to displacements of the valve spool from its balance condition. It is therefore convenient, in order to establish the previously mentioned errors, to measure the displacement of the spool relative to the valve body, and to record these displacements for a series of specified and controlled input functions.

A suitable arrangement for carrying out the above measurements was developed, and a schematic diagram of the equipment used is given in Fig.3-1 opposite. Valve displacements were detected by means of a proximity transducer which was mounted on a bracket attached to the copying slide of the lathe, so that it moved with the slide, and with the detector head in close proximity to a brass pad soldered to the rear face of the copying stylus. In this way system position errors are detected as changes in the gap between the detector head and the brass pad, brass being required since the proximity transducer was of

the inductance type.

The detecting instrument used was a type G 211 B proximity transducer by Southern Instruments, Ltd., with 0.10 in. adjustment and dial readout for the position of the detector head. This unit is shown at A in Fig.3-1, whereas B and C represent the servo valve and hydraulic power supply respectively. The equipment also included an oscillator shown at D which generates a 2 MHz. carrier signal, and the cabinet E contains an F.M. pre-amplifier unit which serves to convert the modulated carrier signal to a d.c. output.

In operation the carrier signal is generated by the oscillator in conjunction with a small coil embedded in the tip of the detector head of the proximity transducer. The frequency of the signal so formed depends on the inductance of this coil, which in turn depends on the proximity of the coil to metal surfaces, preferably non-ferrous metal. A given carrier frequency may therefore be modulated by changing the gap between the detector head and a brass surface, and for small gap changes, up to 0.01 in., the modulating effect is linearly proportional to change in gap size. Modulations are converted to a d.c. output by the pre-amplifier, and supplied to a U.V. recording oscilloscope (F in Fig.3-1) through an attenuator illustrated at G.

The equipment was set up as shown in Fig.3-1, and as the copying stylus followed the template profile, the oscilloscope produced a trace of valve deflections from balance position during the operation. The magnitude of the deflections produced on the oscilloscope by deflect-

ions of the valve was adjusted to a convenient amount by means of the attenuator circuit, which is shown in detail in Fig.3-2 below.

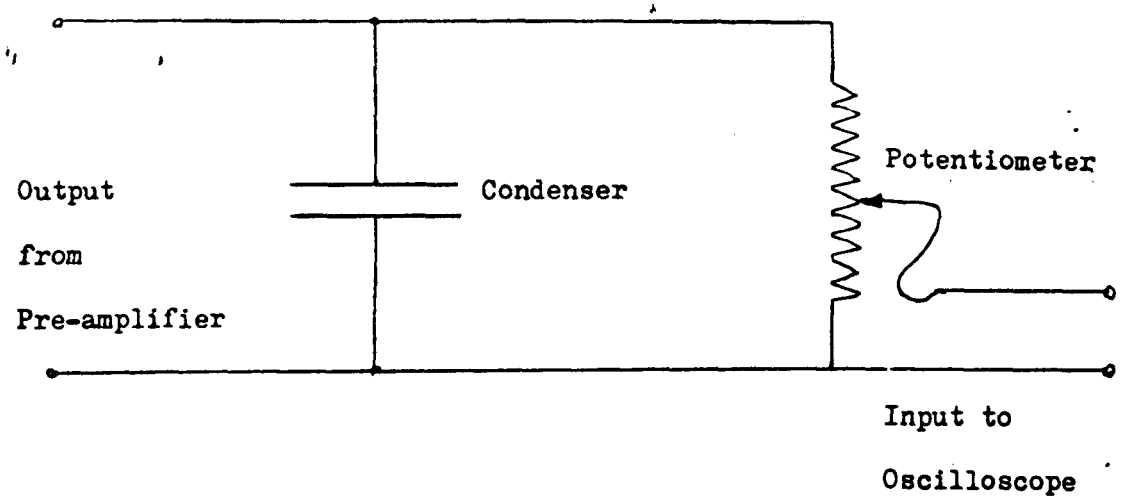

Fig. 3-2 Circuit Diagram of Attenuator

The magnitude of the signal supplied to the oscilloscope was set by means of the potentiometer in the above figure, and the large capacitor fitted across the pre-amplifier output served to reduce unwanted oscillations to an acceptably low value. The value of this capacitor was found by trial.

Input Conditions

In order to test the response of the copying servo it is necessary to apply a known input function, and measure the subsequent response.The previous part of this section has dealt with the equipment employed to measure the response, and it remains therefore to describe the method whereby known input conditions were applied to the servo valve. As already stated, all input functions to the copying servo under normal operating conditions are either zero or ramp functions,

and the equipment has not been designed for, nor is it required to respond to step type or periodically varying input functions. For this reason it was decided in the tests to limit the input functions to ramp types, followed by periods of zero input in order to determine the stability and positioning accuracy of the system.

During copy turning the saddle of the lathe is moved steadily along the bed of the machine by means of the feedshaft, which in turn is driven through a gear train from the main spindle. As the copying stylus contacts the template, which is mounted at the rear of the machine as described in Section 1, the spool valve is deflected producing a corresponding movement of the tool slide. In this way the tool tip is caused to trace out in space the form of the template profile. The magnitude of the ramp input depends, therefore, on both the template form and also on the rate of saddle feed selected by the operator. The manufacturers place specific limits on the profile of templates that the system can follow, and the fact that the purpose of the equipment is to control the path of a tool which is machining metal, in practice puts a limit on the amount of saddle feed that can be selected.

In general it may be said that the above limitations result in very restricted input conditions, both in form and magnitude, when compared to the operating conditions of other types of position servomechanisms. Rapid response is not an important factor with such equipment, and slides of massive proportions may therefore be employed without detracting from the performance of the system. On the other hand high positioning accuracy, and stability are essential to the satis-

factory operation of such equipment.

Standard Template

In order to set up conditions of known input it was necessary to design a standard template of prescribed profile, and also to move the saddle at a controlled and measured rate. Several input ramps can be achieved on a single template, and it was decided to design a profile that would provide both 'worst case' and typical working conditions. Since the copying servo is required to drive the tool slide in two directions, it was necessary to include at least one reducing taper in the profile.

In Fig.3-3 below, a ramp input function is defined as tanΨ, where the time base in the figure is a function of saddle traverse rate.

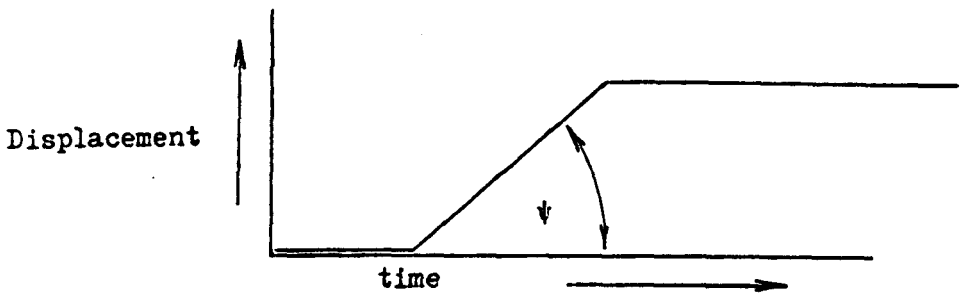

Fig. 3-3 Ramp type Input Function

According to the manufacturers the limiting profile form for this equipment is, 90° shoulders outwards and 30° (half angle) tapers inwards, which results in a profile of the form shown in Fig.3-4 below.

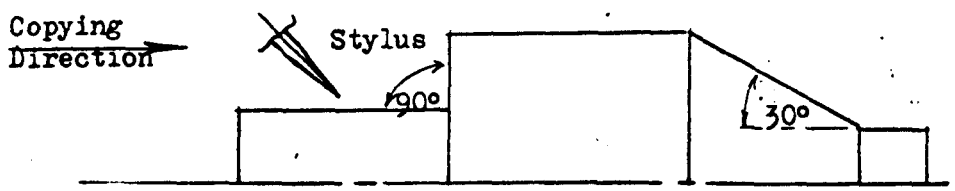

Fig. 3-4 Template Profile employing Makers Limits

Due to the copying slide angle, which is fixed at 30° from the cross slide axis, even the 90° shoulder becomes a ramp with respect to the servo valve. In Fig.3-5, if θ is the angle of the template profile with respect to its own centre line, and ø is the effective angle due to the copying slide alignment, we have:

$$\tan \phi = \frac{\delta Z}{\delta X}$$

where δ Z is the displacement of the spool valve along its own axis and δ X is the displacement of the saddle along the lathe bed

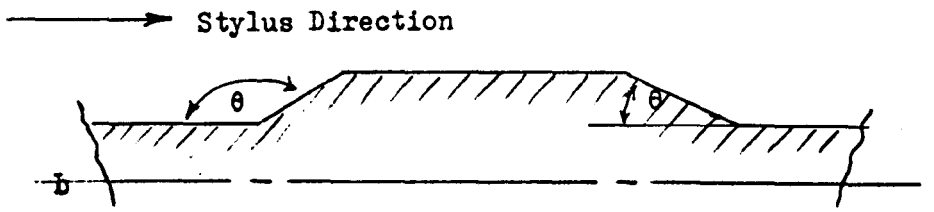

Fig.3-5 Definition of θ the profile angle

We then have the following conditions:

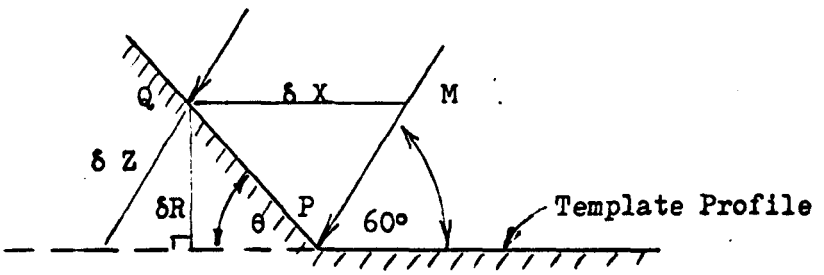

Fig.3-6 Calculation of effective angle ø

By the sin rule in triangle PMQ, Fig.3-6 above:

$$\frac{PQ}{\sin 60^\circ} = \frac{\delta X}{\sin (120 - \theta)^\circ} \quad \ldots\ldots$$

Therefore

$$PQ = \delta X \frac{\sin 60^\circ}{\sin(120 - \theta)^\circ} \quad \ldots\ldots(i)$$

Fig.3-7 Standard Template employed for Response Tests

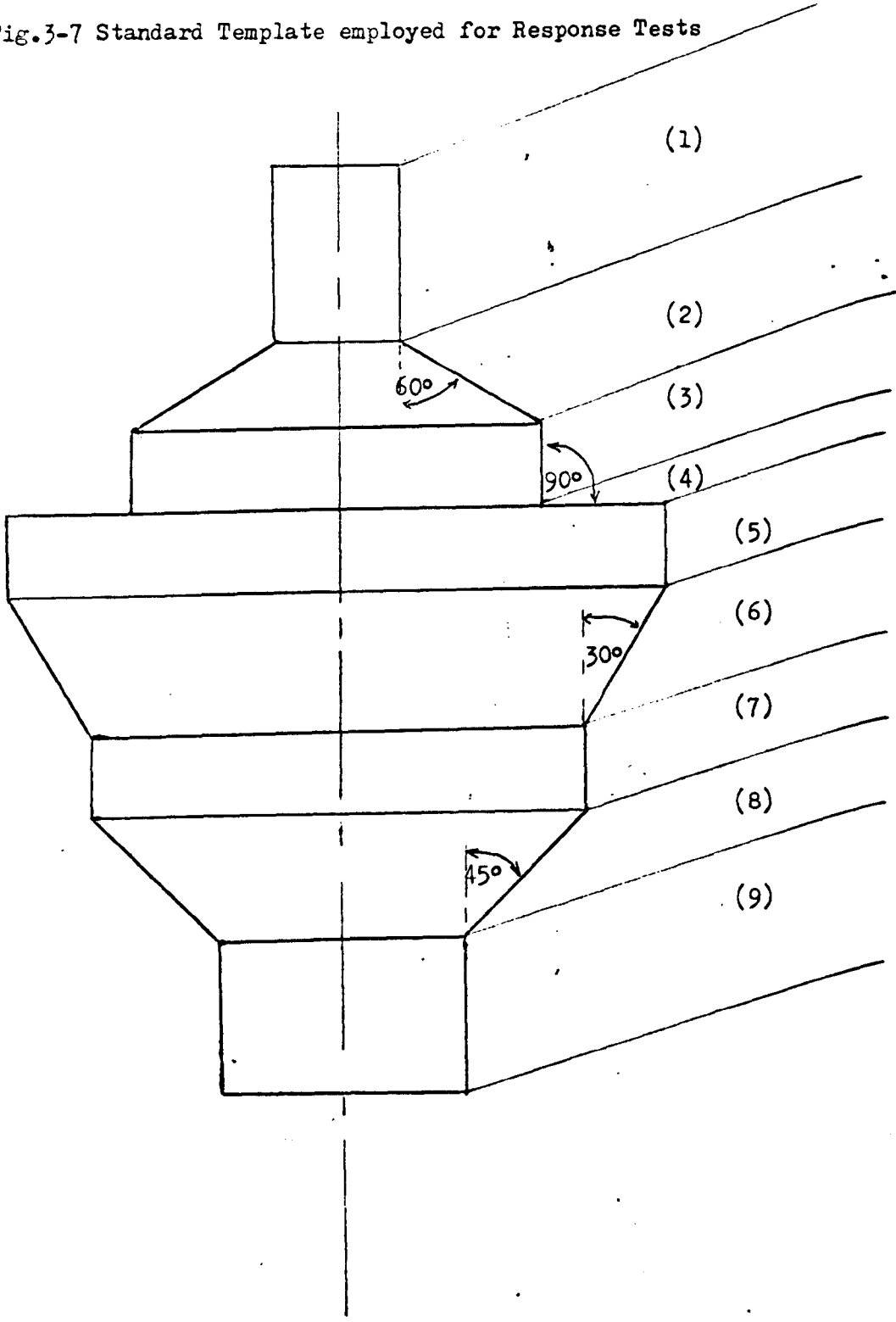

Also

$$\frac{P\,Q}{\delta\,R} = \text{cosec } \theta$$

and $$\delta\,R = \delta\,Z \cos 30^\circ$$

Therefore $$P\,Q = \delta\,Z \frac{\cos 30^\circ}{\sin \theta} \qquad \ldots\ldots(ii)$$

Combining equations (i) and (ii), we have:

$$\delta\,Z \frac{\cos 30^\circ}{\sin \theta} = \delta\,X \frac{\cos 30^\circ}{\sin(120 - \theta)^\circ}$$

Hence $$\frac{\delta\,Z}{\delta\,X} = \frac{\sin \theta}{\sin(120 - \theta)} = \tan \phi$$

Therefore

$$\tan \phi = \frac{\sin \theta}{\sin(120).\cos \theta - \cos(120).\sin \theta}$$

$$\tan \phi = \frac{2\sin \theta}{\sqrt{3} \cos \theta + \sin \theta}$$

Fig.3-7 is a drawing of the template produced for these tests, and it may be seen to comprise nine distinct regions:

1) Parallel region giving no input

2) 60° increasing taper giving $\phi = 45^\circ$ outwards

3) Parallel region giving no input but showing position error

4) 90° shoulder giving $\phi = 63^\circ\ 26'$ outwards

5) Parallel journal showing position error

6) 30° decreasing taper giving ø = 45° inwards

7) Parallel journal showing position error

8) and 9) could not be followed due to stylus interference.

Saddle Traverse Rate

As stated previously the magnitude of the input ramp function depends on the velocity of the saddle along the lathe bed in addition to the profile of the template. It was therefore necessary to control and measure the saddle traverse rate.

Due to the small valve displacements to be measured, the detecting equipment had to be adjusted to a very high sensitivity, which rendered it susceptible to noise pick up. This noise was the result of vibrations in the machine bed and copying slide, which caused the gap between the proximity transducer head, and the associated brass pad the fluctuate in width slightly. Unfortunately it was found during preliminary tests, that the main motor and the headstock gears produced so much vibration in the machine that the output from the proximity transducer was swamped, and all measurements had therefore to be made with the main motor and headstock gears at rest.

This effect made it necessary to set up another method of driving the saddle along the lathe bed during this part of the testing. It was decided to make use of the leadscrew and feedshaft members of the machine, which are coupled together through the gearbox, and which are arranged to drive the saddle at two different speed ranges. Normally the

Fig.3-8 Arrangements for driving the Lathe Saddle employed during the tests on the Hydraulic Servomechanism

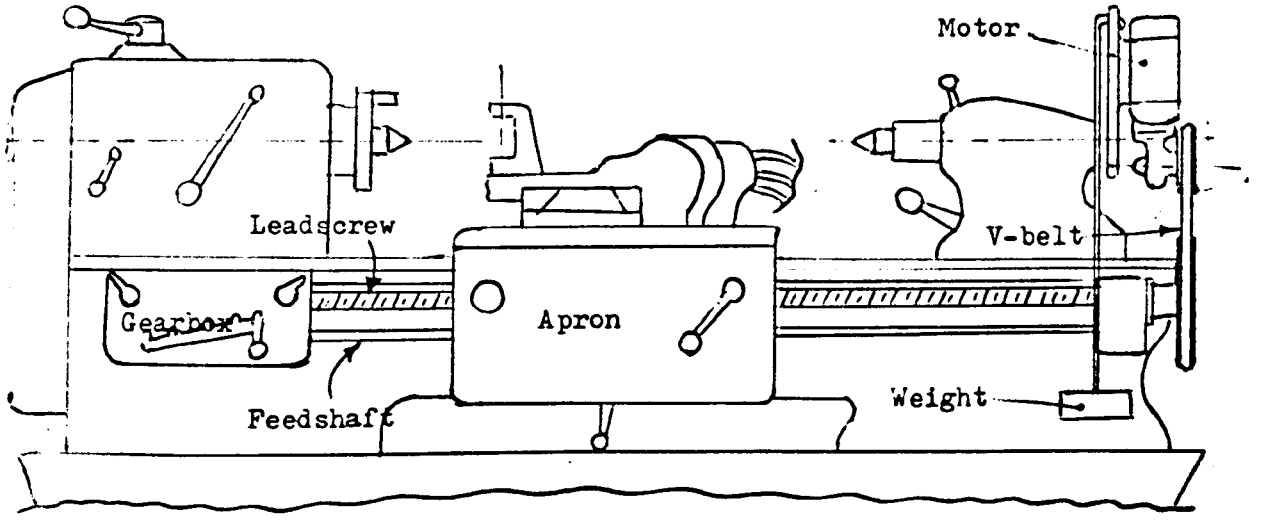

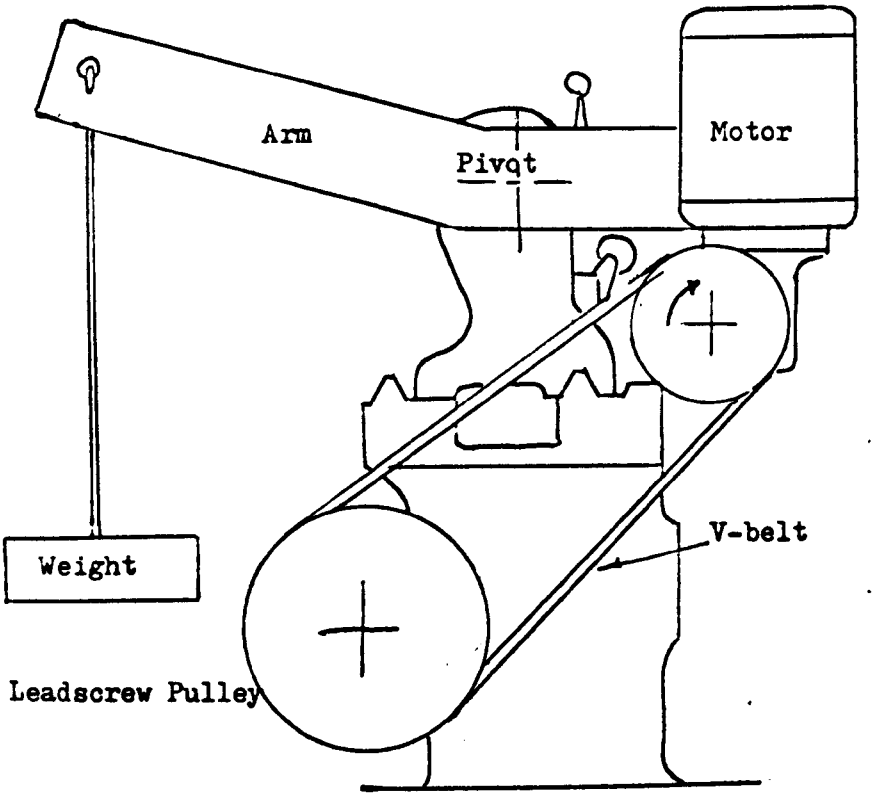

gearbox is driven by a gear train from the lathe spindle, and this drive was disconnected for the tests. An adaptor was made for the tailstock end of the leadscrew, thereby enabling a V-belt driving pulley to be fitted. A small electric motor mounted on a pivoting arm from the tailstock was employed to drive the leadscrew, by means of a V-belt and belt tension was maintained by a counter weight fitted to the arm. This method of driving the leadscrew was adopted since the V-belt afforded good vibration insulation, and the pivoting arm provided for a range of pulley centres which permitted a number of driving ratios to be employed. Fig.3-8 is a drawing showing two views of the arrangements for driving the lathe saddle without excessive vibration.

By engaging leadscrew drive at the gearbox, as for normal screwcutting operations, it was possible to drive the feedshaft member through the gearbox at a range of speeds which could be selected by the normal gearbox controls. For rapid saddle traverse rates, the leadscrew drive from the gearbox was disconnected, and the split nut in the saddle apron was engaged with the leadscrew, whereas slower traverse rates were achieved by driving the saddle from the feedshaft as previously described. Clearly the feed rates indicated by the gearbox chart no longer applied, since the power was derived from the leadscrew. However, it was possible to establish the ratio between feedshaft and leadscrew rotation rates from the screwcutting information given for each gearbox setting, and hence it was possible to calculate saddle traverse rates from the leadscrew speed.

The motor employed to drive the leadscrew was a small universal unit with a worm reduction gear, by M.R.Supplies, Ltd., and under no load conditions, the output shaft ran at 150 rev/min on mains voltage. A further speed reduction of just more than 2:1 was achieved by means of the belt drive, but it was found that the final speed varied according to load. During the tests therefore the actual speed of the leadscrew was measured with an integrating revolution counter, and these values are included in the results.

It was decided to employ two feed rates, one typical of a practical machining operation, and a faster speed to illustrate and measure the hydraulic lag in the servo.

Fast Speed

As already stated this speed was achieved by engaging the split nut in the apron and driving the saddle directly from the leadscrew. Under this load, the leadscrew was rotated at 51 rev/min, and since the pitch of the leadscrew is 0.250 in, the resulting saddle velocity was 12.750 in/min.

It should be mentioned that this traverse rate can be exceeded on an L 6 lathe. Since the machine has a maximum feed rate setting, according to the gearbox chart, of 0.0327 in/rev, and the maximum spindle speed is 2000 rev/min, it is possible to select a saddle traverse rate of no less than 65.4 in/min. Such a rapid feed rate would, however, not be used for copy turning operations, and it was decided that since the

fast speed chosen adequately illustrated hydraulic lag in the servo, there was no point in running at higher feed rates.

Normal Feed

For this feed rate the drive for the saddle was taken from the gearbox as previously described, and it was engaged by means of the normal feed selector lever on the saddle apron. Under this load the leadscrew ran at 65 rev/min, but the saddle moved at a rate according to the gearbox selector setting. A suitable traverse rate was achieved with the gearbox set to provide a feed of 0.0327 in/rev under normal conditions. At this setting the gearbox drives the leadscrew at a rate to produce a 4 t.p.i. thread, hence:

Leadscrew rate = 0.250 in/rev

Feedshaft rate = 0.0327 in/rev

Gearbox ratio is then:

$$R = \frac{0.0327}{0.250} = 0.1306$$

Now under these conditions, the leadscrew revolved at 65 rev/min, which would, under normal conditions, give a saddle velocity of 16.25 in/min

Therefore:

saddle velocity = 16.25 X .1306

= 2.12 in/min

This method of calculation has to be employed since the gearbox chart makes no allowance for the worm gearing in the saddle apron, through which the feedshaft drives the rack and pinion mechanism of

the saddle. A typical feedrate for machining a workpiece to the form of the standard template would be about 0.004 in/rev, and assuming the workpiece material to be mild steel, a suitable spindle speed would be 500rev/min. These values would result in a saddle traverse rate of 2 in/min, which is very close to the normal feed figure selected for the tests.

The effective input ramp functions resulting from the use of the standard template and the saddle feed rates selected are listed below in Table 3.1

Template Region	Profile Angle θ	Effective Angle ϕ	Ramp Input Function $\tan \psi$ (in/min)
2	60° Outwards	45°	Normal +2.12 Fast +12.75
4	90° Shoulder	63° 26'	Normal +4.24 Fast +25.5
6	30° Inwards	45°	Normal -2.12 Fast -12.75

Table 3.1 Effective input ramps due to template profile

Other Variables

In addition to the input conditions, which were standardized as described, two other factors affecting the response of the equipment could be varied. These were the delivery pressure of the hydraulic power unit, and the return spring load on the valve spool.

Since the force acting on the copying slide, which to a large extent

represents the mass of the moving elements of the system, is a function of the delivery pressure, the value of pressure selected affects the response of the system to any input function. The pump in the hydraulic power unit was provided with a bypass passage controlled by a hand operated wheel valve, and the output pressure was indicated by a built-in bourden type gauge. By this means it was possible to adjust the pump delivery pressure from zero to about 600 lbf/in^2, and the manufacturers recommended operating pressure for the system is 150 lbf/in^2.

Tests were conducted at a number of delivery pressures above and below the recommended value, and in this work the results obtained with pressures of 50, 150 and 250 lbf/in^2 are included. In addition some runs were made at pressures up to 400 lbf/in^2, but such values produced violent hunting and accurate measurements of the servo response were not possible.

Normally the L 6 lathe copying servo is fitted with a spool return spring of fixed loading, but since the machine employed for this work was fitted with the prototype of a new 3-way valve, a screw adjustment was provided whereby the spring load could be altered. By means of this screw, the stylus load could be set at any value between zero and approximately 3 lbf, these values being determined by means of a spring balance.

As indicated above, the magnitude of the return spring load controls the stylus load, which should be as low as possible to reduce template wear. However, the return spring load cannot be set too low with-

out adversely affecting the performance of the system. As delivered the valve was set with a return spring load of 1.125 lbf, and in these tests results are included for stylus loads of 0.5,1.0 and 2 lbf.

Results of Tests on the Hydraulic Servomechanism

Having set up the equipment as shown in Fig.3-1, a series of ten passes was made across the template at a range of hydraulic fluid pressures and return spring loads. In addition the saddle velocity was varied as described earlier. At the low saddle speed it was more convenient to record the response traces in three stages, as even the slowest recording rate (0.15 in/s) produced an unreasonably long oscillograph due to the cycle time length. As a result there are 20 oscillograms representing 10 passes, and table A1.1 in Appendix 1 shows the value of pressure and spring load employed in each case, together with the associated ramp input functions and the saddle velocities used.

In order to remove as much oscillation from the signal as possible, the value of the capacitor used in the attenuator circuit (Fig. 3-2) was 250μF. The potential divider part of the circuit in Fig.3-2 was adjusted so that a 1-in deflection of the oscilloscope trace corresponded to a valve movement of 0.00125 in, and all the results were recorded at this sensitivity, which ensures that all the oscillogram traces in Appendix 1 are to the same scale.

The oscillograms in this report are in fact 'Xeroxed' copies of the original oscillograms, which were developed and fixed in the manner

described in Appendix 1. Measurements were then made of the hydraulic lag recorded for each of the ramp inputs employed, and also of the position error of the system after following a given ramp. Measurement of the amplitude of the vibration which may be observed on the traces was not attempted, this amplitude having been attenuated by the previously described circuit(Fig.3-2). Tests were also made with the attenuator capacitor removed, which resulted in very greatly increased vibration. In all passes without the capacitor, except those carried out at hydraulic fluid pressures less than 50 lbf/in^2, these oscillations were very great indeed when the copying slide was moving towards the centre line of the lathe ie. the valve spool under these conditions was being driven to its balance position by the action of the return spring. During outward ramps, that is when following increasing tapers on the template, the oscillations experienced at normal turning feed rates were approximately 0.001 in amplitude.

It should be emphasized that the above mentioned oscillations are the result of changes in the air gap between the detector head of the proximity transducer and the associated brass pad on the copying stylus. Changes in this gap size, especially those which are oscillatory, do not necessarily indicate similar motion of the valve spool or tool slide, since the mounting bracket of the proximity transducer was resilient to a certain degree. Certainly during the very large oscillations it was possible to detect vibrations of the tool slide by touch, but a considerable portion of the oscillation amplitude could be attributed to vibration of the transducer relative to the valve body. This effect is dealt with in greater detail later in this section.

Fig.3-9 Theoretical Response of the Hydraulic Servo

(Ramp type Input Functions)

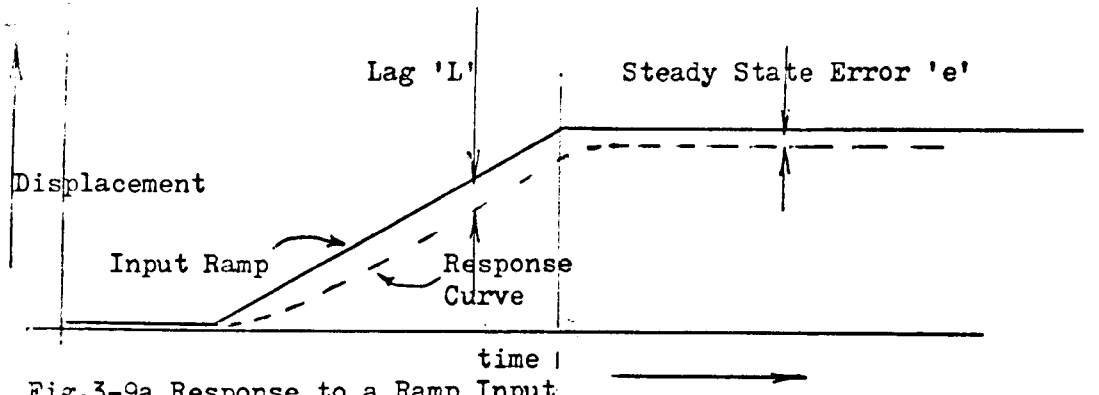

Fig.3-9a Response to a Ramp Input

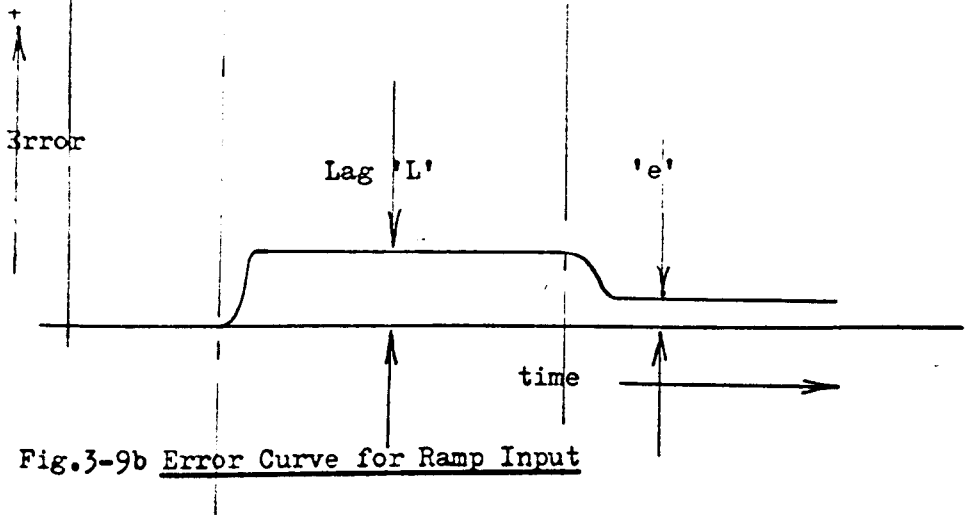

Fig.3-9b Error Curve for Ramp Input

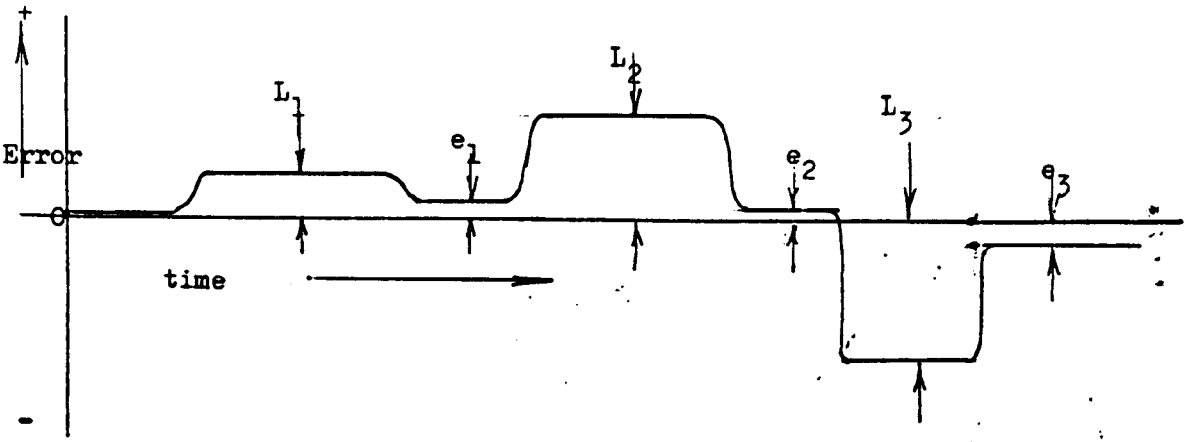

Fig.3-9c Error Curve for Standard Template Profile

Interpretation of Results

In Fig.3-9 is aseries of diagrams representing the theoretical response of a hydraulically operated position servomechanism to ramp type input functions. Fig.3-9 a is the response curve for such a system, to a simple ramp input as given in Ref.6 Section 9, the system being damped to 'dead beat' response. The servo does not respond at once to the ramp since the presence of an error is necessary to generate the drive signal, and the response curve then follows the form of the input ramp with a steady lag until the input ceases. Termination of the input ramp results in the drive signal gradually falling, and the servo slows down. If the system is damped to the 'dead beat' condition, the response curve will not overshoot the command signal and the results should be as illustrated in the diagram. When the system finally comes to rest, it will not in general coincide precisely with the desired position, but will differ from it by a small error known as the 'steady state error' and denoted by 'e' in the figure.

Fig.3-9 b is an error versus time curve for the response curve shown in Fig.3-9 a, the lag error being marked 'L' and the steady state error 'e'.

The standard template employed for these tests, and previously described, provided three usable ramp type input functions for each value of saddle velocity selected. Using the set up illustrated in Fig.3-1, whereby error traces were recorded by means of a U.V. oscilloscope, the theoretical form of such traces is as illustrated in Fig.3-9 c,

In Fig.3-9 c, L_1 is the lag error generated when the system follows the 60° outward taper on the template, L_2 is the lag as the 90° shoulder is negotiated and L_3 occurs as [illegible]es the 30° decreasing taper. The steady state positioning errors between each of these ramp inputs are indicated by e_1 , e_2 and e_3.

The actual traces which are given in Appendix 1 are of the general form of Fig.3-9 c, but with certain modifications. From the traces it is clear that the steady state errors between the inputs are sufficiently small to support the manufacturers stated accuracy for the lathe, namely 0.002 in when copy turning. If the input functions are limited to those that would be encountered during copy turning operations, and also if the makers recommended operating pressure for the hydraulic system is adhered to, the lag of the copying slide is less than 0.0005 in, which implies less than 0.001 in error on workpiece diameter.

However, it was apparent that the equipment responded far more satisfactorily to positive input ramps, that is when the slide was moved away from the lathe axis, than in the reverse direction. In fact it was found that the system tended to oscillate as the slide moved towards the lathe axis, and changes in the loading on the spool valve return spring had little effect on this property. Changes in the pressure of the hydraulic fluid appeared to have most effect on the oscillations, and if the pressure was increased above 200 lbf/in^2 the oscillations became very noticable, reaching unacceptable proportions at 300 lbf/in^2 with the slide moving inwards towards the lathe axis.

The oscillations described in the previous paragraph were not, at the recommended operating pressure, sufficient to impair the performance of the machine. The actual magnitude of these oscillations was not measured for reasons that will be discussed later, but test runs carried out without the attenuator circuit (Fig.3-2) indicated that there was no vibration of the actual copying slide, under recommended operating conditions, even when the error trace showed oscillations to be present in the system.

Modifications to the theoretical error curve may be classified into three divisions:

i) Apparent deviations from the steady state during periods of no input, and also under conditions of steady lag.

ii) General superimposed vibration of constant frequency.

iii) Deflections of large amplitude, and short duration apparent at the start of a steady lag. This occurred for the steeper ramp input functions.

These effects may be explained as follows:

i) The standard template was machined to a high surface finish, but it had nevertheless some surface imperfections, and the sensitivity of the detecting equipment was set at a high value. The high sensitivity was necessitated by the requirement to detect hydraulic lag for low gradient ramp inputs, and the explanation is justified by the fact that similar fluctuations were observed at the same

point on the template at different ramp input rates.

ii) The general vibration at constant frequency experienced throughout this series of tests stems from three main causes:

1. Gear tooth ripple, from the pump in the hydraulic power unit. This is a general problem in equipment of this type, and is the usual forcing agency causother components in the system to vibrate.

2. General vibration of the machine and measuring equipment, induced largely by gear tooth ripple, and actually causing the oscillation on the trace. Attempts were made to reduce the effect of these vibrations to an acceptably low level by the use of the attenuator.

3. Oscillation of the spool valve due to fluid flow effects at small port openings. The valve spool and return spring assembly may be excited to oscillate at their combined natural frequency if a suiable forcing agency is generated by hydraulic turbulence.

The cause mentioned in 2. above is the reason why no attempt was made to measure the amplitude of these general vibrations. As has already been stated the proximity transuder mounting bracket would vibrate if excited, and this caused the gap between the stylus pad and the detector head to vary, hence affecting the trace recorded. Under these conditions, valve deflections cannot be related directly to trace displace-

Fig.3-10 Response Curve for the Hydraulic Servomechanism

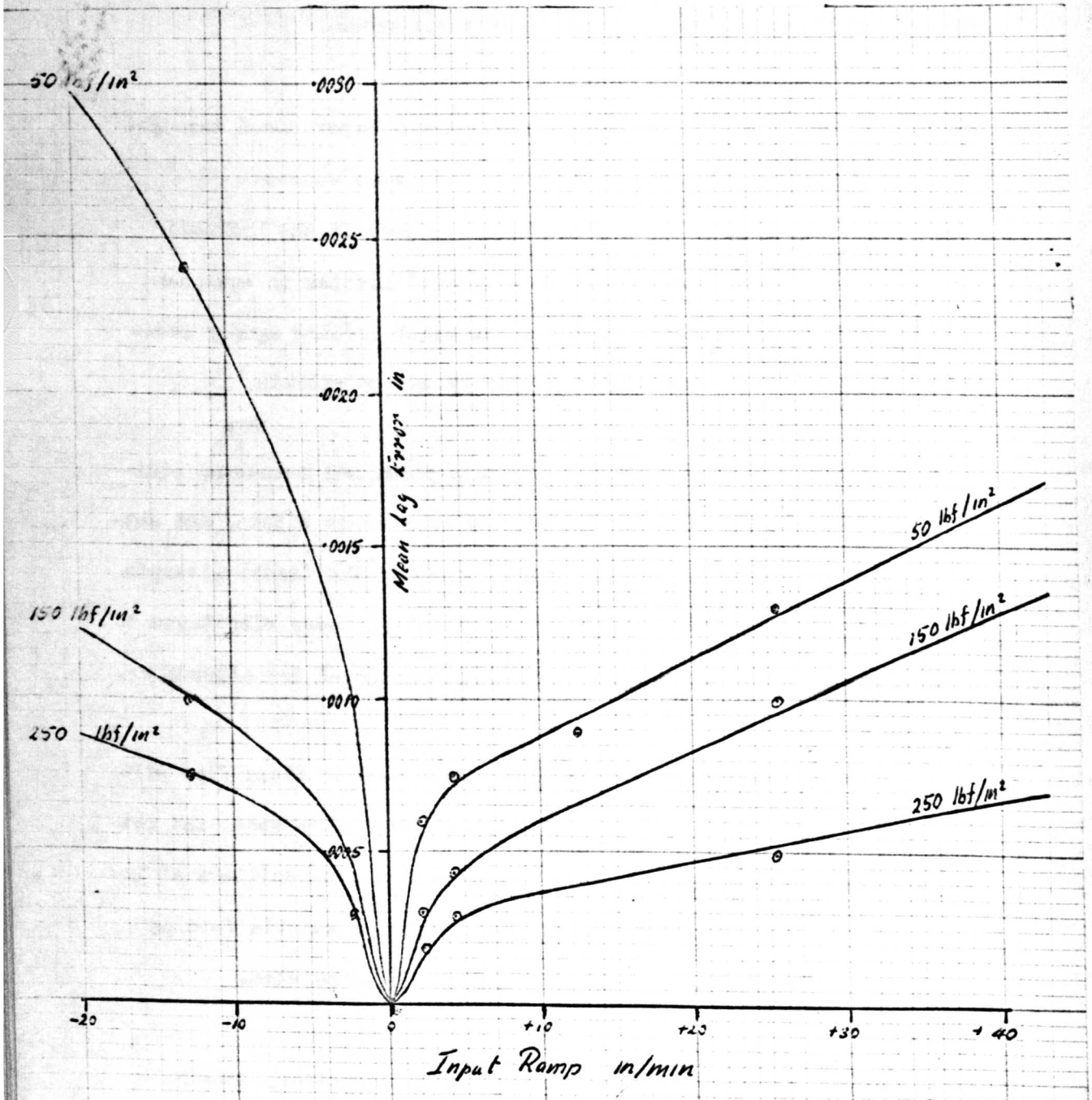

All lag errors taken as positive.

Positive input ramp drives toolslide away from machine axis.

ment. However, the effect is oscillatory, whereas the delection produced by a definite lag error is not, and it was decided to attempt to remove the oscillations in the attenuator circuit.

iii) The large amplitude deflections of short duration experienced at rapid traverse rates are interesting, since they appear to be characteristic of a high sensitivity closed loop positioning system. Such 'spikes'are found in the Electro-Myographic records of animal muscle response, although there are many differences between this system and the 'reflex arc' of biological systems. Mr. J.Korn of Enfield College of Technology has also noticed this effect in another hydraulic servomechanism, and this was partly due to the inertia of the valve spool. (Ref. 7 and 8 Section 9)

Test Results

Detailed test results, including the oscillograms are given in Appendix 1, and error measurements taken from the traces are listed below in Table 3.2, for return spring load equal to 1 lbf. Fig.3-10 is the performance curve for the system, drawn from the value in Table3.2.

Input Ramp in/min	Mean Lag Error 'L' in		
	50 lbf/in^2	150 lbf/in^2	250 lbf/in^2
-12.75	0.00240	0.00100	0.00075
- 2.12	0.00100	0.00050	0.00030
+ 2.12	0.00060	0.00030	0.00018
+ 4.24	0.00075	0.00042	0.00027
+12.75	0.00088	0.00066	0.00040
+25.5	0.00130	0.00100	0.00050

SECTION 4: Analysis of the Digital Servomechanism

A block diagram of the digital servomechanism, described in Section 2 is given below in Fig.4-1.

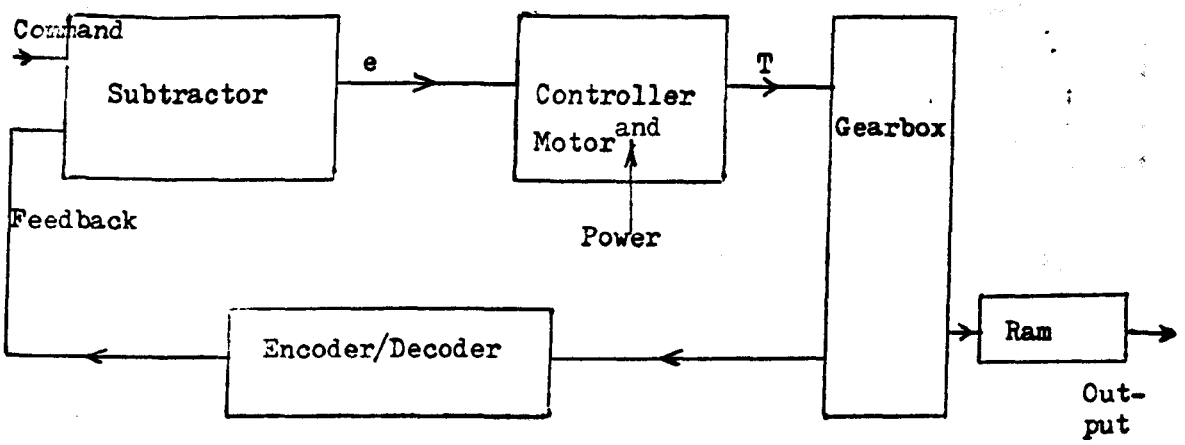

Fig.4-1 Block Diagram of the Digital Servomechanism

Considering the functions of each element of the above system separately, we have:

Subtractor

Both inputs, command and feedback, are in the form of parallel binary numbers on multi-core cables, and the unit then generates the error signal which is also a parallel binary number. In the system described there are in fact two outputs, one providing the difference between the command and the feedback numbers in both magnitude and sign, and the other which provides the signal for the motor controller, which is the next element in the above diagram. The output of this element is, as far as this analysis is concerned, as given in Table 4.1 on the next page.

Error Signal	Output to Motor Controller		
	Low speed	High speed	Sign
$e = 0$	0	0	on or off
$0 < e < e^*$	on	off	on
$e^* \leq e < 0$	on	off	off
$e \geq e^*$	on or off	on	on
$e^* \geq e$	on or off	on	off

where e* is the value of error signal at which the high speed relay is arranged to operate.

Table 4.1 Output from the subtractor element

Since this element contains no mechanical operations it introduces no lag errors of significance to this analysis.

Motor Controller

Input to this element is a 3-core cable carrying the output from the subtractor unit as tabulated above, namely:

1) Lead carrying information concerning the sign of the error signal
2) Lead for small errors, less than e*.
3) Lead for errors in excess of e*

These leads control the settings of three relays, which have the following functions:

1) Reversing switch to change motor field polarity for direction control.
2) Relay controlling the supply of d.c. pulses to the motor armature for low speed running.

3) Relay which when energized supplies 24 volts d.c. to the motor armature for high speed running.

An electronic circuit is used to generate the d.c. pulses for 2) above, from the 24 volt supply, and the mark-to-space ratio of this signal may be adjusted manually as required.

The output from the controller is therefore a double step function, and if for this analysis the motor is included in the element, the output may be taken as torque. In this case the element may be considered as a servo amplifier with non-linear characteristics as shown in Fig.4-2 below.

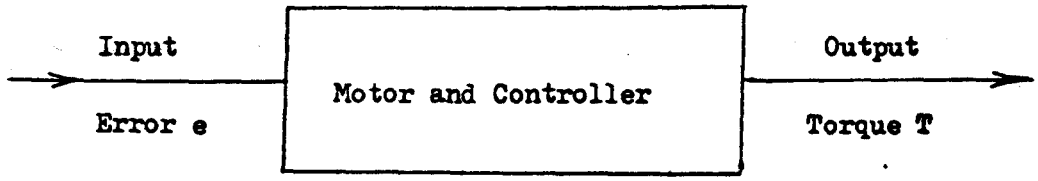

Fig.4-2 Input-Output relationship of the Servo Amplifier

Similarly the characteristic of the element is then as shown in Fig.4-3 below.

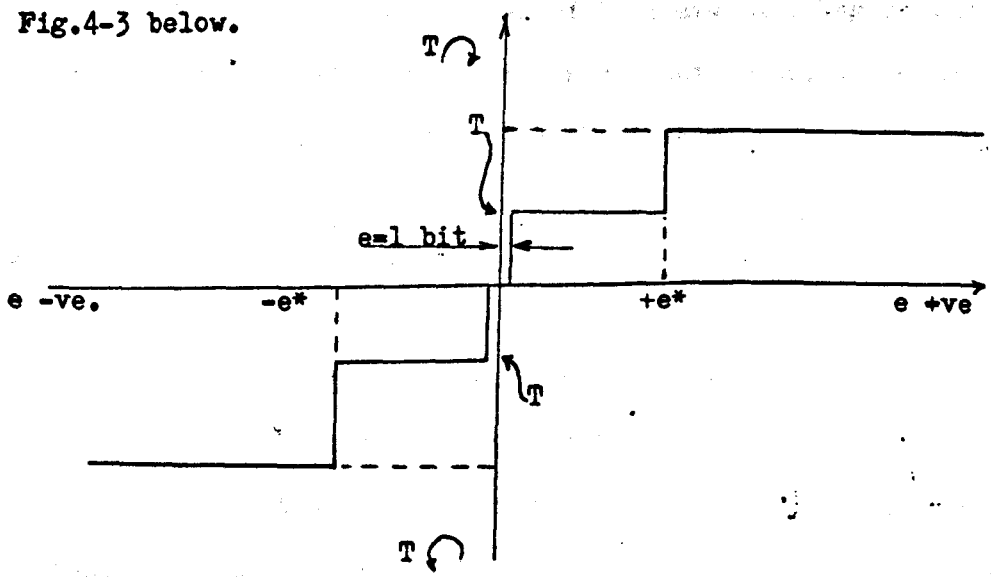

Fig.4-3 Input-Output characteristic of the Servo Amplifier

In operation the servomechanism will only work in the low speed mode, that is with errors less than e* in magnitude. In addition, reversals of direction will not be encountered during a given cycle, although the system will be capable of running in either direction. It is therefore reasonable to consider the element as a unidirectional step torque function generator, and to deal with a given profile in stages, in order to deal with changes in the direction of the ram. The characteristic then reduces to that given in Fig.4-4.

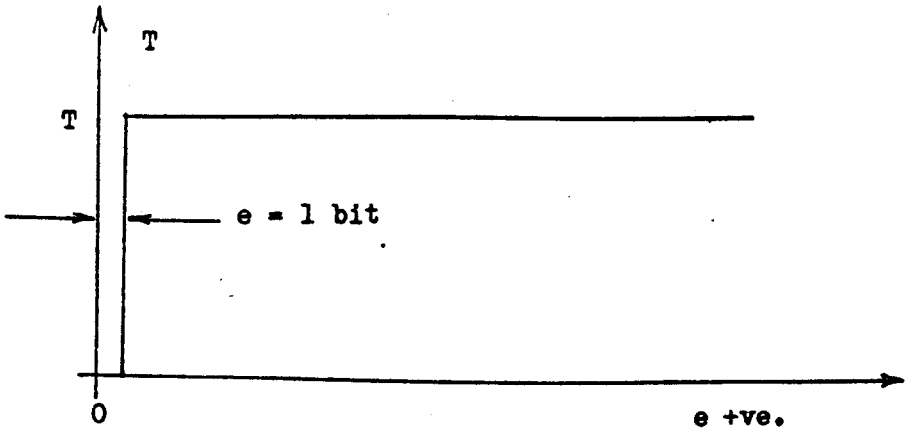

Fig.4-4 Modified Input-Output characteristic

In this element the value of output torque T changes between 0 and T according to the input with a lag of 1 binary bit. Neglecting the lag introduced by the relay, which is only about 10 ms, the element introduces no measurable lag effects to the system.

Encoder and Decoding Logic

The decoding logic comprises a series of solid state 'gates' the function of which is to convert the output from the shaft encoder (V-scan) to match the input of the subtractor (binary code). It contains no mechanical linkages and may therefore be ignored in this analysis.

The encoder is electro-mechanical in operation, and therefore it introduces friction and inertia effects into the system. For the purpose of this analysis, however, it is more convenient to include these mechanical effects with those of the gearbox element, which is dealt with later. The encoder/decoder element as shown in Fig.4-1 may therefore be ignored in the analysis.

Gearbox Unit

For the purpose of this analysis all the mechanical effects in the system are included in this element, except those delays due to the relays in the servo amplifier, which as explained have been ignored.

The gearbox unit comprises a motor driven 3:1 reduction spur gear mechanism, coupled to a screw jack which is fitted with a contact type shaft encoder to provide position feedback signals. Output of the system is the extension or retraction of the screw jack ram, but in fact the ram itself is outside the servo loop, since the position of the ram is infered from the angular orientation of the screw. In this analysis therefore the output of the gearbox unit is taken to be the angular position of the screw.

Mechanical effects introduced by this element include:

Friction: plain and ball bearings, brushes in the motor and the encoder, screw thread and ram friction, also gear tooth friction.

Inertia: rotors of the motor and encoder, spur gears and the screw member, also the linear mass effect of the ram.

Fig.4-5 is a diagram of the general arrangement of the components of the gearbox unit.

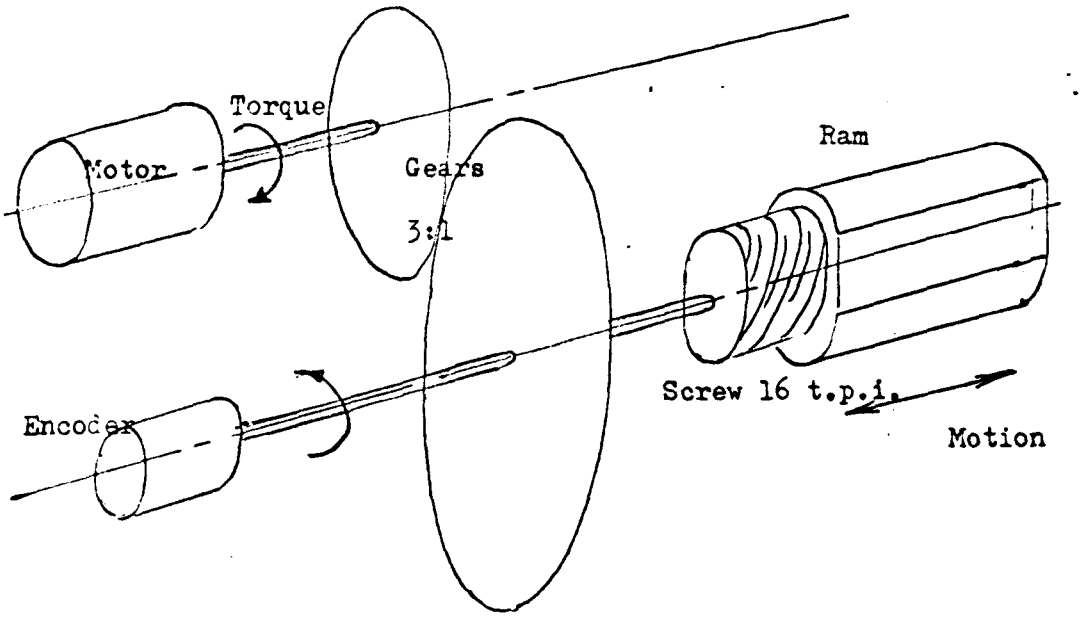

Fig.4-5 General Arrangement of the components of the Gearbox

Analysis of Gearbox Response

Let the applied torque	=	T
combined 'stiction'	=	K
combined friction coeff.	=	c (without e.m. braking)
combined friction coeff.	=	c'(with e.m. braking)
combined inertia effects	=	J
angular displacement of motor shaft	=	θ (linearly related to) (stated output)
differential operator w.r.t. time	=	D

The e.m. (electro magnetic) braking occurs due to the motor field, which is permanently energized. When the armature is receiving current the effect of the field is included in the output torque of the motor, but when the armature is switched off, the field current has the effect of increasing the value of the friction term.

The motion of this element may then be described by the following pair of differential equations, to cover the motor driving and coasting conditions.

$$(JD^2 + cD)\theta = T - K \quad \text{(motor driving)} \qquad \ldots\ldots\text{(iii)}$$

$$(JD^2 + c'D)\theta = 0 \quad \text{(coasting)} \qquad \ldots\ldots\text{(iv)}$$

Both the above equations refer to motion of the shaft in one direction. They may be said to describe the motion provided:

a) the motion is unidirectional, in order that the sign of K may be established.

b) the torque is a continuous function.

As already stated the above conditions are met by the normal running conditions of the system, provided that a given profile is considered in a series of separate sections, none of which required ram direction changes. In practice this limitation will mean that the input is either zero, for journal machining, or a ramp input function for machining tapers or faces.

Considering the motor on response, let $T' = T - K$, then:

$$(JD^2 + cD)\theta = T' \qquad \ldots\ldots\text{(v)}$$

Equation (v) has the auxilliary:

$$k^2 + \frac{c}{J}k = 0$$

with roots,

0 and $-\frac{c}{J}$, hence the complementary function is:

$$A + Be^{-c/J\,t}$$ where A and B are constants.

The particular solution is given by:

$$\theta = \frac{1}{(D^2 + \frac{c}{J}D)} \cdot \frac{T'}{J}$$

$$= \frac{1}{D} \cdot \frac{1}{(\frac{c}{J} + D)} \cdot \frac{T'}{J}$$

$$= \frac{1}{D} \cdot \frac{J}{c} \cdot \frac{T'}{J}$$

$$= \frac{T'}{c}t$$

Combining the particular and complementary solutions we have:

$$\theta = A + B\,e^{\frac{-c}{J}t} + \frac{T'}{c}t \qquad \text{.....(vi)}$$

Boundary conditions are:

$\theta = 0$ at $t = 0$, also $D\theta = 0$ at $t = 0$

Hence:

$$A = -B$$

Also,

$$\frac{T'}{c} = \frac{cB}{J}$$

Therefore, $B = \frac{T'\,J}{c^2}$ and $A = -\frac{T'\,J}{c^2}$

And equation (vi) may then be written as:

$$\theta = \frac{T'J}{c^2} e^{\frac{-c}{J}t} + \frac{T'}{c}t - \frac{T'J}{c^2} \qquad \ldots\ldots \text{(vii)}$$

or

$$\psi(t) = \frac{T'}{c}\left\{\frac{J}{c} e^{\frac{-c}{J}t} + t - \frac{J}{c}\right\} \qquad \ldots\ldots \text{(viii)}$$

The three terms of equation (vii) above may be considered separately, as illustrated in Fig.4-6, and equation (viii) shows that the solution is non-oscillatory.

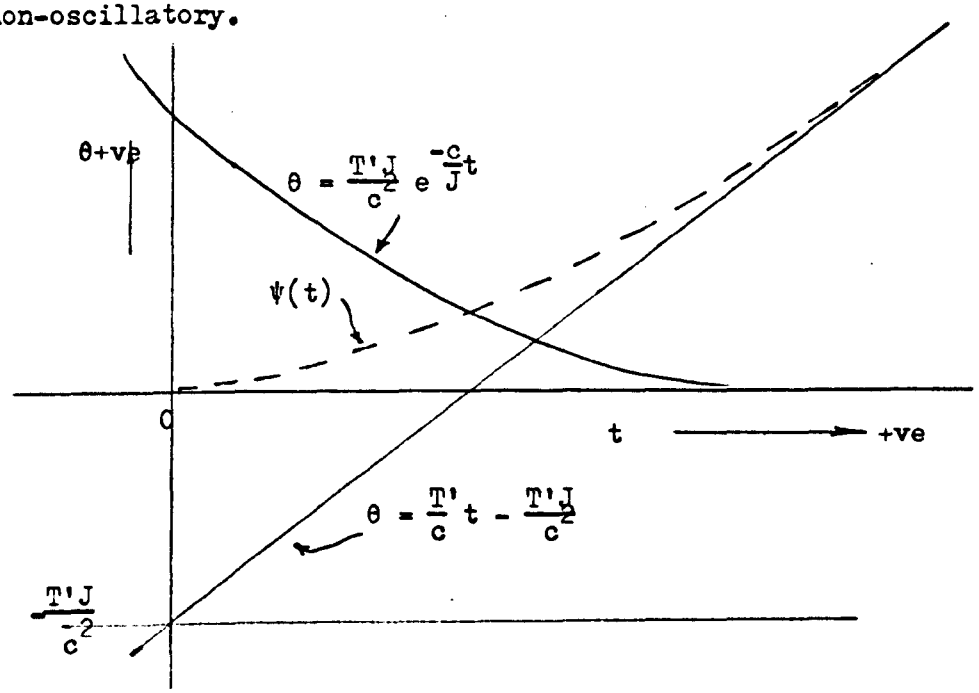

Fig.4-6 The Function $\psi(t)$, and its components

From the above curve it may be seen that the function $\psi(t)$ tends to the line $\theta = \frac{T'}{c}t$, being modified in the early stages by an exponential decay component. The coefficient $\frac{J}{c}$ may be termed the 'time constant' of the system, and is denoted by the symbol $\mathcal{J}$.

If the input to the system is a ramp function, the motor will be

switched on as soon as there is an error of 1 bit, and it will then 'chase' the ramp input until there is again an error of only one bit. At this point the system will switch off the motor and the gearbox will obey the second equation of motion (equation (iv)).

In considering the response of the system, the above mentioned error of 1 bit is conveniently ignored since its effect is non-linear, and as a result the ramp is considered to commence at time -t which is fixed so that the system begins to respond at t = 0. This modification does not alter the form of the functions plotted but serves to simplify the values of the constant terms A and B in equation (vi). When considering the response after motor cut-off the 1 bit uncertainty has to be taken into the calculations, but since there is an accepted discontinuity at this point, it can be done without excessive difficulty.

Fig.4-7 below shows the system response from rest, to the motor cut-off point P, when the response function (motor on), $\psi(t)$ intersects the ramp input function.

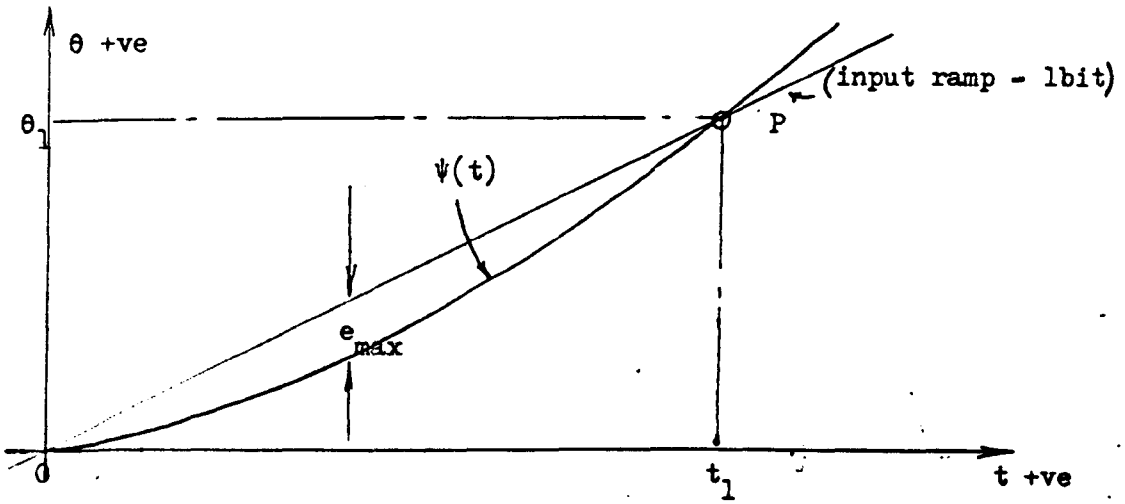

Fig.4-7 Initial response from rest to motor cut-off point

Motor Off Response (Coasting)

As soon as the system achieves an error of less than 1 bit, the motor is switched off by relays in the controller, and the gearbox may then be said to behave according to equation (iv). During this phase of running the motor field is still energized which results in a different effective friction coefficient c'. Hence the equation of motion,

$$(JD^2 + c'D)\theta = 0$$

has the solution:

$$\theta = E + F e^{\frac{-c'}{J}t}$$ where E and F are constants

In this case the boundary conditions depend on the motor cut-off point, these being determined in turn by the form of the input ramp.

In general at the cut-off point P, $\theta = \theta_1$ and $D\theta = \omega = \omega_1$ at t_1

Then:

$$\theta_1 = E + F e^{\frac{-c'}{J}t_1} \qquad .....(ix)$$

and,

$$D\theta = -\frac{c'}{J}.F.e^{\frac{-c'}{J}t} = \omega$$

therefore:

$$\omega_1 = -\frac{c'}{J}.e^{\frac{-c'}{J}t_1}$$

and,

$$F = -\frac{J\omega_1}{c'1} e^{\frac{-c'}{J}t_1}$$

Substituting for F in equation (ix), we have:

$$E = \theta_1 + \frac{J\omega_1}{c'1}$$

Putting these values for the constants E and F into equation (ix), we have the full solution for this condition.

$$\theta = (\theta_1 + \frac{J\omega_1}{c'}1) - (\frac{J\omega_1}{c'}1.e^{\frac{-c'}{J}t_1}).e^{\frac{-c'}{J}t}$$

Let $\frac{J}{c'} = \mathcal{T}'$, a revised time constant for the coasting condition, and this solution may be written as:

$$\theta = \phi(t) = X - Z.e^{\frac{-t}{\mathcal{T}'}} \qquad .....(x)$$

where the constants X and Z are given by:

$$X = \theta_1 + \frac{J\omega_1}{c'}1$$

and

$$Z = \frac{J\omega_1}{c'}1.e^{\frac{-t}{\mathcal{T}'}}$$

A sketch of the function $\phi(t)$ is given below in Fig.4-8, from the motor cut-off point P, and from this curve it may be seen that the function comprises an exponential rise from the point P, and becomes assymptotic to a horizontal line $\theta = X$, where X is the constant defined above.

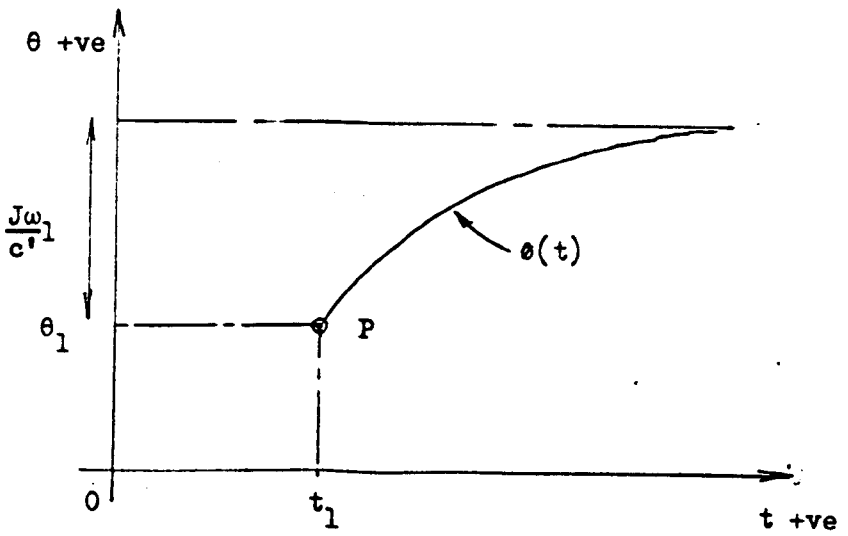

Fig.4-8 The coasting response function $\phi(t)$ from point P

The final value of θ depends on:

θ_1 the starting value

ω_1 velocity at the motor cut-off point

γ' the time constant for the coasting condition

In addition it may be seen that the form of the exponential rise also depends on the time constant γ'.

Combining the motor on and coasting response functions, for a steady ramp input function, it may be seen (Fig.4-9) that there are two possible forms for the complete system response curve, both of which take the form of discontinuous oscillations. Which of these two forms is realized in practice depends on the slope or gradient of the input ramp, for given torque and time constant parameters.

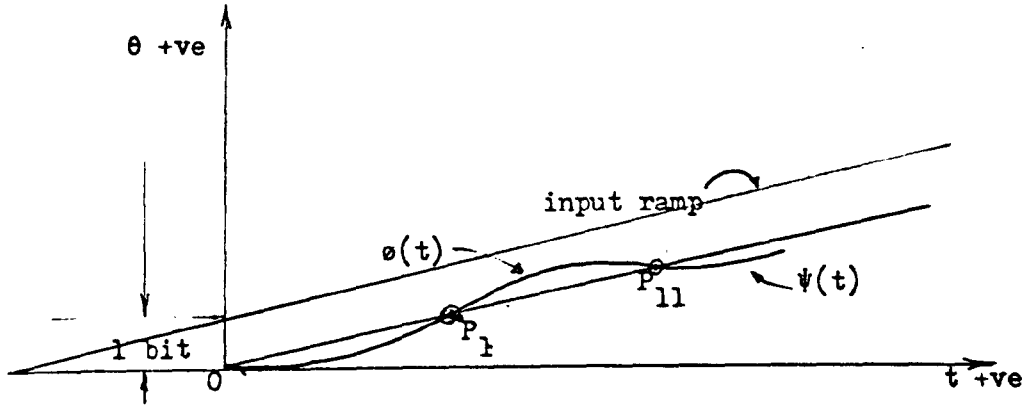

Fig.4-9 a Response to small gradient input ramp

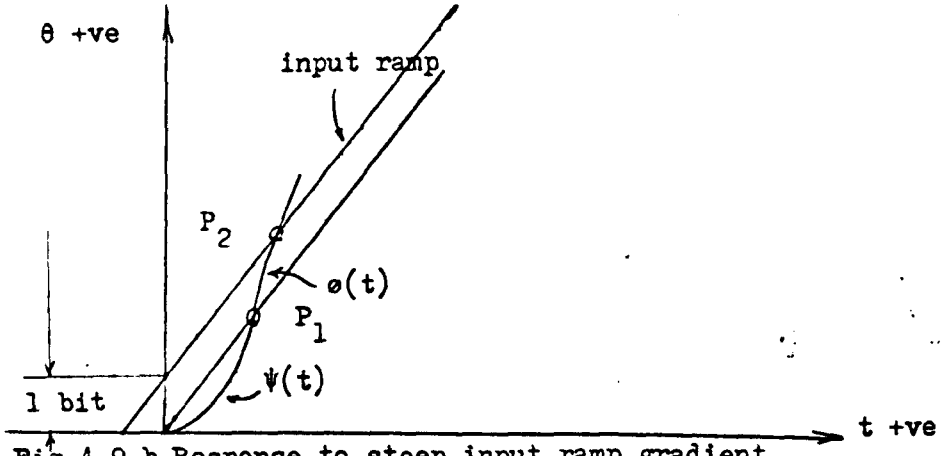

Fig.4-9 b Response to steep input ramp gradient

In the case of the system response to steep input ramps as illustrated in Fig.4-9 b, it may be seen that the ram overshoots its required position, and reaches a point P_2 in Fig.4-10 below, where the motor is switched on again but with opposite field polarity. This results in the ram being reversed, and there is then a second motor cut-off point P_{22}.

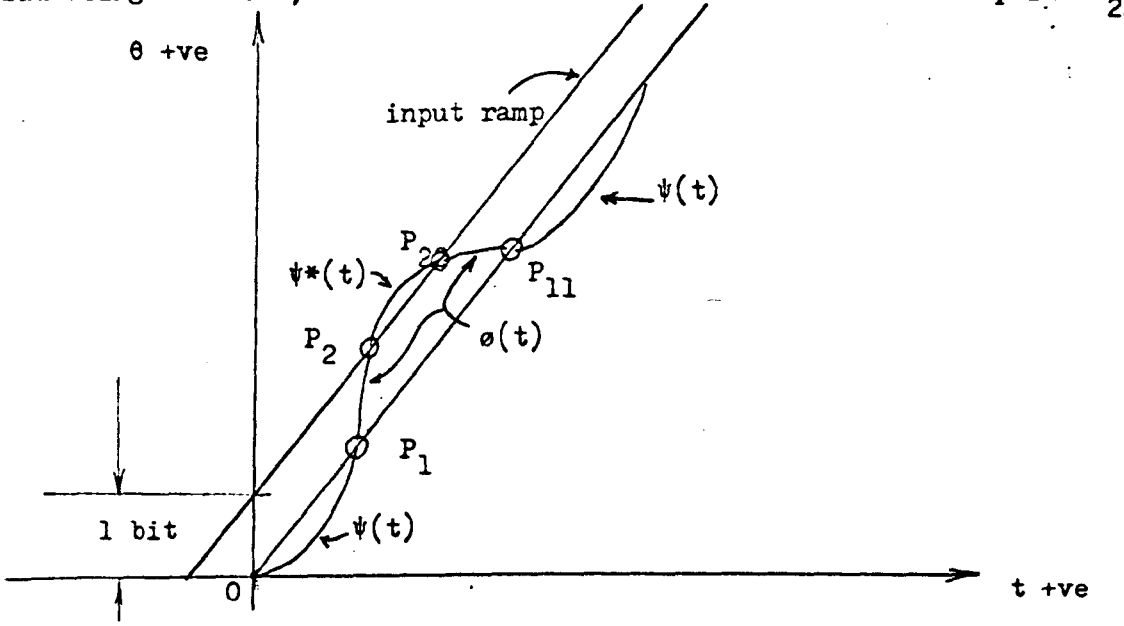

Fig.4-10 Response to steep input ramp, showing overshoot.

The form of the response functions in the above figure is similar to those already derived, but the values for the constant terms are more complex as the system does not start from rest. After the point P_2 we have motor on, but with opposite torque, hence the describing function is:

$$(JD^2 + cD)\theta = -T'$$

The solution of which is:

$$\theta = A' + B'.e^{\frac{-t}{\tau}} - \frac{T'}{c}t$$

and the boundary conditions are:

$$\theta = \theta_2 \text{ at } t = t_2 \text{ , also } \omega = \omega_2 \text{ at } t_2$$

θ_2 and t_2 are the co-ordinates of the point P_2 on the response curve,

which is the intersection of the function $\phi(t)$ and the input ramp taking the 1 bit lag into account.

In general it may be shown that:

$$A' = (\theta_2 + \frac{T'}{c} t_2 + \tau \omega_2 + \frac{T'\tau}{c})$$

$$B' = -\tau . e^{\frac{t}{\tau}2} (\omega_2 + \frac{T'}{c})$$

Which gives the solution:

$$\psi^*(t) = (\theta_2 + \frac{T'}{c} t_2 + \tau \omega_2 + \tau \frac{T'}{c}) - . e^{\frac{t}{\tau}2} (\omega_2 + \frac{T'}{c}) . e^{\frac{-t}{\tau}} - \frac{T'}{c} t \quad ..(xi)$$

The above expression is of the same form as the function $\psi(t)$, equation (viii). Between the point P_{22} and P_{11} in Fig.4-10, the system will follow the function $\phi(t)$, but this time the starting velocity will have a different sign.

Evaluation of System Constants

The solutions to the describing equations given in equations (viii) and (x), include certain coefficients which are constant for the equipment under test. These constants have to be determined in order to plot the theoretical response curve. The constants are listed below:

T' = Effective torque generated when the motor is supplied with d.c. pulses for low speed running.

c = The friction constant, due to bearings, gears , brushes and the ram, in the motor on condition.

c' = Similar to c, but with the motor field energized to produce the previously mentioned electro-magnetic braking effect.

$\mathcal{J} = \frac{J}{c}$ = The time constant, which includes the combined inertia effects of the complete element.

$\mathcal{J}' = \frac{J}{c'}$ = Similar to $\mathcal{J}$, but with c' instead of c.

Effective Torque T'

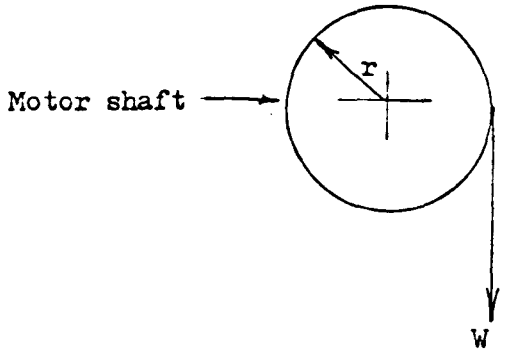

Fig.4-11 Determination of effective torque T'

A light thread was attached to the motor shaft, as shown in Fig.4-11 above, and the value of weight W was determined by experiment, so that the turning moment of the motor at low speed was just cancelled. The torque was then found from the relation:

$$T' = W.r$$

Now,

$r = 0.290$ in (micrometer measurement)

$W = 1.4$ lbf (mean of three tests)

Hence:

$$T' = \frac{1.4 \times 32.2 \times 0.290}{12} \text{ pdl.ft}$$

$$T' = 1.089 \text{ pdl.ft}$$

Considering the accuracy of measurement, $T' = 1.1$ pdl.ft

Friction Constants c and c'

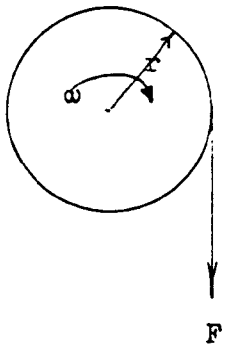

Fig.4-12 Determination of friction constants

These values were determined by applying a known torque to the motor shaft, as shown in Fig.4-12 above, and recording the steady speed reached by the shaft. The tests were made with the motor field on and off in order to obtain values for both c and c'. A subsidiary test was then carried out to find the torque absorbed by the revolution counter which was used to measure the shaft speed. The friction constants were then determined from the following relation:

$$\text{Applied torque} = c \times \text{Angular velocity (steady state)}$$

$$F.r = c.\omega$$

Considering the gearbox unit and the revolution counter,

$$F.r = c''.\omega$$

where F.r is the torque applied to the motor shaft, ω is the steady velocity achieved and c'' is the friction constant including the effect of the revolution counter.

A similar series of results was then obtained for the revolution counter only, by applying the torque to its shaft only, hence:

$$f.r' = c'''.\omega$$

By plotting f.r versus ω, for the revolution counter, the value of

c''' may be found from the slope.

Then:

$$T' = F.r - f.r'$$

$$= c''\omega - c'''.\omega$$

But

$$T' = c.\omega$$

Therefore:

$$\underline{c = c'' - c'''}$$

By repeating these tests with the motor field energized it was possible to obtain a value for c', from the relation:

$$\underline{c' = c^{v} - c'''}$$ (Since c' is not required results are not included in this thesis)

Results from these tests are listed below in Tables 4.2 and 4.3

F (lbf)	F (pdl)	F.r (pdl.ft)	N (rev/min)	ω (rad/s)
.5	16.1	.3888	20	2.093
.75	24.15	.5832	130	13.610
1.00	32.2	.7776	255	26.690
1.25	40.25	.9718	380	39.780

Table 4.2 Determination of friction constant-Gearbox and Counter

f (lbf)	f (pdl)	f.r' (pdl.ft)	N (rev/min)	ω (rad/s)
.25	8.050	.005207	275	28.78
.30	11.270	.006248	355	37.16
.35	14.490	.007291	435	45.54

The number of readings that could be taken for the revolution counter only was limited, at the top end by the limit of 500 rev/min of the counter range, and at the low end by 'stiction' in the instrument which resulted in a threshold torque of 0.22.r' lbf.ft.

Fig. 4-13 Determination of friction constants

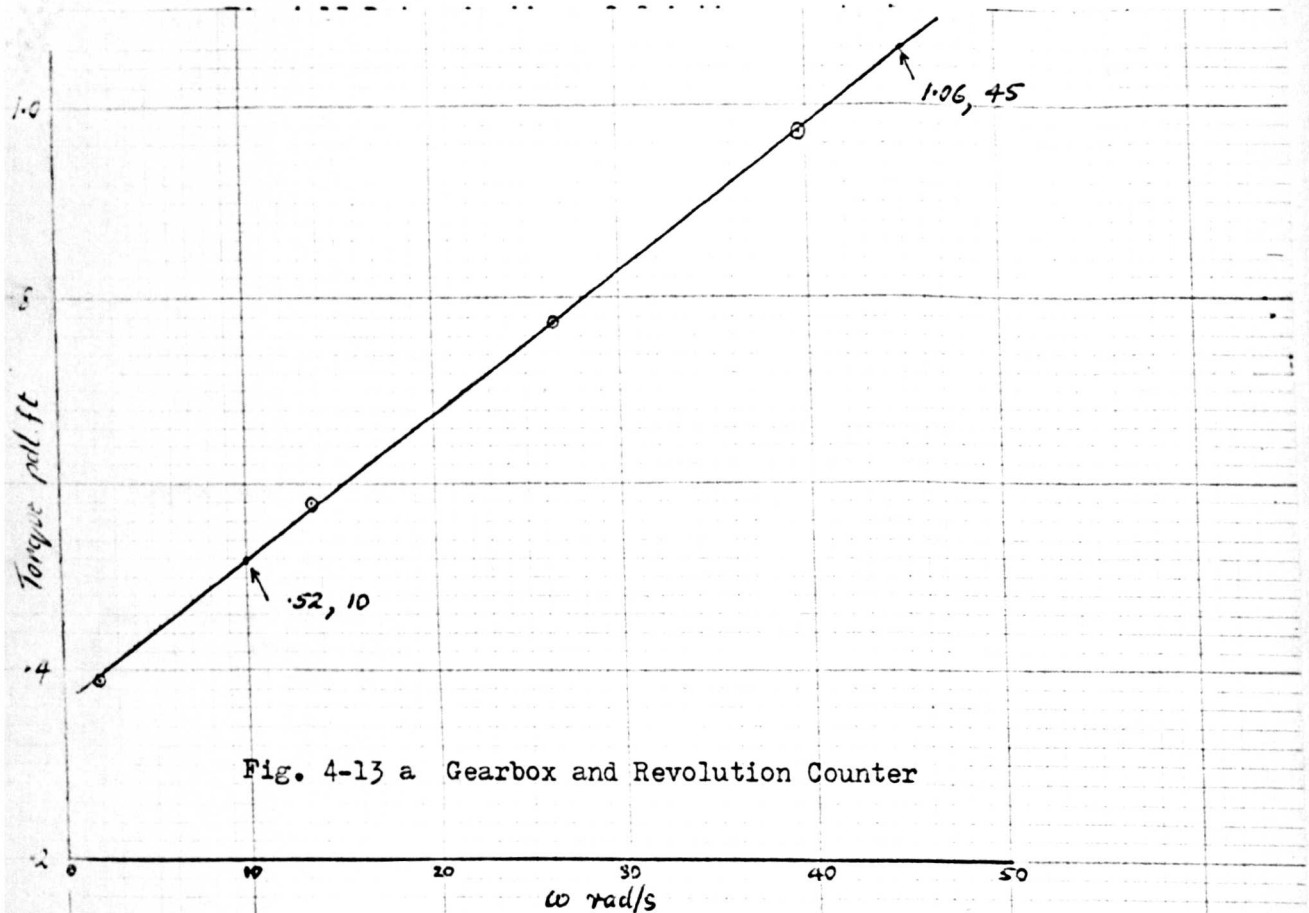

Fig. 4-13 a Gearbox and Revolution Counter

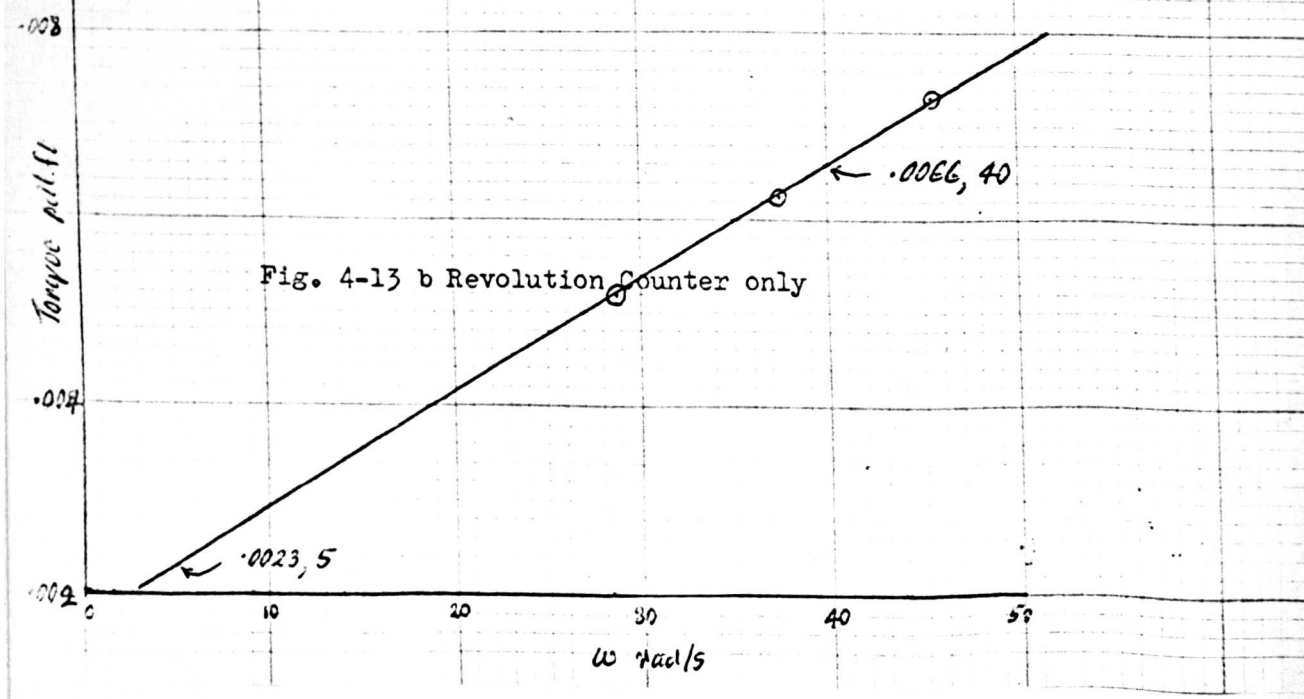

Fig. 4-13 b Revolution Counter only

The results given in Tables 4.2 and 4.3 on the previous page are plotted on two graphs illustrated in Fig.4-13 opposite. From the slopes of these curves the friction constants may be determined:

From Fig.4-13 a,

$$\text{slope} = \frac{1.06 - .52}{45 - 10} = \frac{.54}{35}$$

Therefore

$$c'' = \underline{0.01543 \text{ pdl.ft.s}}$$

From Fig.4-13 b,

$$\text{slope} = \frac{.0066 - .0023}{40 - 5} = \frac{.0043}{35}$$

Therefore

$$c''' = \underline{0.00012 \text{ pdl.ft.s}}$$

By subtraction, and taking into account the accuracy of these measurements, the friction constant is:

$$\underline{c = 0.0153 \text{ pdl.ft.s}}$$

Ratio of Torque to Friction Constant $\frac{T'}{c}$

This term occurs in the function $\psi(t)$, and is given by,

$$\frac{T'}{c} = \frac{1.089}{0.0153}$$

$$= 70.78 \text{ s}^{-1}$$

Considering the accuracy of the tests,

$$\underline{\frac{T'}{c} = 71 \text{ s}^{-1}}$$

The Time Constants $\mathcal{T}$ and $\mathcal{T}'$

It was decided to evaluate the damping ratios by oscillatory methods, the simplest practically being the use of a compound pendulum. In this

method a suitable pendulum is fitted to the motor shaft, with the gear-box unit mounted horizontally, as shown in Fig.4-14 below. The pendulum is then made to oscillate, using the motor shaft as the fulcrum, and the resulting damped oscillations are observed. Measurements are then made of successive amplitudes of swing, and also of the periodic time for the system. In a subsidiary experiment the periodic time for the pedulum is determined for free undamped swings about the same axis, using a knife edge as the fulcrum. Together with the measured mass of the pendulum, and the distance between the centre of gravity of the unit and the axis of the fulcrum, the periodic time for free swings is then used to determine the moment of inertia of the pendulum itself about the axis employed.

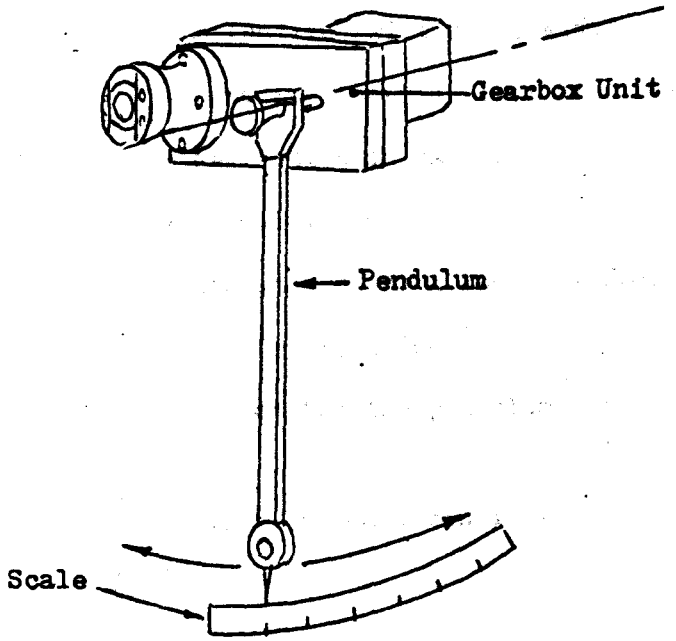

Fig.4-14 Arrangements for determination of time constants

Tests were carried out with the motor field energized, and also with the field switched off, to establish values for the two time constants required, and runs were made with two values for the pendulum inertia.

Use of the Compound Pendulum

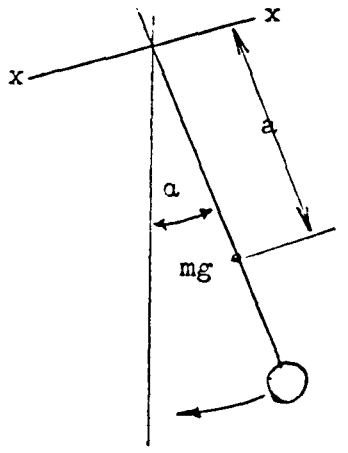

Fig.4-15 Diagram of the compound pendulum

In Fig.4-15 above, let:

J = effective inertia of the gearbox element

c = effective friction constant

J_p = pendulum inertia about axis x-x

α = deflection in radians

m = pendulum mass

a = distance of pendulum c.g. from axis x-x

g = acceleration due to gravity

Then the equation of motion for the pendulum is:

$$(J'D^2 + cD)\,\alpha = -mga \sin\alpha = -mga\,\alpha \text{ (for small } \alpha)$$

where $J' = (J + J_p)$

The oscillatory solution to this equation is:

$$\alpha = R.e^{Pt}.\sin(qt + \beta)$$

where R and β are constants, and P, q are the real and imaginary parts of the roots P + iq, P - iq of the auxilliary equation.

By inspection,

$$P = -\frac{c}{2J'} = -\frac{c}{2(J + J_p)}$$

Now the amplitude of the oscillatory solution is:

$$\text{amplitude} = R.e^{-\frac{c}{2J'}t}$$

Put $k = \frac{c}{2J'}$, and considering only the maximum amplitudes, we have:

$$a_{max.} = R.e^{-kt}$$

hence:

$$\log_e a = \text{Log}_e R - kt$$

k may therefore be determined by plotting the logarithm of successive maximum amplitudes against time, and measuring the slope of the resulting curve:

$$\text{slope} = k = \frac{c}{2(J + J_p)}$$

If two series of tests are run at different pendulum inertias, J_{p1} and J_{p2}, then the slopes of the resulting curves are:

$$2k_1 = \frac{c}{(J + J_{p1})} \qquad \text{.....(xii)}$$

and,

$$2k_2 = \frac{c}{(J + J_{p2})} \qquad \text{.....(xiii)}$$

Combining equations (xii) and (xiii), we have:

$$k_1(J + J_{p1}) = k_2(J + J_{p2})$$

Hence:

$$J = \frac{k_2J_{p2} - k_1J_{p1}}{(k_1 - k_2)}$$

Now,

$$c = 2k_1(J + J_{p1})$$

$$= 2k_1 \left\{ \frac{k_2J_{p2} - k_1J_{p1}}{k_1 - k_2} + J_{p1} \right\}$$

$$= 2.k_1.k_2 \left\{ \frac{J_{p2} - J_{p1}}{k_1 - k_2} \right\}$$

Hence the time constant is given by:

$$\gamma = \frac{J}{c} = \frac{k_2J_{p2} - k_1J_{p1}}{2.k_1.k_2(J_{p2} - J_{p1})} \qquad .....(xiv)$$

Similarly, if the slopes for the motor field on condition are k_{11} for J_{p1}, and k_{22} for J_{p2}, the time constant for the coasting condition is:

$$\gamma' = \frac{J}{c'} = \frac{k_{22}J_{p2} - k_{11}J_{p1}}{2.k_{11}.k_{22}(J_{p2} - J_{p1})} \qquad .....(xv)$$

Pendulum Inertias J_{p1} and J_{p2}

As stated earlier these values were determined from measurements of mass, free period and c.g. position for the pendulum in the two conditions in which it was employed

Considering the pendulum suspended from a knife edge, let:

T = free period of the pendulum

m = mass of the pendulum

K = radius of gyration

a = c.g. position from fulcrum

J_p = moment of inertia about fulcrum axis

Then,

$$T = 2\pi \sqrt{\frac{K^2 + a^2}{ga}}$$

$$T^2 = 4\pi^2 \left(\frac{K^2 + a^2}{ga}\right)$$

Now,

$$J_p = m(K^2 + a^2)$$

Therefore:

$$T^2 = 4\pi^2 \frac{J_p}{mga}$$

The two required pendulum inertias are:

$$J_{p1} = \frac{m_1 \cdot g \cdot a_1 \cdot T_1^2}{4\pi^2} \quad \text{and} \quad J_{p2} = \frac{m_2 \cdot g \cdot a_2 \cdot T_2^2}{4\pi^2}$$

The following measurements were made directly on the pendulum:

m_1	= 1.1 lbf	m_2	= 0.65 lbf
T_1	= 1.94 s	T_2	= 1.90 s
a_1	= 26.95 in	a_2	= 19.60 in

Hence J_{p1}:

$$J_{p1} = \frac{1.1 \times 32.2 \times 26.95 \times 1.94^2}{4.\pi^2 \times 12}$$

$$= 7.586 \text{ lb.ft}^2$$

or, considering accuracy of measurement $J_{p1} = 7.6 \text{ lb.ft}^2$

Also, J_{p2} is:

$$J_{p2} = \frac{0.65 \times 32.2 \times 19.6 \times 1.9^2}{4.\pi^2 \times 12}$$

$$= 3.127 \text{ lb.ft}^2$$

or considering accuracy of measurement,

$$J_{p2} = 3.1 \text{ lb.ft}^2$$

Pendulum fitted to motor shaft

Readings of maximum amplitude obtained during successive swings with the pendulum mounted on the motor shaft, are listed in Tables 4.4 and 4.5.

Table 4.4 Pendulum amplitudes with motor field off

Heavy Pendulum			Pendulum		
α °	α(rad)	$\text{Log}_e \alpha$	α °	α(rad)	$\text{Log}_e \alpha$
15.00	.2618	-1.3402	15.00	.2618	-1.3402
13.90	.2426	-1.4164	12.80	.2234	-1.4988
12.95	.2260	-1.4872	10.70	.1868	-1.6777
12.00	.2094	-1.5834	8.70	.1518	-1.8853
11.10	.1937	-1.6415	6.65	.1161	-2.1533
10.15	.1772	-1.7305	4.80	.0838	-2.4794
9.25	.1615	-1.8234	3.00	.0524	-2.9489
8.40	.1466	-1.9201	1.45	.0253	-3.6770
7.55	.1318	-2.0267	.40	.0070	-4.9619
6.65	.1161	-2,1533	0	0	
5.75	.1004	-2.2988			
4.95	.0864	-2.4488			
4.15	.0725	-2.6252			

Table 4.4 continued from previous page

Heavy Pendulum			Light Pendulum		
α °	α(rad)	$\log_e \alpha$	α °	α(rad)	$\log_e \alpha$
3.4	.0593	-2.8702			
2.65	.0463	-3.1176			
1.95	.0341	-3.4235			
1.35	.0236	-3.7915			
.70	.0122	-4.4063			
.40	.0070	-4.9619			
.10	.0017	-6.3772			
0	0				

Table 4.5 Pendulum amplitudes with motor field on

Heavy Pendulum			Light Pendulum		
α °	α(rad)	$\log_e \alpha$	α °	α(rad)	$\log_e \alpha$
15.00	.2618	-1.3402	15.00	.2618	-1.3402
13.90	.2426	-1.4164	12.70	.2217	-1.5605
12.85	.2243	-1.4948	10.40	.1815	-1.7066
11.85	.2069	-1.5755	8.15	.1423	-1.9498
10.85	.1894	-1.6638	6.10	.1065	-2.2395
9.90	.1728	-1.7557	4.20	.0733	-2.6132
8.95	.1562	-1.8566	2.30	.0401	-3.2164
8.00	.1396	-1.9689	.85	.0149	-4.2064
7.25	.1266	-2.0667	.20	.0035	-5.6550
6.40	.1117	-2.1921	0	0	
5.45	.0951	-2.3529			
4.60	.0803	-2.5220			
3.70	.0646	-2.7396			

Fig. 4-16 Pendulum amplitude curves for determination of time constants

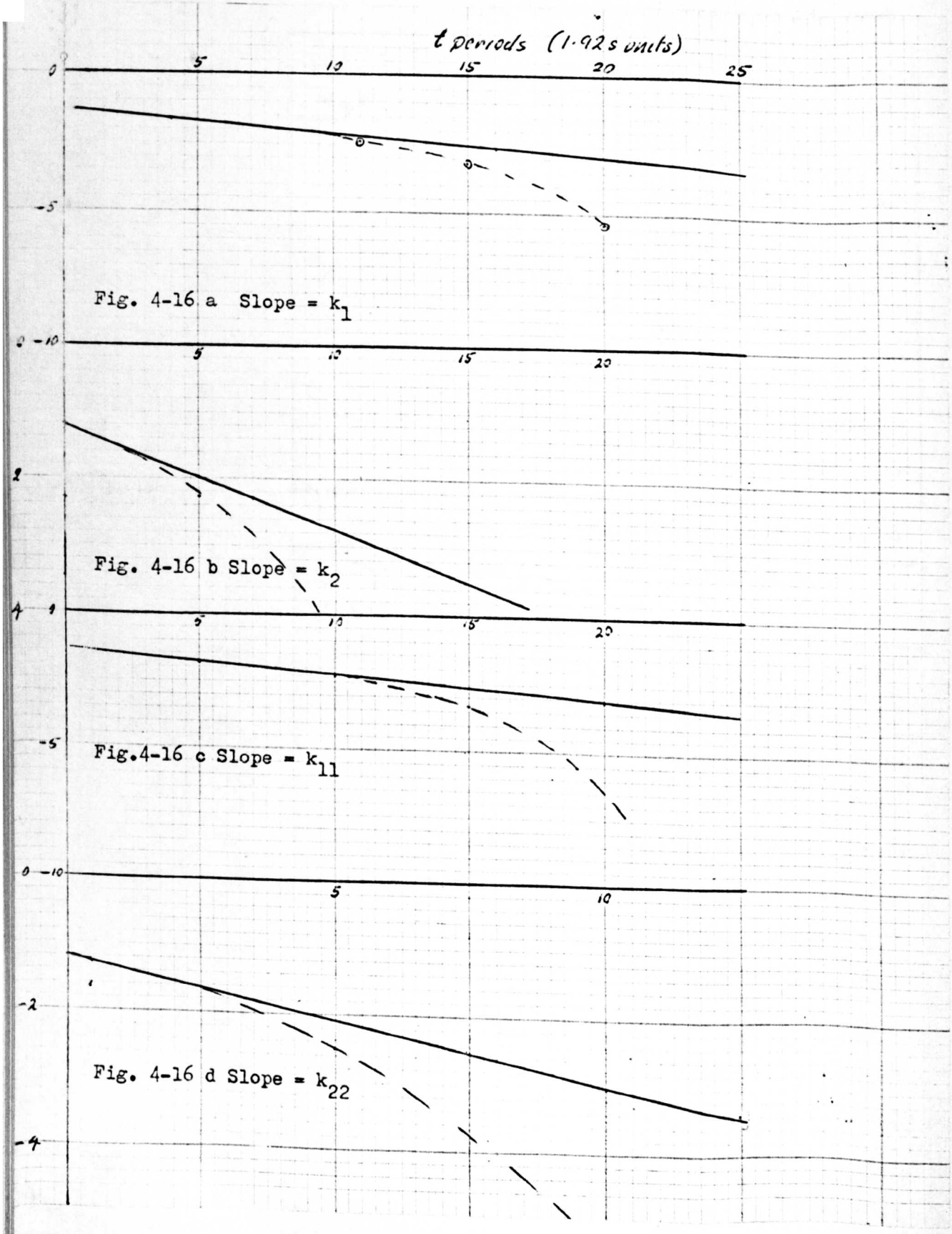

Table 4.5 continued from the previous page

Heavy Pendulum		
α °	α(rad)	$\text{Log}_e \alpha$
3.05	.0533	-2.9318
2.35	.0410	-3.1942
1.60	.0279	-3.5792
1.00	.0175	-4.0456
.55	.0096	-4.6460
.35	.0061	-5.0095
0	0	

The readings listed in Tables 4.4 and 4.5, are plotted on the curves given in Fig.4-16 opposite. Inspection of these curves reveals that, although the analysis has suggested that they should be straight lines, they are in fact curved as shown in Fig.4-17 below.

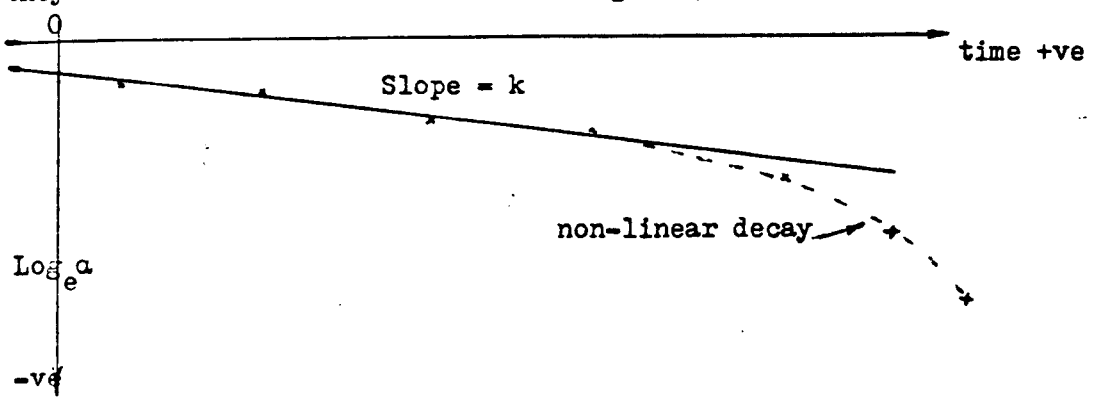

Fig.4-17 Decay of pendulum amplitude

It would appear that the straight line is modified as time increases by a decay function. Such a function could be explained by the action of non-linear effects, such as 'stiction' and backlash in the gearbox unit. This explanation is reasonable, since as time increases, the deflection caused by the pendulum swing decreases, and it should be

remembered that the overall mechanical advantage to the motor shaft in this unit is such that a pendulum deflection of nearly 5° is necessary to advance the ram by 0.001 in.

It is assumed then that the linear portions of the curves in Fig.4-16 provide the required values of slope, and that the curved portions are due to non-linear effects which increase greatly as deflections approach a small value.

From the curves in Fig.4-16, the following values of slope have been measured:

No braking effect	Heavy Pendulum	$k_1 = .0434\ s^{-1}$
	Light Pendulum	$k_2 = .0827\ s^{-1}$
With braking effect	Heavy Pendulum	$k_{11} = .0456\ s^{-1}$
	Light Pendulum	$k_{22} = .0936\ s^{-1}$

Calculation of Time Constants

The expression for the time constants has been derived as:

$$y = \frac{k_2 J_{p2} - k_1 J_{p1}}{2 \cdot k_1 \cdot k_2 (J_{p2} - J_{p1})}$$

Substituting the calculated values for k_1, k_2, J_{p1} and J_{p2}, we have:

$$= \frac{3.127 \times .0827 - 7.586 \times .0434}{2 \times .0827 \times .0434(3.127 - 7.586)}$$

$$= 2.211\ s$$

Similarly, substituting for k_{11}, k_{22}, J_{p1} and J_{p2}, we have:

$$y' = \frac{3.127 \times .0936 - 7.586 \times .0456}{2 \times .0936 \times .0456(3.127 - 7.586)}$$

$$= 1.397 \text{ s}$$

However, considering the accuracies of the measurements employed for these calculations, we may write:

$$\underline{y = 2.2 \text{ s}}$$

and

$$\underline{y' = 1.4 \text{ s}}$$

Input Ramp Functions

It has been shown in Section 3, that for a lathe tool to machine a 90° shoulder by copy turning, the saddle velocity being constant at 2.12 in/min, the copying slide has to retract at 4.24 in/min. From this figure the associated system response may be deduced thus:

Ram velocity = 4.24 in/min

= 0.0704 in/s

≑ 142 bits/s

Let ω_m = angular velocity of the motor shaft in rad/s, then

Input function = required ω_m

$$= \frac{142 \times 360 \times 3 \times 2\pi}{360 \times 128}$$

= 20.97 rad/s

≑ 21 rad/s

similarly other input ramp function may be calculated. In this work three ramp inputs have been tested theoretically, namely:

21 rad/s equivalent to 90° shoulder at 2.12 in/min

10.5 rad/s equivalent to 90° shoulder at 1.06 in/min

or a taper at a faster saddle velocity

also 5.25 rad/s

Theoretical Response Path

Using the response functions derived in this section, equations (viii), (x) and (xi), together with the system constants calculated and measured, the response of the system to the input ramps listed above was calculated. Since this task,if carried out by hand would be very tedious, use was made of a general purpose digital computer to calculate the co-ordinates of the response curve. The computer programme is fully described in Appendix 2, but the actual values calculated are not included in this thesis in the interests of space saving.

These co-ordinates were, however, used to plot response curves, which are given in Figs 4-18, 4-19, 4-20 and 4-21. The first three curves are the theoretical responses to the three input ramp functions employed, whereas Fig.4-21 is an enlarged drawing of the initial response to the 21 rad/s input ramp.

Theoretical mean lag errors are then determined from these response curves, and these results are listed in Table 4.6.

Fig.4-18 Theoretical Response to 21 rad/s input ramp

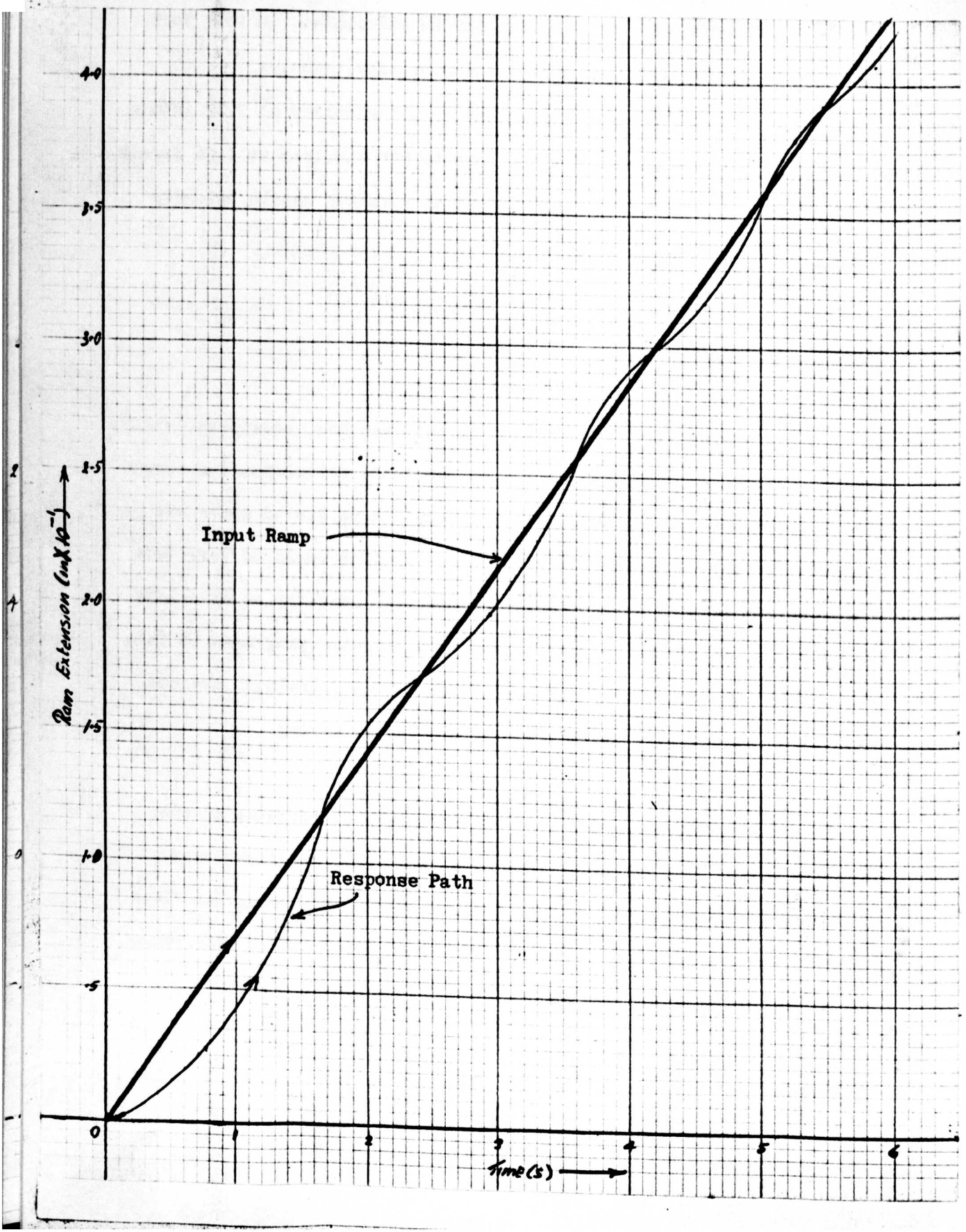

Fig.4-19 Theoretical Response to 10.5 rad/s input ramp

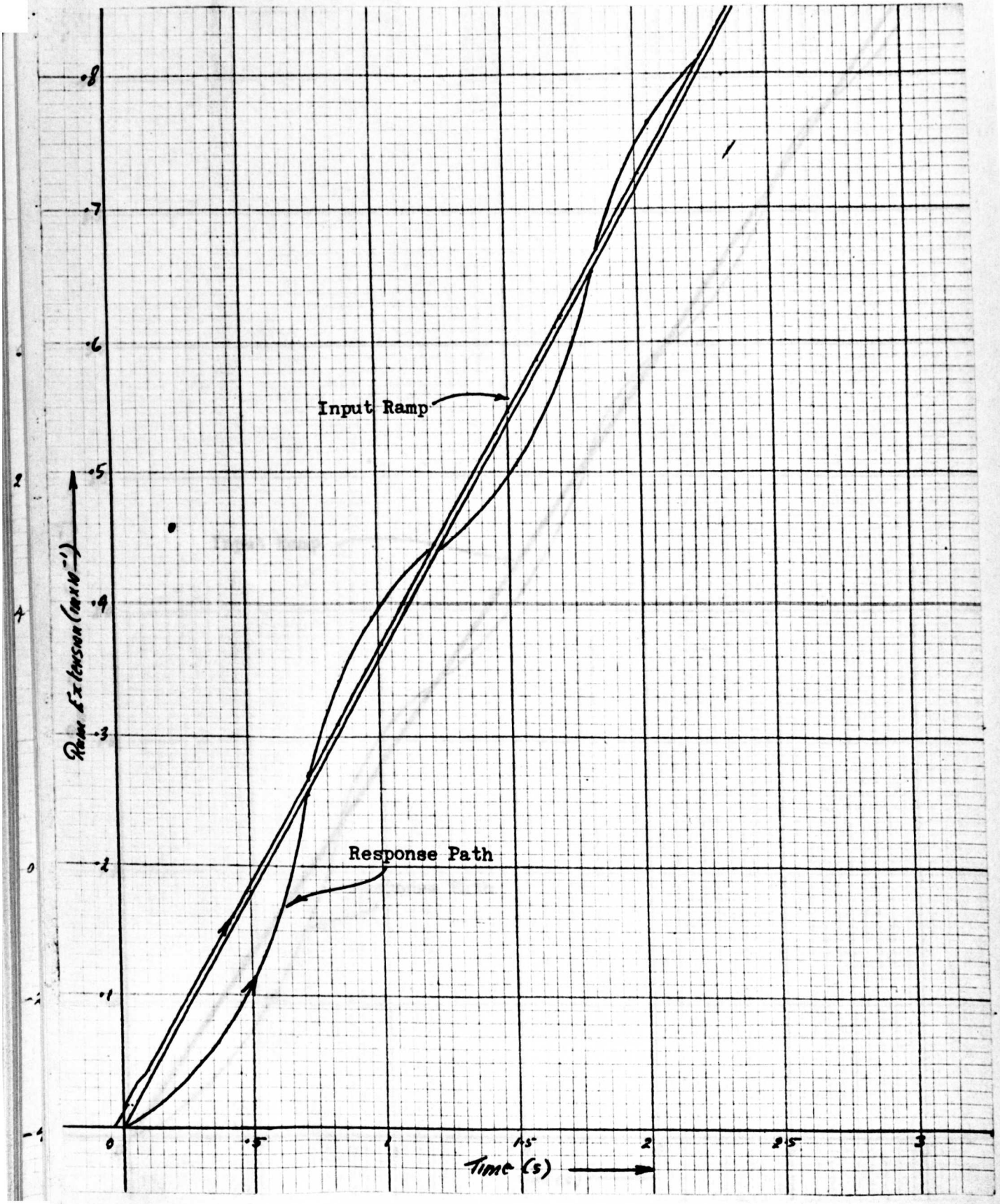

Fig.4-20 Theoretical Response to 5.25 rad/s input ramp

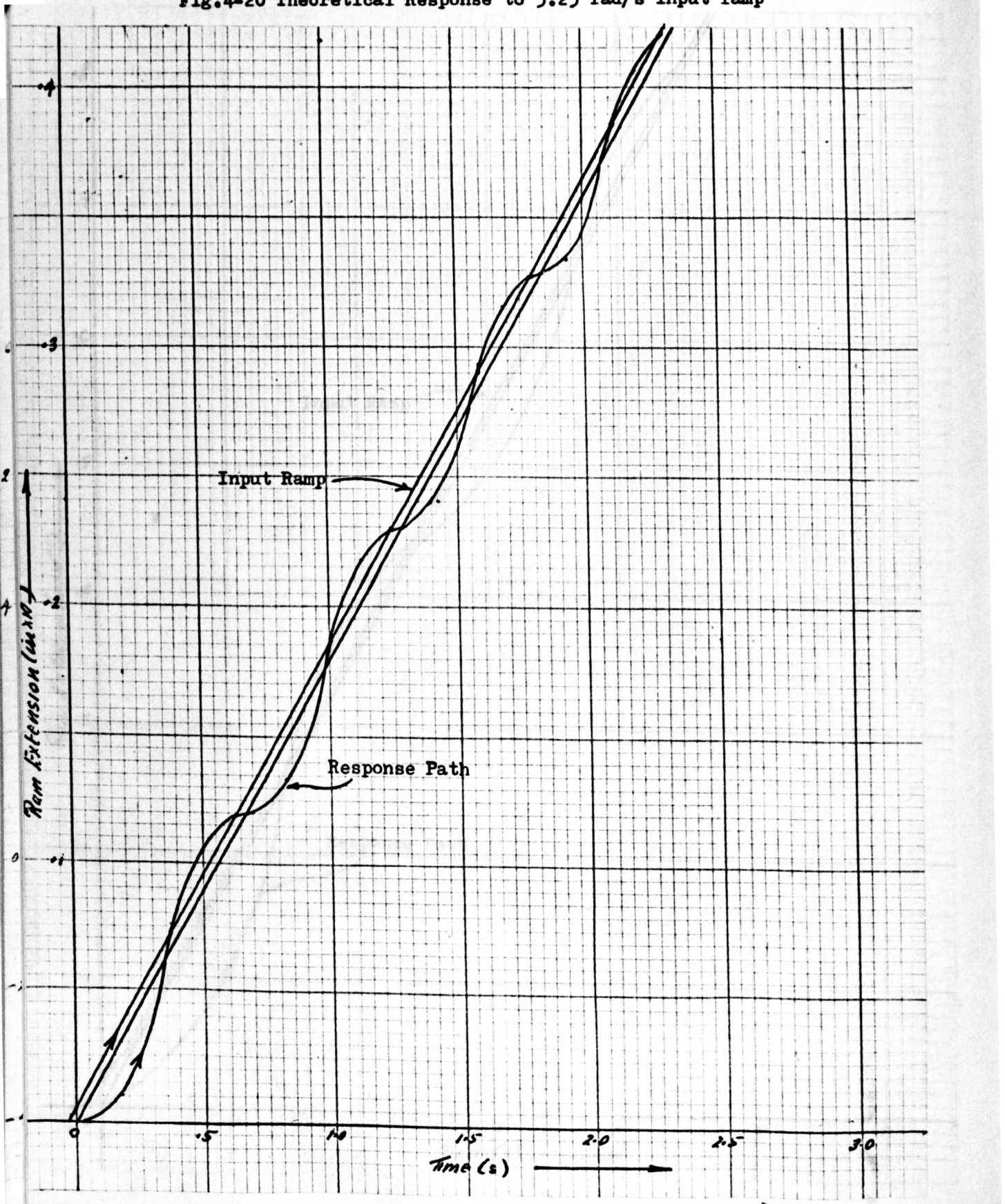

Fig.4-21 Initial Response to 21 rad/s input ramp

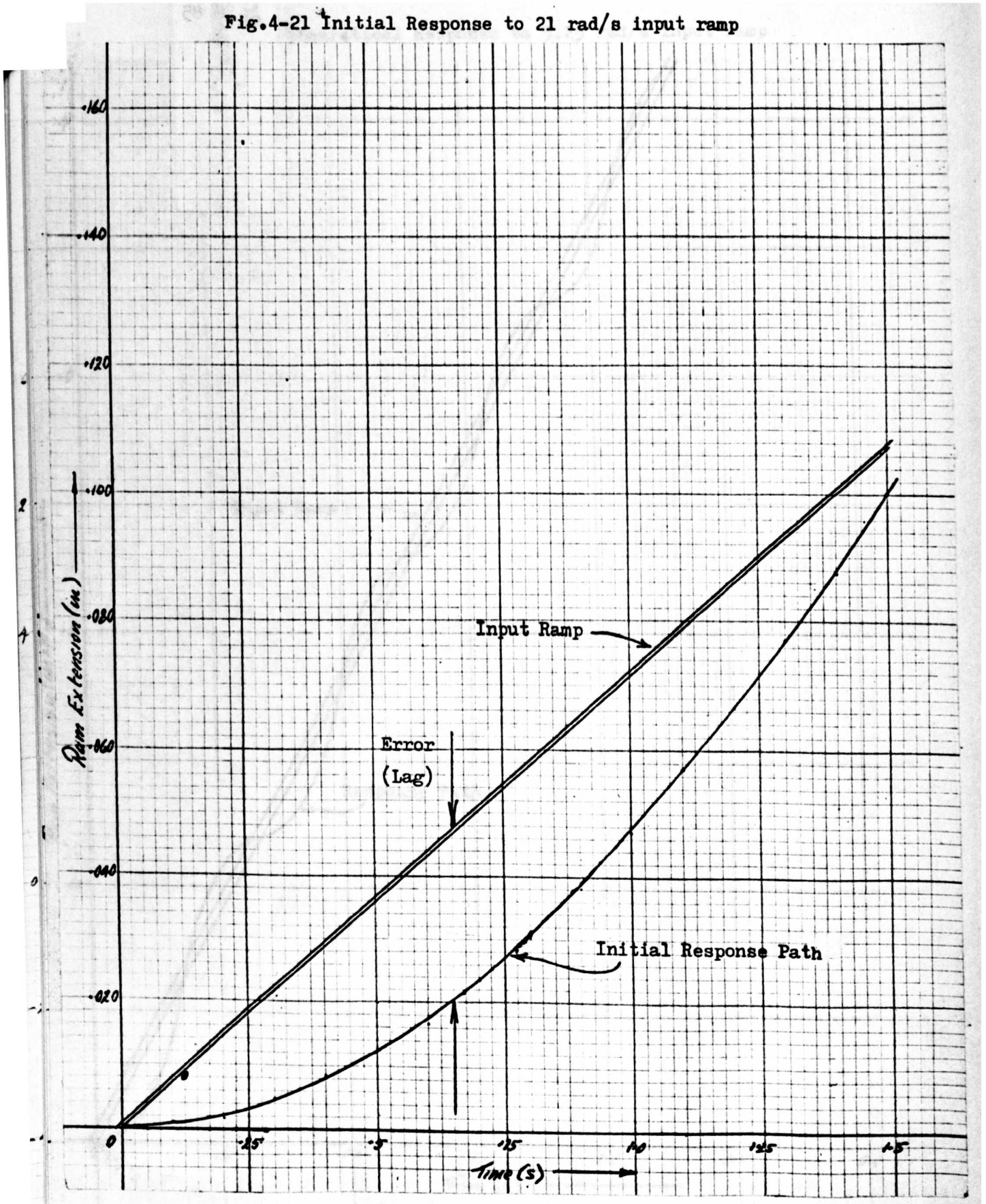

Table 4.6 Theoretical mean lag errors

Input Ramp Gradient (rad/s)	Maximum Amplitude after 5th. Oscillation (in)	Mean Lag (in)
5.250	0.0010	0.0005
10.500	0.0025	0.0013
21.000	0.0035	0.0018

As may be seen from the theoretical response curves given in Figs. 4-18, 4-19 and 4-20, the response path oscillates about the input ramp, and the maximum lag error generated tend to decrease with time. These maximum lag errorsare plotted against oscillation number in Fig.A2-3, from the values in Table A2.5, Appendix 2, and the above values for'Maximum amplitude after 5th oscillation'in Table 4.6, are taken from Fig.A2-3. The mean lag error is then deduced by assuming that it is one half the maximum error.

Fig.5-1 Schematic Diagram for Response Tests on the Digital Servomechanism

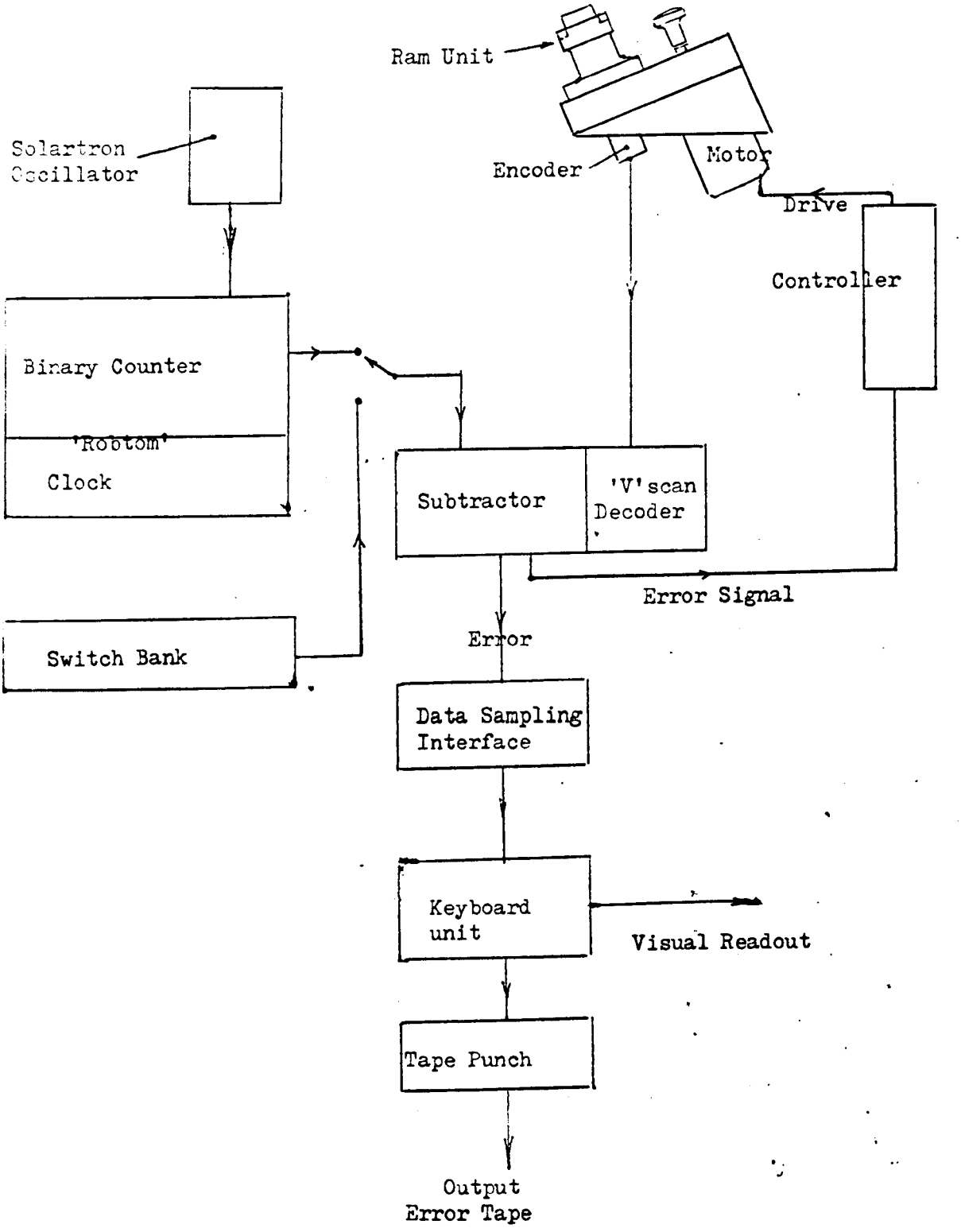

SECTION 5 : Response Tests on the Digital Servomechanism

The procedure adopted for testing the response of the digital equipment was similar in principle to that employed for the hydraulic system already described in Section 3. The system was subjected to a series of known input signals, and arrangements were made to measure and record the system lag and positioning errors.

Since the equipment employs digital command and position feedback signals, the arrangements for input signals and also the recording of errors, had to be digital in nature. A schematic diagram of the set-up used to carry out these tests is shown opposite in Fig.5-1, from which it may be seen that three additional items of equipment were employed. Since it was very easy to test the system for response to step type input functions this was also included in the work, even though this type of input signal would never be applied in practice.

As with the hydraulic servo, the type of input signal for which the system has to be tested is the ramp function, and both forward and reverse response is required. Since commands to the digital servo take the form of 12-bit parallel numbers in binary code, suitable ramp input functions may be generated by means of a binary counter unit. Hence forward ramps correspond to an increasing count, whereas reverse ramps may be simulated by a decreasing count. In addition the counting rate provides a measure of the ramp gradient.

Step type input functions are formed simply by the application of a parallel binary number to the subtractor, and since provision

already exists for this facility on the prototype control cabinet, such tests are included in this work.

A series of suitable ramp and step inputs was then applied to the input at the control cabinet, and records were made of the error signal generated by the subtractor element of the system, as the electrically driven ram followed the prescribed command. For convenience the gear-box element was removed from the lathe for these experiments, and as the error signal was found to vary so rapidly during each run, the results were recorded automatically on punched paper tape.

Due to the delay introduced by the time taken to punch out a given error, it was not possible to provide a continuous readout of the error signal, and a data sampling technique was therefore adopted. The sampling period employed was governed by the punching speed of the tape equipment.

In addition, the tape punch equipment which was obtained for another project, operates at a different voltage level from the digital servo, and it is also relay operated. It was not possible therefore to drive the tape punch directly from the output of the subtractor unit, and an interface had to be provided. This requirement, together with the above mentioned data sampling need, was therefore overcome by the introduction of a specially built data sampling interface unit. This unit was controlled by a 'clock' circuit which is described later, together with the method for establishing the 'on' time of the unit.

From the punched tape output, a series of tables of results was

Fig.5-2 The 'Robtom' logic planning machine employed in the digital servo response tests

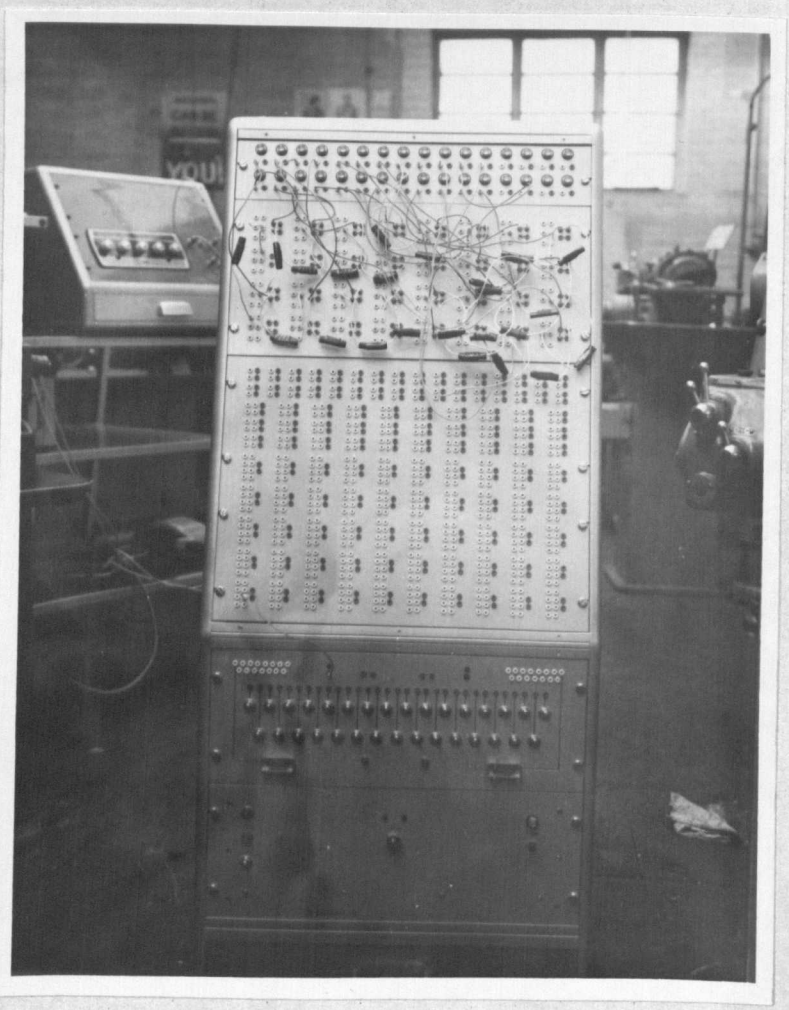

drawn up, and these are included in this thesis in Tables A3.1 to A3.13 in Appendix 3. Response curves were then prepared from the tabulated errors, and these are also included in Appendix 3, in Fig.A3-1 to A3-18.

Input Functions

In Fig.5-1 reference is made to a machine which is know as 'Robtom', and which is used in these tests to provide the required input ramp functions and also to opearte the data sampling interface unit. This machine which is illustrated opposite in Fig.5-2 was designed by the author and two co-workers in 1966, and its description was published in that year (Ref 9 Section 9).

'Robtom' is best described as a solid state logic planning machine, designed to assist research workers in the fields of control and computing. It was developed from the small logic tutors employed to train engineers in logic design, and provides a large number of elements which may be coupled together by the well established patching technique using the sockets provided on the front panel. In addition to standard NOR logic elements, the machine is provided with a number of bistable circuits, and also some input and output devices. A suitable power supply is built into the base of the cabinet, and the panels of logic elements are detachable, so that they may be replaced with panels of other elements as required.

Housed in a 36-in tall sloping front cabinet, the machine has a drawer for patching cords at the bottom, and the remaining vertical

portion of the cabinet by the 10 volt stabilized d.c. power supply, and the input switch panel. This last mentioned panel carries two push button switches, 31 tumbler switches and a pair of 15-way miniature sockets whereby external equipment may be connected to the machine. All connections from the switches and sockets are brought to patching sockets at the front of the panel to give maximum versatility.

The larger panel on the sloping front of the machine carries the main NOR logic in the form of 112 separate elements: 32 single input, 30 twin input and 50 four input gates. In each case the input and output connections are brought to patching sockets on the panel. Silicon planar transistors are employed and the circuit diagram for a twin input NOR element is given below in Fig.5-3.

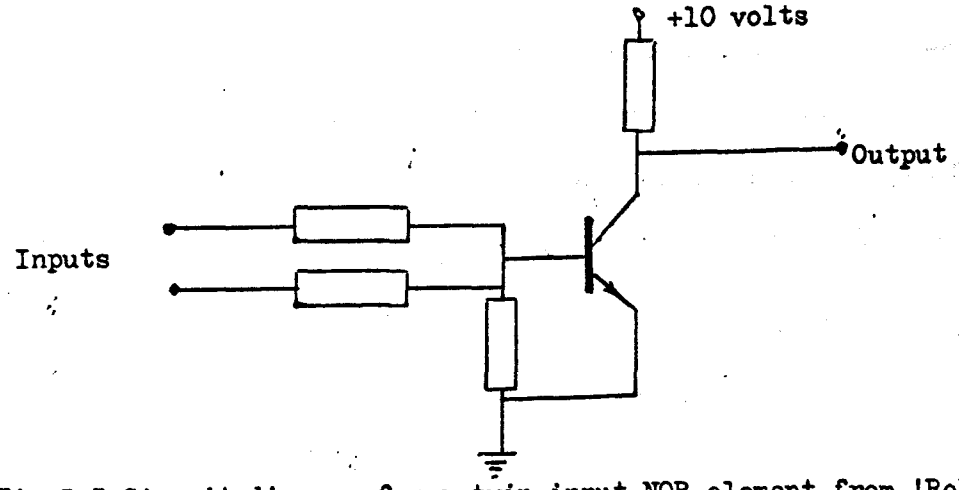

Fig.5-3 Circuit diagram for a twin input NOR element from 'Robtom'

The panel above the main logic unit is provided with 32 bistable circuits in four rows, each having two d.c. inputs, two outputs and a separate a.c. input, the latter being employed when the machine is to be operated as a counter.

A circuit diagram for one of the bistable elements is given below in Fig.5-4

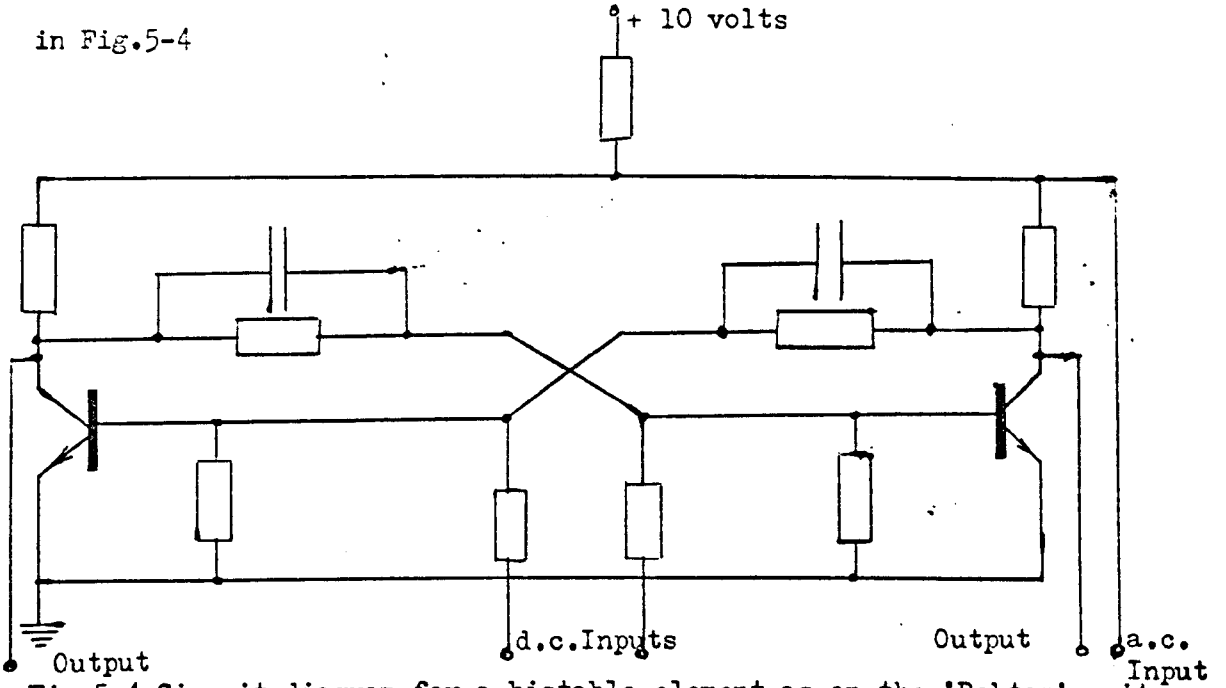

Fig.5-4 Circuit diagram for a bistable element as on the 'Robtom' unit

Output from the machine takes the form of two rows of signal lamps, 16 red and 16 green, each being fitted with a drive amplifier. Patching sockets are provided at both the input and the output of the drive amplifiers, so that they may be used as additional single input NOR elements if necessary. The circuit diagram for a drive amplifier and lamp is given below in Fig.5-5.

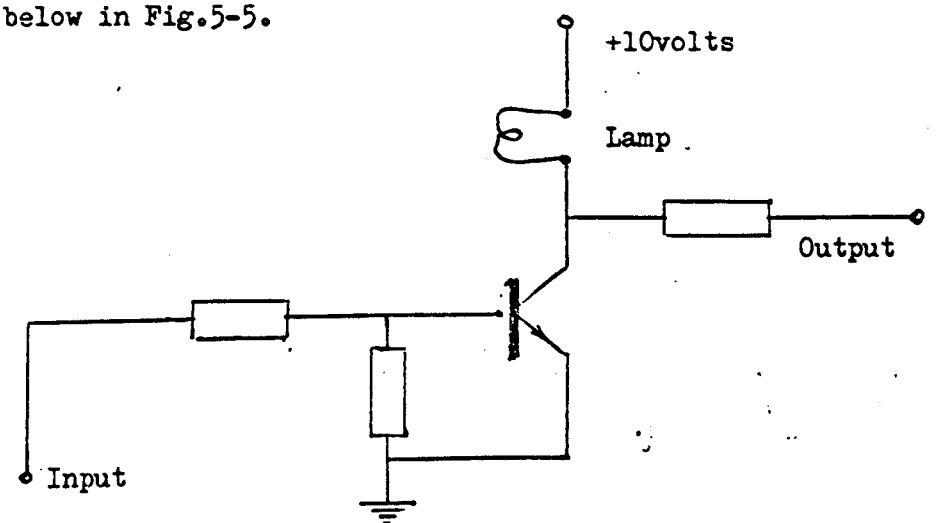

Fig.5-5 Circuit diagram for lamp and drive amplifier from 'Robtom'

In order to set up the 'Robtom' machine to operate as a binary counter it is necessary to couple a number of bistable elements in series as shown below in Fig.5-6. From this diagram it may be seen that the connection is made from the output of one stage, through a small coupling capacitor to the a.c. input of the subsequent stage. The output is then taken from either output of each stage, depending on requirements, ie. decreasing or increasing count and convention adopted.

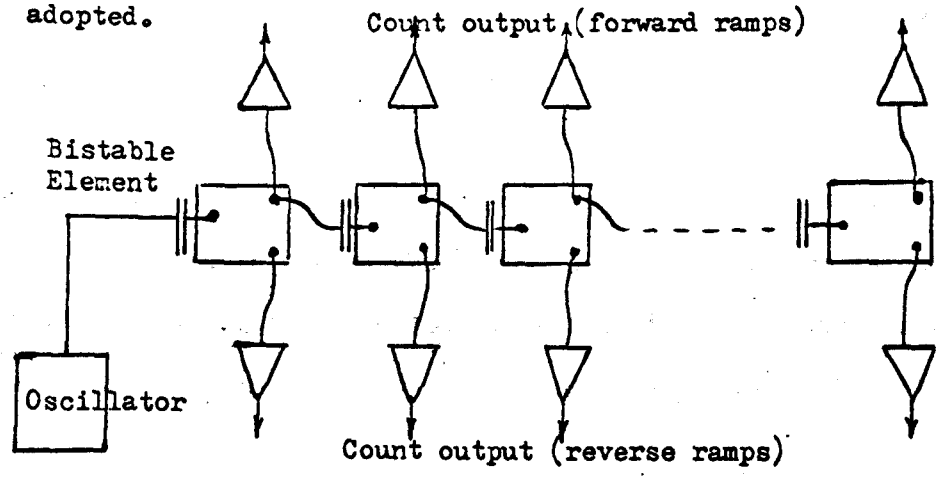

Fig.5-6 Arrangements for patching bistable elements to form a binary counter

The outputs are then patched to the input sockets of the drive amplifiers located on the panel above, and the associated signal lamp signifies the state of the bistable elements to which it is connected. A series of lamps so coupled will therefore show a binary count if the first bistable element in the chain is supplied with a regular pulse of suitable magnitude, since each bistable element halves the frequency of the signal which is driving it.

In this particular application, a problem was presented by the fact that the logic in the 'Robtom' machine employs silicon transistors

which are operated from +10 volts, whereas the logic in the subtractor unit of the servomechanism uses germanium transistors supplied from -15 volts. It was necessary that the output from the counter should form the input to the digital servo, and this end was achieved by coupling the +10 volt line on 'Robtom' to the 0 volt line on the servo power supply. In this way, zero outputs from 'Robtom' acted as negative pulses on the servo input at a level of - 10 volts. It was then only necessary to change the convention adopted for the counter, so that when one stage was off this in fact corresponded to a count. The resulting effect is a phase change, which is easily accommodated by taking the counter output from the opposite side of each bistable element to that connected to the signal lamps. Hence when a lamp is on on 'Robtom' indicating a count, the output socket of the associated drive amplifier falls to 0 volts, which the subtractor accepts as a -10 volt drive signal.

In this manner a 12-channel binary counter was patched up on the 'Robtom' machine, the first stage being driven by a Solartron variable frequency R-C oscillator. The output frequency of the oscillator could be set between 10 Hz and 1 MHz, and the amplitude of the signal could be varied from 0 to 20 volts. Although the output from the oscillator was sinusoidal, only about 1 volt was required to operate the bistable elements, and the unit therefore drove the counter satisfactorily with its output level set at + 10 volts. The input ramp gradient was set by adjusting the frequency of the R-C oscillator, and values were chosen to provide comparable ramps to those employed for testing the response of the hydraulic servo in Section 3.

Ramp Gradient

In the series of tests carried out on the hydraulic servo, the worst case considered was that due to negotiating a 90° shoulder for forward ramps, and a 30° reducing taper for reverse ramps. The former case requires that the tool slide should retract at twice the saddle velocity, whereas the latter condition is simulated by moving the slide towards the lathe axis at the same speed as the selected saddle traverse rate.

As indicated the actual value of ramp gradient depends on the saddle velocity required, and in the hydraulic tests, Section 3, two saddle velocities were employed, in addition to three template regions which gave rise to the following input conditions:

Normal feed	+ 4 in/min
	+ 2 in/min
	- 2 in/min
Rapid feed	+ 25 in/min
	+ 12.5 in/min
	- 12.5 in/min

These values being corrected to the nearest .5 in/min.

Each bit on the digital servo is equivalent to a ram extension of 0.000489 in, or very nearly 0.005 in, hence an input ramp to simulate slide motion at 1 in/min, would be provided by a binary count with the rate of change of the least significant digit of 2048 bits per minute.

Since in this application we have a binary counter circuit which is driven from a variable frequency oscillator, the output from which produces a two bit change for each cycle, the frequency in Hz required to simulate a 1 in/min ramp is :

$$\text{drive frequency} = \frac{2048}{60 \times 2} \text{ Hz}$$

Step Inputs

As described in Section 2, the control cabinet of the digital servomechanism is fitted with a bank of tumbler switches, which forms the input system for the prototype equipment. By setting up a binary number on this switch bank, it is possible to supply an input command to the servo which is very close to a step function.

For this purpose, in this part of the tests, the 'Robtom' machine was disconnected from the input of the subtractor, and replaced by the normal input connection from the switch bank. The ram was then extended to 0.5 in from its zero datum position, and the switch corresponding to a further 1-in extension was depressed. As the ram moved to its commanded setting, the errors generated were recorded using the equipment in Fig.5-1. Similarly by switching off the command a reverse step was simulated.

Stylus Loading

In operation the ram unit will be in contact with the copying stylus of the Harrison hydraulic servomechanism, and as my be seen in Section 1, this results in a load equivalent to the spool valve return

spring load, being applied to the end of the ram. In these tests the gearbox unit was removed from the lathe, and it was therefroe necessary to simulate this stylus loading. In addition since in Section 3, three different values of spool valve return spring load were employed, it was necessary to simulate each of these values. For these tests, the gearbox unit was mounted on a bench with the ram axis aligned vertically, as shown below in Fig.5-7. It was found that the ram itself weighed 0.50 lbf, and hence the vertical mounting simulated 0.5 lbf stylus loading. For the remaining values weights were manufactured, and positioned on the top of the ram during the relevant test runs.

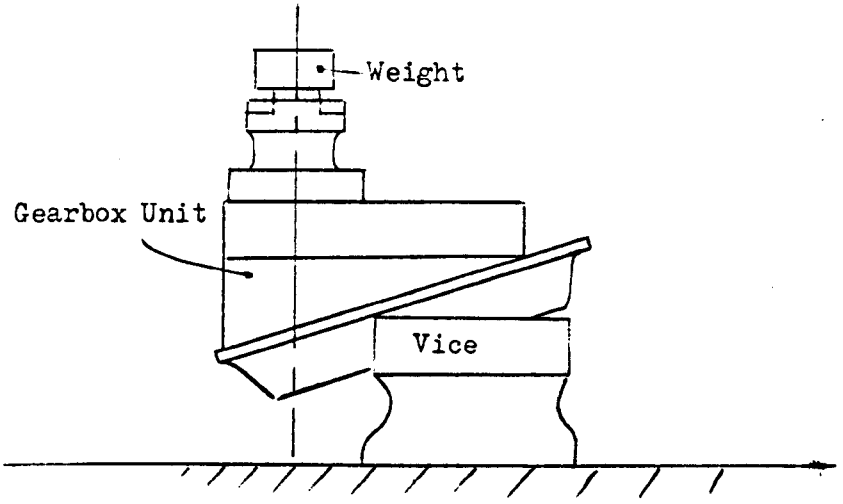

Fig.5-7 Arrangements for simulating stylus loading

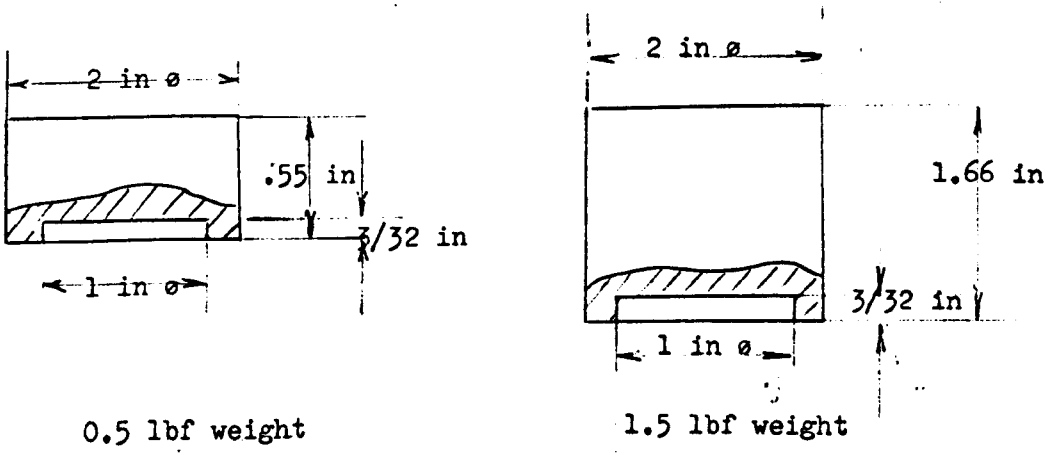

Fig.5-8 Weights used to simulate stylus loading

Fig.5-9 The A.P.T. Equipment used for recording errors during response tests on the digital servomechanism

Data Handling

As the digital servo responds to the error signal generated by subtracting the position feedback signal from the input function, a visual readout of the instantaneous error is displayed on a row of 12 amber signal lamps, with a thirteenth lamp indicating the sign of the error. During a given response the error signal is liable to change rapidly, and it is not possible to write down the changes. For this reason it was decided to arrange for the error to be recorded automatically during each test run.

A suitable machine was available for recording the error automatically, when generated during the testing, the equipment having been obtained as tape preparation units for the numerical control project mentioned in Ref.5, Section 9. Comprising two units, the tape preparation equipment was built by Automatic Punched Tape, Ltd., and is illustrated opposite in Fig.5-9. It includes a standard 8-hole tape punch, coupled to a special binary keyboard.

The special design of the keyboard arises from the requirements of the numerical control project, whereby it is convenient to set up two 12-bit binary words at the same time. This information is then automatically punched out on three successive characters on the tape. This function is carried out by relay logic, and a uniselector mechanism, housed in the keyboard unit, this latter member serving to operate the tape punch three times in rapid succession. The first punching action deals with the first 8 bits of one of the 12-bit

commands, the next character on the tape contains the last four bits of the first command and the first four bits from the second command, whereas the third character in the series covers the remaining 8 bits from the second command.

This machine was made to operate entirely automatically, by connecting each terminal setting buttons to a 25-way socket mounted on the front of the keyboard unit. For normal operation, the operation of a setting button connects together two leads which in turn actuate a relay. By bringing these leads to an external socket, it was possible to connect each pair of leads automatically, including those leads which control the tape punch unit.

A further modification was necessitated by the fact that during normal operation, the relays controlling the punch are arranged to lock on until the uniselector has operated three times. In this application, this would have resulted in the maximum number of '1's being recorded all the time, and this locking system was therefore removed. For example, in the event of the signal 101 changing to 010 the number recorded would be 111, since all three relays have been energized. It is still, however, necessary to lock on the numeral relays during the action of the tape punch, and this was effected externally in the data sampling interface unit.

The stated punching time for the tape punch unit is 100 ms, and since in this application three characters are punched in succession and a uniselector is used to drive the unit, a time of 400 ms was necessary to print out an error statement. This time was in fact

Fig.5-10 Circuit diagram of the Data Sampling Interface

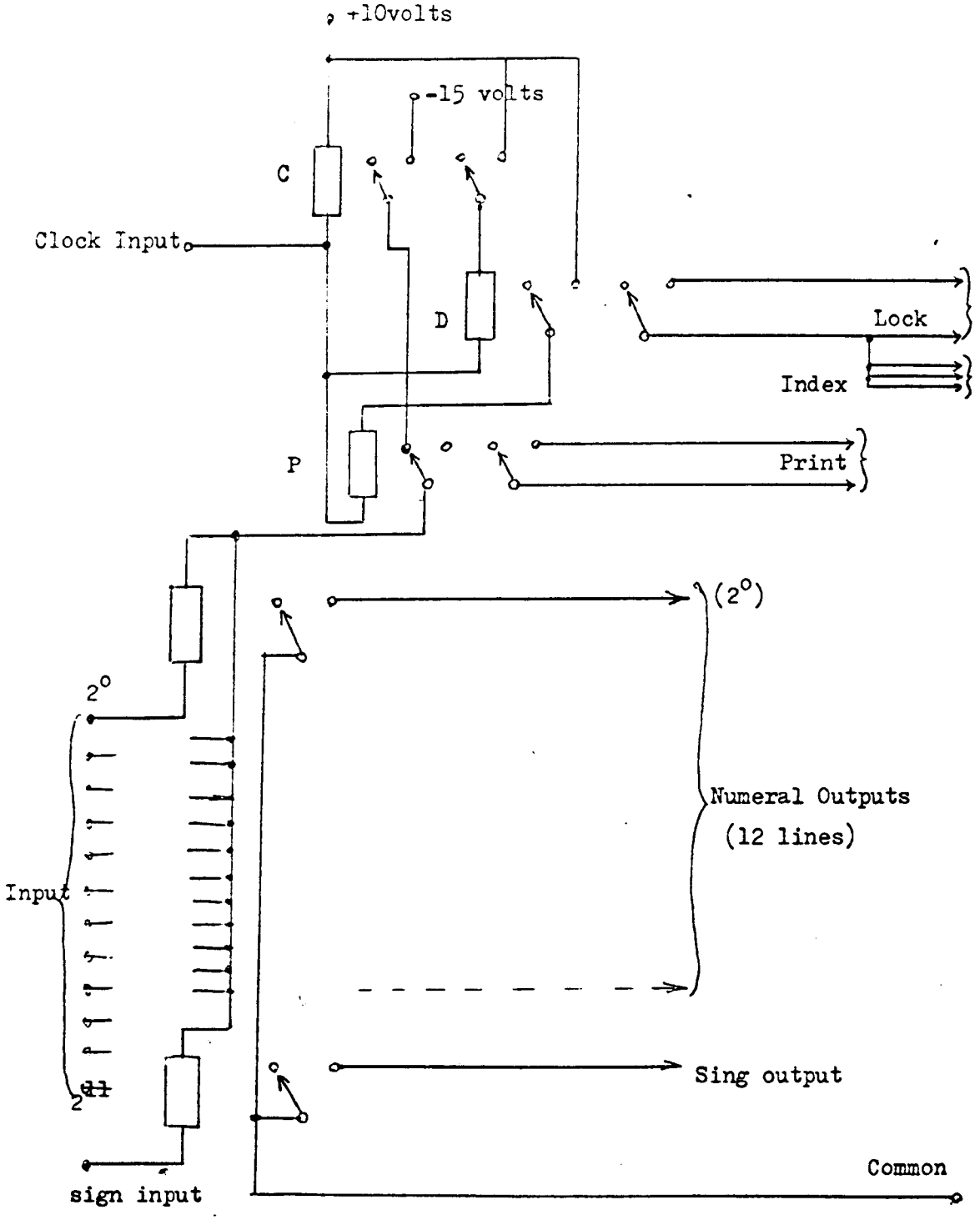

determined by experimental trial. The time lag necessary to operate the tape punching equipment necessitated the development of the data sampling interface and its associated driving clock.

Data Sampling Interface Unit

In order to link together the 12-bit error signal supplied by the subtractor of the servomechanism to the equipment which had been adapted to record the error automatically, a unit was built which sampled the error signal periodically. At fixed intervals, this unit provided a command to the tape punch which caused it to print out the error as it stood at the instant of command. During printing the sampling action was arrested, and the frequency of printing was set as high as possible within the limits of the tape punch.

The keyboard unit employs relays operated at a level of 50 volts, and since the uniselector which is an essential part of the equipment, also operates at 50 volts, it was decided to use relays in the data sampling unit. This decision provides for the isolation of the voltage level in the A.P.T. equipment from the -15 volt level of the subtractor output, and also results in a convenient method of cutting off the sampling action during print out.

A small unit was therefore built to carry a total of 16 miniature 15-volt relays, and the circuit for this unit is shown opposite in Fig.5-10. In operation this equipment is actuated by signals from the subtractor, which drive the coils of the numeral and sign relays, and also from the clock circuit on the 'Robtom' machine which

is described later. When a numeral relay is energized in the interface unit, its contacts short out the relevant keyboard relay circuit, thereby setting up the information on the keyboard which provides a visual readout by means of signal lamps mounted inside the setting buttons.

Unfortunately the operation of any key causes any subsequent key to lock on. This effect, together with the fact that the least significant bit in each character (binary '1') is used as a marker on the tape, these keys being shorted at each sampling, made it absolutely essential to sample the error for an instant only. If the keyboard unit is permanently coupled to the error output from the interface unit, a completely false signal results.

In order to achieve instant sampling, the numeral relays are only connected to the -15 volt line for a short period. Drive pulses from the clock circuit are fed to the coil of the clock relay (C in Fig.5-10) and the contacts of this relay are used to connect the numeral and sign relays to the -15 volt line thereby initiating the sampling period. The remaining contacts are used to energize the delay relay (D in Fig.5-10). This relay has two sets of contacts, the first being used to energize the keyboard locking on facility, and the second set are employed to actuate the print relay (P in Fig.5-10). As its name implies, relay P shorts the print button circuit thereby actuating the tape punch, and its spare contacts break the connection between the numeral and sign relays and the -15 volt line, which ends the

sampling period. The length of the sampling period employed was the time taken for these three relays to operate in series, about 30 ms.

It was found that this system operated extremely satisfactorily provided that the clock frequency was not too high. At high clock frequencies, sampling periods were initiated during an incomplete punching cycle from the previous sampling. If the errors in the two sampling periods concerned differed, the signal to the tape punch would change while the unit was operating which would cause it to jam.

Clock Circuit.

It was decided to employ a free running multivibrator circuit as the clock for these tests, since a suitable unit could be rapidly patched up on 'Robtom'. The circuit used is shown below in Fig.5-11, and by changing the values of coupling capacitors, C_1 and C_2, it was possible to achieve suitable frequencies and pulse shapes.

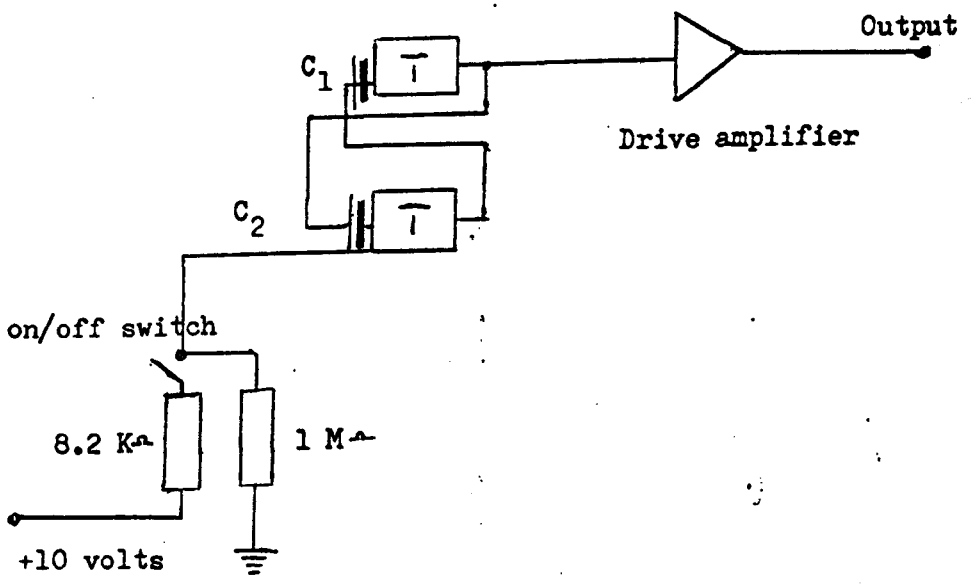

Fig.5-11 Circuit diagram for the clock.

It was found that suitable conditions were achieved when the capacitors were set at 4 and 8 μF respectively. In addition, the 'Robtom' machine also afforded the facility of switching the clock on and off, and the output from the clock was fed to the data sampling interface unit through one of the drive amplifiers on the top panel of the machine. Hence the associated signal lamp produced flashes in time with the clock.

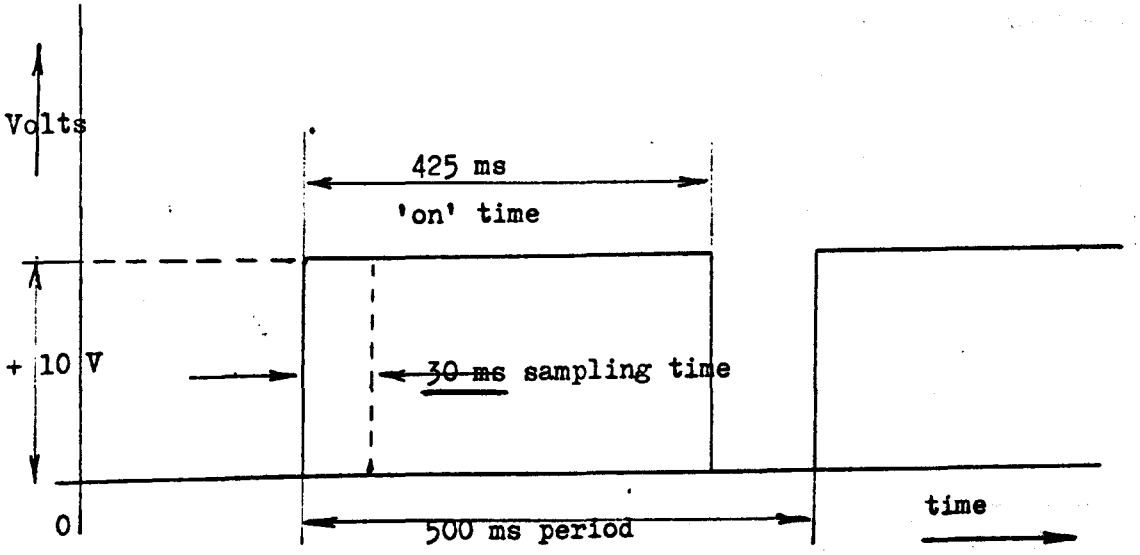

Fig.5-12 Clock pulse shape.

Fig.5-12 shows the pulse shape, which is the output from the clock amplifier supplied to the coil of the clock relay on the data sampling interface unit. It will be seen that the frequency of the clock was 2 Hz, but that the 'on' time was 425 ms., to give the punch unit time to complete its cycle. The amplitude of the clock output signal was +10 volts, and it was switched off by connecting 10 volts to one side of the multivibrator by means of a tumbler switch.

In drawing the error curves it is necessary to know the frequency of the clock pulse, since this establishes the relationship between sampling instants. This measurement was made by driving the counter for a known period from the clock instead of the Solartron oscillator, and taking readings at the counter output before and the timed period. Subtracting these two binary numbers establishes the number of pulses delivered by the clock, and the timing period was set at 100 s. to ensure a high degree of accuracy. The actual results obtained were:

Counter output at start = 000000100001

Counter output at finish = 000011100111

count = 198

≑ 200

Period = 100 s., hence

clock period ≑ 500 ms.

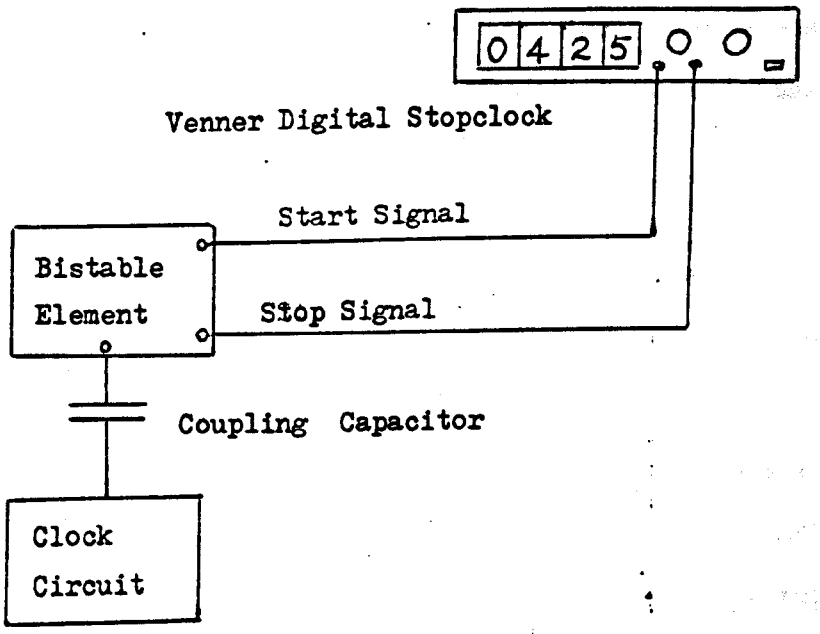

Fig.5-13 Arrangements for measuring clock pulse length.

In order to ascertain the clock pulse length, a different method was employed, and the circuit used is shown on the previous page in Fig.5-13. Use was made of a Venner Millisecond Stopclock for this measurement, which was switched on by a positive pulse and off by a similar pulse fed to another input socket.

The output from the clock circuit was therefore fed via a coupling capacitor to the a.c. input of one of the bistable elements on the 'Robtom'. Outputs were then taken from each side of this element so that the clock pulse leading edge put the element in a state which started the stopclock, and the end of the pulse changed the state of the element which stopped the stopclock. The time interval between these two signals was shown digitally on the screen of the Venner unit, and since this device is fitted with an automatic reset facility, it was possible to run the clock for a long period and to observe a series of readings on the stopclock thereby enabling an average determination to be made. The result of 50 such observations indicated a clock pulse length of 425 ms.

Output Tape Format.

Since a large number of readings results from a series of ramp inputs and a data sampling period of 500 ms., it was decided to employ a special tape format. The tape punch equipment as previously described is arranged to print out three characters in succession, and each of these characters is in plain binary code, the associated keys being so marked on the keyboard unit. The large number of errors resulting from the series of test runs would result in difficulties in reading

the tape unless some provision is made to indicate on the tape when an error has in fact been recorded. It was decided to employ the position 1 in each character as a parity check to achieve this end.

The maximum possible error that the system can have may be expressed as a 12-bit binary word so the remaining seven holes in the first character, and five holes in the second character, are used to carry this information. In addition, the sign of the error signal was indicated by the presence of absence of a hole in the tape at the most significant position in the third character of the series. A hole in the tape indicated a positive error or lag in the case of increasing ramps and vice versa. A diagram showing the output tape format employed is given below in Fig.5-14.

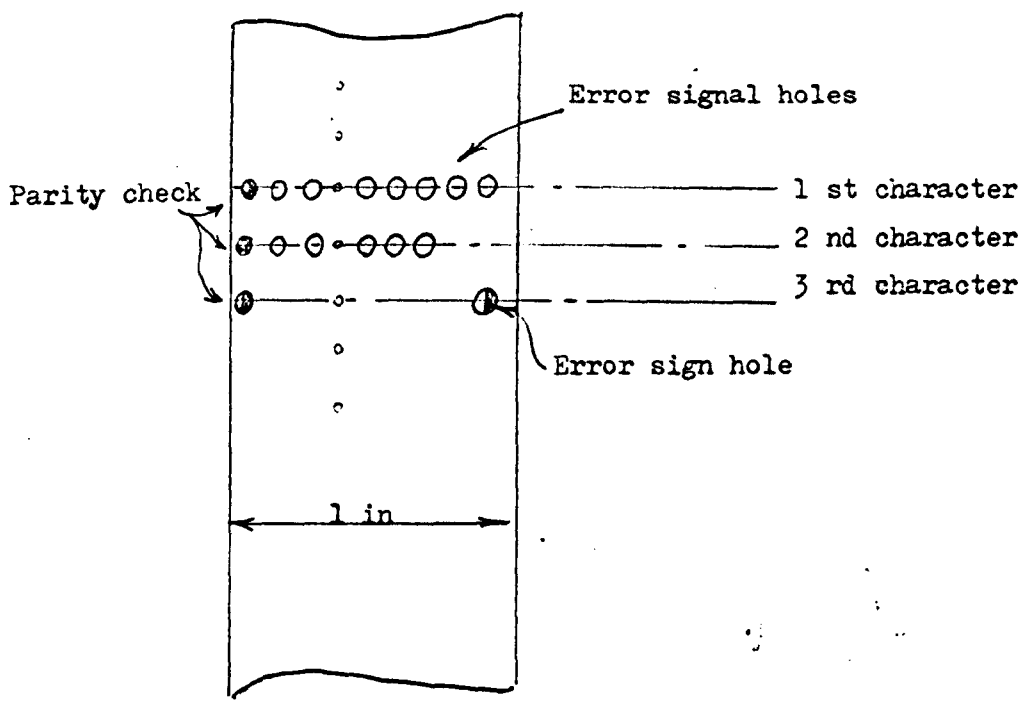

Fig.5-14 Error tape format employed.

Results

Results for the tests carried out were recorded on 18 punched paper tapes, and it was found more convenient to read these tapes by eye since the computer available was not fitted with tape reading equipment.

Detailed records of these results are not included in this thesis in the interests of space saving, but the curves of error v time which were obtained from them are included in Appendix 3. The error curves for step input functions are given in Figs.A3-6 to A.3-11, and the results for ramp input functions are given in Figs. A3-12 to A3-23.

From each curve the value of the mean position error e* was deduced by drawing a line on the associated graph. Values of e* were tabulated for the various input conditions and also for the stylus loadings employed. Table 5.1 gives the mean position error at a constant stylus loading of 1 lbf, whereas 5.2 provides information at various stylus loads for all the input functions.

Ramp Rate in/min	Ramp Number	Mean Error e* in
+ 25	10	.1875
+ 12.5	11	.1750
+ 4	7	.0035
+ 2	8	.0025
- 2	9	.0035
- 12.5	12	.1750

Table 5.1 Mean lag for stylus load of 1 lbf

Fig. 5-15 Response curve for the digital servomechanism
1 lbf stylus load.

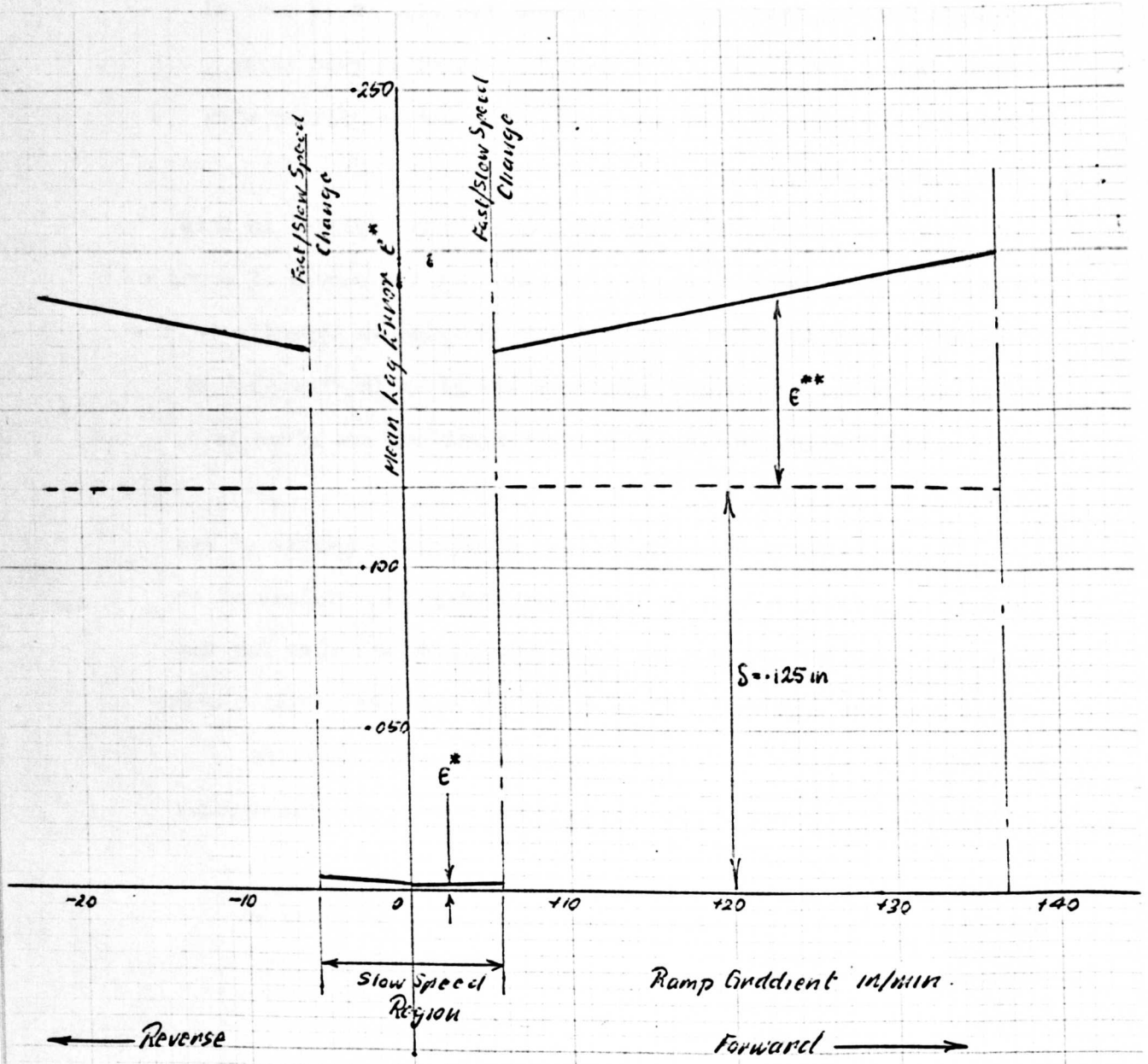

Ramp Rate in/min	Ramp Number	Stylus load lbf	Mean error e* in
+ 4	13	.5	.0035
+4	7	.5	.0035
+ 4	16	.5	.0035
+ 2	14	1.0	.0025
+ 2	8	1.0	.0025
+ 2	17	1.0	.0025
- 2	15	2.0	.0035
- 2	9	2.0	.0035
- 2	18	2.0	.0035

Table 5.2 Mean lag at various stylus loads.

The input parameters employed for the ramp numbers listed in Tables 5.1 and 5.2 are given in Appendix 3 Table A3.2.

The resulting performance curve is shown opposite in Fig.5-15, this graph being prepared from the values of mean lag error given in Table 5.1 on the previous page (1 lbf stylus load). A description of the preparation of the performance curve is included in Appendix 3.

Fig.6-1 Diagram of the modified gearbox unit.

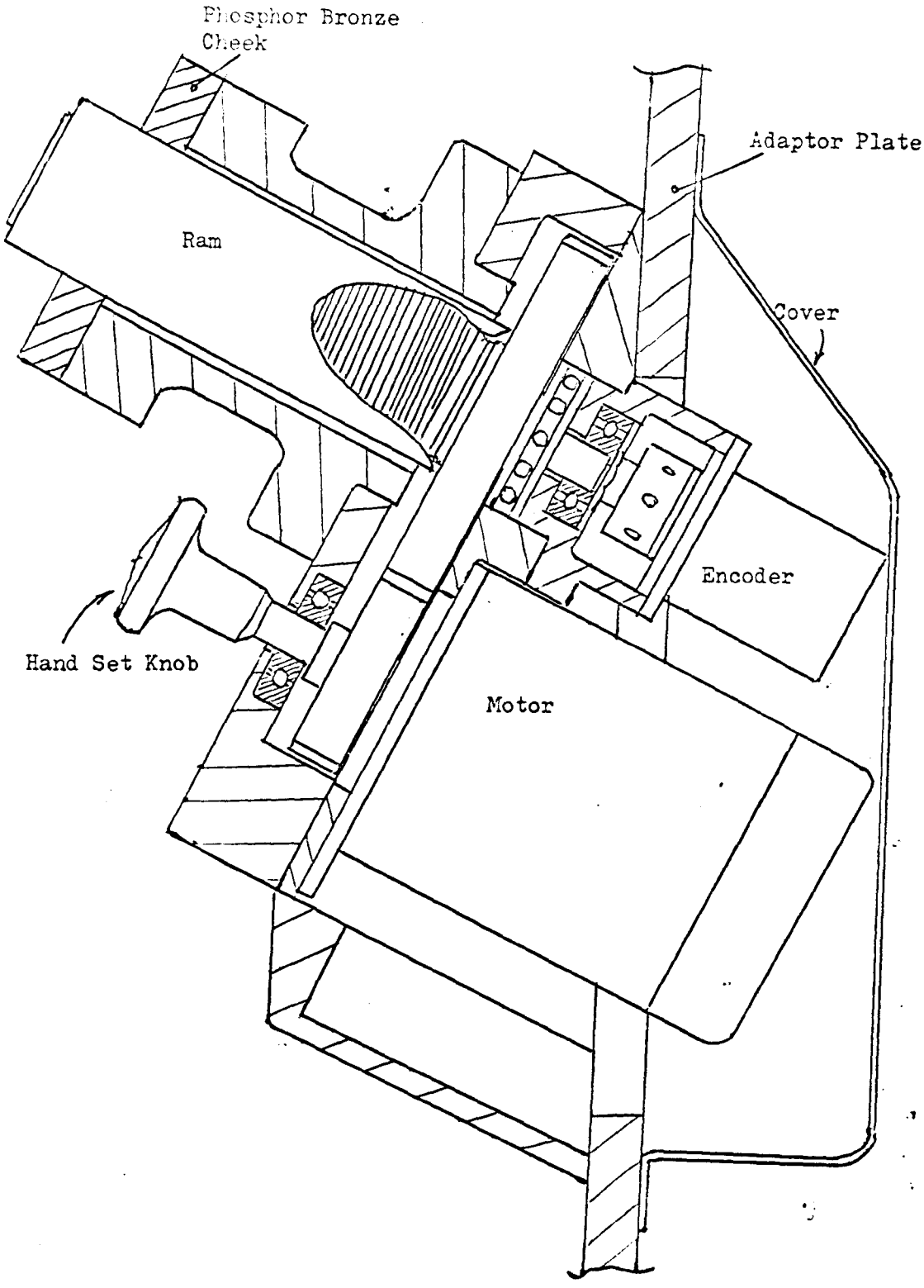

SECTION 6 : Mounting the digital servomechanism on the lathe

In the previously mentioned papers (Ref.5 - Section 9) the gear box unit described was a prototype mechanism to test the principle of the system. It was fitted with a universal electric motor which was available at that time, and no attempt was made to design the gear-box casing so that it could be adapted to fit any particular machine. In addition, the end of the ram was designed for mounting a dial indicator in order to facilitate positional accuracy tests.

In order to adapt this mechanism so that it could be mounted on the saddle of the L.6 lathe, it was necessary to redesign some of the components, and also to fit a smaller and more powerful electric motor. Fig.6-1 opposite is a cross sectional drawing of the modified unit showing the mounting of the motor and the shaft encoder, and a view of the unit with the rear cover removed is shown below in Fig.6-2.

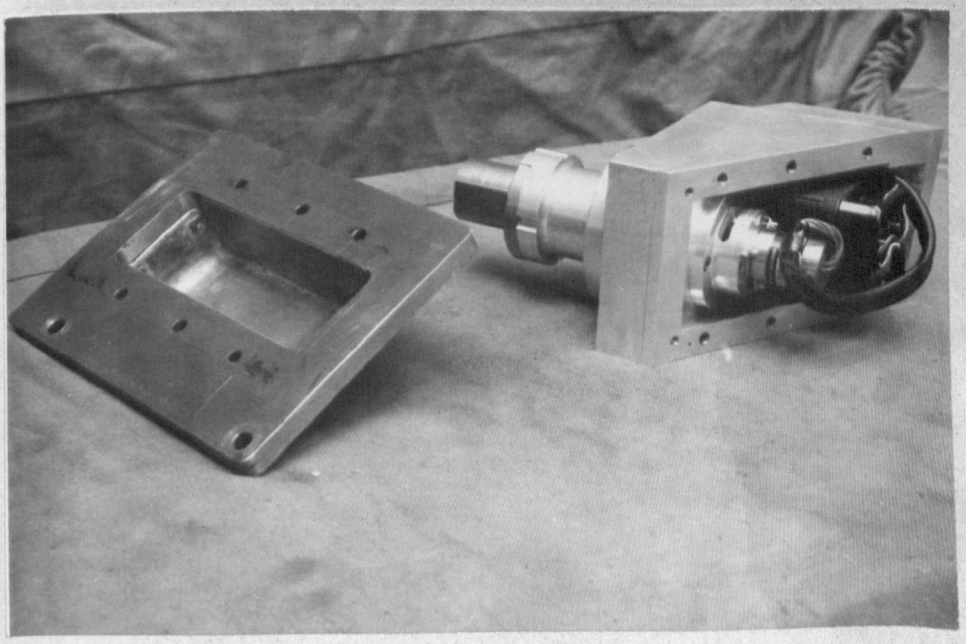

Fig.6-2 View of the gearbox unit with cover plate removed.

Fig.6-4 Modified gearbox casings.

(cross section)

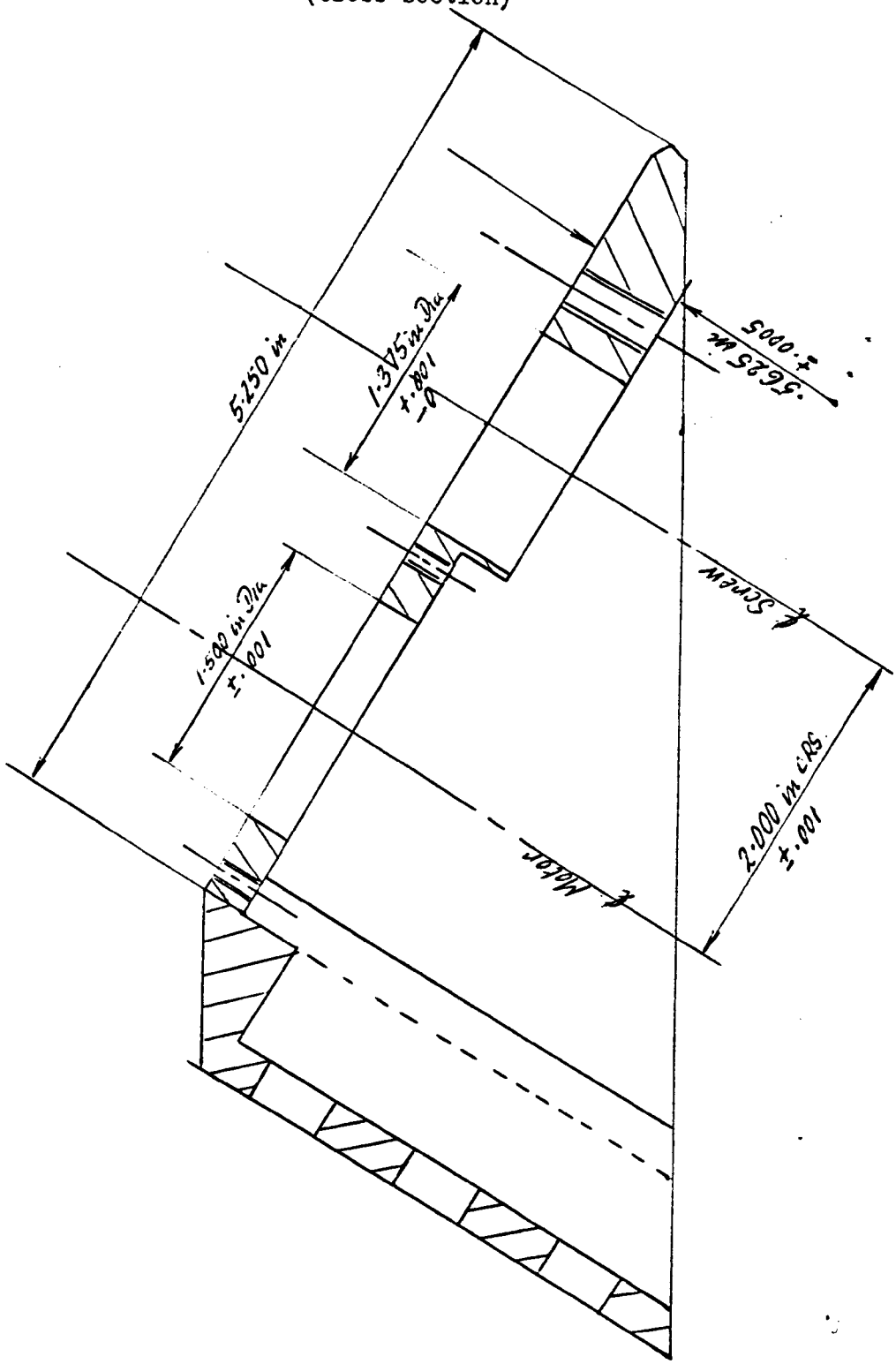

After removing the 'T' slotted member that carries the template centres at the rear of the lathe bed, a steel plate was machined and fitted to the rear of the saddle. A drawing of the plate is shown below in Fig.6-3.

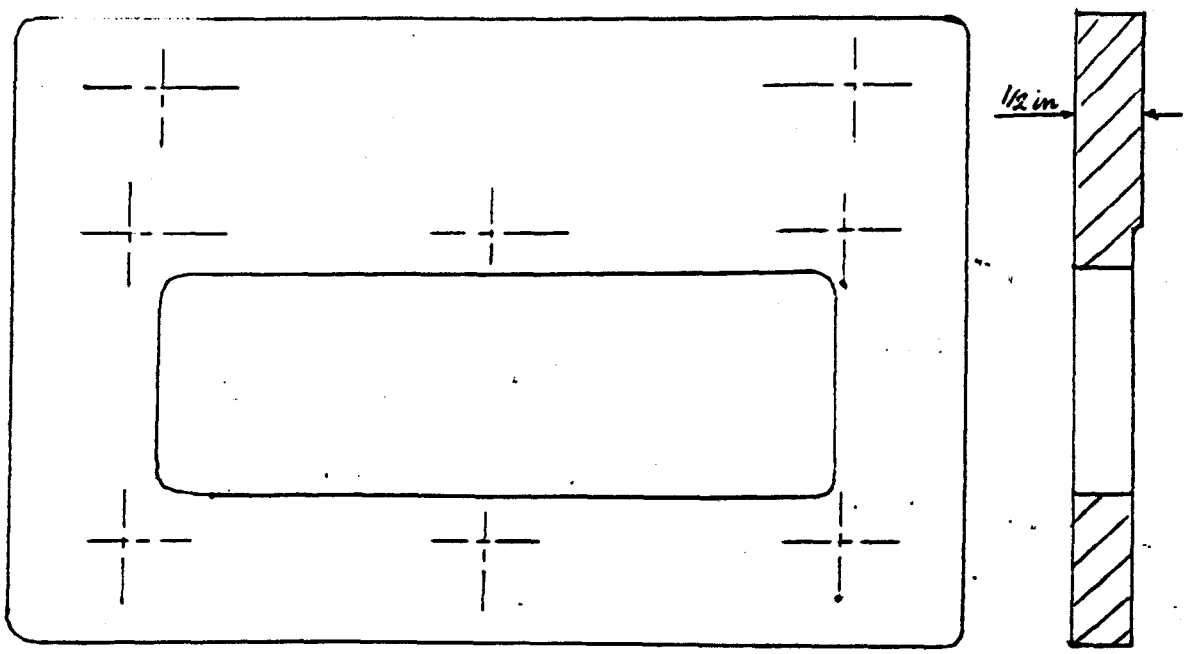

Fig.6-3 Adaptor plate for gearbox unit.

Since the copying slide of the Harrison lathe is angled by 30° from the cross slide axis, it was necessary for the ram axis of the unit to be aligned by a similar amount. This end was achieved by re-designing the gearbox casings, the drawings of which are provided opposite in Fig.6-4.

Photographs showing two views of the modified gearbox unit mounted on the lathe saddle are given on the following page in Figs. 6-5 and 6-6.

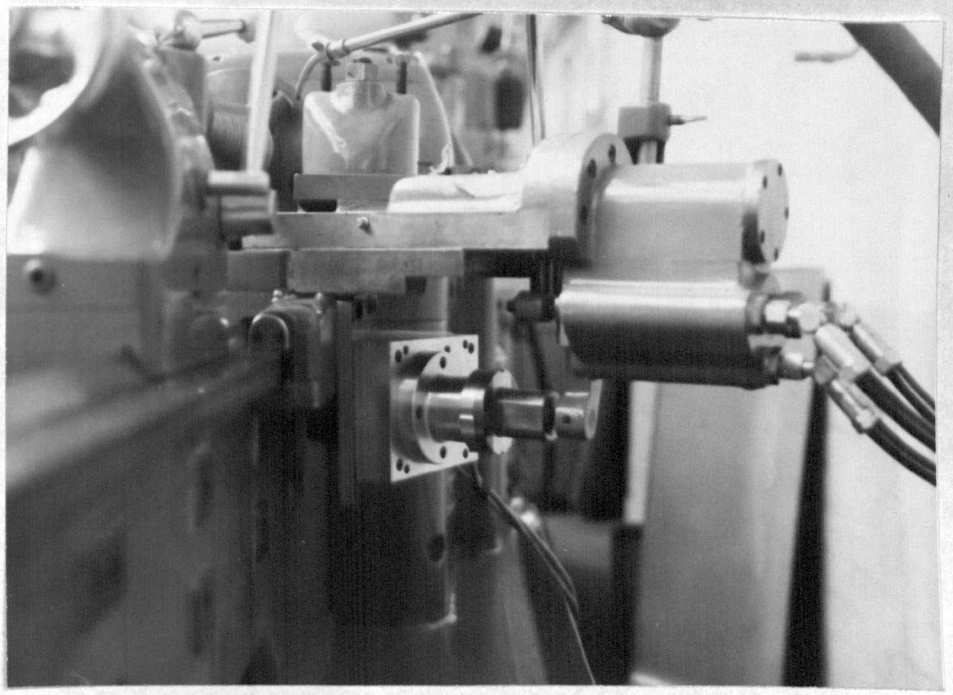

Fig.6-5 Gearbox unit viewed from tailstock end.

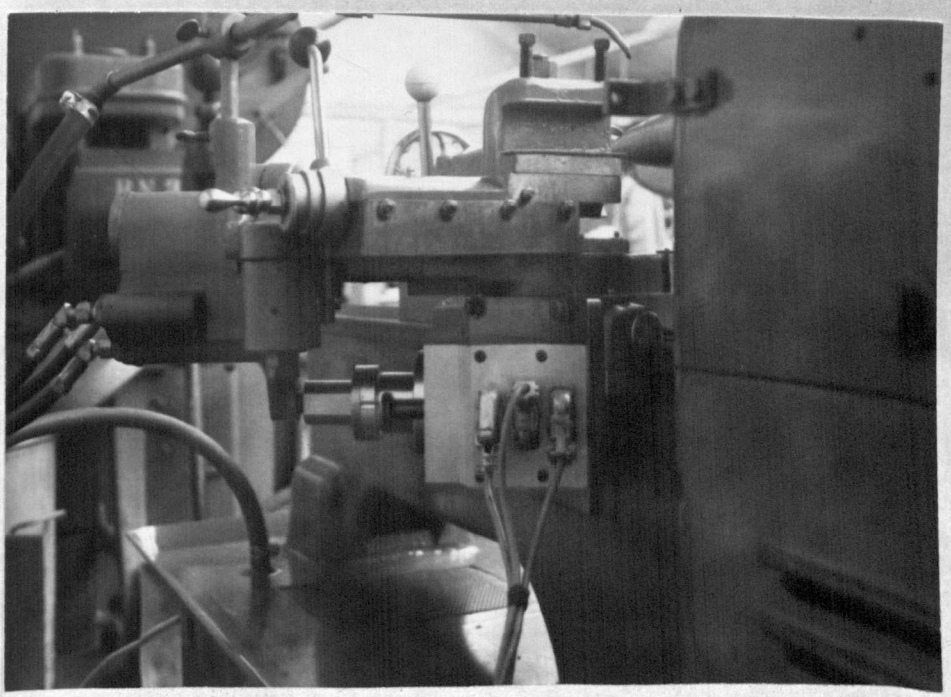

Fig.6-6 Gearbox unit viewed from headstock end.

Although by the use of the type B12/154 Pullin servo motor, the overall depth of the unit was reduced considerably, it was still necessary to arrange for the encoder motor to project through the adaptor plate. When the casings had been designed to give an absolute minimum ram projection from the face of the adaptor plate, and the conventional copying stylus had been replaced by the spherical button, it was still found to necessitate excessive retraction of the copying slide.

The result of the above-mentioned problem is to make it necessary to have a great tool projection, in order that the tool nose should be on the lathe axis with the ram at its zero datum point. It was felt that such a limitation could be tolerated in the prototype but future development must certainly include attempts to reduce tool overhang.

A sheet metal casing was fitted at the rear of the adaptor plate to shield the encoder and motor from oil and coolant during operation of the lathe, and this component necessitated redesign of the rear saddle gib strip due to interference. All electrical connections from the gearbox unit were brought to three sockets, two 15-way subminiature connectors for the lag and lead brushes of the encoder and one 4-way socket for the motor supply. These sockets were mounted on an aluminium cover fitted to the end of the gearbox, which is readily demountable to facilitate inspection. The gearbox unit was thereby completely enclosed in order to protect its electrical connections during operation of the machine.

Modifications to the ram included the removal of the dial indicator mounting, and the fitting of a hardened steel end plate which contacts

the spherical button mounted in the stylus holder. It was also found necessary to provide an end stop for the ram, since the encoder counts back from its maximum immediately after reaching the zero datum. If there is any overshoot in the positioning of the ram as it approaches the zero datum, the error signal becomes extremely large and in the wrong sense so that the motor is supplied with full power driving it further from the zero datum. The result of this effect was found to be jamming of the ram screw, and the trouble was overcome by fitting a 3/8-in steel ball to the rear face of the ram end plate. It was arranged that the ball contacted the end of the ram screw at the point where the encoder read zero, by adjusting the orientation of the encoder shaft relative to the screw when the ball was in contact. This modification together with a view of the end plate and spherical stylus button are shown below in Fig.6-7.

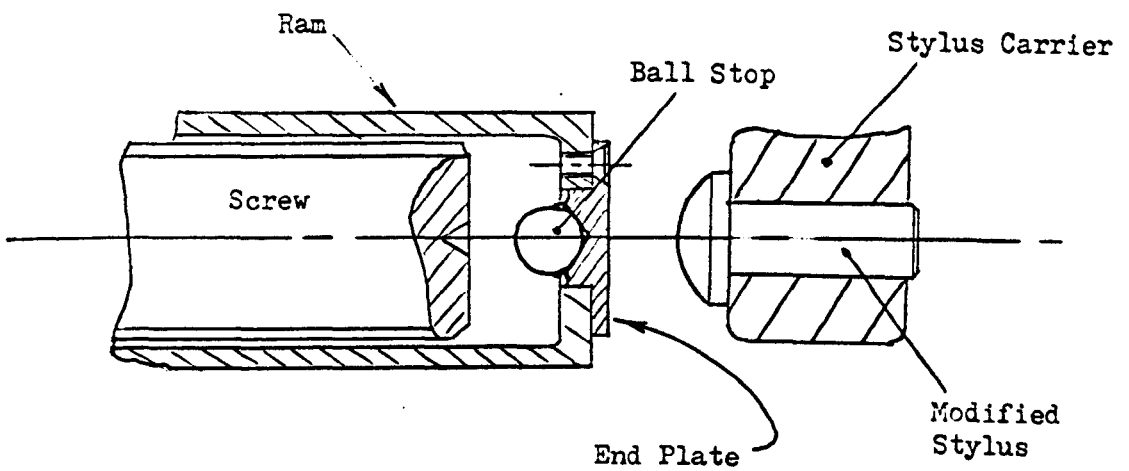

Fig.6-7 Modifications to ram and stylus.

Introduction of the Pullin servo motor resulted in a considerable change in the system characteristics described in Ref.5-Section 9. It was therefore necessary to alter the high/low speed changeover point. Bench tests indicated that in order to avoid violent hunting, it was necessary to supply the motor with greatly reduced power when the ram reached a position giving an error of 0.125 in. This was achieved by changing the connections to the motor control unit from the subtractor, and also by adjusting the preset potentiometer on the motor control unit. Under these conditions the gearbox unit was found to operate satisfactorily.

From the theoretical analysis of the digital equipment given in Section 4, it may be seen that the response characteristics depend on the value of the friction constant in the gearbox unit. It was originally thought that sufficient control over this constant would be achieved by adjusting the bronze cheeks on the ram housing, but in practice this method of adjustment was not found to be successful. An improvement to this unit would be achieved if a mechanical brake with manual adjustment were fitted directly to the motor shaft, in order to give direct control over thevalue of the effective friction constant.

As mentioned earlier in this section, the modified gearbox unit necessitated excessive lathe tool overhang, which resulted in chatter under certain conditions. In an attempt to stiffen the lathe tool, an 'L' section steel member was brazed to the tool shank and a sketch of this modification is shown overleaf in Fig.6-8.

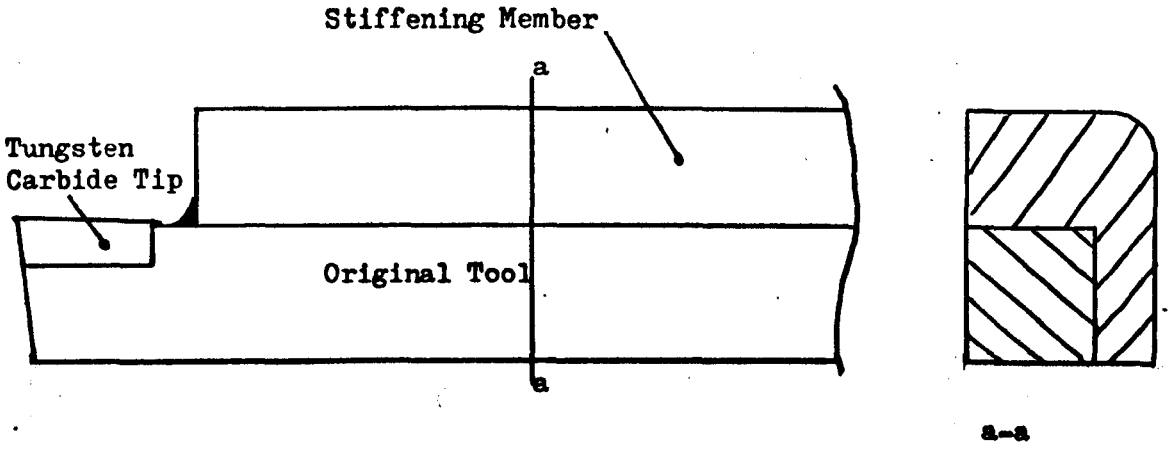

Fig.6-8 Modified lathe tool.

Other modifications to the machine included the provision of a metal shield over the previously mentioned electrical sockets to prevent coolant from interfering with these connections. In addition, it was arranged that the saddle was driven along the bed of the machine by the lead screw, instead of the feedshaft, and in order to achieve the necessary feed rate for turning operations, special change wheels were fitted to the machine. This latter modification is not essential to the work described in this thesis, but is required for the numerical control project of which these tests form a part.

Setting procedure

When the gearbox unit has been fitted to the lathe saddle, it is necessary to position the stylus relative to the ram. This is achieved by energizing the hydraulic supply of the copying servo and causing the slide to move until the stylus contacts the end of the ram. In general, it will be found that the axis of the stylus does not coincide with the axis of the ram due to relative horizontal components resulting from the copying slide angle, and these axes may be brought

into coincidence manually by means of the cross slide control wheel. When this has been achieved, it is not necessary to move the cross slide again, in fact it is important that once an accurate datum has been achieved with the gearbox unit the cross slide position should not be changed, and for this reason the gib strips are screwed up as tightly as possible.

With the stylus button and ram correctly aligned, the copying slide hand lever is fully released so that the slide moves under the control of the ram only. It was found that at normal running pressure the lathe servo satisfactorily followed the motion of the ram, in fact the most rapid ram retraction rate that could be achieved did not result in separation of the ram and stylus.

In order to relate the diametral settings of the lathe tool to ram extensions, a simple calculation has to be carried out which serves to accommodate the copying slide angle and also the bit size chosen for the digital system. The relation is as follows:-

$$\text{Command} = \text{Diameter} \times \text{machine constant } (\lambda)$$

Diameters so calculated would be in decimals of an inch, and the command would also be in decimal notation. In order to make use of this number, therefore, it is necessary to convert it to a 12-bit binary word.

The value of the machine constant λ may be calculated theoretically, or determined experimentally and both methods were employed.

The diagram in Fig.6-9 overleaf shows the relation between ram extension and work diameter where σ is the angle of the copying slide (30°).

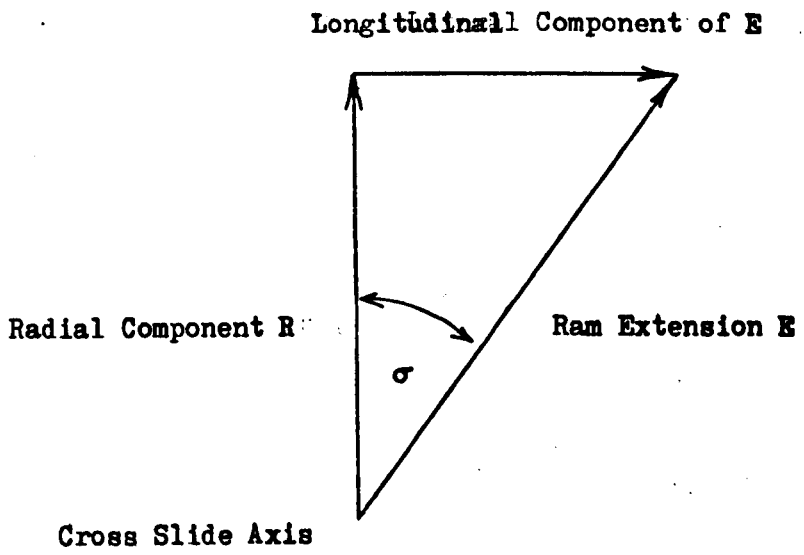

Fig.6-9 Relation between ram extension and work diameter.

In the above figure:

$$E \cos \sigma = R = 0.5\, D$$

where E = ram extension

R = Radial component of E

σ = slide angle

D = workpiece diameter

Hence,

$$E = \frac{D \sec \sigma}{2}$$

where D, E are in inches.

In this system 1 in. = 2048 bits, and the ram command is given by:

$$E_c = E \times 2048$$

Hence,

$$E_c = 1024.D\sec\sigma$$

Since we define the machine constant λ as:

$$E_c = D.\lambda$$

we have,

$$\lambda = 1024 \sec\sigma$$

taking σ as 30°

$$\lambda = \frac{1024}{.866}$$

$$= \underline{1182.4}$$

In order to operate the machine, the ram is brought to its zero datum position, thereby ensuring that the copying slide is fully forward. There is an additional tool slide mounted on the copying slide of the lathe which carries the tool post, and which is manually adjustable. This slide is then adjusted until the tool tip is close to the axis of the lathe. An accuracy of $\pm$ 0.010 in. is adequate for this adjustment, which may be effected by sighting the tool point relative to the centre mounted in the lathe spindle.

A suitable workpiece is then selected, 2-in. diameter material was employed for these tests, and mounted between centres in the lathe. The required command for a particular diameter, say 1.950 in., is then calculated and converted to a binary word, which is then set up on the bank of tumbler switches on the control cabinet. This operation will result in the ram positioning itself and taking the tool slide with it. If a cut is then taken at this setting, the diameter generated on the workpiece may be measured with a micrometer, and the tool point may then be adjusted to accommodate any error by means of the previously mentioned hand-operated tool slide. When correct adjustment has been achieved, the gibs of this tool slide should be tightened to prevent unwanted movement. Once the correct adjustment has been achieved at one diametral setting, it should only

be necessary to alter the position of this tool slide to accommodate tool wear, or if the tool itself has to be changed. If correct adjustment is not achieved, resulting diameters will include a constant error.

In these tests, the machine constant λ was taken as 1170 to observe the effects resulting from an incorrect value, then at 1183, 1182 and 1182.5. The range of ram extension available made it possible to handle workpiece diameters up to 3 in. and the tests were conducted initially at 0.05 in. and later at 0.10 in. intervals. Commands were calculated using four figure log tables, and binary commands were determined using a technique involving successive division by 2.

Early tests were carried out starting with the largest diameter and working through the smaller diameters of the series. Each diameter machined was stopped before the previous cut had been completely removed, and when the series had been completed the tool was reset for each cut again to check the repeatability of the system.

In order to avoid errors due to inaccuracies in the lathe, all diametral measurements were taken at the tailstock end of the workpiece. This procedure resulted in all diameters measured being machined from the same point on the lathe bed, and rendered the tests independent of parallel turning errors inherent in the lathe.

Fig.7-1 Positioning Accuracy of the Digital Servo
(Ref.5 Section 9)

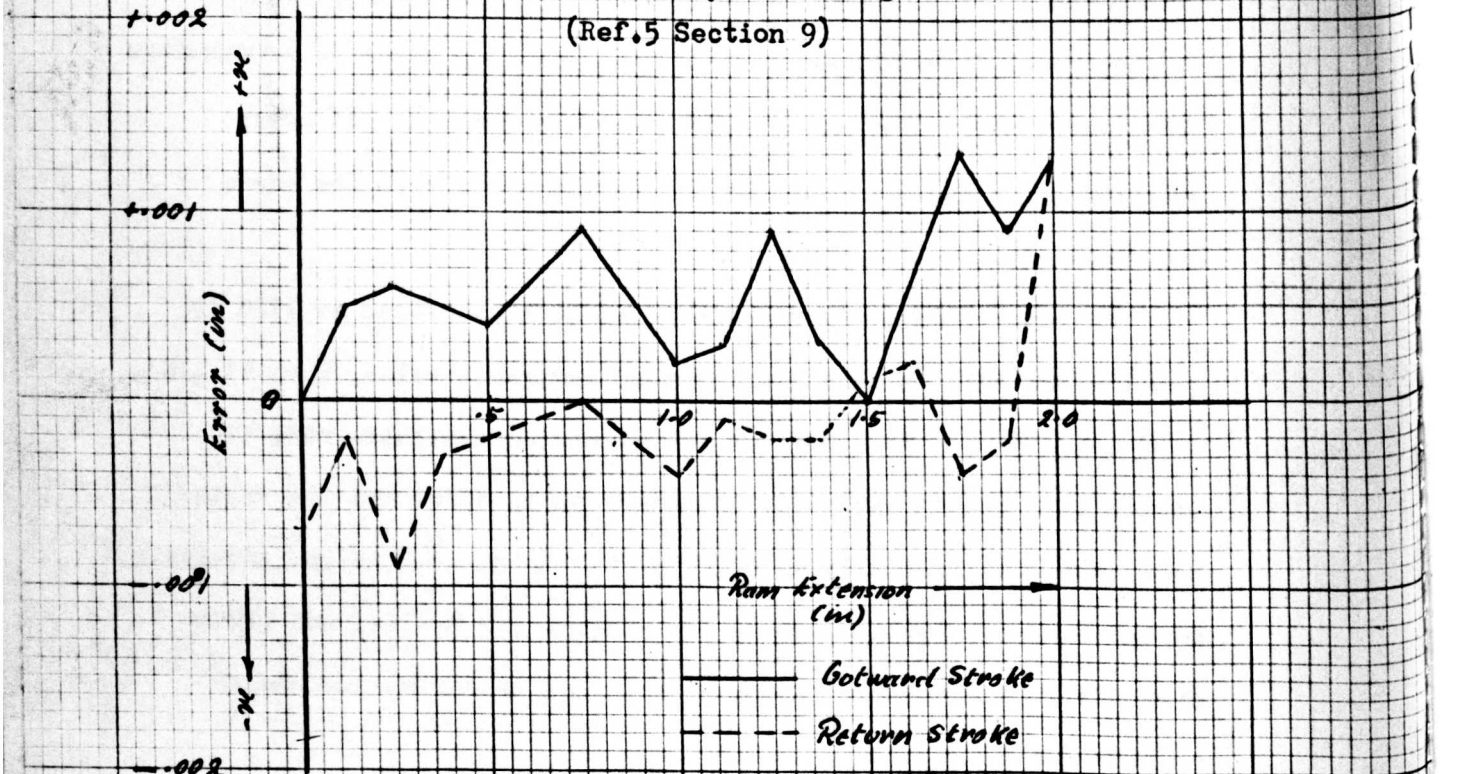

Fig.7-2 Error curve for the first test

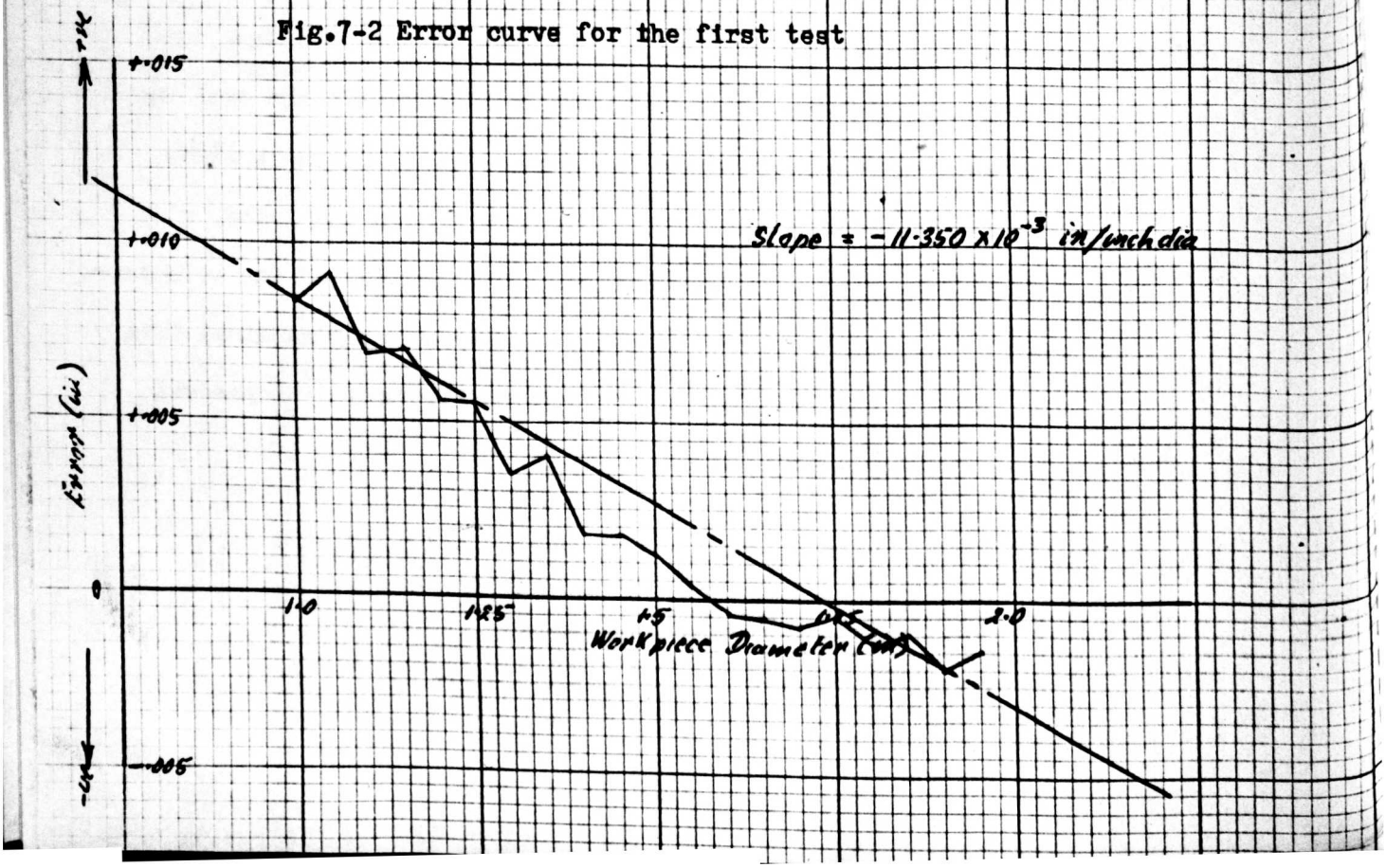

SECTION 7 : Machining Tests

Detailed results of machining tests are included in this thesis in Appendix 4. These results are tabulated in Tables A4.2 to A4.9, and the error curves plotted from these values are given in this section in Figs.7-2 to 7-9. In addition, Appendix 4 includes the tabulated (Table A4.1)results from positioning accuracy tests carried out on the prototype digital position servomechanism as published in Ref.5 Section 9.For comparison with the error curves in this section, these latter figures are plotted in Fig.7-1 opposite, showing the inherent positioning error of the system.

First Test

Using a 2-in diameter mild steel test piece, a series of cuts was taken without coolant at a spindle speed of 409 rev/min, between diameters 1.950 and 1.500 in. The machine constant used to calculate the necessary binary input commands was 1170, and the results are given in Table A4.2, Appendix 4, and the corresponding error curve is drawn in Fig.7-2 opposite.. From the slope of this curve it is possible to calculate a more accurate value for the machine constant λ.

In Fig.7-2 the broken line represents the mean slope of the curve and this line has a slope of - 0.01135 in per in, which indicates that the value λ = 1170 produces an error of 0.01135 in per inch workpiece diameter. If the tool had been correctly zeroed on the lathe axis, the command to generate a diameter equal to 1 in, would have resulted in

Fig.7-3 a Error curve for the second test

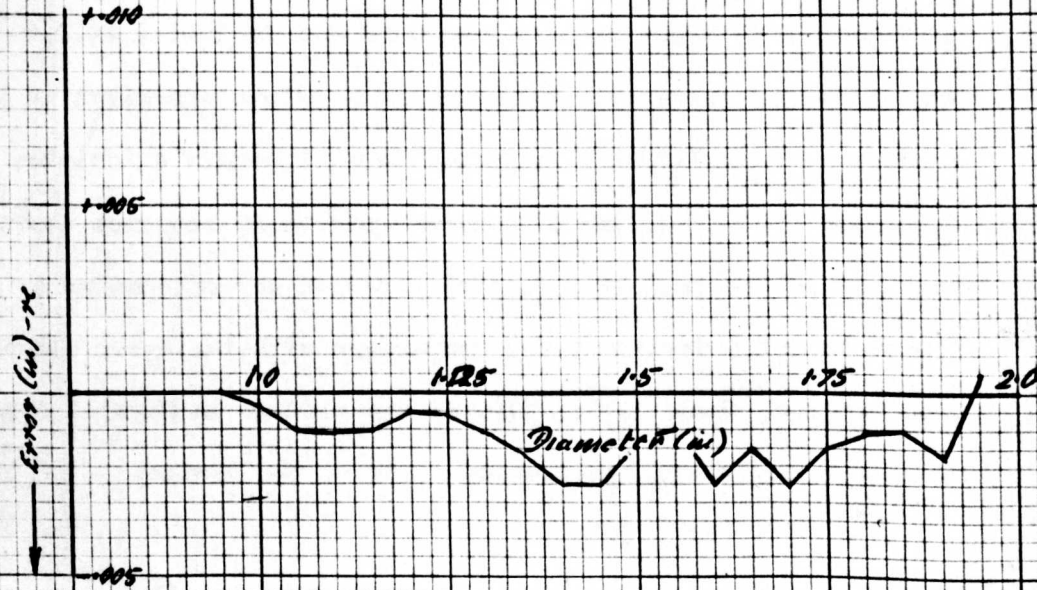

Fig.7-3 b Repeatability curve for the second test

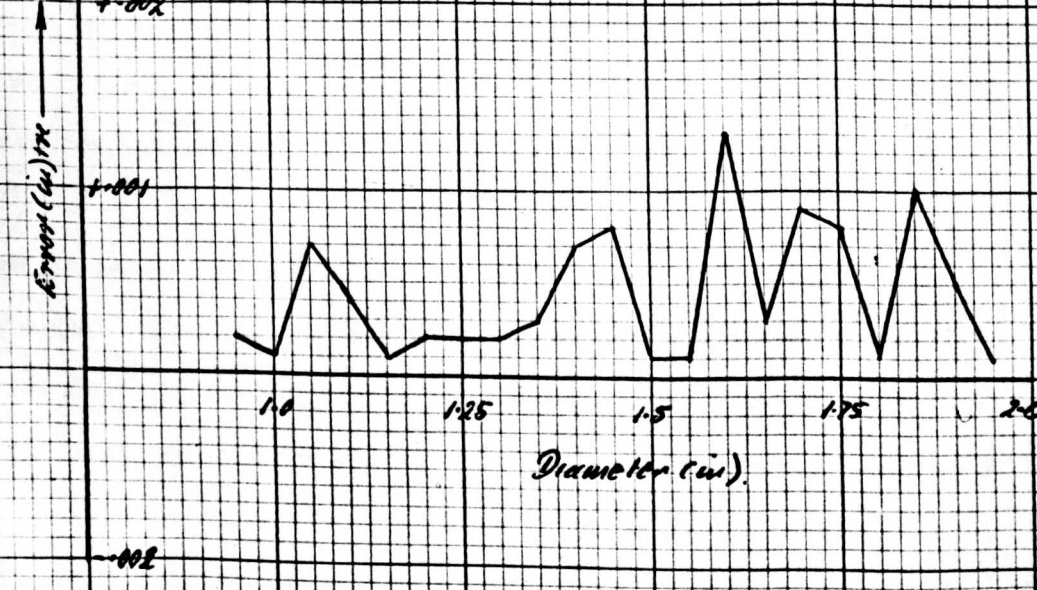

a diameter of 0.98665 in being machined.

The theoretical value for λ, which was calculated in Section 6, is:

$$\lambda = 1182.4$$

and this value results in one binary bit being equivalent to 0.000845 in on workpiece diameter. If this figure is used to modify the value of λ we have:

$$\begin{aligned} \text{Actual } \lambda &= 1170 + 11.35 \times 1.1824 \\ &= 1170 + 13.42 \\ &= 1183.4 \end{aligned}$$

For the next test $\lambda = 1183$ was used.

Second Test

Using the above value for λ , a second series of machining operations was carried out on a second and similar test piece. In this case the tests were again conducted without coolant, and the number of cuts was increased to include 1-in diameter. This series of cuts indicated that the machine constant was much more accurate, although the settings chosen due to test piece size only covered half the range of the ram. In addition to the initial cuts, a further series was taken at the same command settings in order to investigate the repeatability of the equipment. Results from these tests are listed in Table A4.3, Appendix 4, and the resulting error and repeatability curves are given opposite in Fig.7-3 a and Fig.7-3 b.

Fig. 7-4 Error curve for the third test

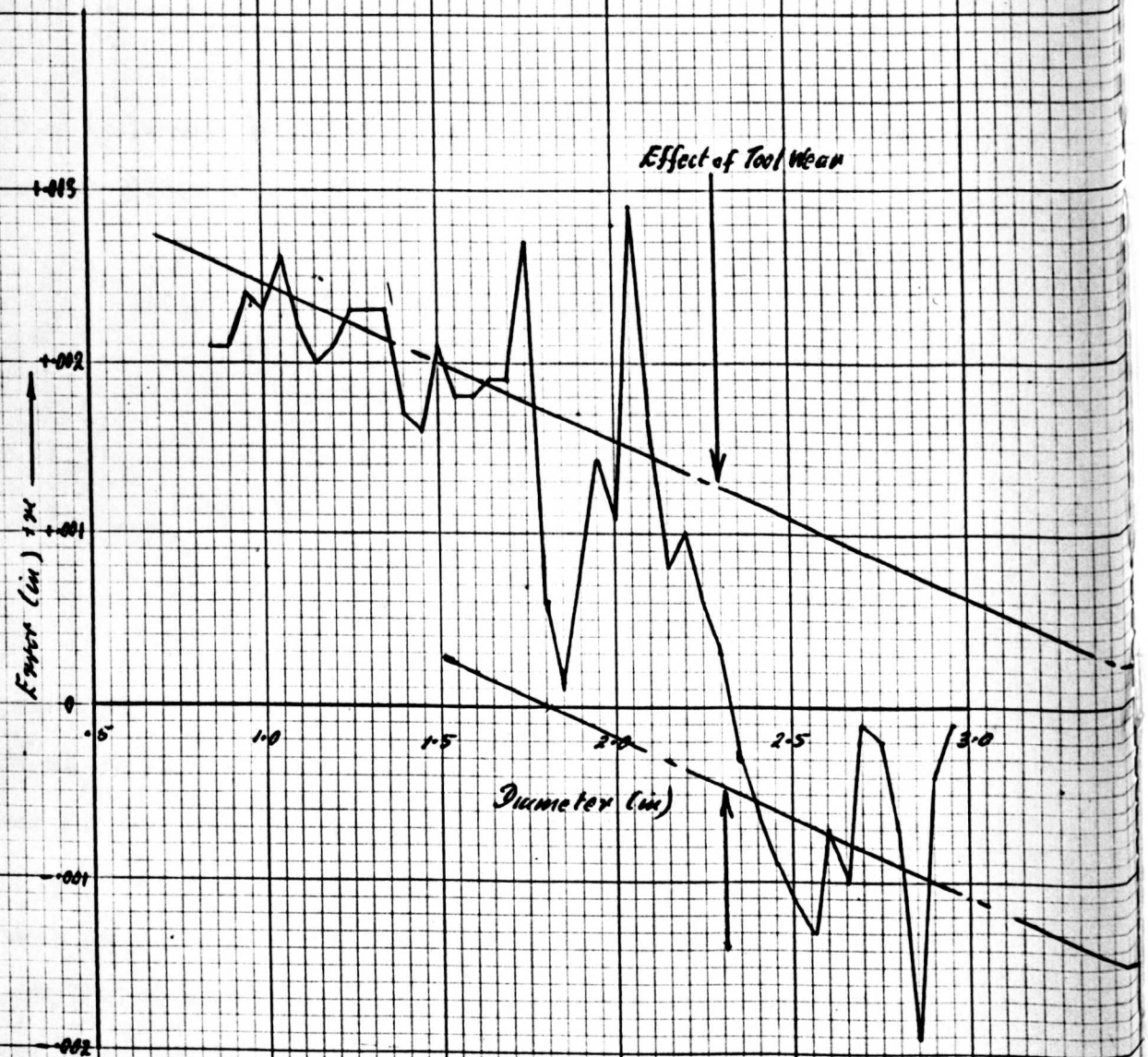

Third Test

This test was carried out in order to check the value of the machine constant in use of the full range of the ram unit. For this reason a 3-in diameter mild steel test piece was employed, and at the resulting higher cutting speeds it was decided to use coolant. The first attempt at this test was a failure due to coolant getting into the gearbox casing and short circuiting the electrical connections, which resulted in a breakdown of the position error feedback signal. For this reason the sheet metal cover described in Section 6 was fitted to the lathe saddle so that protection was afforded to the plugs and connectors which coupled the encoder to the subtractor unit.

The second attempt produced results which clearly indicate that the tool had suffered wear, which is a major difficulty with this type of control system. After machining accurately from 2.950 in to 2.350 in, the curve in Fig.7-4 opposite shows that there is a sudden jump in the errors produced, so that the lathe then consistently machined oversize. Due to this effect it was not possible to carry out a repeatability check. Results from this test are given in Table A4.4 Appendix 4. The cause of the tool wear was thought to be chatter at the larger diameters, and the spindle speed was therefore changed back to the value employed for dry cutting (409 rev/min) in an attempt to reduce its effect.

In addition, the tool was reground with a larger tool nose radius (approximately 0.030 in).

Fig. 7-5 a Error curve for the fourth test

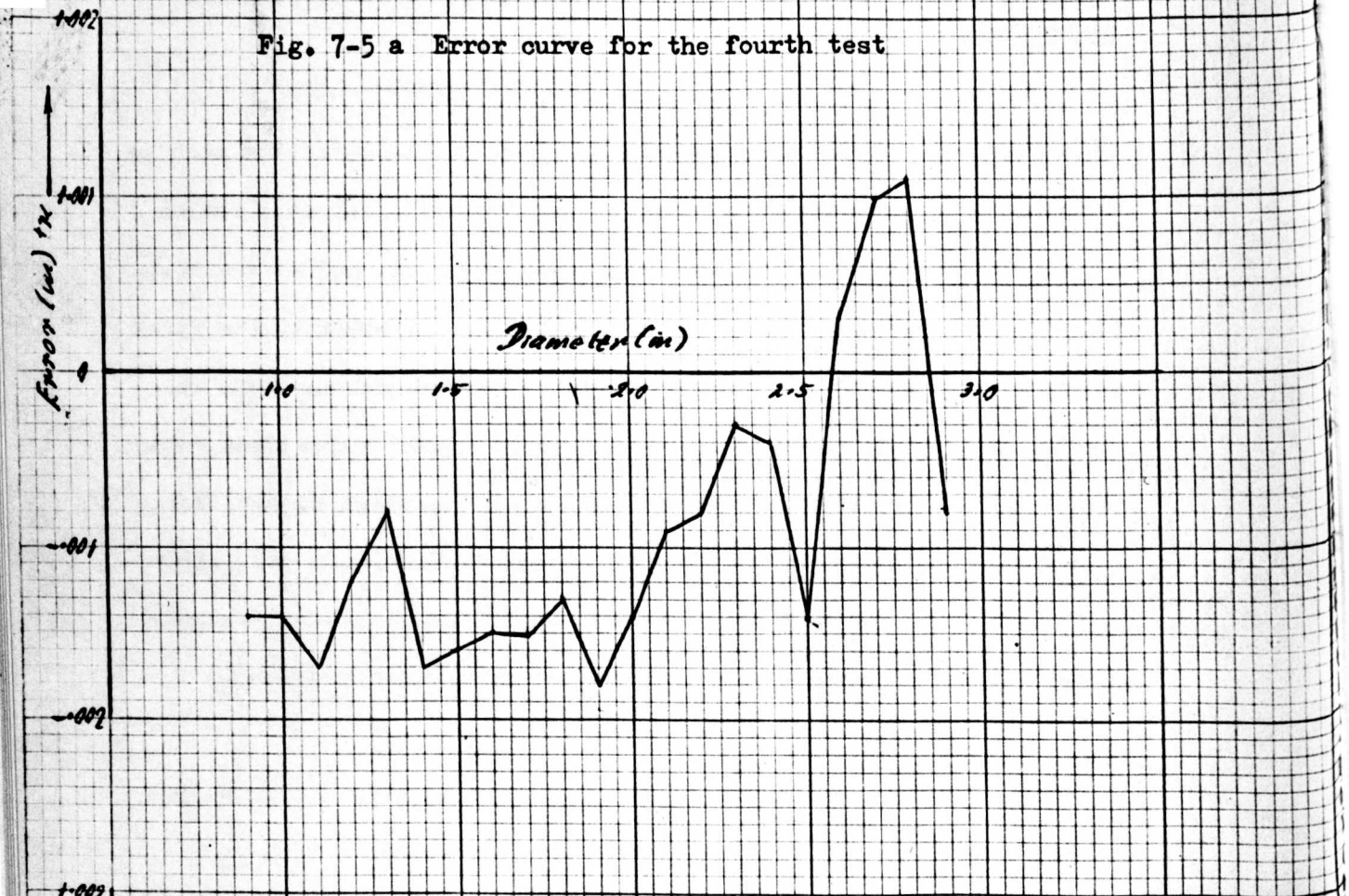

Fig. 7-5 b Repeatability curve for the fourth test

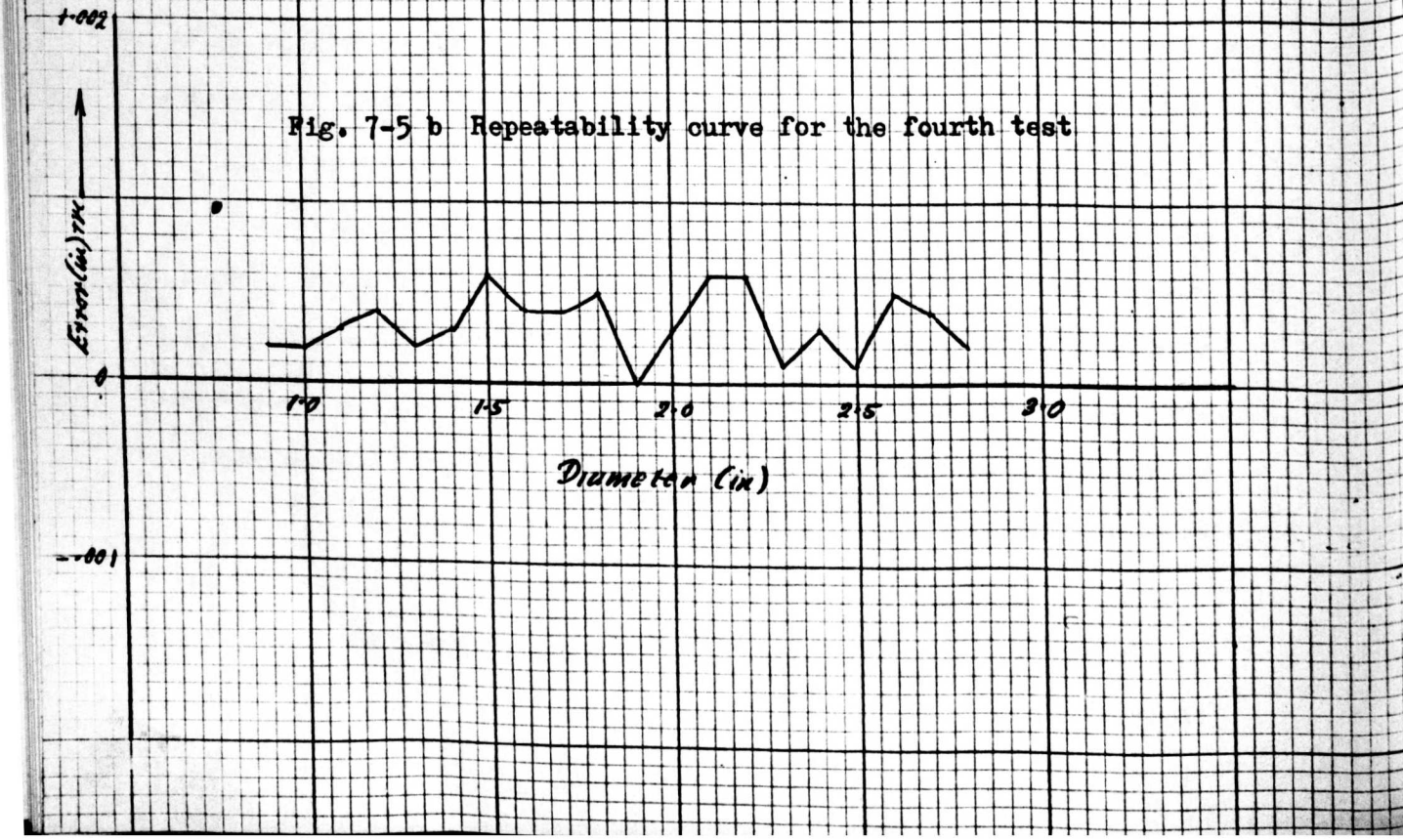

Fourth Test

Due to the results being affected by tool wear as described, it was decided to repeat the conditions of the third test, using another mild steel test piece. This test became the fourth, but in order to save time it was also decided to change the diametral settings from 0.050 in intervals on workpiece diameter to 0.10 in steps. The range of the tests was not however altered.

The reground tool mentioned on the previous page was employed and the results achieved were good, there being no apparent tool wear. It was therefore possible to run a complete repeatability check, and this was achieved by repeating each diameteral setting as described in the second test.

Detailed results obtained during the fourth test are listed in Appendix 4 , Table A4.5, whereas the error and repeatability curves plotted from these results are shown opposite in Figs. 7-5 a and 7-5 b respectively.

Fifth Test

As the results from the previous test appeared to be very good it was decided to repeat the run under the same conditions. This then

Fig.7-6 Error curve for the fifth test

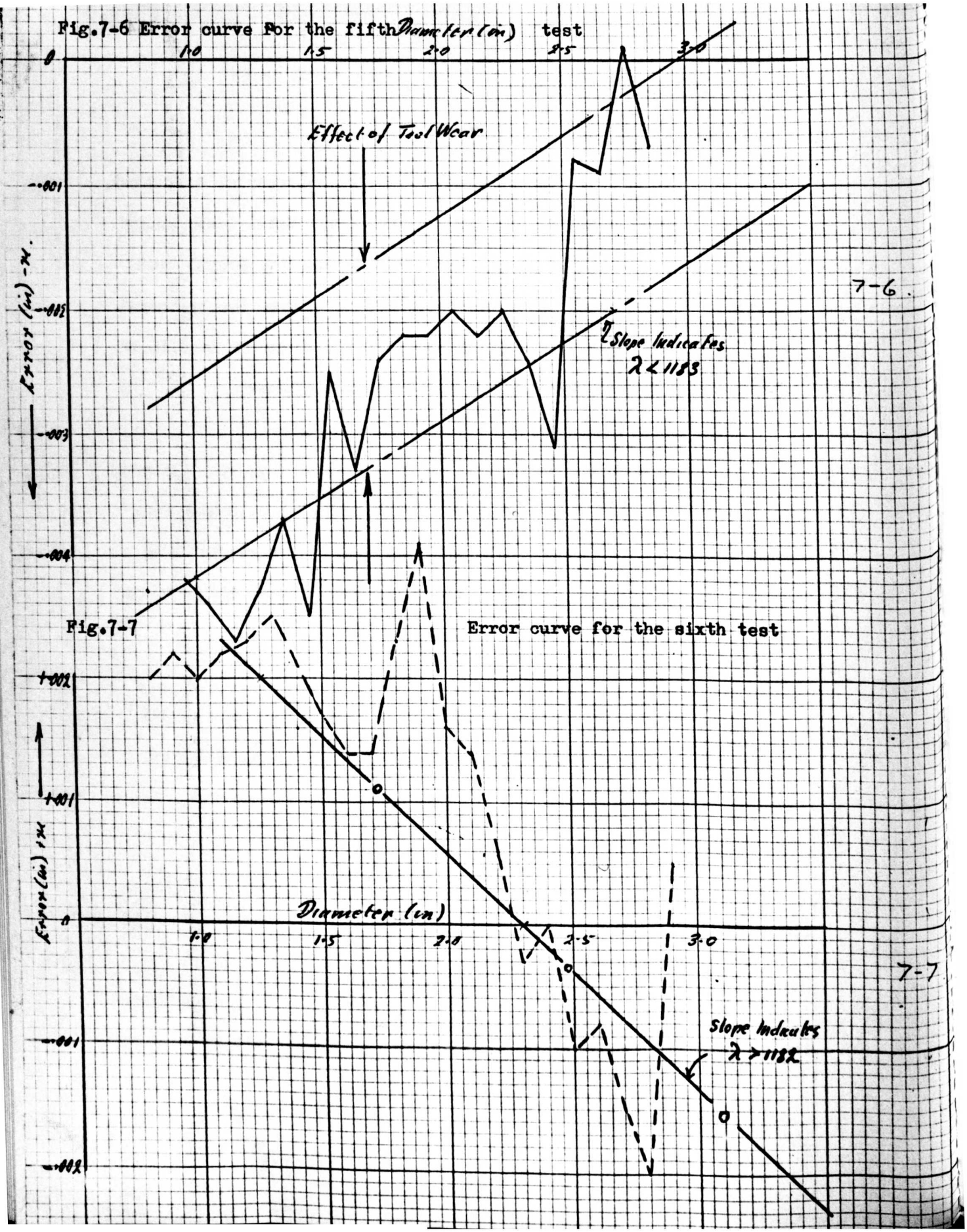

Fig.7-7 Error curve for the sixth test

became the fifth test, and the results are given in Table A 4.6 Appendix 4, and the associated error curve is opposite in Fig.7-6. The tool was not resharpened between tests four and five, and the setting of the slide was not changed.

The results indicate that the machine constant $\lambda = 1183$ is too great, and that this value produces an error of 0.0099 in per inch which increases with diameter. Since 1 binary bit is nearly equivalent to 0.0009 in, the subsequent test was performed using $\lambda = 1182$.

Sixth Test

Using a new 3-in diameter mild steel test piece, and a machine constant of $\lambda = 1182$, a further series of test cuts was made at diameteral intervals of 0.10 in.

Severe chatter was experienced however during these cuts, which again caused tool wear. The error curve for this run, opposite in Fig.7-7, clearly shows the same faults as Fig.7-4, indicating that approximately 0.001 in had been laost from the tool tip. Detailed results for this test are given in Table A4.7, Appendix 4.

It is however possible to observe that the value of the machine constant is not correct at 1182, but that too much adjustment had been made. It was deduced therefore that the machine constant for the system was in fact 1182.5, which agrees very well with the calculated value of 1182.4, and all subsequent tests were carried out using $\lambda = 1182.5$.

Fig.7-8 Error curve for the seventh test

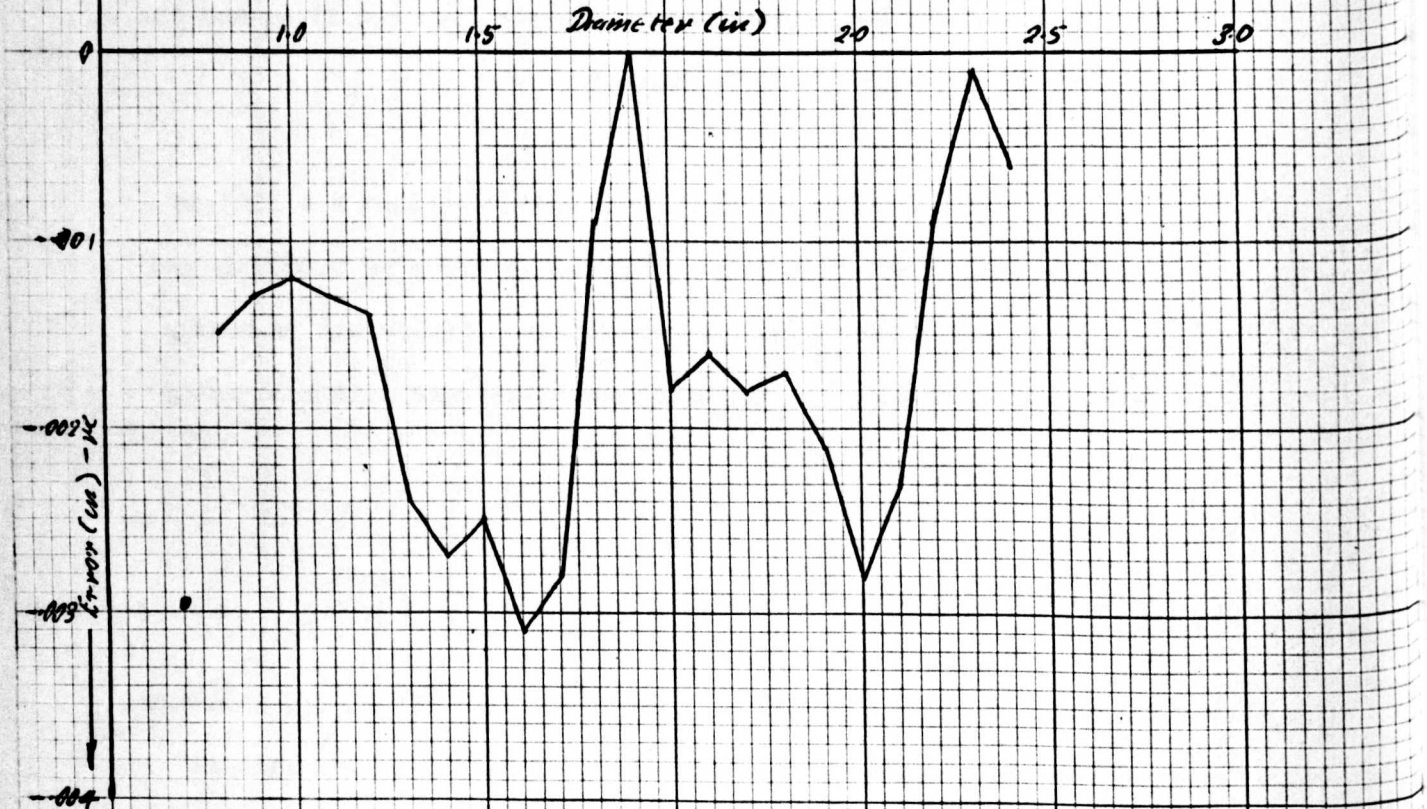

Fig.7-9 Error curve for the eighth test

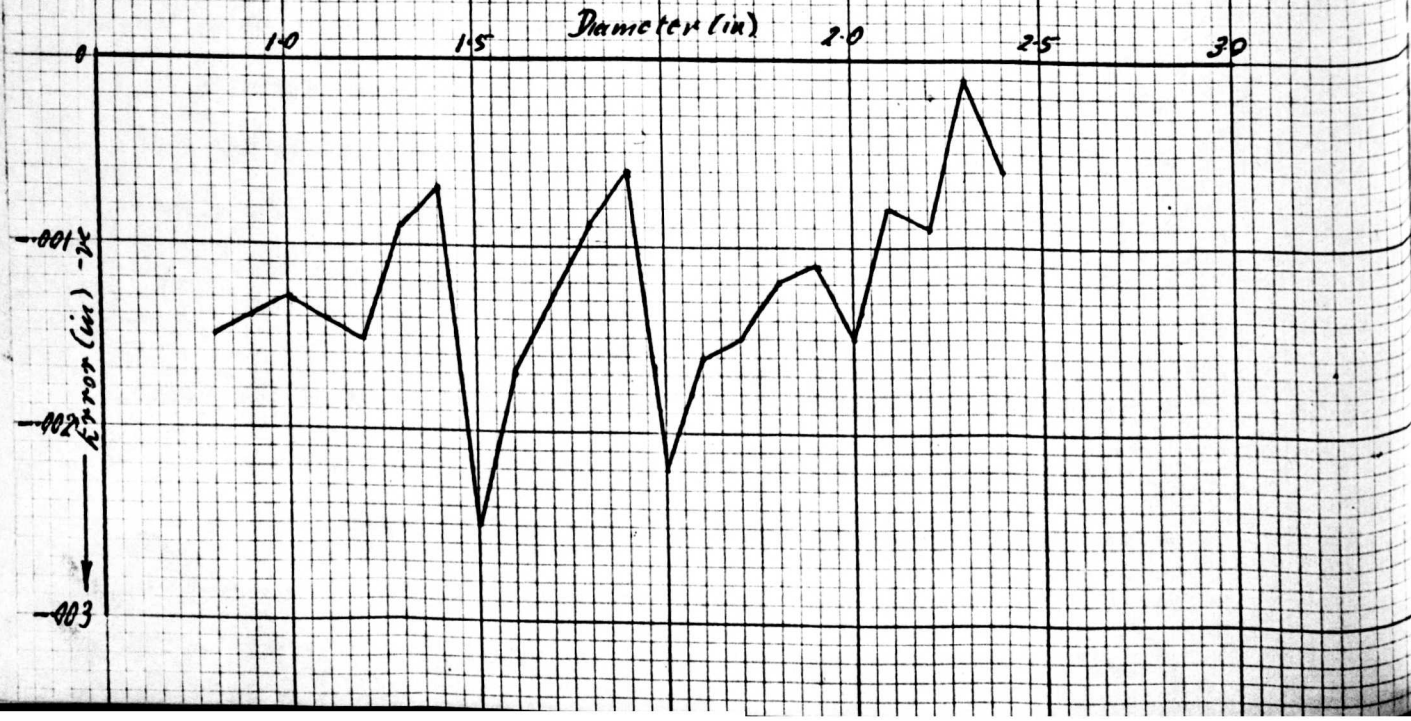

In a further attempt to reduce chatter, the lathe tool was stiffened as described in Section 6, Fig.6-8, and the remaining runs were performed using Duralumin test pieces. In addition a new live centre was fitted to the lathe tailstock.

Seventh Test

Using a 3-in diameter Duralumin test piece machining tests were carried out at a range of diameters between 2.900 in and 0.800 in, at 0.10 in diametral intervals. Spindle speed employed was 818 rev/min and the operations were carried out without coolant. Since previous work had shown the repeatability of the equipment, it was decided that no further checks of this kind were necessary.

Detailed results for the seventh test are given in Table A4.8, Appendix 4, and the corresponding error curve is opposite in Fig.7-8.

Eighth Test

In order to check the results of the seventh test a further run was carried out on a second Duralumin test piece at the same settings. Results for this test, which confirmed the previous run, are given in Table A4.9, Appendix 4, and the associated error curve is plotted opposite in Fig.7-9.

General Comments

During these machining tests a tungsten carbide tipped tool was used on both mild steel and Duralumin test pieces. As stated the tool

nose radius was increased by regrinding from the small value as supplied by the manufacturers, to approximately 0.030 in. This was done in attempt to reduce tool wear, but it certainly served to increase chatter as well.

It was apparent from these tests that the tool wear problem is critical for this type of system, since its effect is doubled when translated into workpiece diametral errors. The problem, however, exists in any machine tool where workpiece diameter is inferred from slide position, as is the case with all machines at present in commercial use such as numerically controlled machine tools, automatics and capstan lathes. The usual solution to the problem is to ensure that sufficient roughing operations are performed before the finishing cut to ensure that the final size is achieved by means of a lightly loaded cutter. Attempts have also been made to obtain position feedback signals directly from the workpiece, which apparently eliminates this problem, but apart from the difficulty in producing such signals, it is not possible to use them in an automatic cycle without some form of adaptive control system, except in operations where one dimension only is under control. Automatic size grinding is the only example where such feedback signals have been employed successfully.

A further point which should be emphasized is the critical effect of tool point height. If the tool point is not set so that it cuts on centre, then a varying error will be produced by an automatic positioning system as the workpiece diameter increases. It was noticeable in this system, that due to excessive tool overhang,

which has been dealt with earlier in Section 6, it was possible to deflect the lathe tool below centre during cutting by taking a heavy cut. This effect resulted in varying errors when different depths of cut were employed, and for this reason the depth of cut was held constant during these tests, except for the change from 0.050 in to 0.10 in.

A degree of 'hunting' of the ram was experienced during the tests, and this condition was found to occur at the same positions on the ram. It was decided that 'hunting' arose from varying friction constant values in the gearbox unit as the ram extended, and the condition was easily checked by light hand pressure on the hand set knob of the unit.

SECTION 8 : Conclusions

Harrison Hydraulic Copying System

The relevance of this equipment to the thesis lies in the necessity of ignoring the lag effects associated with the hydraulic positioning system fitted to the L 6 lathe, in order to justify the treatment applied to the complete tool positioning system. This can only be done if these lag effects are sufficiently small compared to those of the digital equipment to render the hydraulic equipment capable of being treated as a solid link.

The response tests carried out on the hydraulic system, which are fully described in Section 3 with detailed results in Appendix 1, illustrate that the lag of the equipment is less than 0.001 in provided that it is operated over its normal range at the manufacturers recommended pressure and stylus loading. This value of lag is sufficiently low to enable the system to be treated as a solid link in this work, and the assumption is therefore justified.

Digital Equipment

In the theoretical analysis of the digital equipment, Section 4, a large number of assumptions had to be made in order to enable the non-linear response of the system to be treated mathematically. These assumptions included the treatment of the gearbox member as a unidirectional device. This was only done, however, within a given phase of

operation, and since the unit can only reverse by changing phase the assumption is justified. The computer programme, Appendix 2, provided results which are plotted and tabulated in Section 4, and these results may be seen to follow the predicted path, which implies that the mathematical description of the motion of the ram unit would in fact produce an oscillatory response of the type indicated in Section 4.

Unfortunately for the reasons outlined in Section 5, it was not possible to provide a continuous record of the error signal during the response tests carried out on the digital equipment. The result of using the data sampling technique was that no information was available concerning position error between sampling instants, and as the error curves in Section 5 show, this information would have indicated more clearly the extent of the non-linear oscillations. An attempt was made, however, to take this loss of information into account when estimating the actual mean lag figures associated with each response curve. From these lag figures it may be seen that the digital equipment was some three to four times slower in response to comparable input ramps than the hydraulic servo.

Comparison of Theoretical and Actual Response for the Digital System

From the figures listed in Table 4.6, Section 4, and from the actual values of response obtained in Section 5, it is possible to compare the theoretical response with that actually measured for input ramp gradients of about 4 and 2 in/min. Study of the results will show that the actual values were in excess of the calculated figures, but

that they were of the same order. Table 8.1 below provides these figures for comparison, and it is considered that they justify the mathematical treatment applied in Section 4. Complete parity would have been remarkable, when the errors of measurement, assumptions and measurement techniques are considered.

Approximate Input Ramp (in/min)	Calculated Error (in)	Actual Error (in)
4	0.0018	0.0035
2	0.0013	0.0025

Table 8.1 Actual and Theoretical Lag Errors

Due to the method of measuring the errors which has been employed, it is not possible to state that the theoretical values are too low. If however they are too low, this could be explained as being due to incorrect values being measured for motor torque and gearbox friction constant.

Positioning Accuracy of the Equipment Mounted on the Lathe

The results of the last two machining tests carried out on aluminium workpieces are given in Figs.7-8 and 7-9, from which it may be seen that the position error of the equipment is almost within its stated accuracy of $\pm$ 1 binary bit (= $\pm$ 0.001 in on diameter).

Apart from errors introduced by innaccuracies in the lathe itself, another possible source of error arises from the dependance of the system on the accuracy of the ram screw thread. An accuracy curve for this member is included in Section 7, Fig.7-1, but the effect of these errors

Fig.8-1 Effect of Ram screw inaccuracies on workpiece diameter

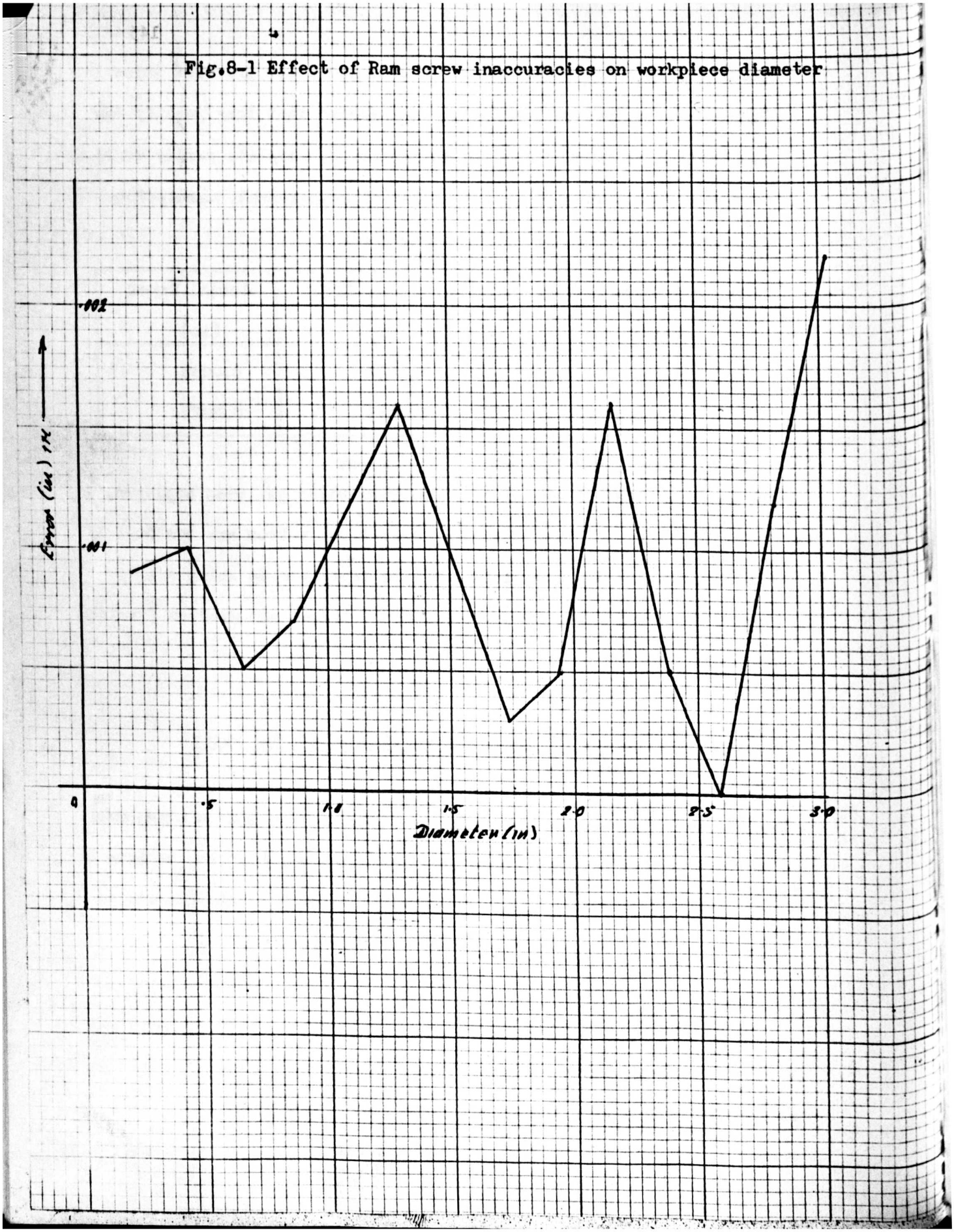

on workpiece diameter is modified by the angled copying slide. Table 8.2 below provides the modified errors due to inaccuracies in the ram screw, and these values have been used to draw the error curve opposite Fig.8-1.

The errors included in Fig.8-1 arise largely from pitch errors in the screw, and comparison of this figure with the error curves in Section 7, Figs.7-2 to 7-9, reveals that the pitch errors do indeed affect the workpiece size.

Nominal Ram Extension (in)	Resulting Diameter (in)	Error (in)
.125	.206	+ .0009
.250	.433	+ .0010
.375	.650	+ .0005
.500	.866	+ .0007
.750	1.297	+ .0016
1.000	1.732	+ .0003
1.125	1.947	+ .0005
1.250	2.165	+ .0016
1.375	2.380	+ .0005
1.500	2.598	0
1.625	2.810	+.0012
1.750	3.030	+.0022
1.875	3.245	+.0016
2.000	3.464	+.0022

SECTION 9 : References

Specific References

1. Handbook for the Harrison 12-in swing centre lathe model L 6

2. Tracer Controlled Copying Lathes — H.C.Town

3. Design of Hydraulic Control System — Lewis and Stern

4. Electrohydraulic Servomechanisms — A.C.Morse

5. A Digital Position Servomechanism — F.J.Robinson, G.A.H.Thomas
   (Machinery 13/10/65 and 17/11/65)

6. Automatic Control — C.R.Webb

7. The Electrical Activity of the Nervous System — M.A.B.Brazier

8. Automatic Control of Viscosity from Blending Systems — J.Korn
   (University of London M.Phil Thesis 1967)

9. 'Robtom', a new Logic Aid to Teaching and Research — F.J.Robinson, G.A.H.Thomas, R.Zgorski
   (Design Electronics September 1966)

General References

Principles of Servomechanisms — Brown and Campbell

Fluid Power Control — Blackburn, Reethoff and Shearer

Servomechanism Theory — G.J.Thaler

Automatic Control Systems — Kuo

APPENDIX 1

Detailed results of response tests on the Harrison Hydraulic Copying System

Oscillogram Number	Delivery Pressure lbf/in^2	Ramp Number	Stylus Load lbf	Saddle Speed in/min	Recording Speed in/s
1	50	1,2,3	1	12.75	0.3
2	150	1,2,3	1	12.75	0.3
3	250	1,2,3	1	12.75	0.3
4	50	1	1	2.12	0.15
5	50	2	1	2.12	0.15
6	50	3	1	2.12	0.15
7	150	1	1	2.12	0.15
8	150	2	1	2.12	0.15
9	150	3	1	2.12	0.15
10	250	1	1	2.12	0.15
11	250	2	1	2.12	0.15
12	250	3	1	2.12	0.15
13	150	1,2,3	0.5	12.75	0.3
14	150	1	0.5	2.12	0.15
15	150	2	0.5	2.12	0.15
16	150	3	0.5	2.12	0.15
17	150	1,2,3	2	12.75	0.3
18	150	1	2	2.12	0.15
19	150	2	2	2.12	0.15
20	150	3	2	2.12	0.15

Table A1.1 Details of parameters employed during each test run.

Preparation of Oscillograms

In order to include the oscillograms in this thesis, it was necessary to copy them, which in turn necessitated fixing the traces in the manner outlined below.

Kodak 'Linagraph' recording paper was used in the orcilloscope, and after exposure to daylight for about 30 seconds which made the trace visible, the oscillograms were processed as follows:

i) Immersed in Kodak permanizing solution for between 1 and 1.5 min, in daylight at room temperature. Sol- agitated by hand during this part of the development.

ii) Placed in acid stop bath for period of 10 seconds.

iii) Fixed in Kodak solution for 4 to 5 min at room temperature.

iv) Washed in cold running water for about 15 min, then dried in air at room temperature.

The resulting oscillograms, which had a medium grey background, were then copied on a Rank Xerox machine.

Detailed Results

Table A1.1 opposite, lists the parameters employed during the various test runs, and relates them to the oscillograms. In the table the ramp numbers in the third column correspond to the following regions on the test template. The actual value of the input ramp function also depends on the saddle feed employed as already explained.

Ramp Number	Template Region
1	2 (60° outwards taper)

Oscillogram Number	Ramp No.	Input Function in/min	Mean Lag Error 'L' in	SteadyState Error 'e' in
1	1	+12.750	+.00088	-.00050
1	2	+25.500	+.00130	+.00042
1	3	-12.750	-.00240	-.00100
2	1	+12.750	+.00066	-.00012
2	2	+25.500	+.00100	+.00038
2	3	-12.750	-.00100	-.00038
3	1	+12.750	+.00040	-.00012
3	2	+25.500	+.00050	+.00012
3	3	-12.750	-.00075	-.00012
4	1	+ 2.120	+.00060	+.00050
5	2	+ 4.240	+.00075	+.00080
6	3	- 2.120	-.00100	-.00075
7	1	+ 2.120	+.00030	-.00025
8	2	+ 4.240	+.00042	+.00050
9	3	- 2.120	-.00050	-.00025
10	1	+ 2.120	+.00018	0
11	2	+ 4.240	+.00027	+.00025
12	3	- 2.120	-.00030	-.00010
13	1	+12.750	+.00050	-.00020
13	2	+25.500	+.00100	+.00030
13	3	-12.750	-.00120	-.00020
14	1	+ 2.120	+.00040	-.00020
15	2	+ 4.240	+.00070	+.00060
16	3	- 2.120	-.00080	-.00050
17	1	+12.750	+.00050	-.00020
17	2	+25.500	+.00080	+.00020
17	3	-12.750	-.00150	-.00030
18	1	+ 2.120	+.00020	-.00020
19	2	+ 4.240	+.00050	+.00040
20	3	- 2.120	-.00060	-.00040

Table A1.2 Tabulated Error values from the Oscillograms

Ramp Number	Template Region
2	4 (90° shoulder)
3	6 (30° decreasing taper)

Recording Speed

Recording speed is the rate of travel of the paper in the oscilloscope. This velocity was adjusted to give a trace length of practical size. Although changes in the recording speed result in lag traces increasing or decreasing in length, they do not affect the size of the trace deflection, and all traces are therefore to the same scale on the ordinate axis.

Error Measurements

Lag and steady state error was measured directly from the oscillograms, after the deflection scale had been established using the screw adjustment and dial gauge on the detector head. It was found that with the equipment set up as already described a deflection of 5 mm on the oscilloscope beam was produced by a gap change of 0.00025 in. Mean lad and steady state errors were then measured from each oscillogram, and these results are listed opposite in table A1.2.

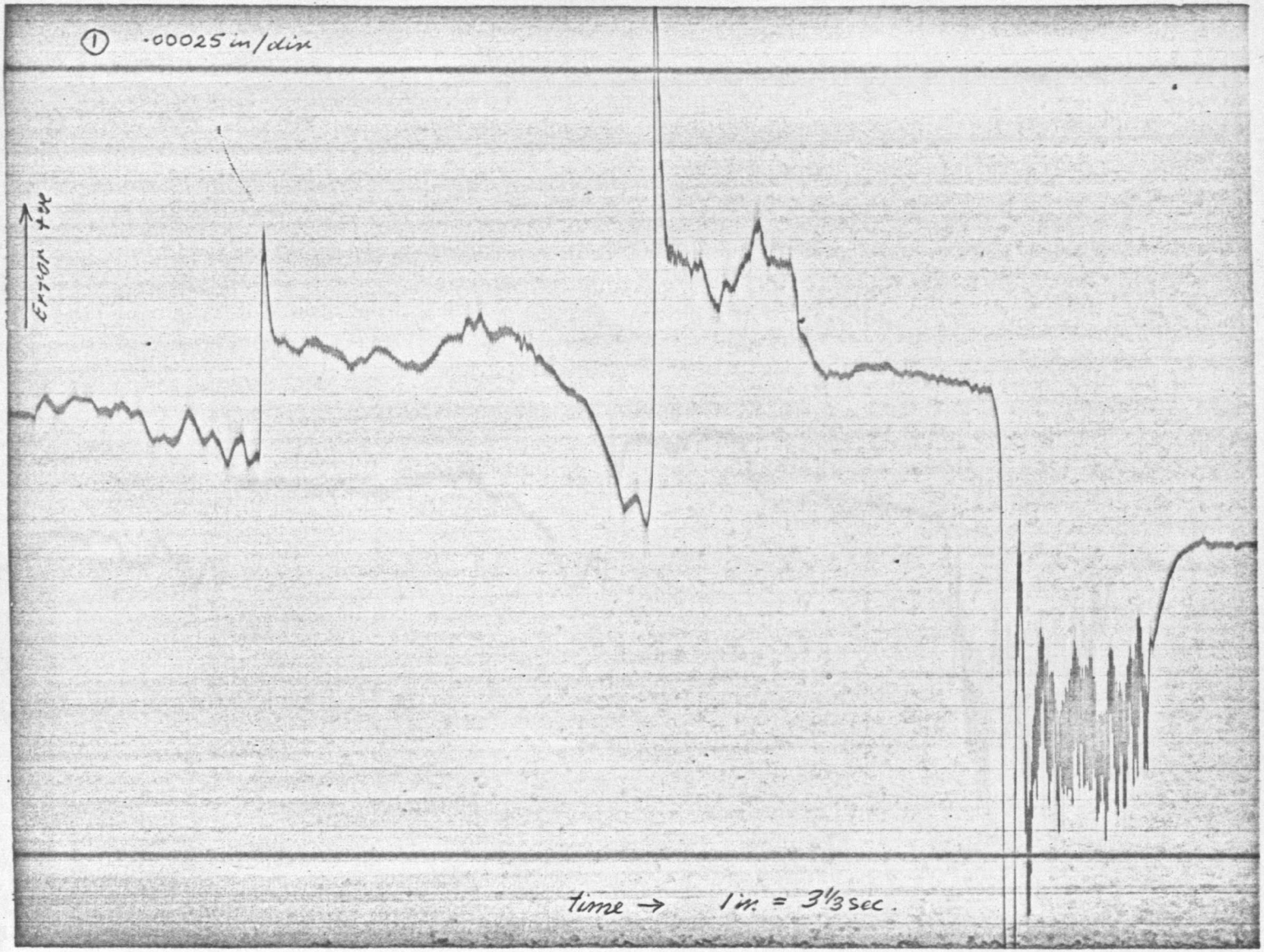
① .00025 in/div
Extension
time → 1 in. = 3⅓ sec.

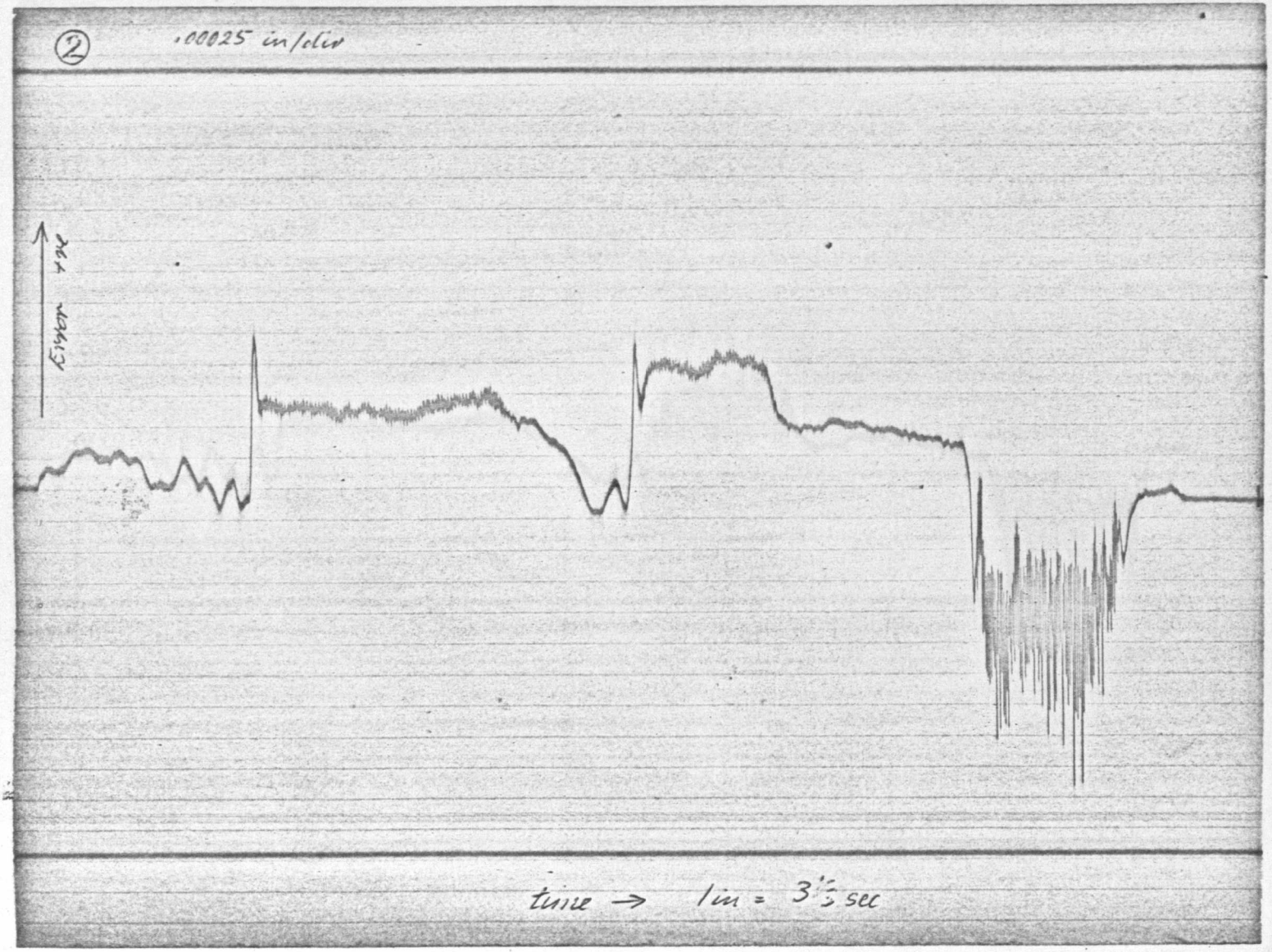
②
.00025 in/div
time →
1in = 3⅓ sec

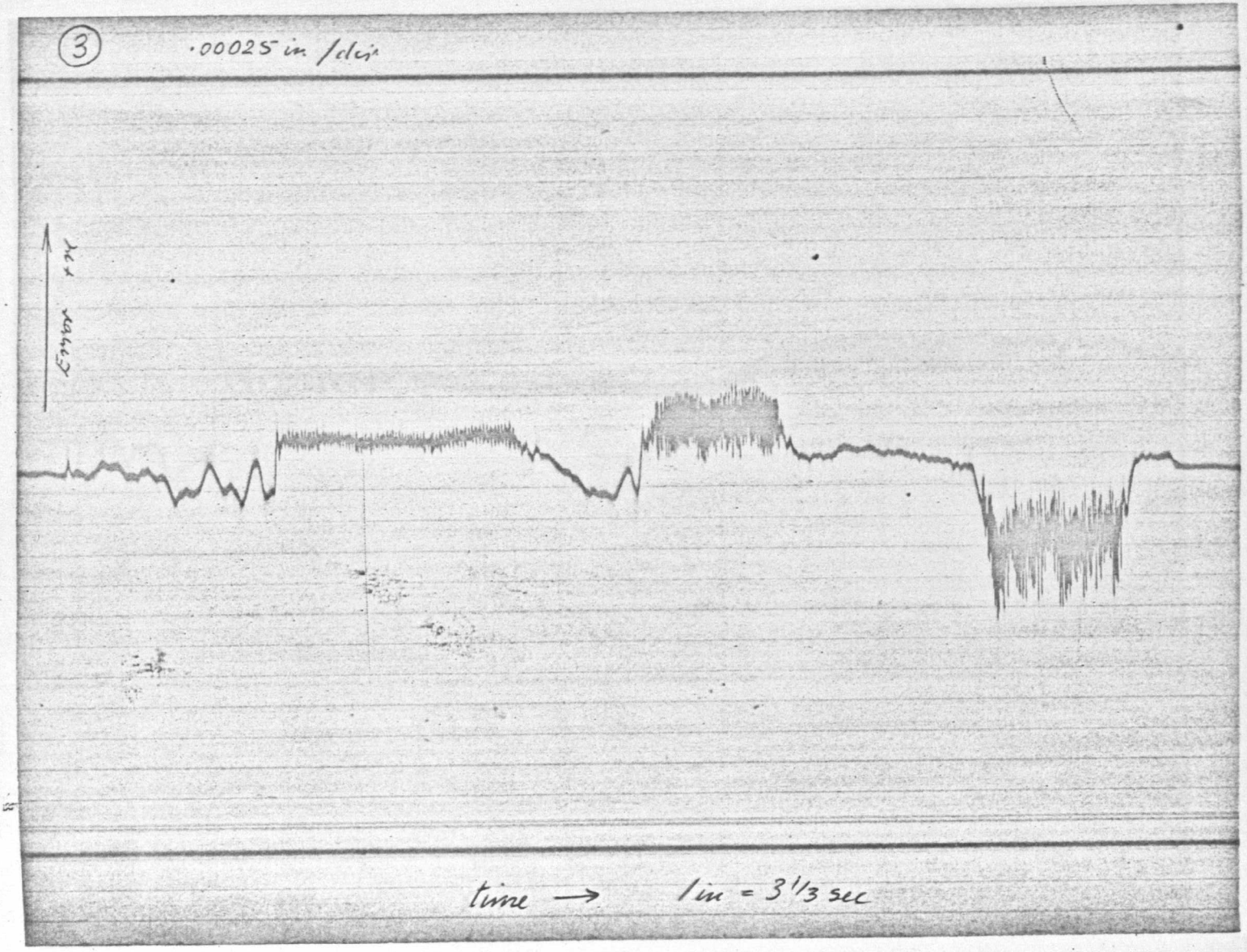
(3)
·00025 in /div
time →
1 in = 3 1/3 sec

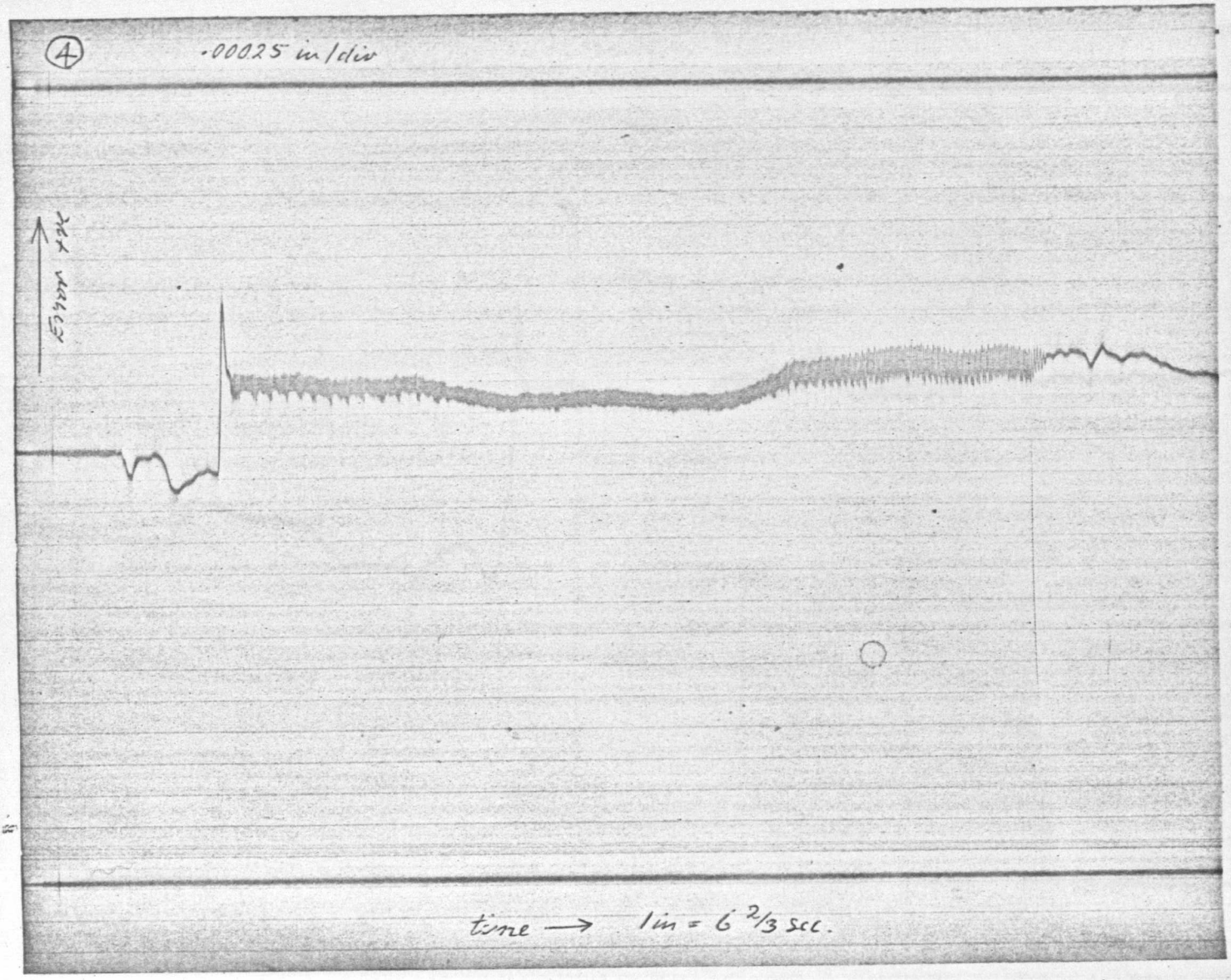
④
.00025 in/div
time → 1in = 6 2/3 sec.

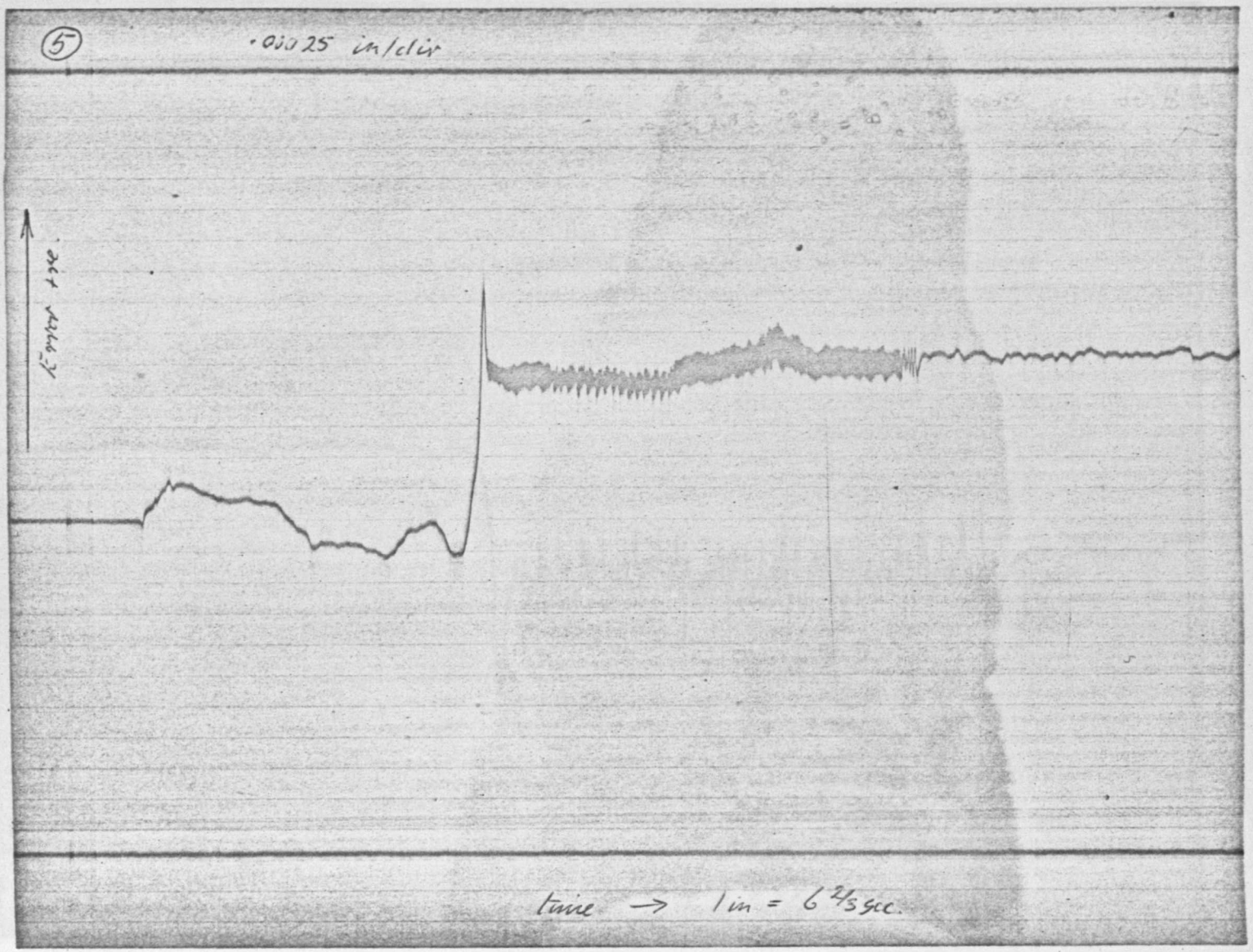
5
.00025 in/div
time → 1 in = 6 2/3 sec.

(6)
.0025 cm/div
x - axis
time → 1 in = 0.1/35 sec

Extension
.0005 in/div
time →
1 in = 2 1/3 sec

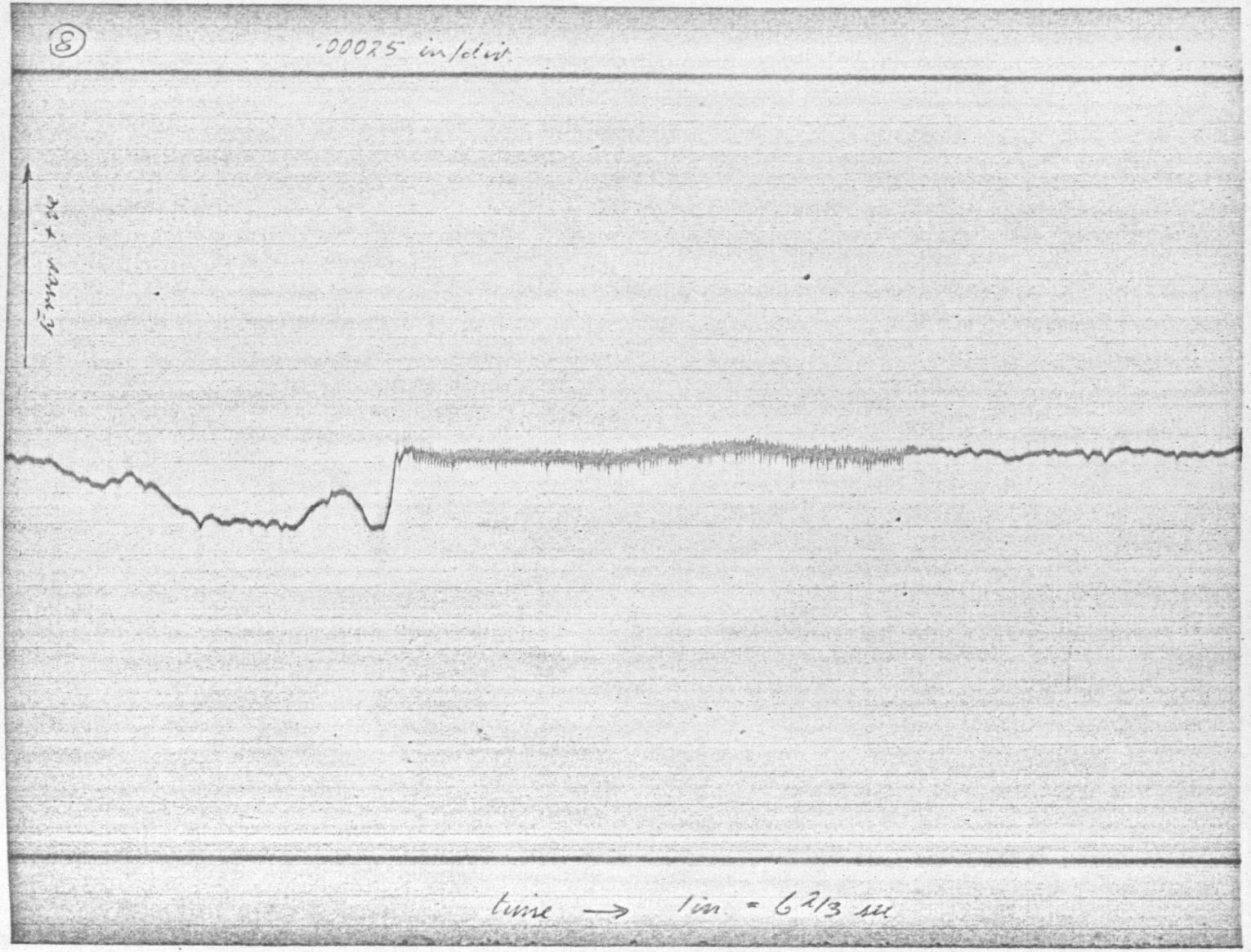
(6)
·00025 in/div.
time → 1in. = 6 2/3 sec

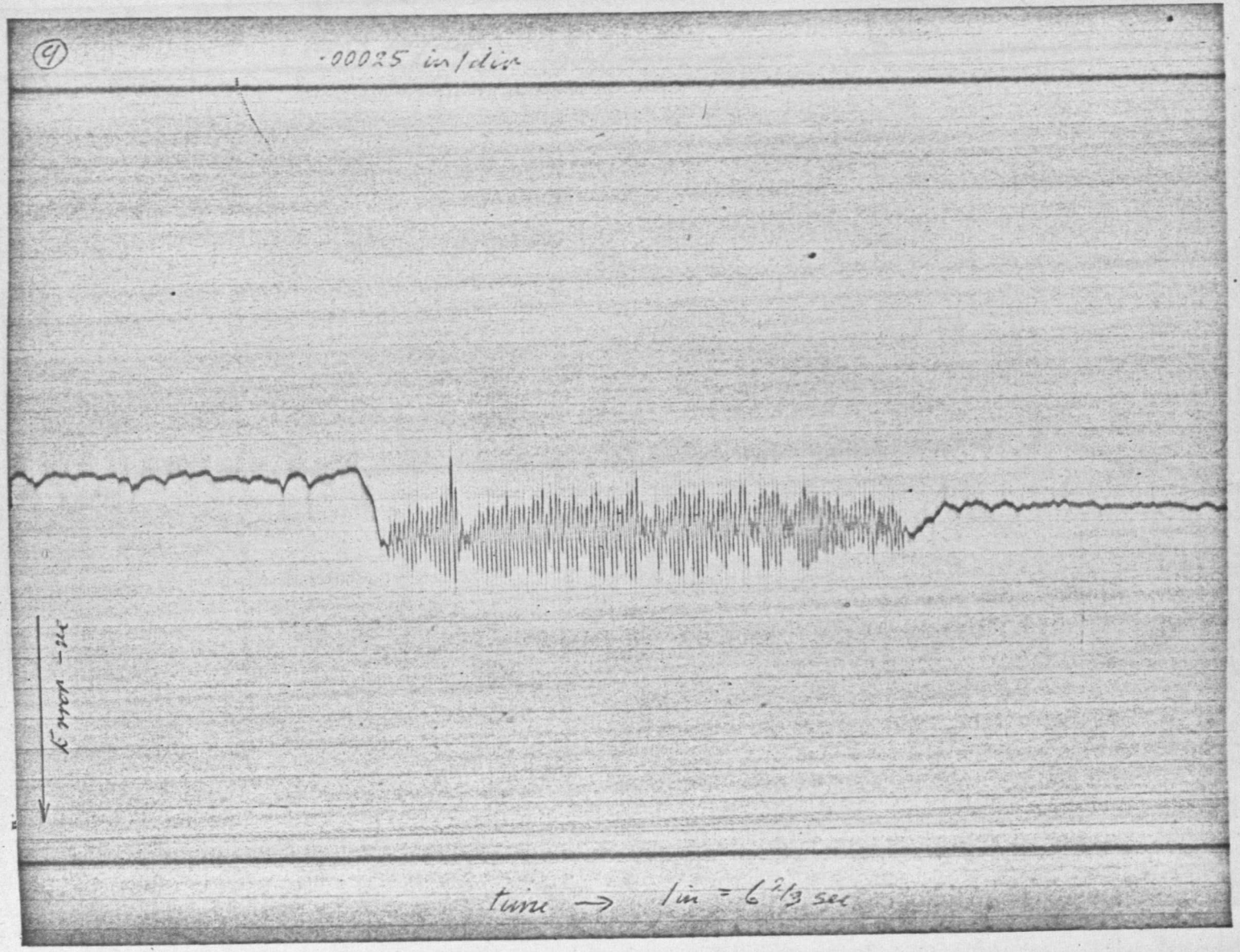
(4)
·00025 in/div
time →
1 in = 6 2/3 sec

(10)

.00025 in/div

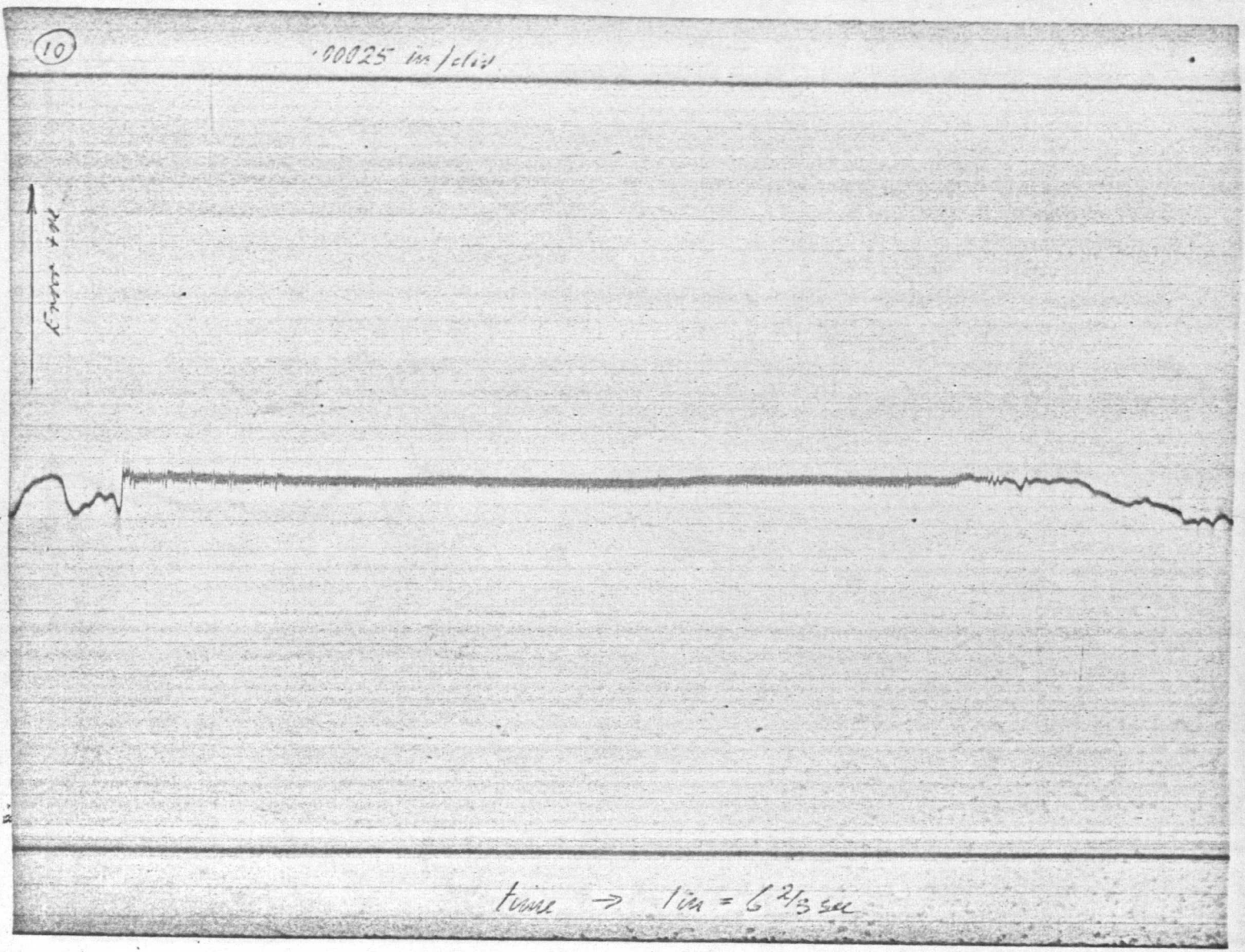

(11) .00025 in/div

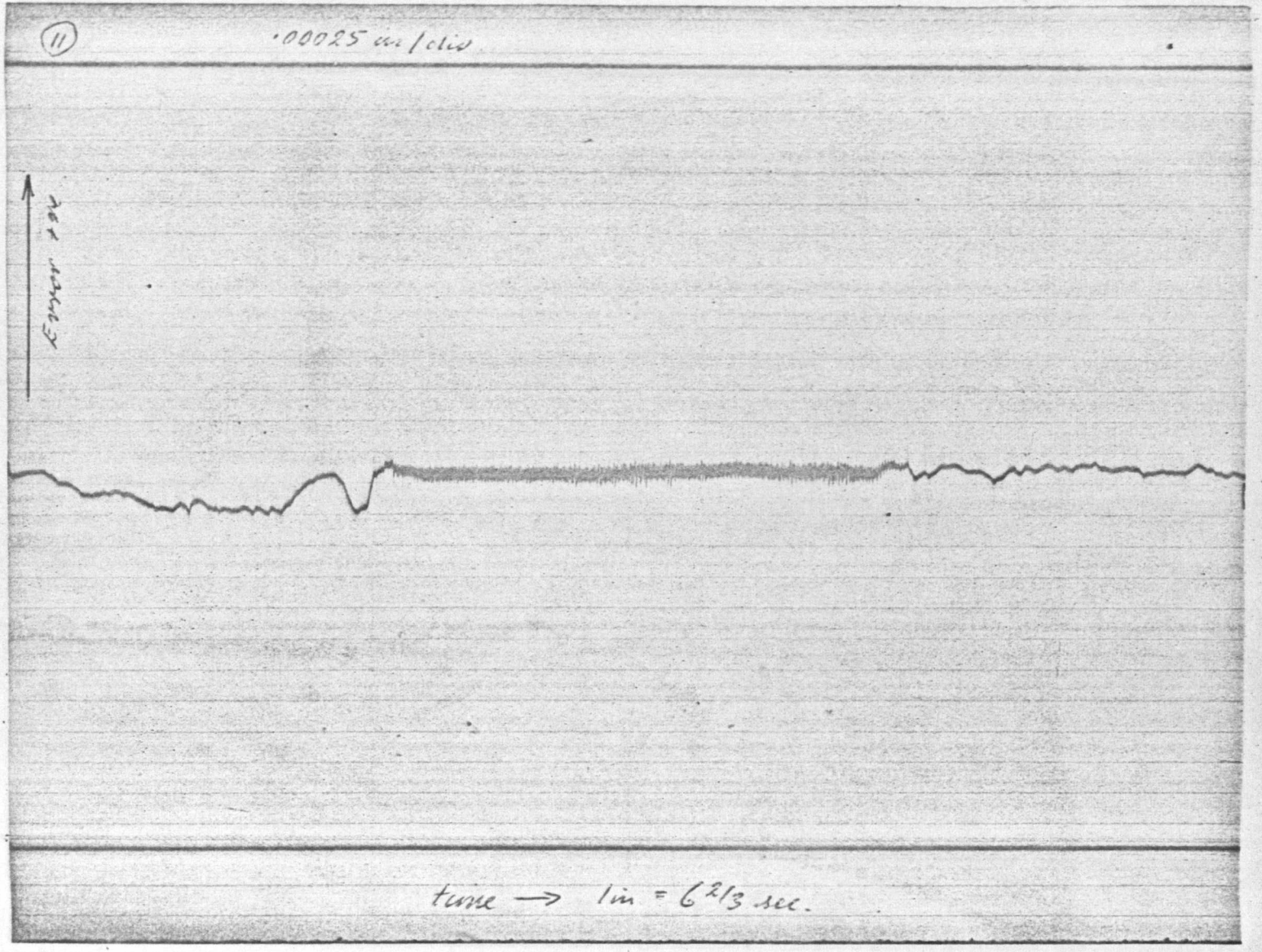

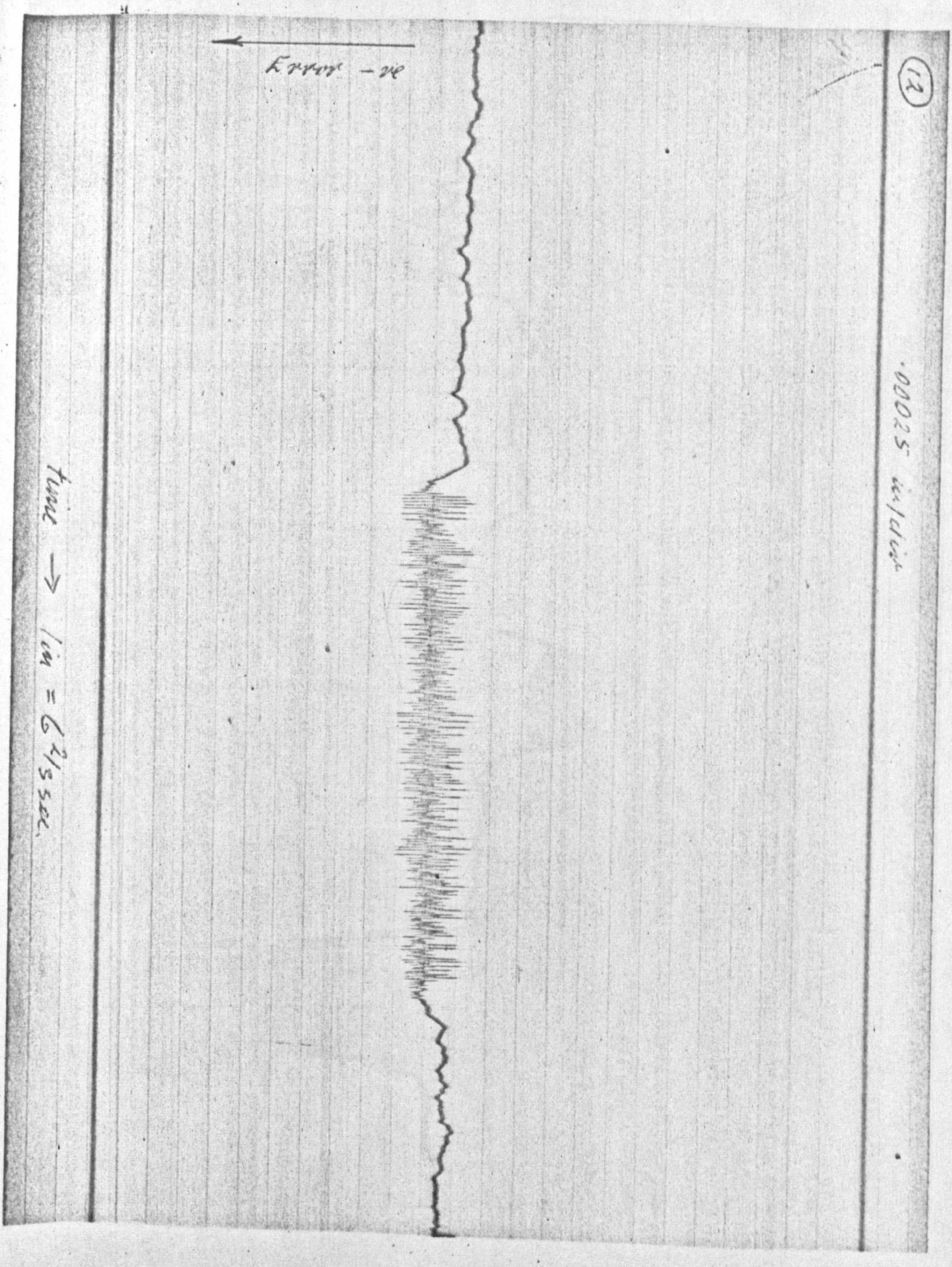
Error -ve
(12)
.00025 in/div
time → 1in = 6 2/3 sec.

(13)

.00025 in/div

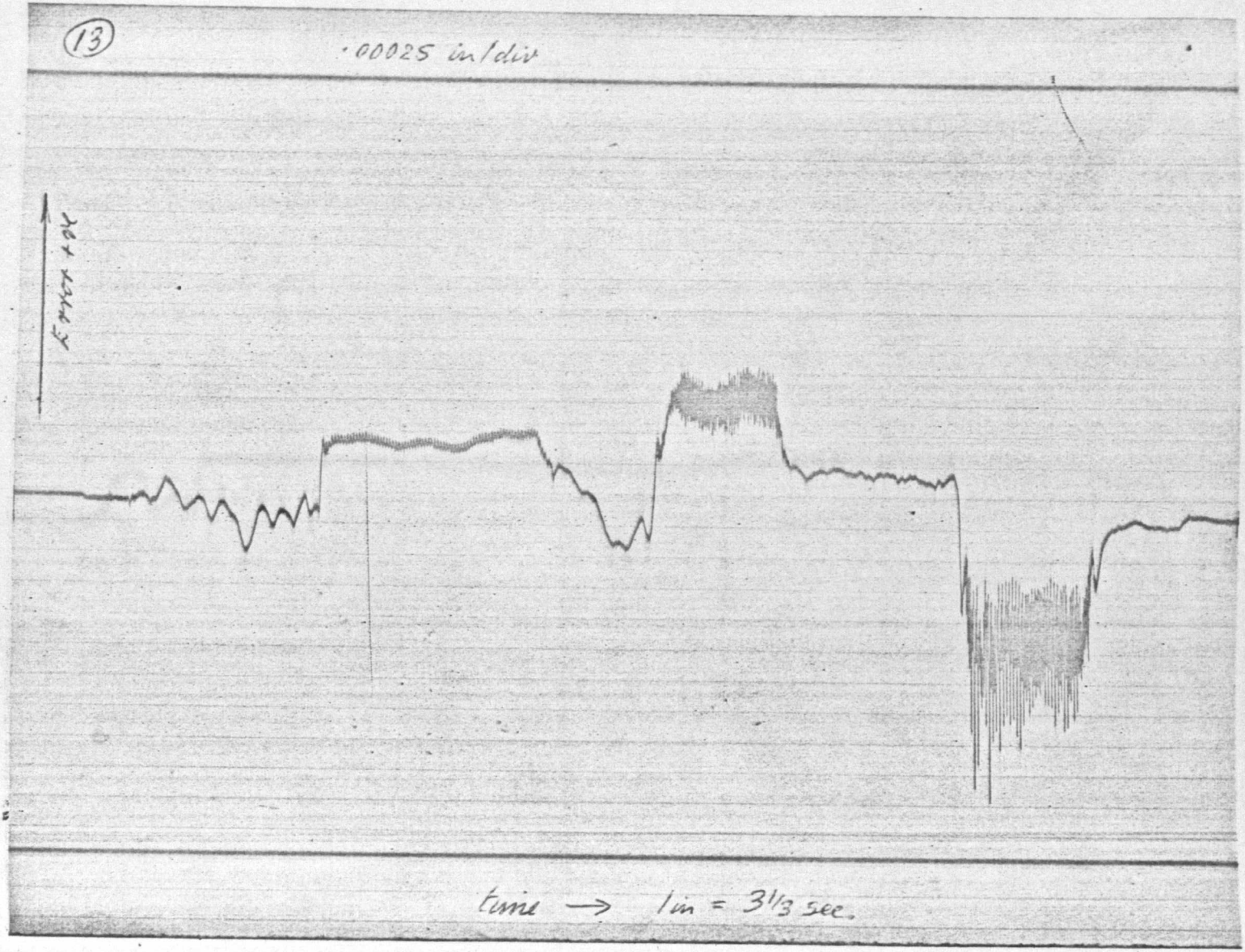

Error axis.
(14)
.00035 in/div
time → 1in = 6 2/3 sec

(15) .00025 in/div

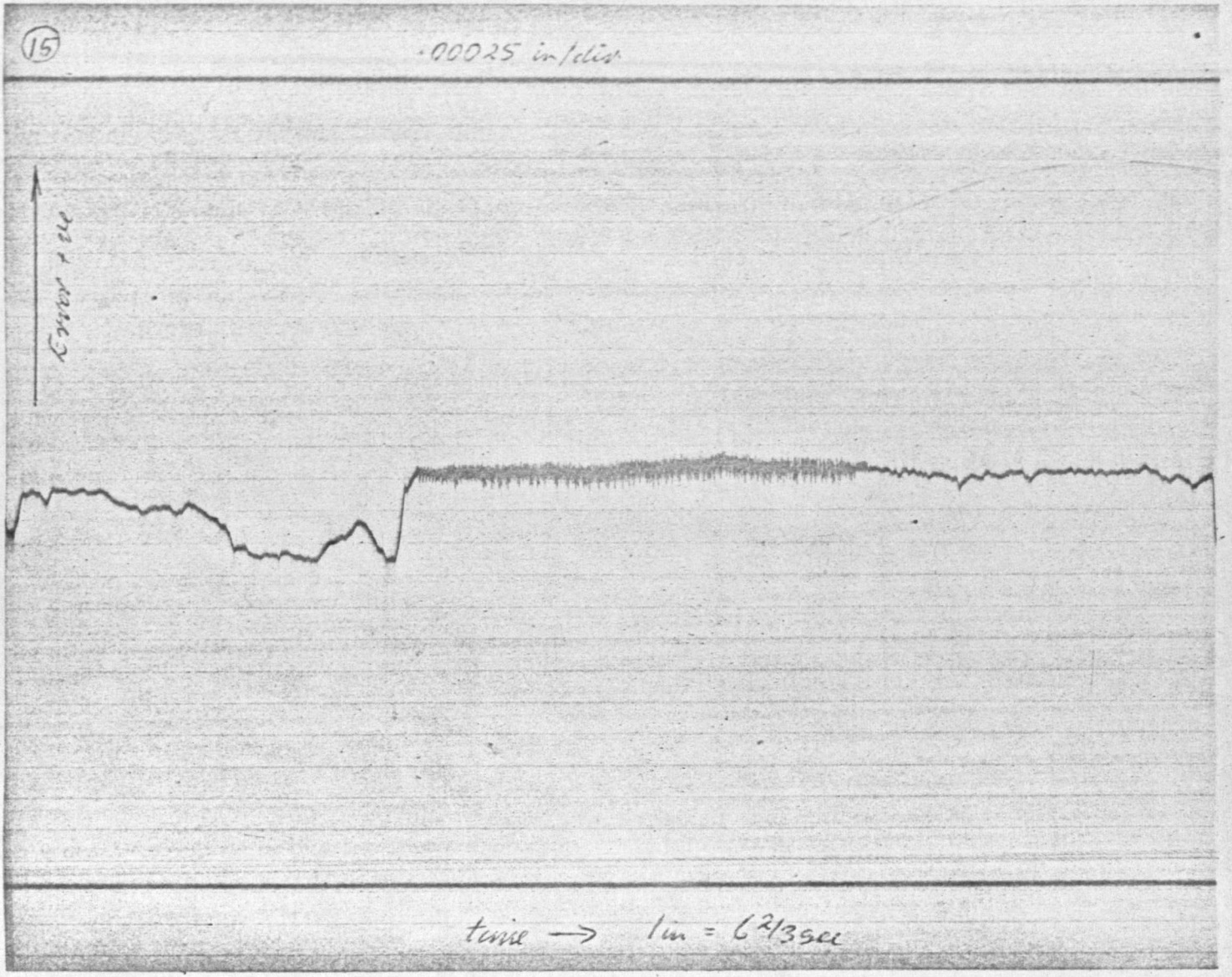

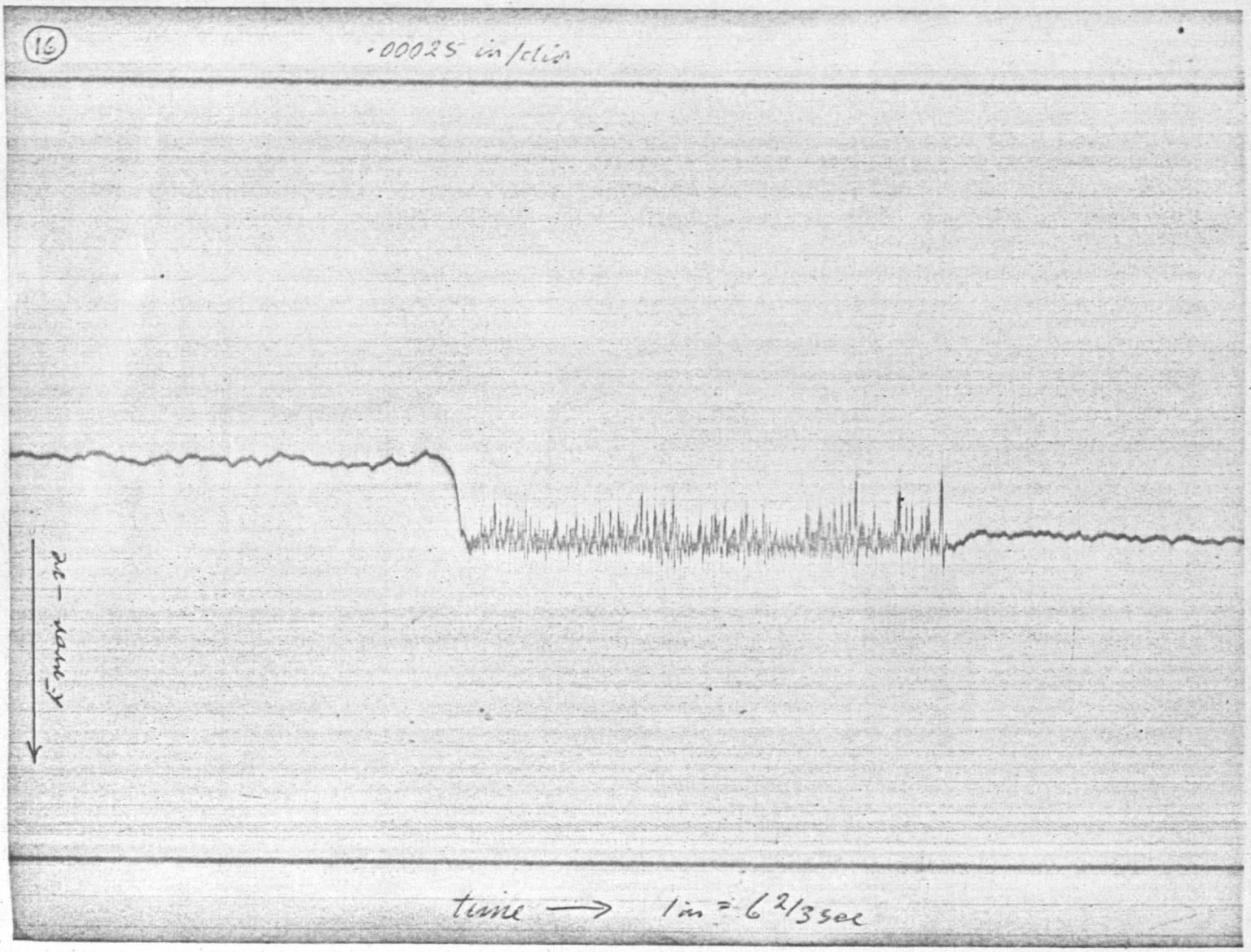
16
.00025 in/division
time → 1 in = 6 2/3 sec

(17) .00025 in/div

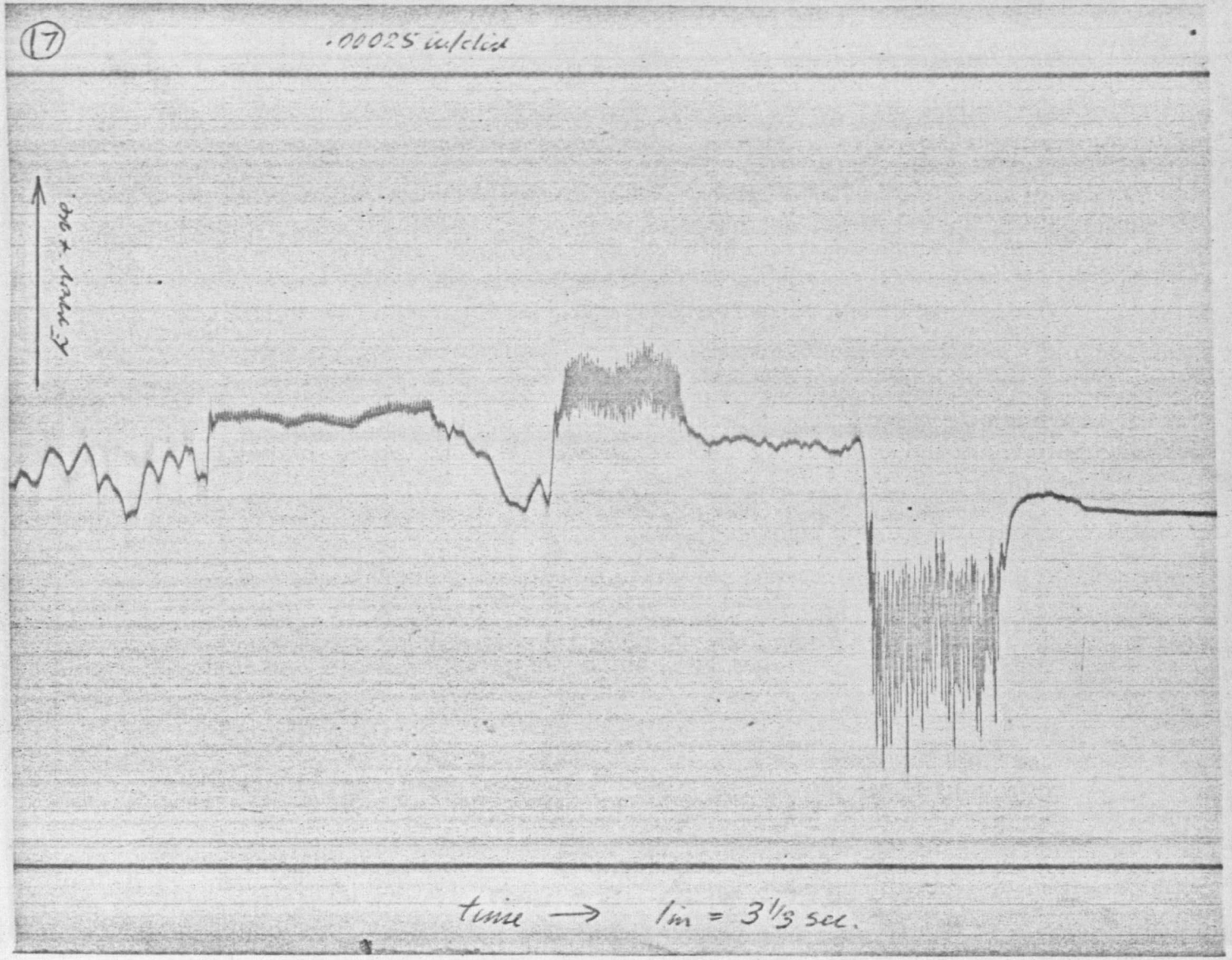

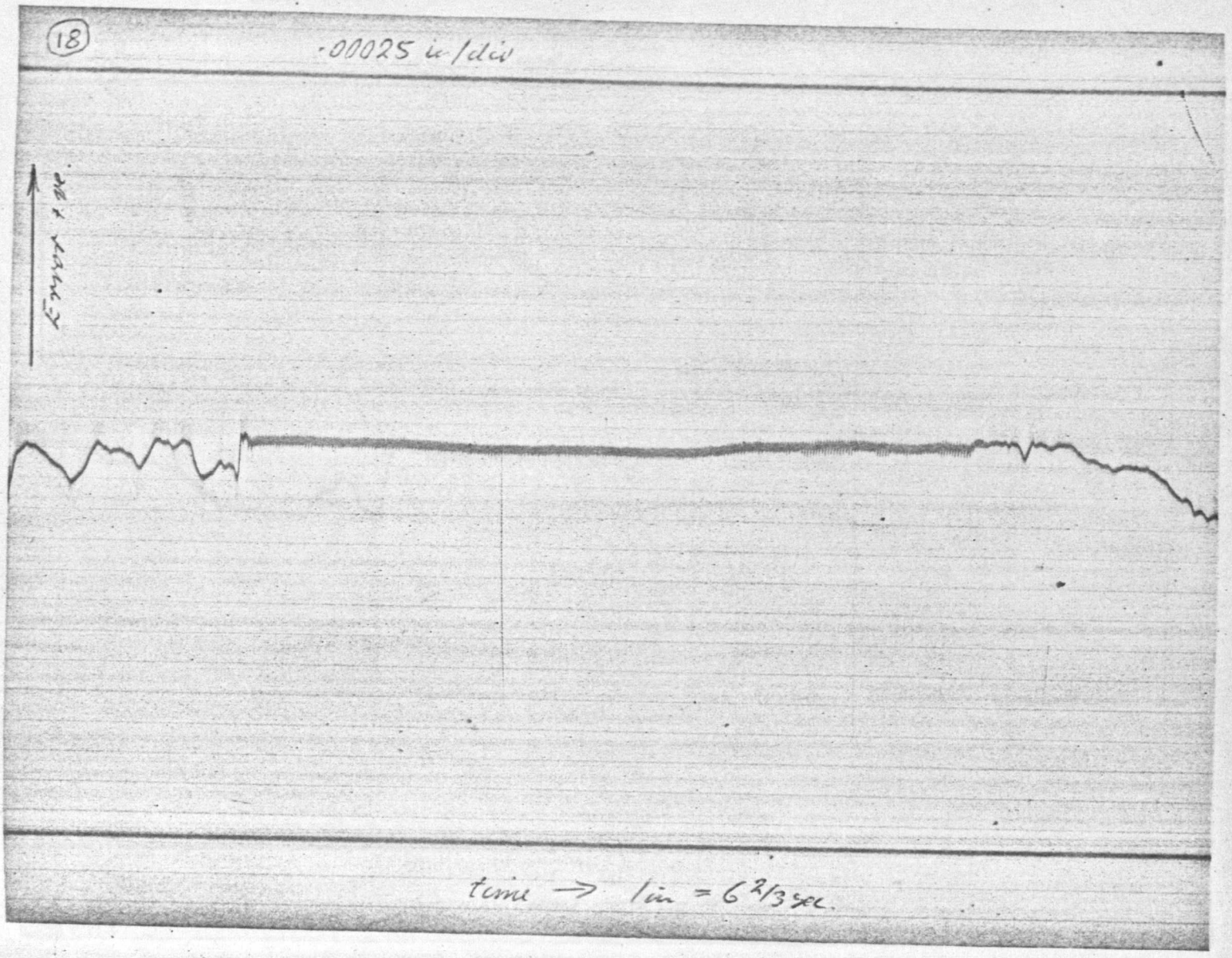
(18)
.00025 in/div
time → 1 in = 6 2/3 sec.

(19)

.00025 in/div

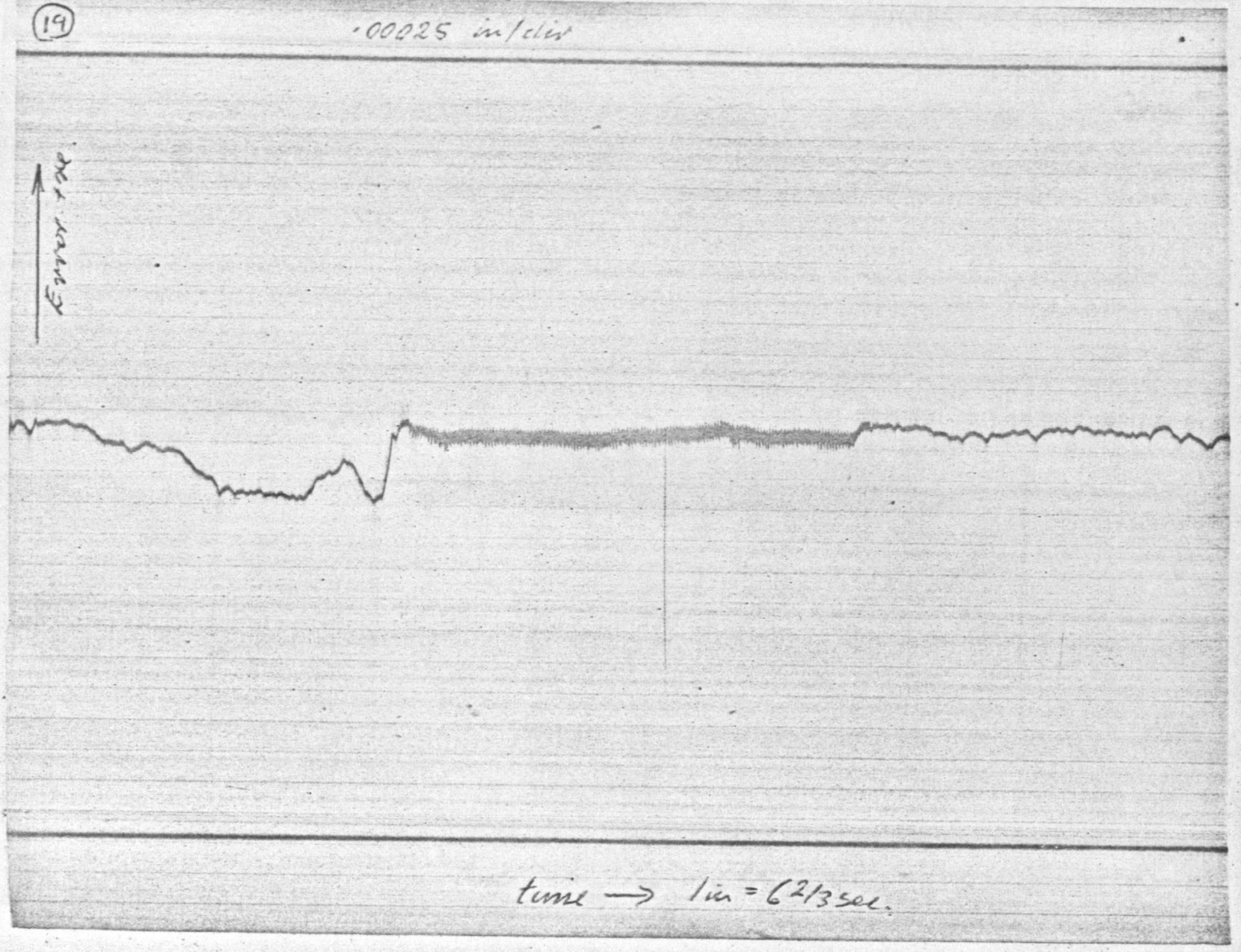

(20) .00025 in/div

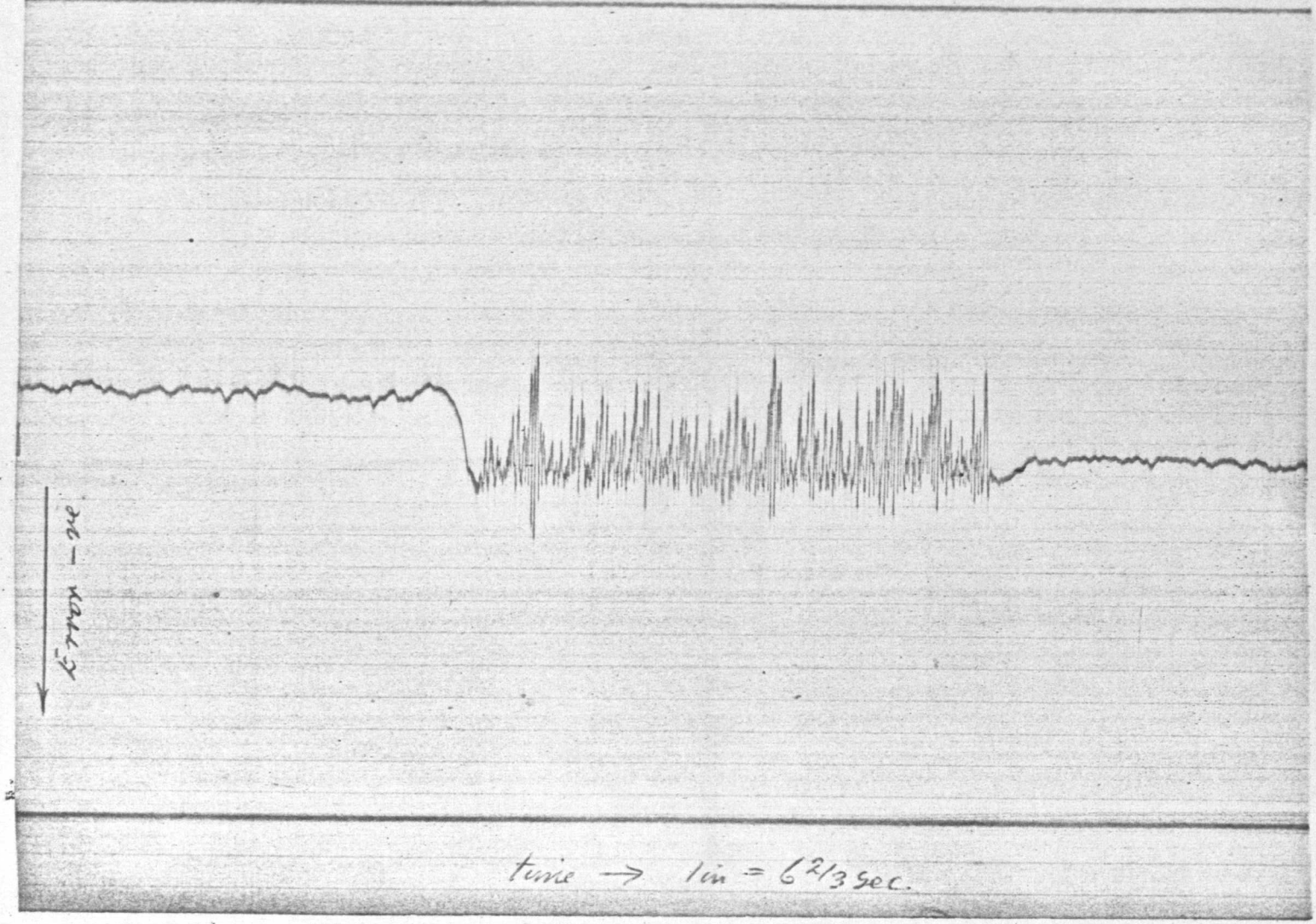

APPENDIX 2

Computer programme for theoretical response of the digital servomechanism

Computer Programme

The computer employed for calculating stations on the theoretical response curve of the digital servomechanism, was a Honeywell model 120 system installed at Enfield College of Technology. In this installation, the machine can only be operated by the computer staff, who also prepare the input cards from programmes written on standardized forms.

The programme written for this work is largely due to the efforts of Stanley Millward, who has also co-operated with me in preparing the block diagram of the programme given in Fig.A2-1. The machine was operated with the high level language 'Fortran D', and some difficulty was experienced in making the programme run. This was due to trouble with the fortran compiler supplied by Honeywell, and necessitates a number of procedural changes in programming.

Normally with fortran programmes it is possible to write in format statements as necessary, but it was found that this procedure resulted in these statements being stored in such a way that the programme tended to overwrite them. After some time it was discovered that by writing the format statements in one block at the end of the programme, their positioning in the machine store was satisfactory, and no overwriting occurred.

The complete programme is given on the following pages, together with an explanation of the labels used in Table A2.1 overleaf. It will be noticed that the ramp input functions are plotted by the machine as straight lines on the form

$$\theta = K.T \quad (RMP = K * T)$$

where:

K = constant defining the ramp gradient in rad/s

T = time in s

Source Listing

```
      INTEGER I,CT
      LOGICAL L1,L2,L3,L4
      REAL  TAU 1,TAU 2, K
      CT = 0
      DO 444 J=1,3
      READ(2,13)TAU1,TAU2,K,TONC1
      WRITE (3,20)
      WRITE(3,21)TAU1,TAU2,K,TONC1
      WRITE(3,14)
      B=0.1472621
      A=-B
      T1=0
      TH1=0
      W1=0
    1 R=TONC1-W1
      DO 2  I=1,1000
      D=I
      T=(D-1.0)/100.+T1
      Z=T1-T
      Q=Z/TAU1
      THETA=TH1-TAU1*R*(1.6-EXP(Q))-TAU1*Z
      W=TONC1-R*EXP(Q)
      RMP=K*T
```

{Initial Conditions}

{Phase 1}

Table A2.1 Explanation of labels employed in the computer programme.

Programme Label	Symbol	Description
TAU1	τ	Time constant (motor on)
TAU2 or TAUDASH	τ'	Time constant (motor off)
TONC1	T/c	Torque/motor on friction constant
TONC2	T/c'	Torque/motor off friction constant
K		Ramp gradient constant
T	t	Time (s)
THETA	θ	Deflection
TH1	θ_1	Deflection at P_1
TH2	θ_2	Deflection at P_2
W	ω	Velocity (angular) rad/s
B		1-bit inherent error
EPS	e	Error (rad)
SM		A small quantity to prevent the computer dealing with 0
RMP		Value of ramp input
EXP		Code for the exponential

```
      EPS=RMP-THETA
      IF((I.GT.10).AND.(EPS.LE.0))GOTO5
      EPS=EPS+B
      WRITE(3,4)T,RMP,THETA,EPS,W
    2 CONTINUE
    5 TEST=0.
    3 CONTINUE
      Z=T1-T
      Q=Z/TAU1
      THETA=TH1-TAU1*R*(1.0-EXP(Q))-TONC1*Z
      W=TONC1-R*EXP(Q)
      RMP=K*T
      EPS=RMP-THETA
      DEPS=K-W
      T2=T-EPS/DEPS
      DIFF=ABS(T2-TEST)
      SM=0.000001
      TEST=T2
      T=T2
      IF(DIFF.GT.SM) GOTO3
    6 CONTINUE
      TH2=THETA
      W2=W
      KT=1
   17 CONTINUE
    7 DO 8 I=1,1000
      D=I
      T=T2+(D-1.0)/1000
      Z=T2-T
      Q=Z/TAU2
      THETA =TH2+W2*TAU2*(1.0-EXP(Q))
      W=W2*EXP(Q)
      RMP=K*T
      EPS=RMP-THETA
      IH=074
      IF(KT.EQ.1.AND.EPS.LE.A) GOTO201
      IF(EPS.GT.SM.AND.I.GT.3) GOTO11
      EPS=EPS+B
```

{Phase 1 continued}

{Locate P_1}

{Initial Conditions Phase 11}

{Phase 11}

```
      WRITE(3,30)T,RMP,THETA,EPS,W
    8 CONTINUE
   11 TEST=0
   12 CONTINUE
      Z=T2-T
      Q=Z/TAU2
      THETA=TH2+W2*TAU2*(1.0-EXP(Q))
      W=W2*EXP(Q)
      RMP=K*T
      EPS=RMP-THETA
      DEPS=K-W
      T=T-EPS/DEPS
      DIFF=ABS(EPS)
      T1=T
      IH=116
      IF(DIFF.GT.SM) GOTO12
      TH1=THETA
      W1=W
      CT=CT+1
      IF(CT.LT.5) GOTO1
      IF(CT.EQ.5) GOTO444
   10 CONTINUE
  201 CONTINUE
      SM=0.00001
      KT=2
      Z=T2-T
      TEST=T
      Q=Z/TAU2
      THETA=TH2+W2*TAU2*(1.0-EXP(Q))
      W=W2*EXP(Q)
      RMP=K*T+B
      F=RMP-THETA
      DF=K-W
      T=T-F/DF
      DIFF=ABS(F)
      TEST=T3
      IF(DIFF.GT.SM) GOTO201
```

{Phase 2 continued}

{Locate P_{11}}

{Initial conditions Phase 1}

{Locate P_2}

```
      T3=T                                  {Initial conditions Phase 111}
      W3=W
      TH3=THETA
      DO 211 I=1,2000
      D=I
      T=(D-1.0)/100.+T3
      Z=T3-T
      Q=Z/TAU1
      R=TONC1-W3
      THETA=TAU1*R*(1.o-EXP(Q))+TONC1*Z+TH3
      W=R*EXP(Q)-TONC1
      RMP=K*T+B
      IH=156                                {Phase 111}
      EPS=RMP-THETA
      CONTINUE
      WRITE(3,456)T,RMP,THETA,EPS,W
      CONTINUE
      IF(EPS.GT.0.00001.AND.I.GT.3) GOTO22
211   CONTINUE
 22   CONTINUE
 40   TEST=T
      Z=T3-T
      Q=Z/TAU1
      R=TONC1+W3
      THETA = TAU1*R*(1.0-EXP(Q))+TONC1*Z+TH3
      W=R*EXP(Q)-TONC1
      RMP=K*T+B                             {Locate P22}
      F=RMP-THETA
      DF=K-W
      T=T-F/DF
      DIFF=ABS(F)
      TEST=T
      IH=202
      IF(DIFF.GT.SM)  GOTO40
113   CONTINUE
      T2=T                                  {Initial conditions Phase 11}
      W2=W
```

```
      TH2=THETA                          {Initial conditions Phase 11}
      KT=2
      GOTO 17
  444 CONTINUE
    4 FORMAT(1H ,5F10.5)
   13 FORMAT(4F10.5)
   14 FORMAT(1H4,3X,5H TIME,5X,5H RAMP,4X,6H ANGLE,4X,4H EPS,6X,3H W)
   20 FORMAT(1H1,10H TAU ,10H TAUDASH,10H T,7H TONC)
   30 FORMAT(5F10.5)
   31 FORMAT(I10)
   21 FORMAT(1H ,4F10.5)
   67 FORMAT(1H ,F10.5)
   97 FORMAT(I10)
  400 FORMAT(1H ,10X,2F10.5)
  456 FORMAT(5F10.5)
      END
```

A block diagram of the computer programme is given on the following pages and Fig.A2-2 defines the various regions and points of intersection on the theoretical response curve to ramp type input functions.

In the programme more general forms of the response functions were employed, and these formulae are given below:

Phase 1

$$\theta = \theta_1 - \mathcal{T}(T/c - \omega_1)(1 - e^{\frac{t_1 - t}{\mathcal{T}}}) - T/c(t_1 - t) \qquad \text{eq(a)}$$

Phase 11

$$\theta = \theta_2 + \omega_2 x \mathcal{T}'(1 - e^{\frac{t_2 - t}{\mathcal{T}'}}) \qquad \text{eq(b)}$$

Phase 111

$$\theta = \theta_3 + \mathcal{T}(T/c + \omega_3)(1 - e^{\frac{t_3 - t}{\mathcal{T}}}) + T/c(t_3 - t) \qquad \text{eq(c)}$$

Fig.A2-1 Block diagram of the Computer Programme

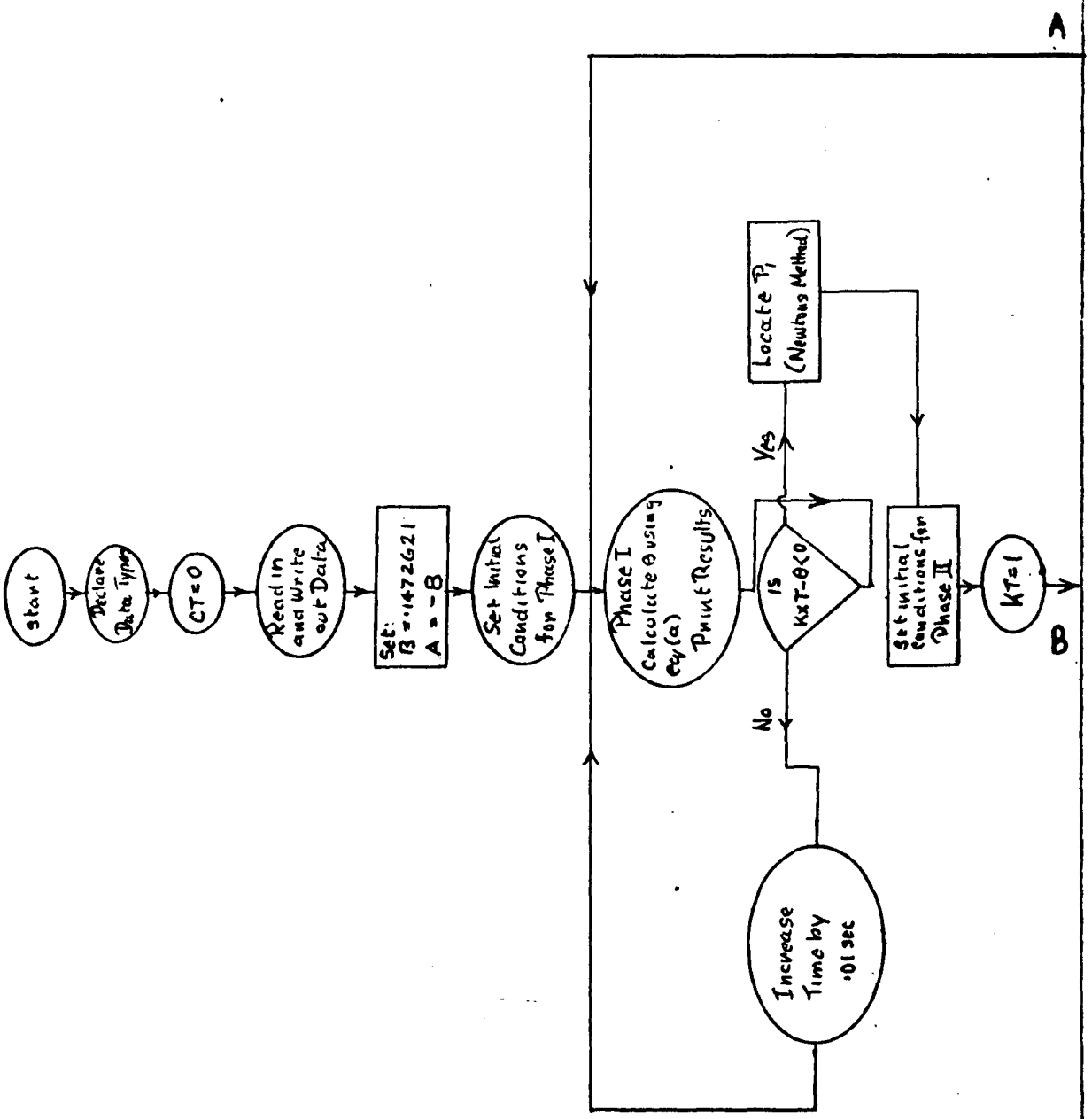

Fig.A2-1

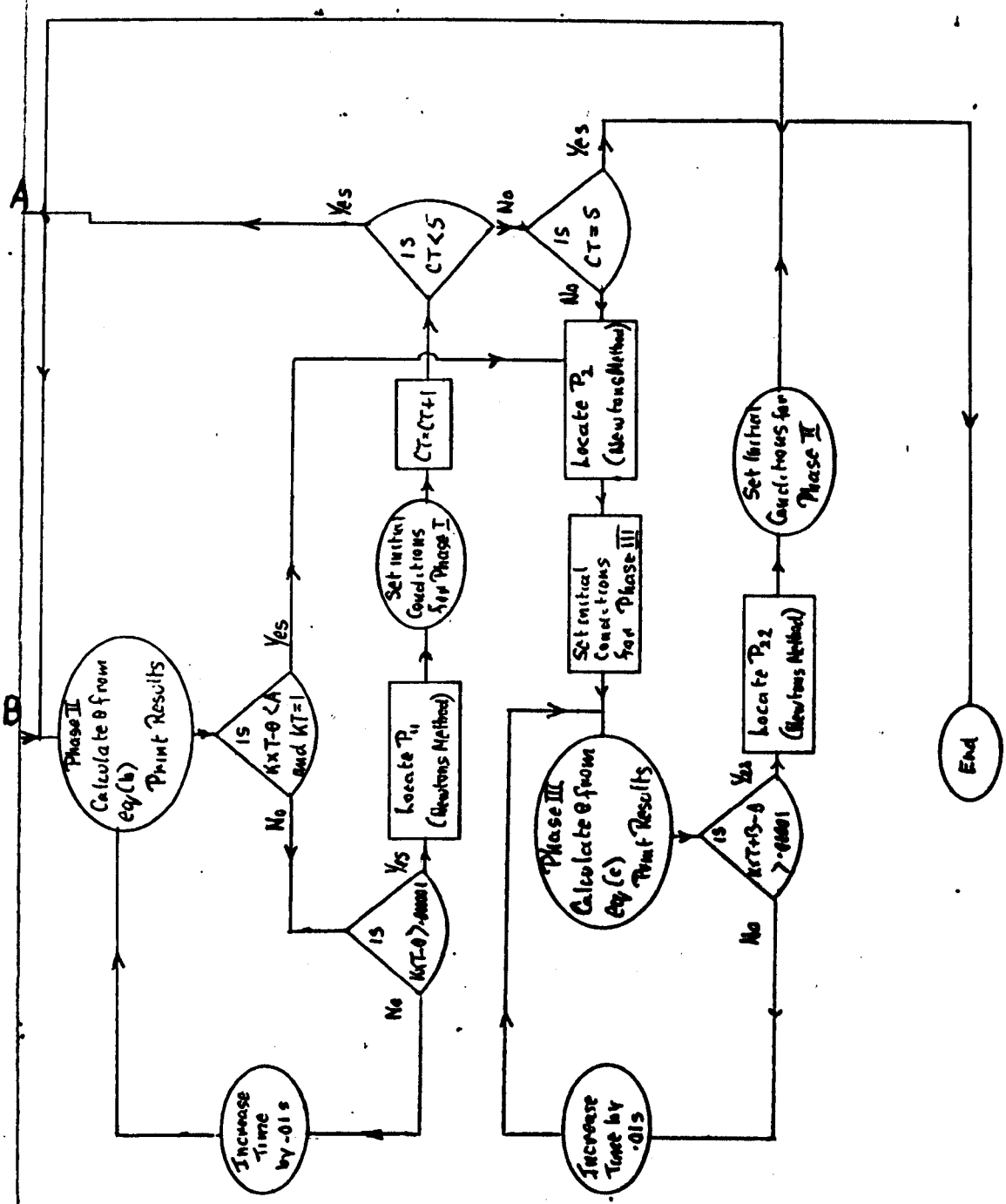
A
B
IS CT<5
Yes
No
IS CT=5
Yes
No
Locate P_1 (Newtons Method)
Set initial Conditions for Phase III
Phase III Calculate θ from eq.(c) Print Results
IS |KT+3-θ| >.0001
Yes
No
Locate P_{32} (Newtons Method)
Set initial Conditions for Phase II
End
CT=CT+1
Set initial Conditions for Phase I
Locate P_{11} (Newtons Method)
IS |KT-θ|>.0001
Yes
No
Phase II Calculate θ from eq.(b) Print Results
IS KxT-θ<A and KT=1
Yes
No
Increase Time by .01s
Increase Time by .01s

Fig.A2-2 Theoretical Response Curve - Explanation of Stations

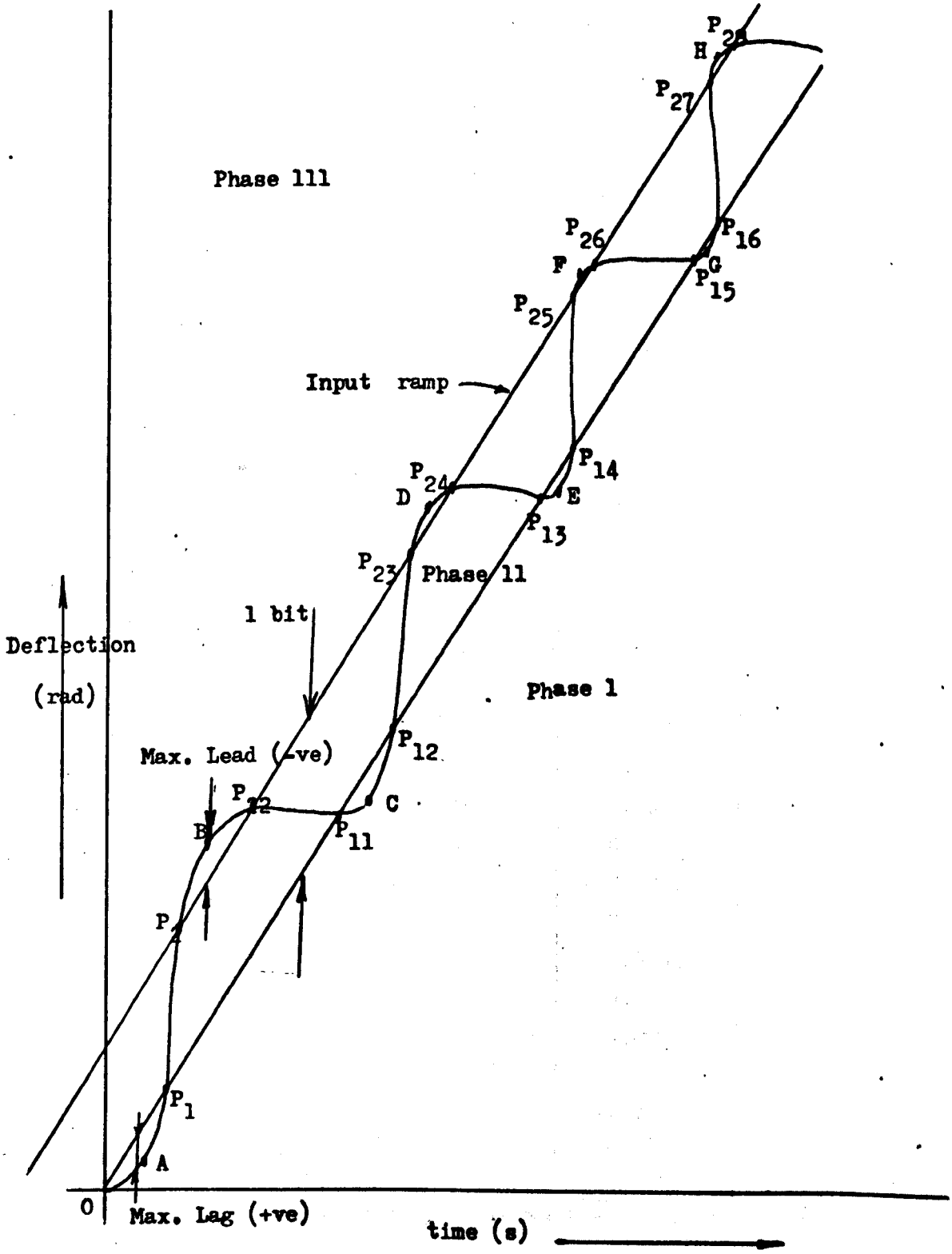

Table A2.2 Theoretical response to 21 rad/s input ramp

(Input Ramp = 21 rad/s)

Station	Time (s)	Error (rad)	Error (in)
0	0	.14726	0.0005
A	.77000	7.77488	0.0264
P_1	1.64491	.14726	0.0005
P_2	1.65396	0	0
B	2.03196	-2.79311	-0.0095
P_{22}	2.38555	0	0
P_{11}	2.39573	.14726	0.0005
C	2.95573	4.03569	0.0137
P_{12}	3.56795	.14726	0.0005
P_{23}	3.58032	0	0
D	3.85033	-1.54819	-0.0053
P_{24}	4.12472	0	0
P_{13}	4.13815	.14726	0.0005
E	4.57815	2.47838	0.0084
P_{14}	5.04507	.14726	0.0005
P_{25}	5.06069	0	0
F	5.26069	-0.95880	-0.0033
P_{26}	5.48965	0	0
P_{15}	5.50647	.14726	0.0005
G	5.86647	1.68237	0.0057
P_{16}	6.24215	.14726	0.0005
P_{27}	6.26128	0	0
H	6.43128	-0.6384	-0.0022
P_{28}	6.61085	0	0
P_{17}	6.63126	.14726	0.0005
J	6.93126	1.22137	0.0042
P_{18}	7.24648	.14726	0.0005
P_{29}	7.26934	0	0
K	7.39924	-0.43836	-0.0015
P_{210}	7.56030	0	0

These results have been used to plot curve Fig.4-18, Section 4.

Table A2.3 Theoretical response to 10.5 rad/s input ramp

(Input Ramp = 10.5 rad/s)

Station	Time (s)	Error (rad)	Error (in)
0	0	.14726	0.0005
A	.3600	1.94554	0.0066
P_1	.7240	.14726	0.0005
P_2	0.7398	0	0
B	.9698	-1.0595	-0.0036
P_{22}	1.2184	0	0
P_{11}	1.2356	.14726	0.0005
C	1.5256	1.36786	0.0046
P_{12}	1.8318	.14726	0.0005
P_{23}	1.8510	0	0
D	2.0510	-0.73005	-0.0025
P_{24}	2.2482	0	0
P_{13}	2.2688	.14726	0.0005
E	2.5188	1.01767	0.0034
P_{14}	2.7721	.14726	0.0005
P_{25}	2.7948	0	0
F	2.9648	-0.52257	-0.0018
P_{26}	3.1309	0	0
P_{15}	3.1550	.14726	0.0005
G	3.3650	.79001	0.0027
P_{16}	3.5875	.14726	0.0005

These results have been used to plot curve Fig.4-19, Section 4.

Table A2.4 Theoretical response to 5.25 rad/s input ramp

(Input Ramp = 5.25 rad/s)

Station	Time (s)	Error (rad)	Error (in)
0	0	.14726	0.0005
A	.1700	.58520	0.0020
P_1	.3425	.14726	0.0005
P_2	.3727	0	0
B	.5027	-.31445	-0.0011
P_{22}	.6422	0	0
P_{11}	.6743	.14726	0.0005
C	.8243	.48421	0.0016
P_{12}	.9747	.14726	0.0005
P_{23}	1.0092	0	0
D	1.1292	-.23982	-0.0008
P_{24}	1.2446	0	0
P_{13}	1.2812	.14726	0.0005
E	1.4112	.40943	0.0014
P_{14}	1.5461	.14726	0.0005
P_{25}	1.5854	0	0
F	1.6854	-.18391	-0.0006
P_{26}	1.7915	0	0
P_{15}	1.8331	.14726	0.0005
G	1.9531	.35246	0.0012
P_{16}	2.0676	.14726	0.0005
P_{27}	2.1121	0	0
H	2.2021	-.14105	-0.0005
P_{28}	2.2926	0	0
P_{17}	2.3398	.14726	0.0005

These results have been used to plot curve Fig.4-20, Section 4.

Table A2.5 Theoretical initial response to 21 rad/s input ramp

(Input Ramp = 21 rad/s)

Time (s)	Error (rad)	Error (in)
0	.14726	0.0005
.10	2.08831	0.0071
.20	3.72093	0.0127
.30	5.05881	0.0172
.40	6.11506	0.0208
.50	6.90218	0.0235
.60	7.43214	0.0253
.70	7.71637	0.0262
.80	7.76578	0.0264
.90	7.59081	0.0258
1.00	7.20143	0.0245
1.10	6.60717	0.0225
1.20	5.81713	0.0198
1.30	4.84002	0.0165
1.40	3.68414	0.0125
1.50	2.35744	0.0080
1.60	.86750	0.0030
1.64491	.14726	0.0005
1.65396	0	0

The results have been used to plot the initial response curve given in Fig.4-21, Section 4.

Fig.A2-3 Decrease in lag amplitude with time

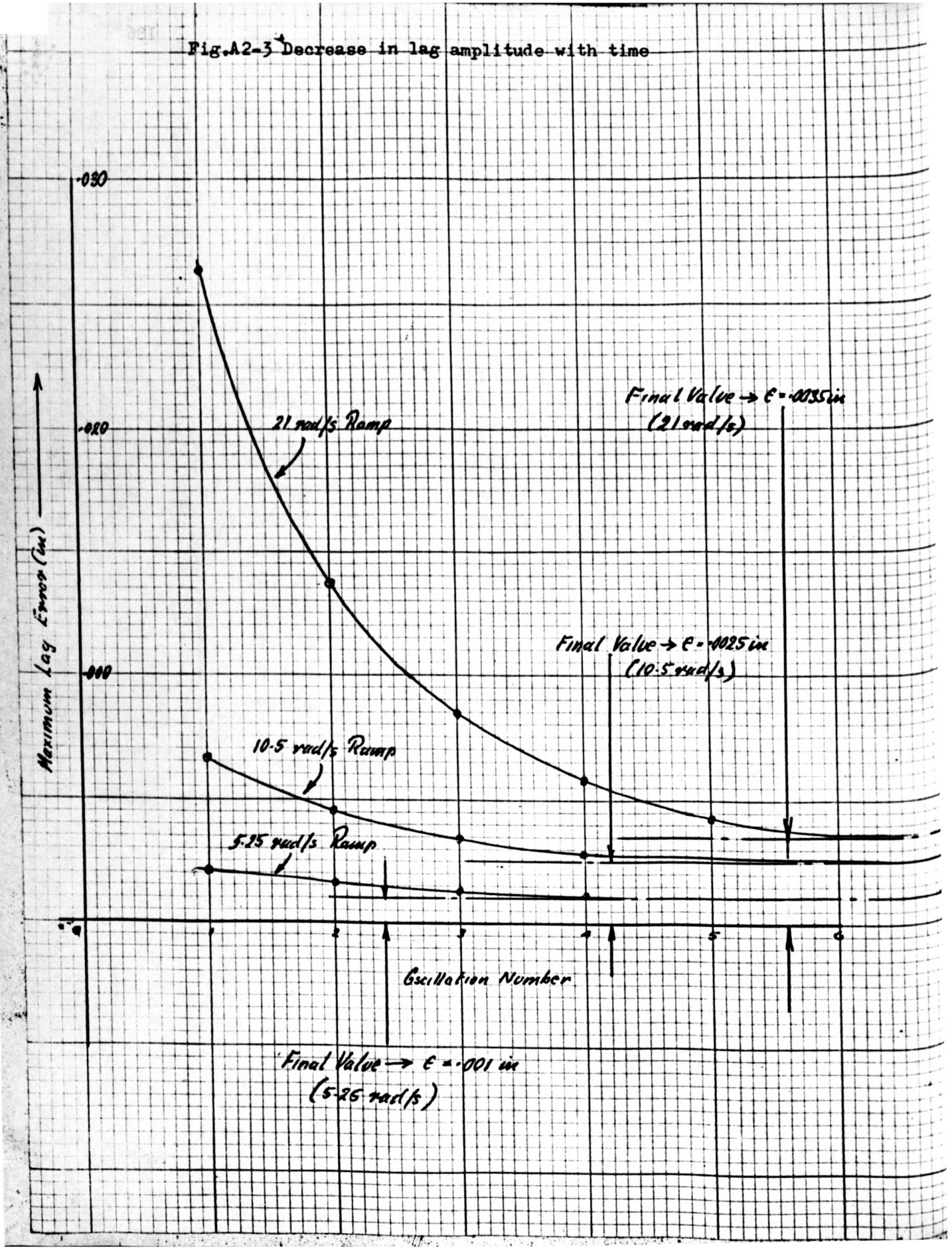

Interpretation of Computer Results

The results from the computer programme for theoretical response of the digital system to three input ramps are listed in condensed form in Tables A2.2, A2.3, A2.4 and A2.5, and these values have been used to plot the response curves included in Section 4. As stated in that section, it is clear that the amplitudes of the error oscillations decrease with time, and in Table A2.5 below these lag amplitudes are listed.

Input Ramp (rad/s)	Maximum Lag Error (in)				
5.250	0.0020	0.0016	0.0014	0.0012	
10.500	0.0066	0.0046	0.0034	0.0027	
21.000	0.0264	0.0137	0.0084	0.0057	0.0042
Oscillation Number	1	2	3	4	5

These results have been used to plot the curves in Fig.A2.3 opposite, which may be seen to tend to values indicated in the figure.

APPENDIX 3

Detailed results of the response tests on the digital servo-mechanism.

Interpretation of Results - Step input response

The digital system is a two speed device without proportional control, and it is arranged that the system runs at high speed when the error number exceeds 255 (equivalent to a ram travel of approximately 0.125 in). For errors between 255 and zero, the driving motor is supplied with d.c. pulses to provide a low speed running condition so that the ram does not overshoot the command setting. The mark-to-space ratio of these pulses was adjusted by means of a preset potentiometer fitted to the motor control unit, and this adjustment was established by trial.

The anticipated response of the system to a step input is shown below in Fig.A3-1.

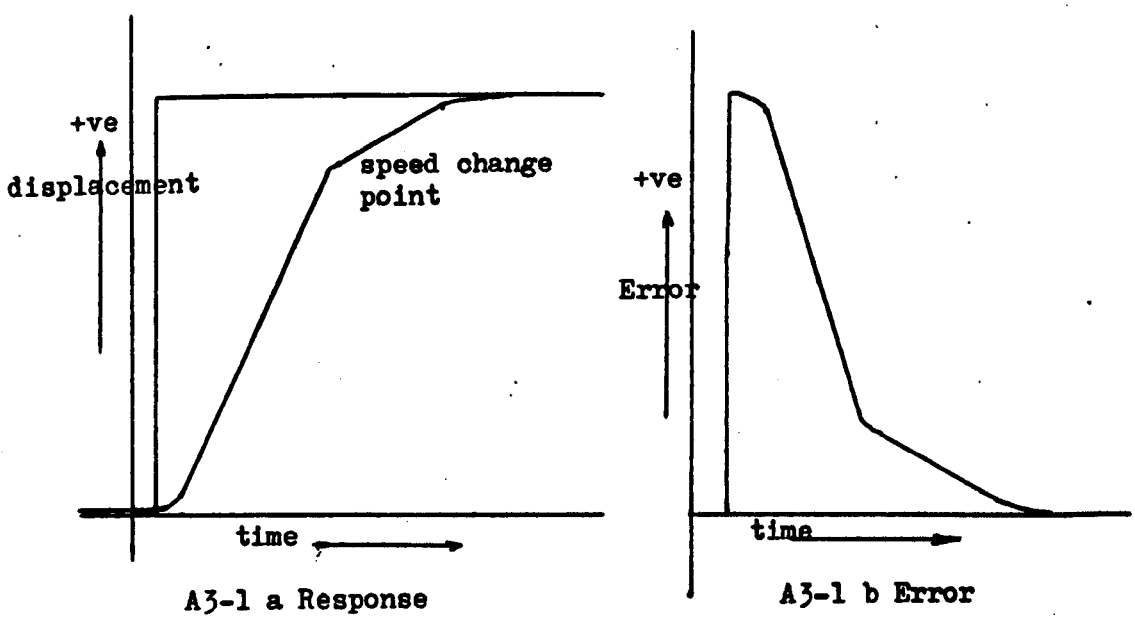

A3-1 a Response

A3-1 b Error

Fig.A3-1 Anticipated response to a step input function.

Rounding of corners in the above curves is due to inertia effects, and the ram extension speeds are given by the slopes of the two portions of the response curve.

In order to plot the performance curve, Fig.5-15 Section 5, for the system at 1 lbf stylus loading, values of the slopes obtained from the response curves in Figs.A3-7 and A3-10 were used, and average values were then calculated as follows:-

From Fig.A3-7 Fast $\frac{2.3 \times .25}{1.0} \times 60 = 34.5$ in/min

Slow $\frac{.5 \times .25}{1.3} \times 60 = 5.77$ in/min

From Fig.A3-10 Fast $\frac{1.65 \times .25}{.64} \times 60 = 38.7$ in/min

Slow $\frac{.47 \times .25}{1.3} \times 60 = 5.42$ in/min

Hence average speeds are:-

Fast = 36.6 in/min

Slow = 5.6 in/min

Owing to the use of the sample data interface unit, no information is available concerning the ram position between the sampling points. For this reason, it is not possible to say precisely where the step occurred on the time base of each curve. The step certainly occurred between the points 0 and 1 on the base, but its position has to be estimated from the slope of the fast portion of each curve. This point is made uncertain by the rounding effects of inertia already mentioned, although in this case high accelerations were made possible by the use of a high torque motor and low component inertias, which served to reduce these rounding effects to a minimum.

Ramp Inputs

In considering a position servomechanism without proportional control, it may be said that such equipment can only follow a ramp type input function provided that the ramp gradient is less than the response speed of the system. If this condition is achieved, the system follows an input ramp in a series of steps as shown below in Fig.A3-2.

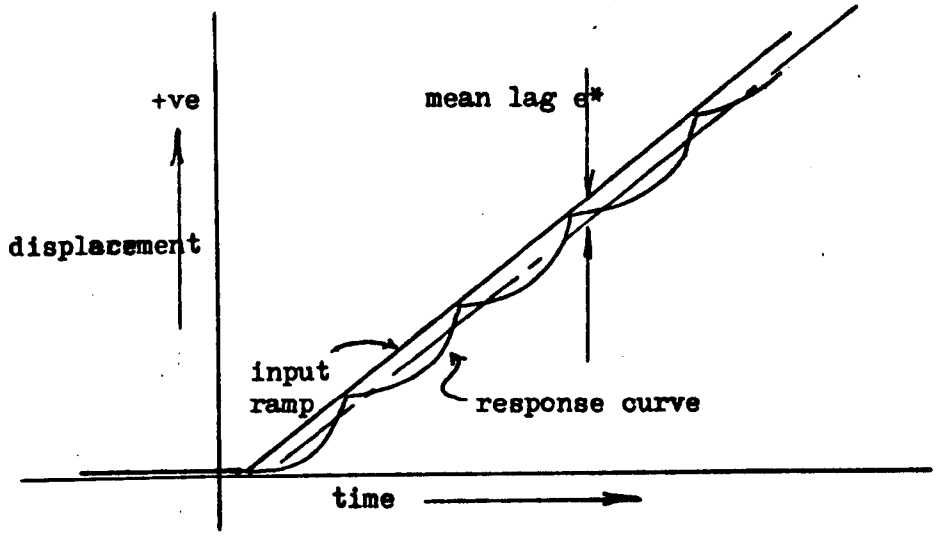

Fig.A3-2 Response of a non proportional servo to an input ramp.

In the above diagram, the mean lag error e* is defined as the average value of position error as the equipment attempts to follow the input signal.

Response of a two speed servo

As previously stated, the system used in these tests was provided with two preset response speeds, and it was arranged that the mechanism changed speed at a definite value of error signal.

Provided that the input ramp gradient does not exceed the slow speed response, the system will behave as the simple non-proportional equipment already considered. When ramp gradients in excess of the slow speed, but less than the fast speed, are applied to the system, the error builds up to the predetermined speed change point and then follows a line parallel to the ramp but displaced vertically below it by an amount δ as shown below in Fig.A3-3. The value of δ is determined by the preset changeover point from slow to fast response, and the nature of the response curve is similar to that shown in Fig.A3-2.

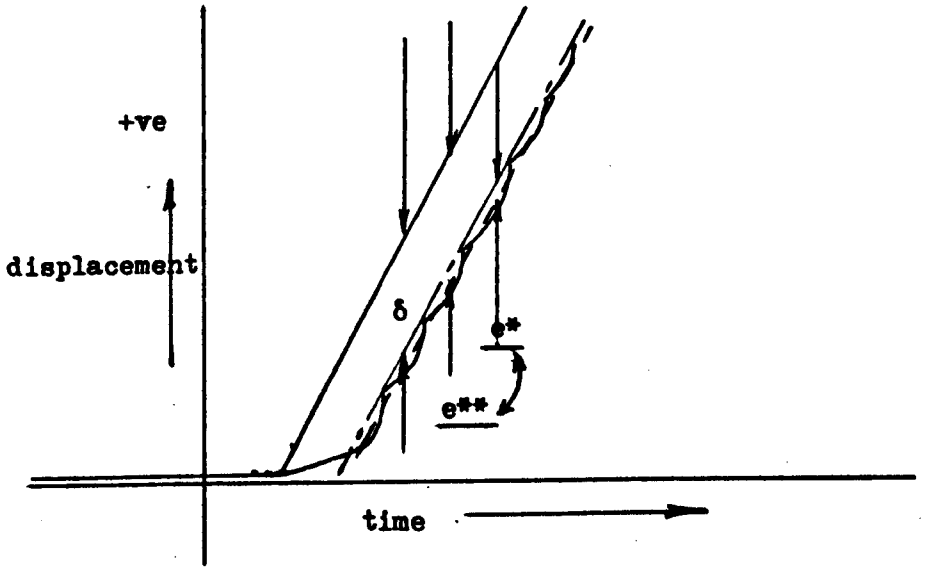

Fig.A3-3 Two speed system response to input ramp.

In the above case, the mean lag error is made up of two parts:

$$e^* = (e^{**} + \delta)$$

The value of e^{**} will change with input ramp gradient.

Performance curve

Due to having a speed changeover point at a predetermined error value, and also having preset response speeds, the performance curve for a two speed system will have the discontinuities shown overleaf in Fig.A3-4.

Fig.A3-4 Form of the performance curve for the digital servomechanism.

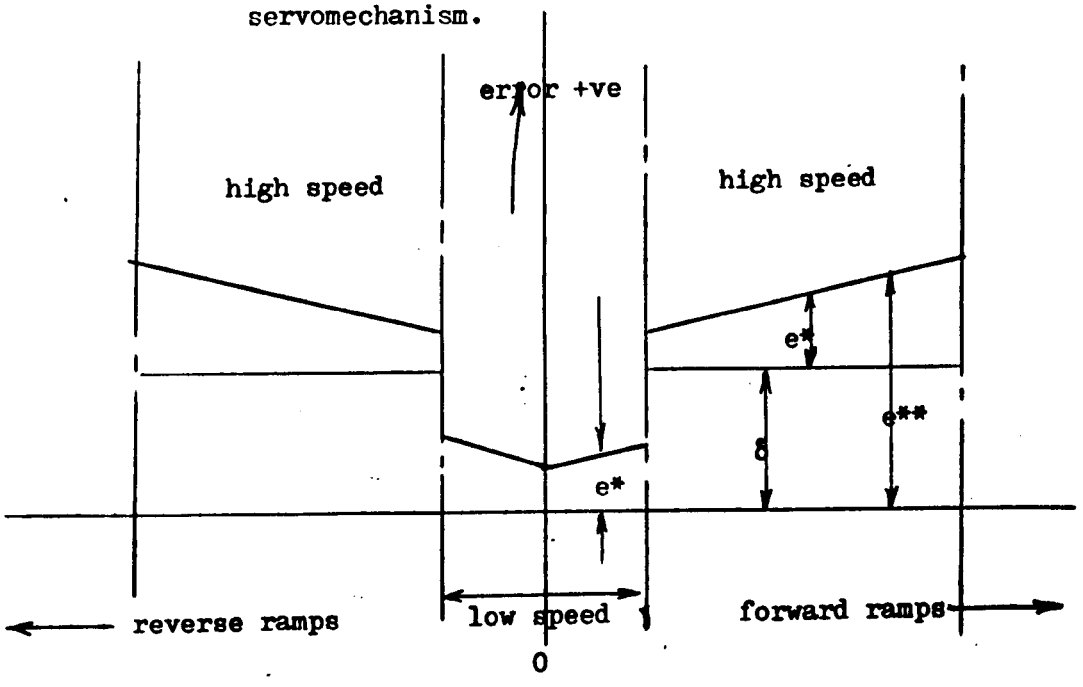

Fig.A3-5 Explanation of the error curve.

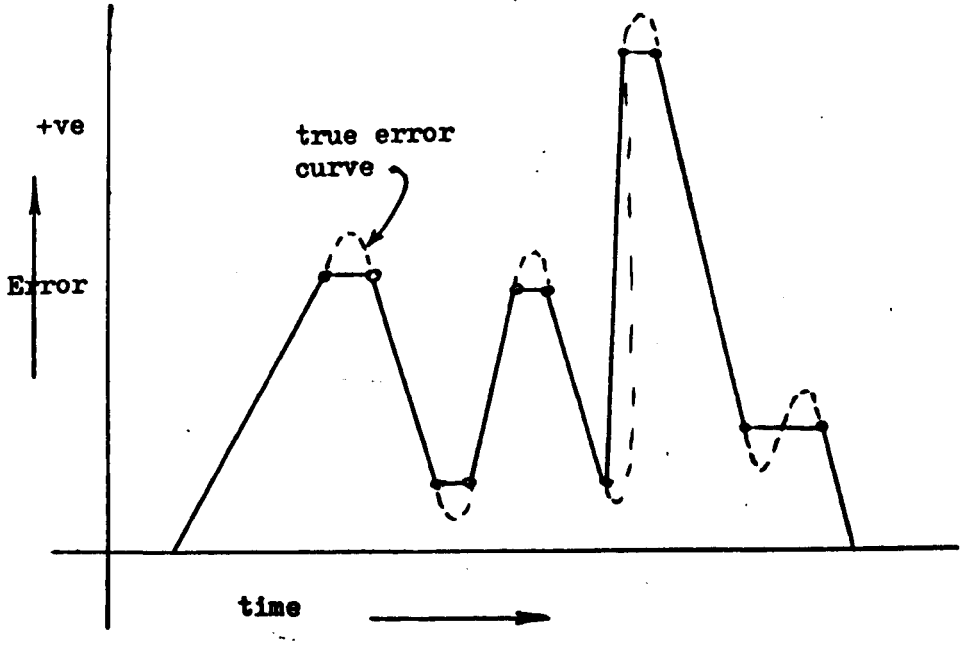

The form of the performance curve shown opposite in Fig.A3-4 is linear between discontinuities. This is an assumption which has been made in the actual response curve, Fig.5-15 Section 5, which was necessitated by the number of points on the curve actually obtained during these tests.

Error Curves

In this thesis, the results obtained have been recorded and plotted as error curves, Figs.A3-6 to A.3-23, rather than the response curves that have been discussed. In addition, the values of error obtained can only be said to have existed at a given instant, there being no information between sampling points.

For clarity, the error curves have been drawn by connecting together the plotted points with straight lines, as shown opposite in Fig.A3-5 by the full lines. In fact, the true error curve would certainly follow the course shown by the dotted lines, with the rounding effects due to inertia as illustrated. This has been taken into account in determining the mean lag error values listed in Tables 5.1 and 5.2 in Section 5.

Test runs - Step Inputs.

A series of six runs using step input functions was carried out on the digital servomechanism, by means of the switch bank as previously described in Section 5, to provide a 1-in step up or down. The simulated stylus loading was varied using the weights described in Section 5, and the following table shows the parameters for each run in this series.

Loading	.5 lbf	1 lbf	2 lbf
'up' step	1	2	3
'down' step	4	5	6

Table A3.1 Parameters for step input tests

An 'up' step corresponds to a sudden change in ram extension from .5 to 1.5 in.

A 'down' step corresponds to a sudden retraction of the ram from 1.5 to .5 in.

Ramp Inputs.

A series of twelve runs using ramp input functions was carried out, using the 'Robtom' machine as described in Section 5, to generate 6 different input functions. In addition, the simulated stylus loading was varied in the same way as for the step input tests.

The frequencies used corresponded to the ramp gradients described in Section 5 which makes these tests comparable to those carried out on the hydraulic servomechanism (Section 3). Table A3.2 on the following page gives the parameters employed for each run.

Test No.	Stylus load lbf	Ramp Gradient in/min	Drive Frequency Hz	Count Direction
7	1.0	+ 4	78	up
8	1.0	+ 2	39	up
9	1.0	- 2	39	down
10	1.0	+ 25	488	up
11	1.0	+ 12.5	244	up
12	1.0	- 12.5	244	down
13	.5	+ 4	78	up
14	.5	+ 2	39	up
15	.5	- 2	39	down
16	2.0	+ 4	78	up
17	2.0	+ 2	39	up
18	2.0	- 2	39	down

Table A3.2 Parameters for ramp input tests.

Count direction 'up' corresponds to an increasing binary count which results in an extension of the ram.

Count direction 'down' corresponds to a decreasing binary count which causes the ram to retract.

As stated in Section 5, the detailed readings of the error tapes are not included in this thesis, but the error curves drawn from them are given on the following pages in Figs. A3-6 to A3-23.

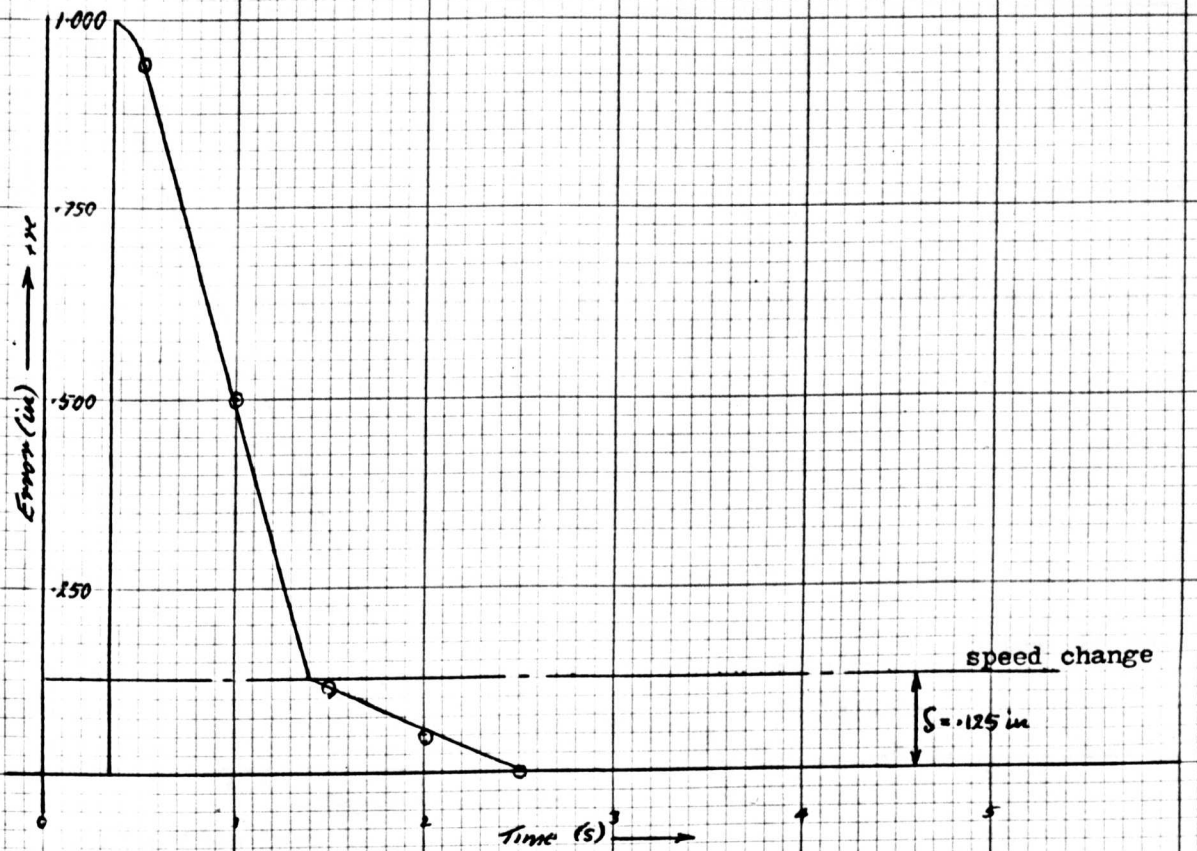

Fig. A3-6 Step Test 1

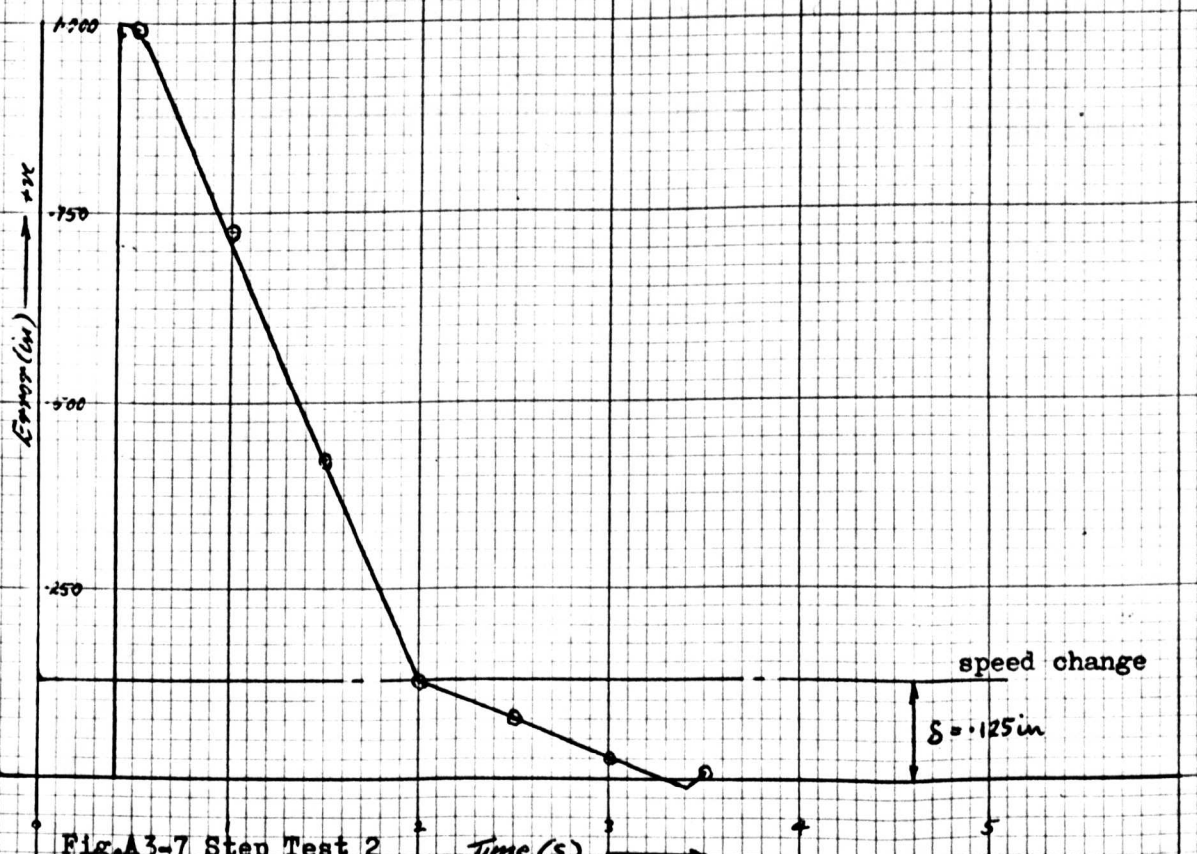

Fig.A3-7 Step Test 2

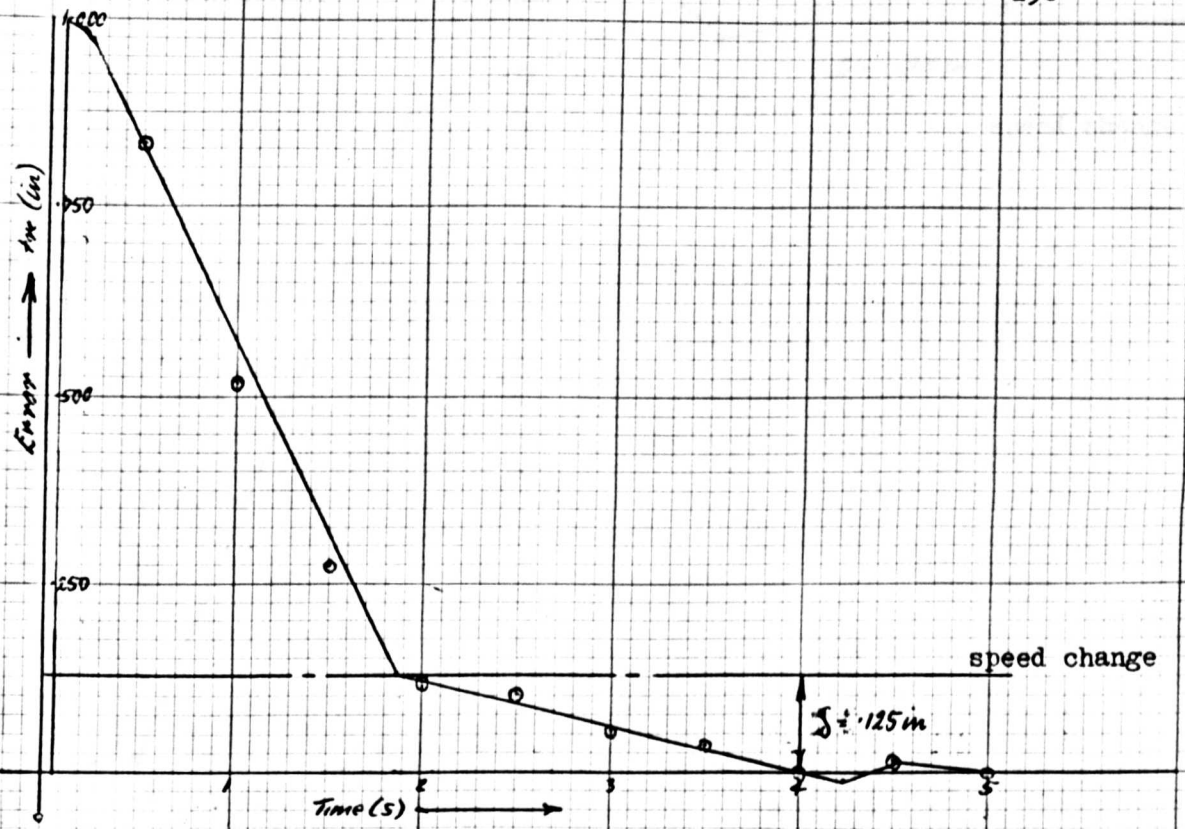

Fig.A3-8 Step Test 3

Fig.A3-9 Step Test 4

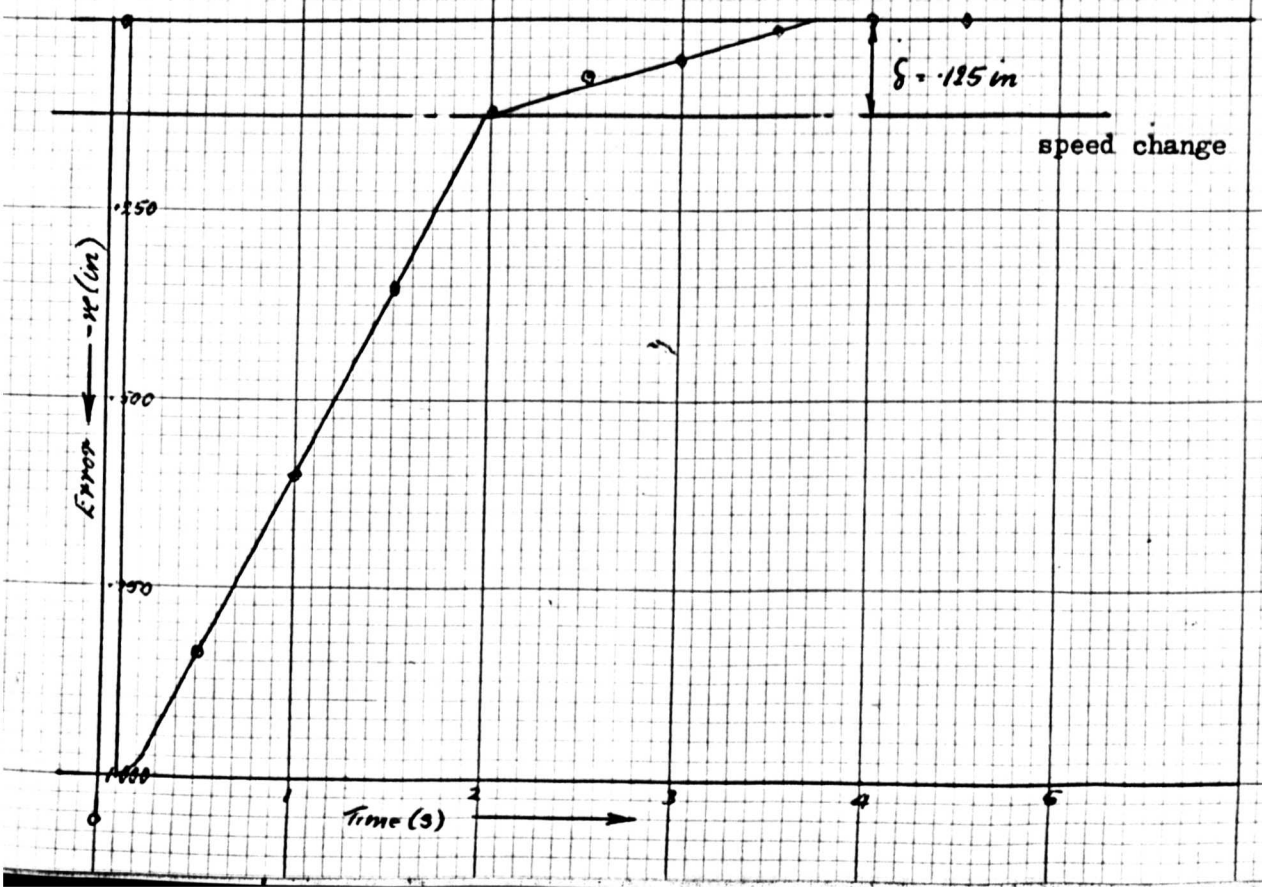

Fig.A3-10 Step Test 5

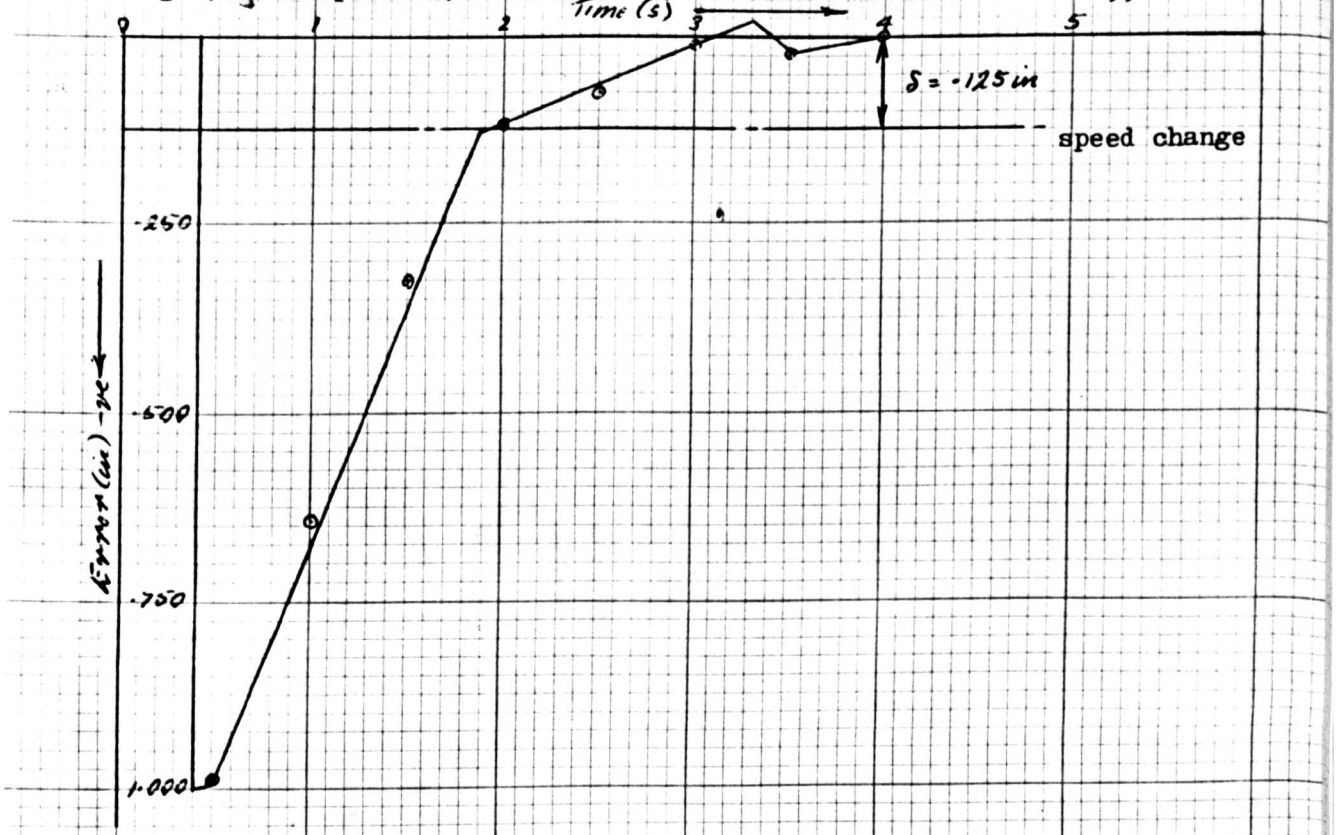

Fig.A3-11 Step Test 6

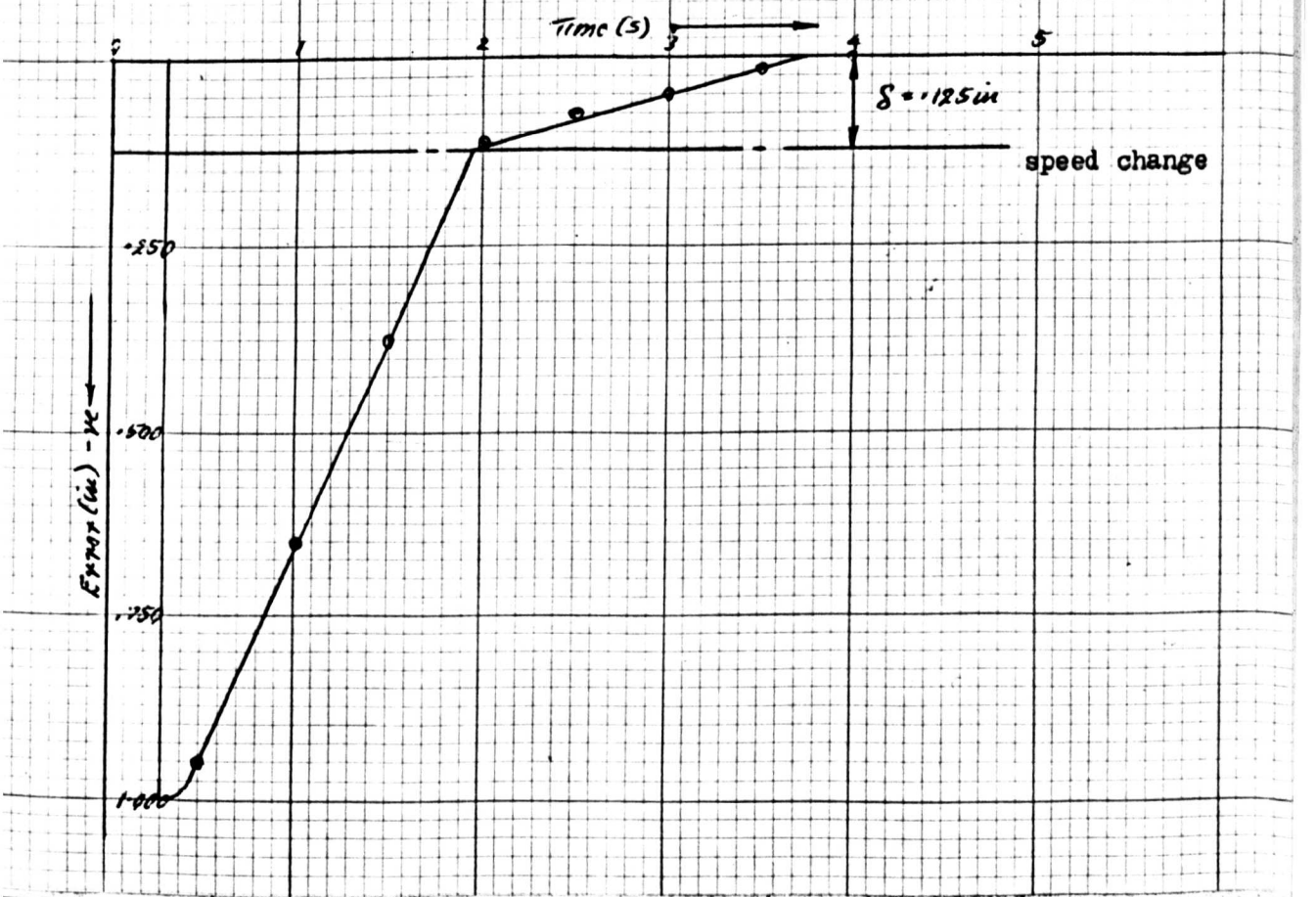

Fig.A3-12 4 in/min forward ramp 1 lbf stylus load

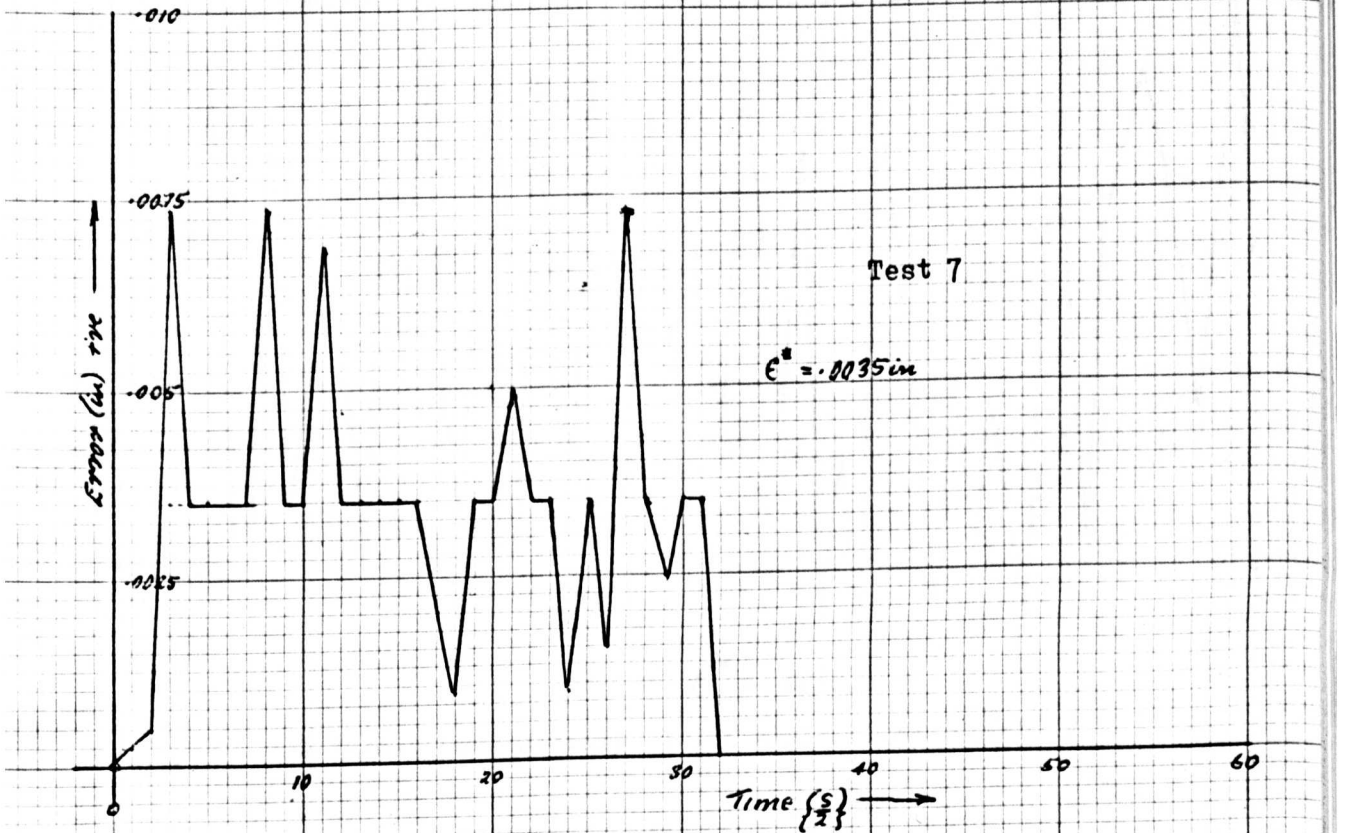

Fig.A3-13 2 in/min forward ramp 1 lbf stylus load

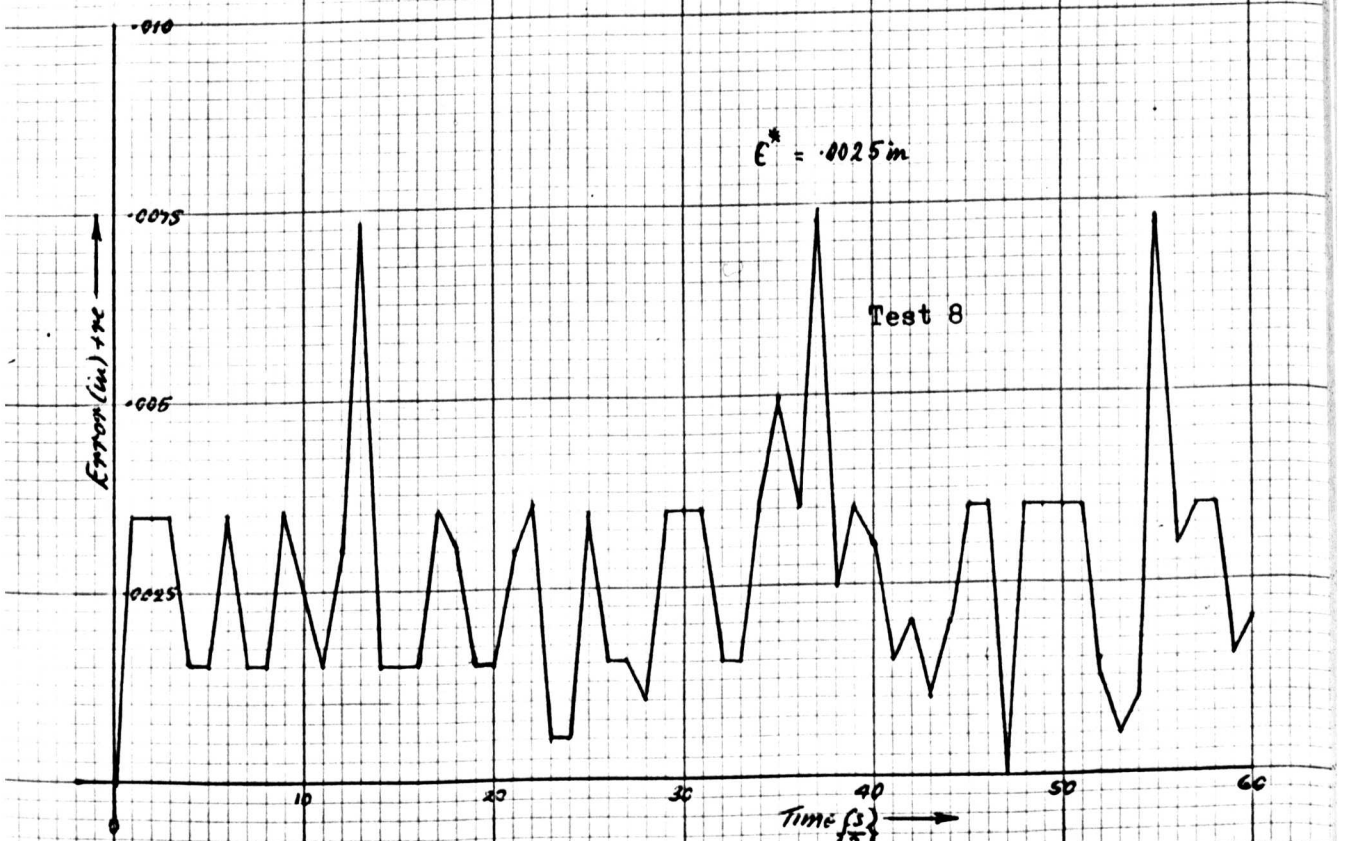

Fig.A3-14

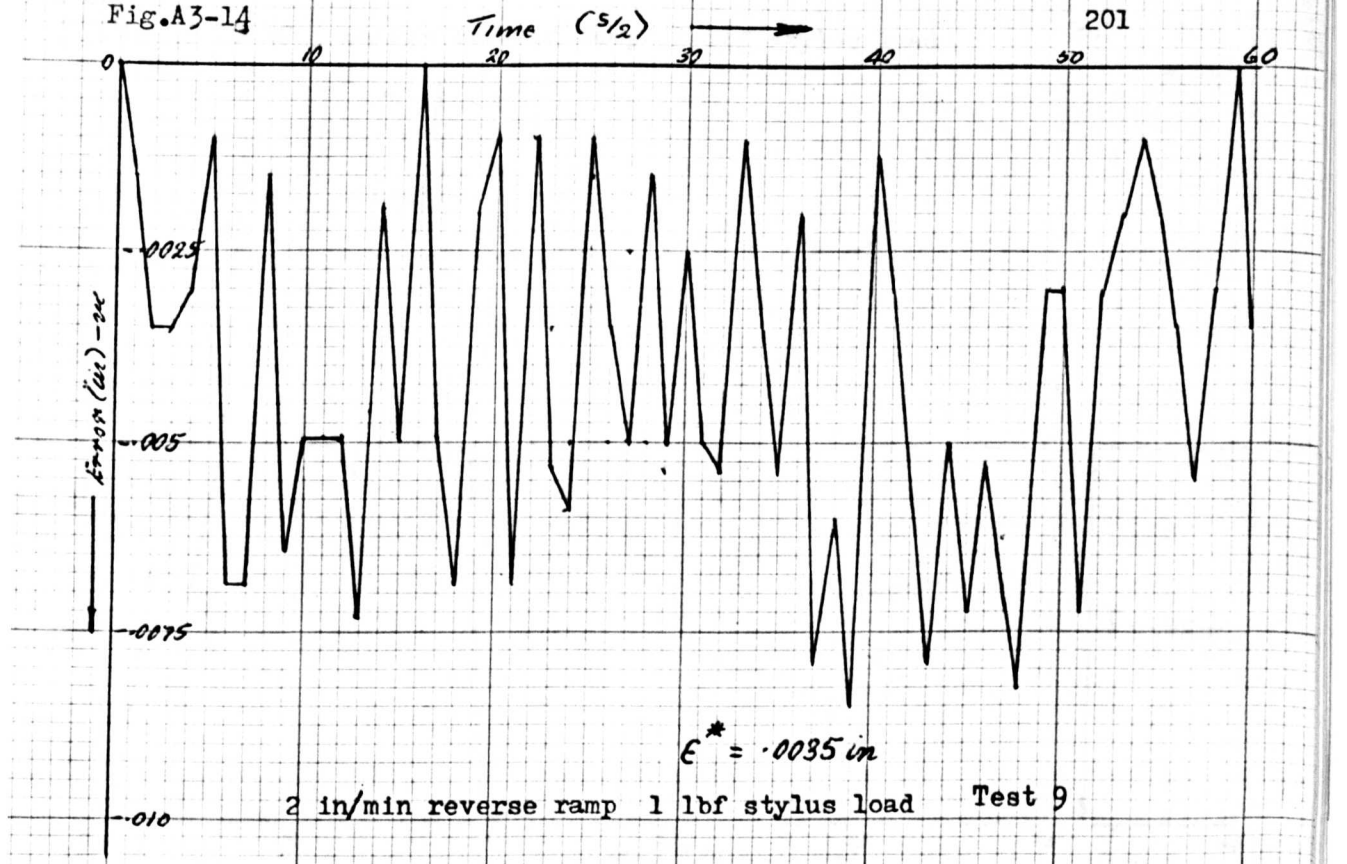

2 in/min reverse ramp 1 lbf stylus load Test 9

Fig.A3-15 25 in/min forward ramp 1.0 lbf stylus load

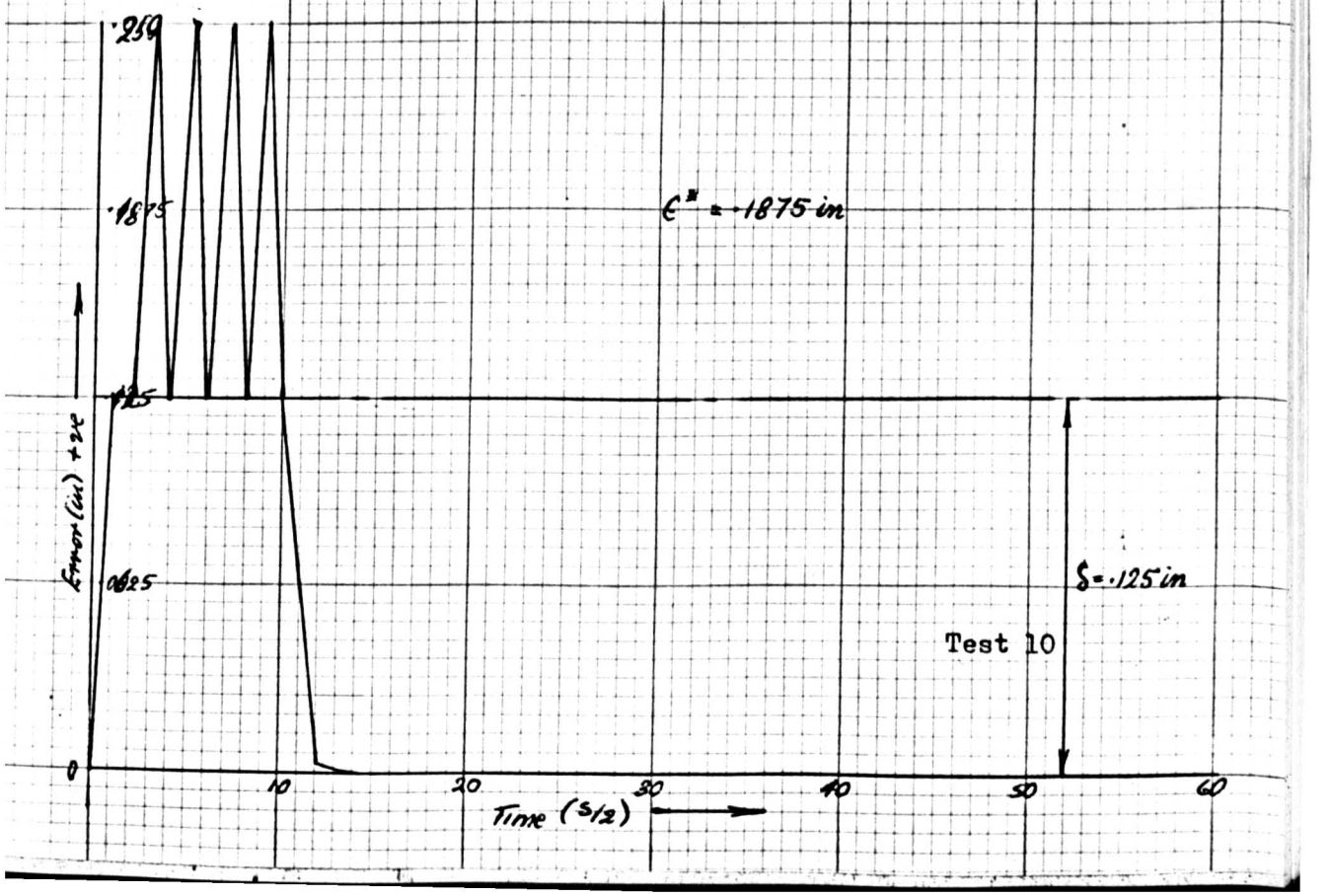

Fig.A3-16 12.5 in/min forward ramp 1 lbf stylus load

Fig.A3-17 12.5 in/min reverse ramp 2 lbf stylus load

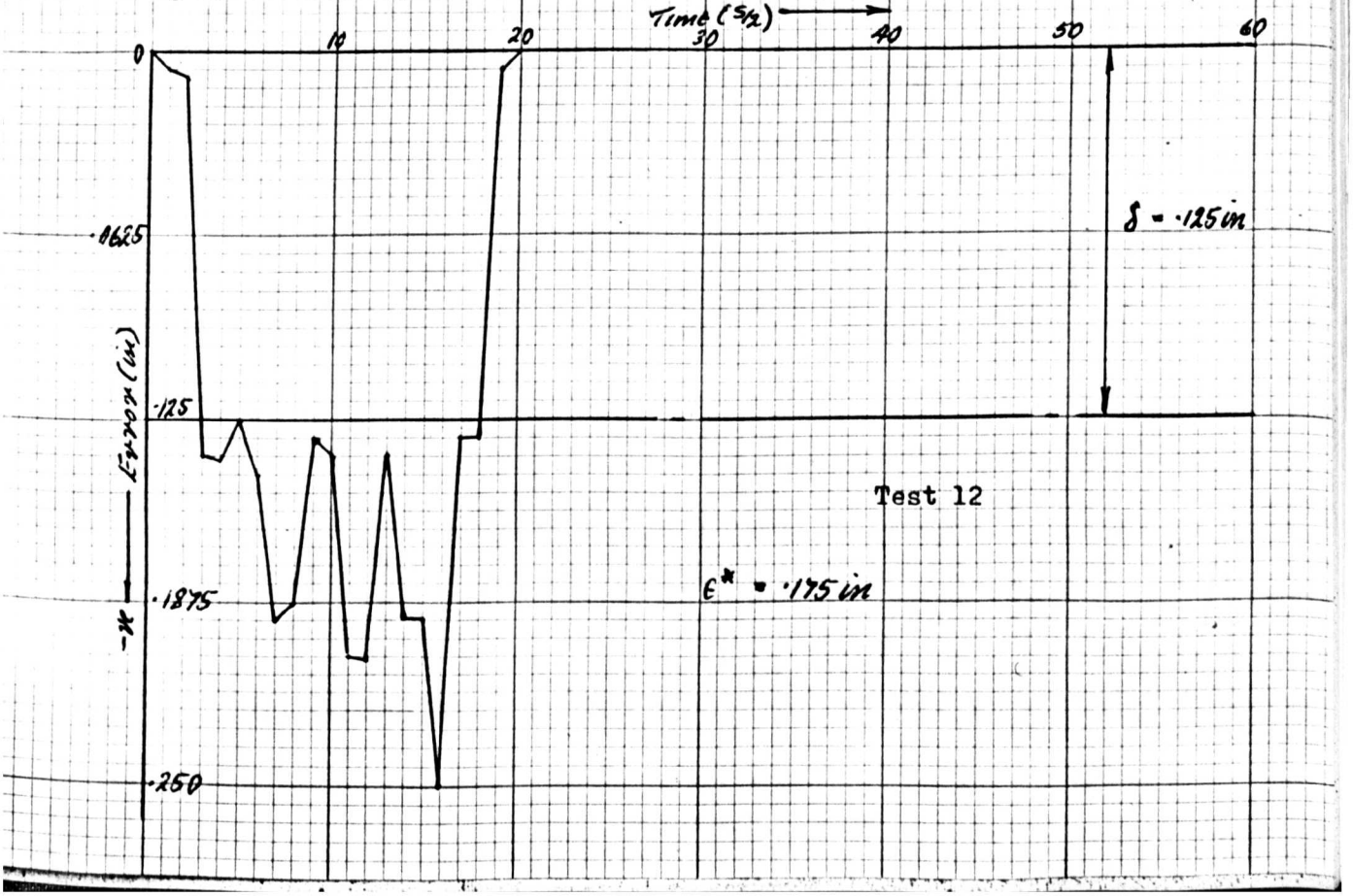

Fig.A3-18. 4 in/min forward ramp 0.5 lbf stylus load

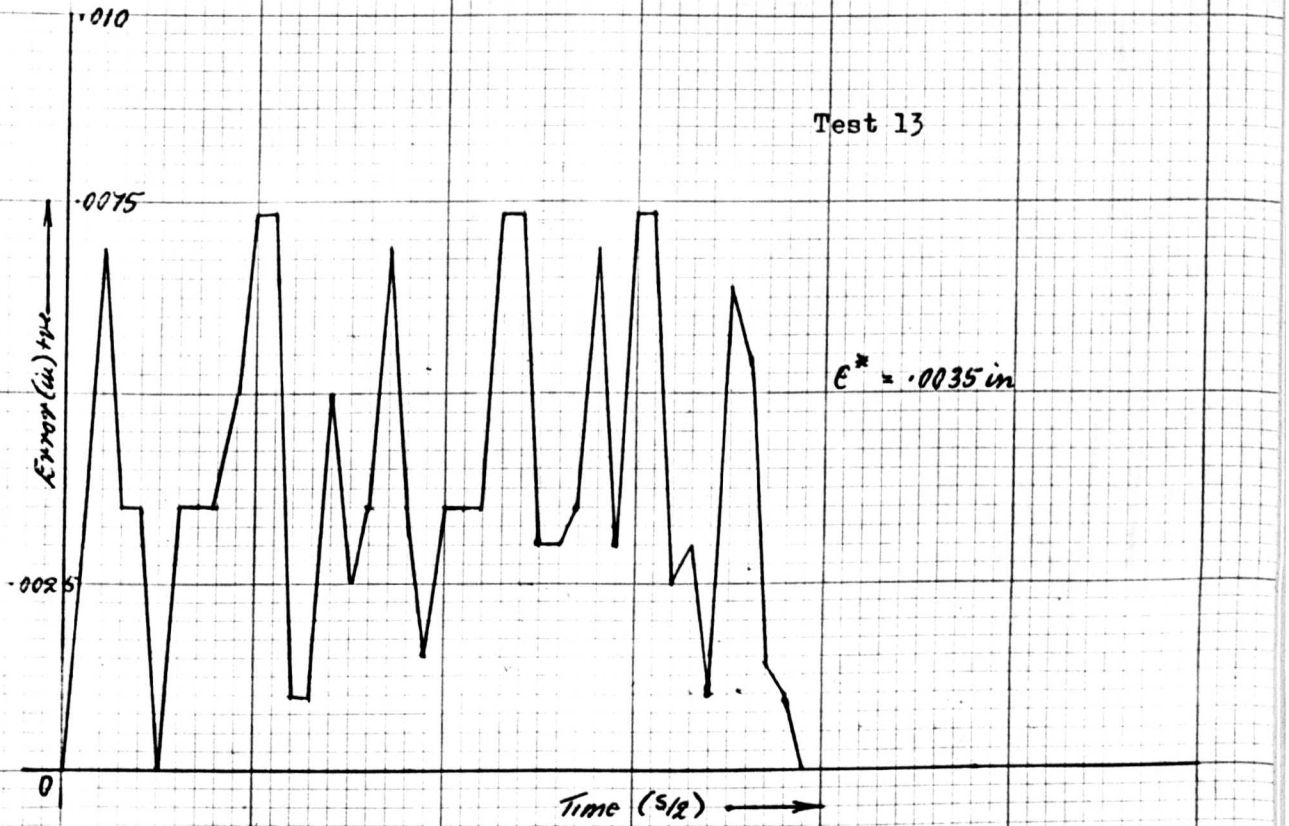

Fig.A3-19 2 in/min forward ramp 0.5 lbf stylus load

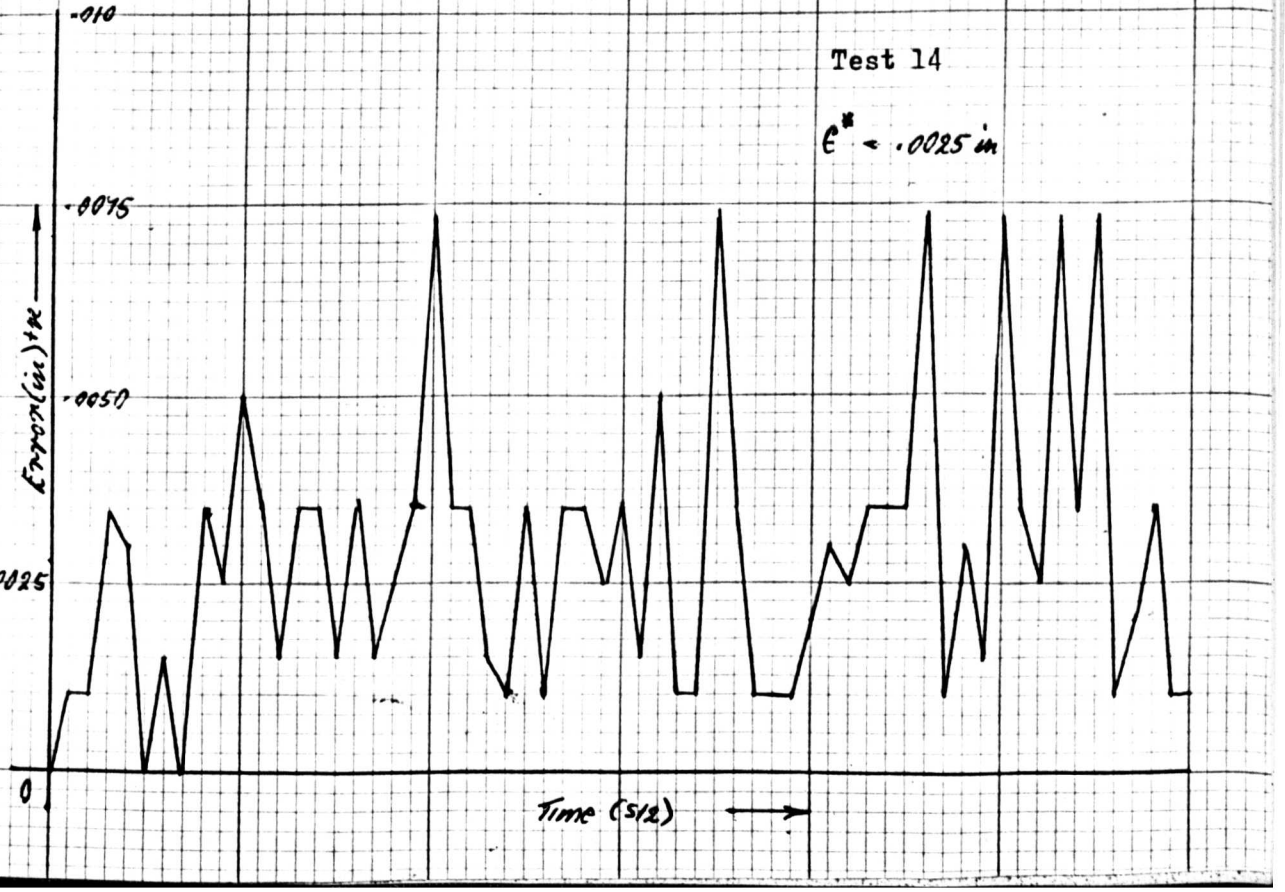

Fig.A3-20 2 in/min reverse ramp 0.5 lbf stylus load

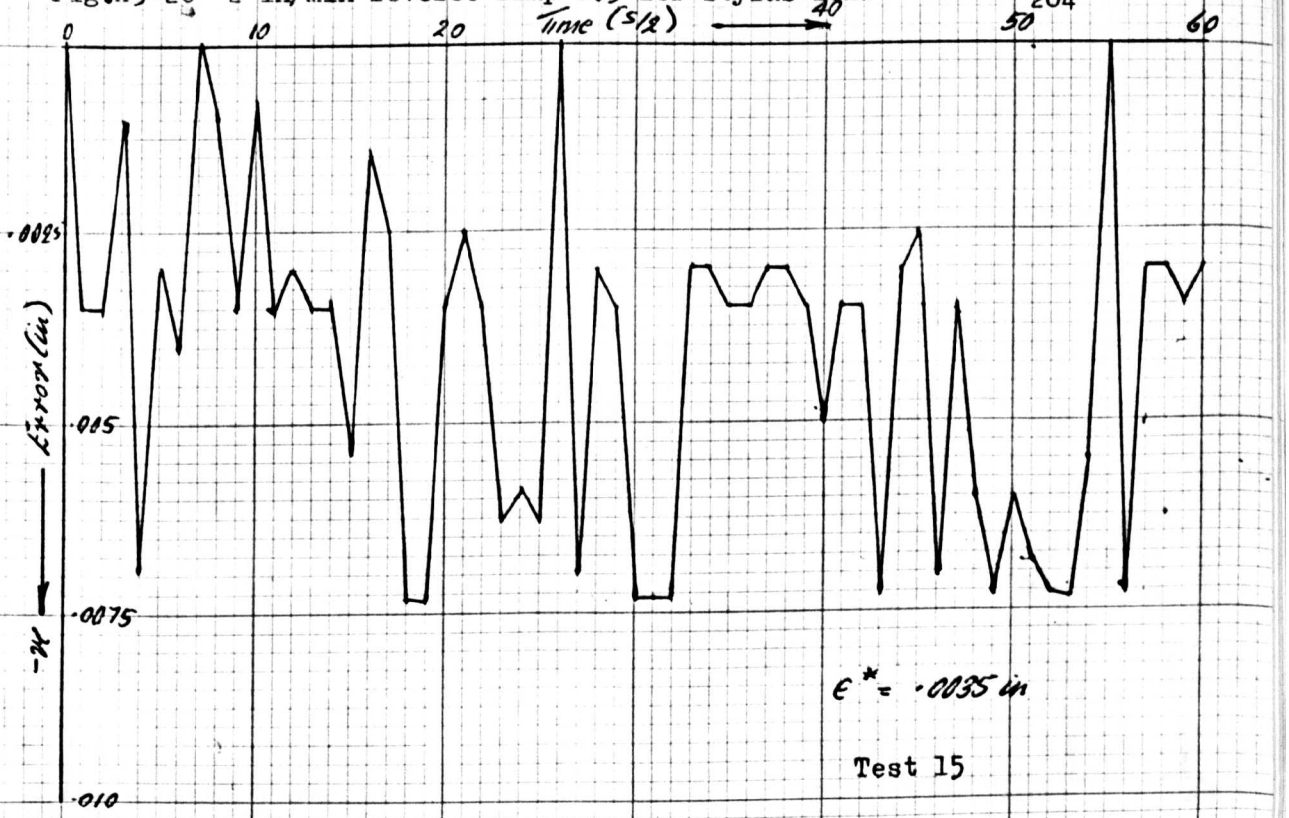

Fig.A3-21 4 in/min forward ramp 2 lbf stylus load

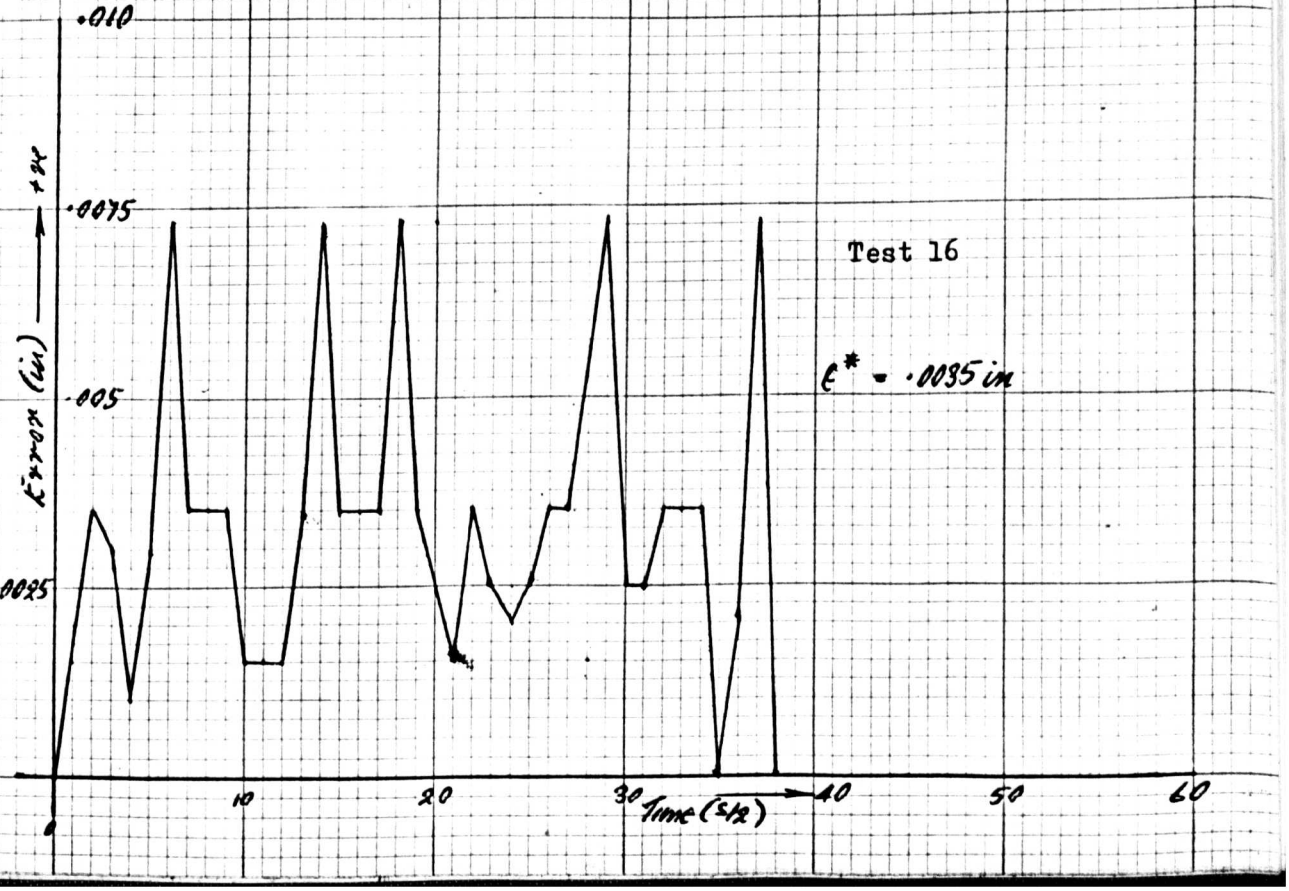

Fig.A3-22 2 in/min forward ramp 2 lbf stylus load

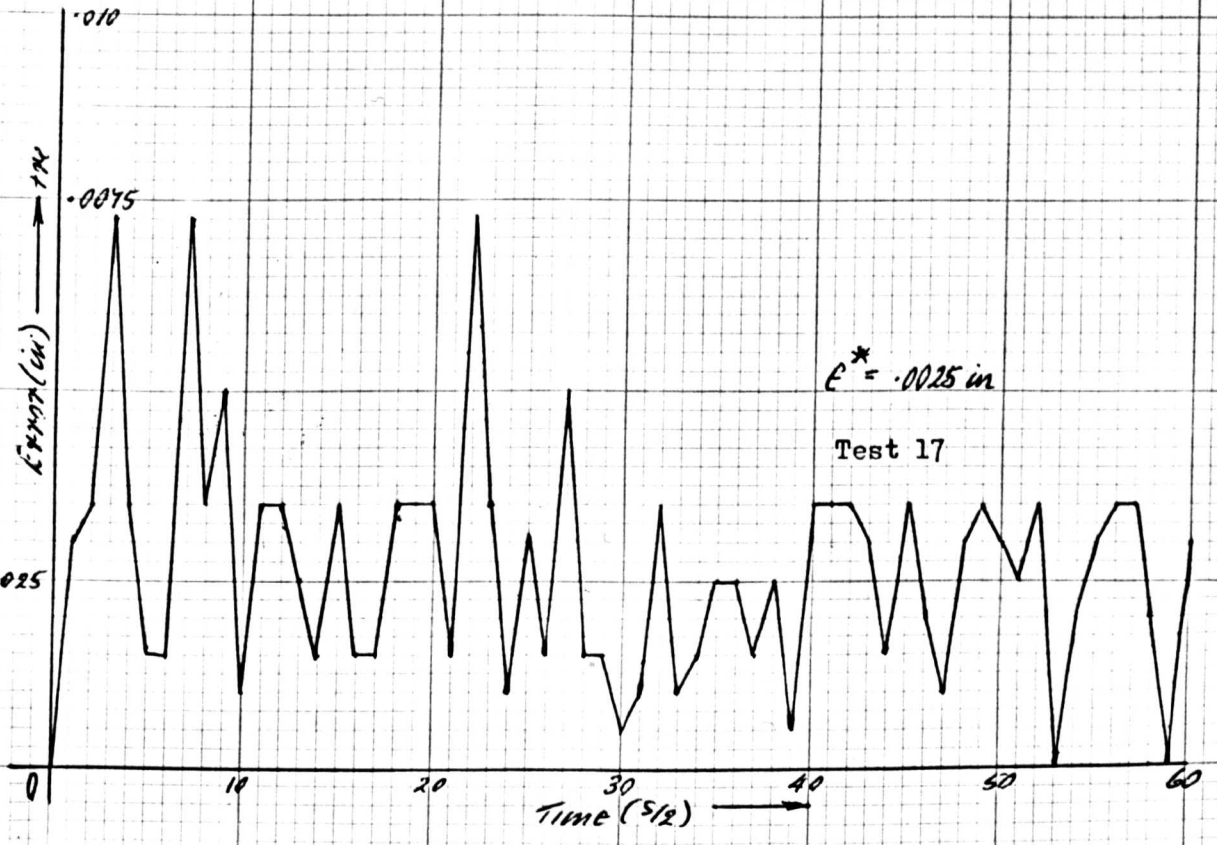

Fig.A3-23 2 in/min reverse ramp 2 lbf stylus load

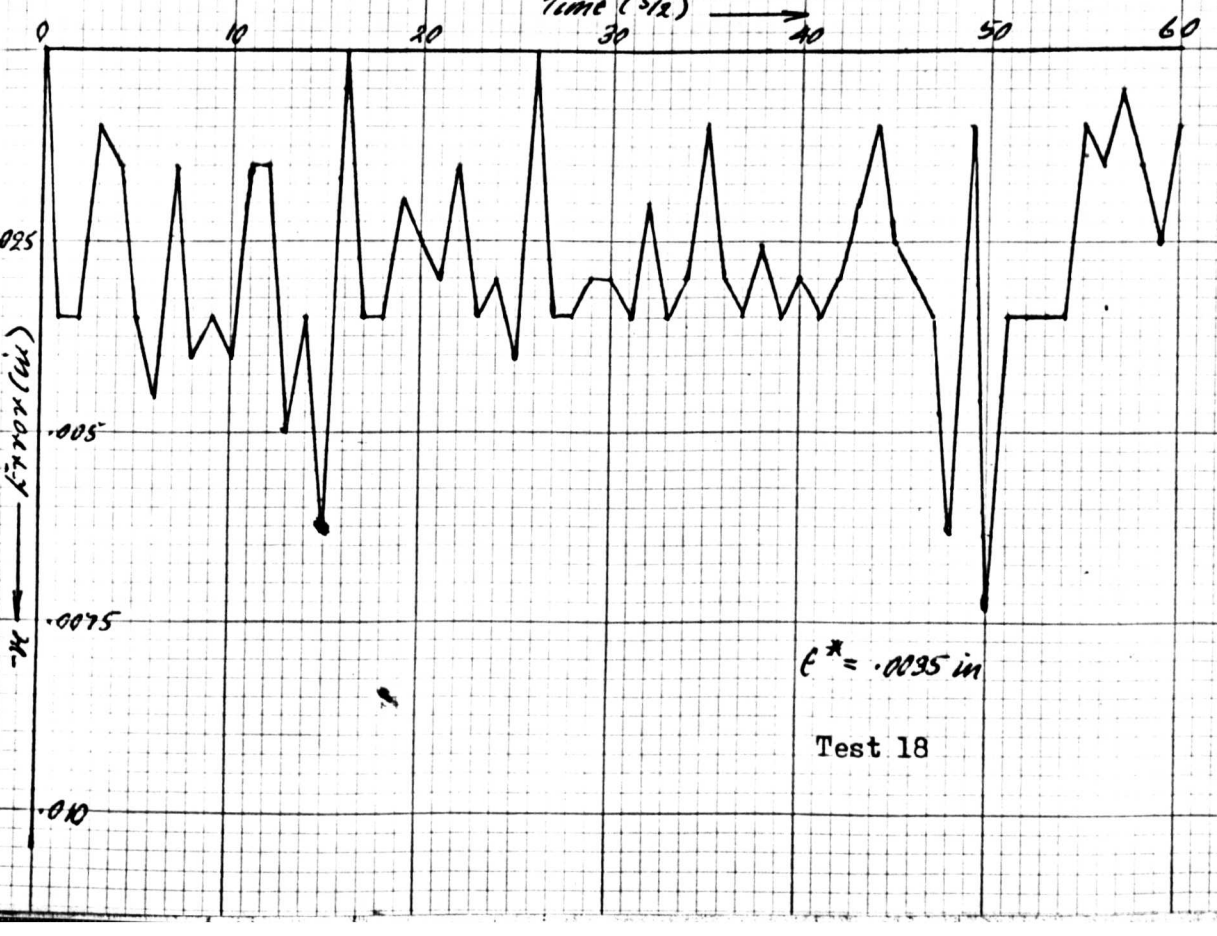

APPENDIX 4

Detailed results of machining tests carried out with the digital servomechanism fitted to the Harrison L 6 copying lathe

Table A4.1 - Detailed results of positioning accuracy tests on the Digital Servomechanism (Ref.5 S 9). These results are plotted in Fig.7-1 S 7.

Ram Extension (in)	Error (in)
.1245	+ .0005
.2494	+ .0006
.4996	+ .0004
.7491	+ .0009
.9998	+ .0002
1.1247	+ .0003
1.2491	+ .0009
1.3747	+ .0003
1.5000	0
1.6243	+ .0007
1.7487	+ .0013
1.8741	+ .0009
1.9982	+ .0013
1.8752	- .0002
1.7504	- .0004
1.6248	+ .0002
1.4999	+ .0001
1.3752	- .0002
1.2502	- .0002
1.1251	- .0001
1.0004	- .0004
.7500	0
.5002	- .0002
.3753	- .0003
.2509	- .0009
.1252	- .0002
.0007	- .0007

Table A4.2 - Detailed results of First machining test. These values are plotted in Fig.7-2 S 7. (λ = 1170).

Required Diameter (in)	Actual Diameter (in)	Error (in)
1.950	1.9485	- .0015
1.900	1.8980	- .0020
1.850	1.8490	- .0010
1.800	1.7988	- .0013
1.750	1.7497	- .0003
1.700	1.6993	- .0007
1.650	1.6495	- .0005
1.600	1.5996	- .0004
1.550	1.5503	+ .0003
1.500	1.5012	+ .0012
1.450	1.4518	+ .0018
1.400	1.4018	+ .0018
1.350	1.3540	+ .0040
1.300	1.3035	+ .0035
1.250	1.2555	+ .0055
1.200	1.2056	+ .0056
1.150	1.1570	+ .0070
1.100	1.1069	+ .0069
1.050	1.0592	+ .0092
1.000	1.0084	+ .0084

Table A4.3 - Detailed results of Second test. These values are plotted in Figs.7-3a and 7-3b. (λ = 1183).

Required Diameter (in)	Actual Diameter (in)	Error (in)	Repeatability (in)
1.950	1.9505	+ .0005	.0002
1.900	1.8983	- .0017	.0005
1.850	1.8489	- .0011	.0010
1.800	1.7988	- .0012	.0001
1.750	1.7479	- .0021	.0008
1.700	1.6970	- .0030	.0009
1.650	1.6480	- .0020	.0003
1.600	1.5971	- .0029	.0013
1.550	1.5491	- .0009	.0001
1.500	1.4987	- .0013	.0001
1.450	1.4475	- .0025	.0008
1.400	1.3975	- .0025	.0007
1.350	1.3483	- .0017	.0003
1.300	1.2988	- .0012	.0002
1.250	1.2494	- .0006	.0002
1.200	1.1996	- .0004	.0002
1.150	1.1490	- .0010	.0001
1.100	1.0989	- .0011	.0004
1.050	1.0490	- .0010	.0007
1.000	.9997	- .0003	.0001
.950	.9500	0	.0002

Table A4.4 - Detailed results of Third test. These values are plotted in Fig. 7-4 Section 7. (λ = 1183).

Required Diameter (in)	Actual Diameter (in)	Error (in)
2.950	2.9499	- .0001
2.900	2.8996	- .0004
2.850	2.8481	- .0019
2.800	2.7993	- .0007
2.750	2.7498	- .0002
2.700	2.6999	- .0001
2.650	2.6490	- .0010
2.600	2.5993	-..0007
2.550	2.5487	- .0013
2.500	2.4989	- .0011
2.450	2.4491	- .0009
2.400	2.3994	- .0006
2.350	2.3497	- .0003
2.300	2.3003	+ .0003
2.250	2.2506	+ .0006
2.200	2.2010	+ .0010
2.150	2.1508	+ .0008
2.100	2.1017	+ .0017
2.050	2.0529	+ .0029
2.000	2.0028	+ .0028
1.950	1.9511	+ .0011
1.900	1.9014	+ .0014
1.850	1.8501	+ .0001
1.800	1.8006	+ .0006
1.750	1.7520	+ .0026
1.700	1.7019	+ .0019
1.650	1.6519	+ .0019
1.600	1.6018	+ .0018
1.550	1.5518	+ .0018
1.500	1.5021	+ .0021
1.450	1.4516	+ .0016
1.400	1.4017	+ .0017
1.350	1.3523	+ .0023
1.300	1.3023	+ .0023
1.250	1.2523	+ .0023
1.200	1.2021	+ .0021
1.150	1.1520	+ .0020
1.100	1.1022	+ .0022
1.050	1.0526	+ .0026
1.000	1.0023	+ .0023
.950	.9524	+ .0024
.900	.9021	+ .0021
.850	.8521	+ .0021

Table A4.5 - Detailed results of Fourth test. These values are plotted in Fig.7-5a and Fig.7-5b, Section 7. (λ = 1183).

Required Diameter (in)	Actual Diameter (in)	Error (in)	Repeatability (in)
2.900	2.8992	- .0008	
2.800	2.8011	+ .0011	.0002
2.700	2.7010	+ .0010	.0004
2.600	2.6003	+ .0003	.0005
2.500	2.4986	- .0014	.0001
2.400	2.3996	- .0004	.0003
2.300	2.2997	- .0003	.0001
2.200	2.1992	- .0008	.0006
2.100	2.0991	- .0009	.0006
2.000	1.9986	- .0014	.0003
1.900	1.8982	- .0018	0
1.800	1.7987	- .0013	.0005
1.700	1.6985	- .0015	.0004
1.600	1.5985	- .0015	.0004
1.500	1.4984	- .0016	.0006
1.400	1.3983	- .0017	.0003
1.300	1.2992	- .0008	.0002
1.200	1.1988	- .0012	.0004
1.100	1.0983	- .0017	.0003
1.000	.9986	- .0014	.0002
.900	.8986	- .0014	.0002

Table A4.6 - Detailed results of Fifth test. These values are plotted in Fig.7-6 Section 7. (λ = 1183).

Required Diameter (in)	Actual Diameter (in)	Error (in)
2.850	2.8493	- .0007
2.750	2.7502	+ .0002
2.650	2.6491	- .0009
2.550	2.5492	- .0008
2.450	2.4479	- .0031
2.350	2.3476	- .0024
2.250	2.2480	- .0020
2.150	2.1478	- .0022
2.050	2.0480	- .0020
1.950	1.9478	- .0022
1.850	1.8478	- .0022
1.750	1.7476	- .0024
1.650	1.6467	- .0033
1.550	1.5475	- .0025
1.450	1.4455	- .0045
1.350	1.3463	- .0037
1.250	1.2457	- .0043
1.150	1.1453	- .0047
1.050	1.0456	- .0044
.950	.9458	- .0042

Table A4.7 - Detailed results of Sixth test. These values are plotted in Fig.7-7 Section 7. (λ = 1182).

Required Diameter (in)	Actual Diameter (in)	Error (in)
2.900	2.9005	+ .0005
2.800	2.7980	- .0020
2.700	2.6985	- .0015
2.600	2.5992	- .0008
2.500	2.4990	- .0010
2.400	2.4000	0
2.300	2.2997	- .0003
2.200	2.2006	+ .0006
2.100	2.1014	+ .0014
2.000	2.0016	+ .0016
1.900	1.9031	+ .0031
1.800	1.8023	+ .0023
1.700	1.7014	+ .0014
1.600	1.6014	+ .0014
1.500	1.5017	+ .0017
1.400	1.4016	+ .0016
1.300	1.3025	+ .0025
1.200	1.2023	+ .0023
1.100	1.1022	+ .0022
1.000	1.0020	+ .0020
.900	.9022	+ .0022
.800	.8020	+ .0020

Table A.4.8 - Detailed results of Seventh test. These values are plotted in Fig.7-8 Section 7. (λ = 1182.5).

Required Diameter (in)	Actual Diameter (in)	Error (in)
2.900	2.8994	- .0006
2.800	2.7999	- .0001
2.700	2.6991	- .0009
2.600	2.5977	- .0023
2.500	2.4972	- .0028
2.400	2.3979	- .0021
2.300	2.2983	- .0017
2.200	2.1982	- .0018
2.100	2.0984	- .0016
2.000	1.9982	- .0018
1.900	1.9000	0
1.800	1.7991	- .0009
1.700	1.6972	- .0028
1.600	1.5969	- .0031
1.500	1.4975	- .0025
1.400	1.3973	- .0027
1.300	1.2976	- .0024
1.200	1.1985	- .0015
1.100	1.0986	- .0014
1.000	.9987	- .0013
.900	.8986	- .0014
.800	.7985	- .0015

Table A4.9 - Detailed results of Eighth test. These values are plotted in Fig.7-9 Section 7. (λ = 1182.5).

Required Diameter (in)	Actual Diameter (in)	Error (in)
2.900	2.8994	- .0006
2.800	2.7999	- .0001
2.700	2.6991	- .0009
2.600	2.5992	- .0008
2.500	2.4985	- .0015
2.400	2.3989	- .0011
2.300	2.2988	- .0012
2.200	2.1985	- .0015
2.100	2.0984	- .0016
2.000	1.9978	- .0022
1.900	1.8995	- .0005
1.800	1.7991	- .0009
1.700	1.6987	- .0013
1.600	1.5983	- .0017
1.500	1.4975	- .0025
1.400	1.3993	- .0007
1.300	1.2991	- .0009
1.200	1.1985	- .0015
1.100	1.0986	- .0014
1.000	.9987	- .0013
.900	.8986	- .0014
.800	.7985	- .0015